Towards Stabilised Cyclocarbons

Daniel R. Kohn

St Hilda's College

University of Oxford

A thesis submitted for the degree of

Doctor of Philosophy

Michaelmas 2017

Towards Stabilised Cyclocarbons

D.Phil. Thesis, Michaelmas 2017

Daniel Kohn, St Hilda's College, University of Oxford

This thesis describes synthetic efforts towards isolating cyclo[*n*]carbons. These elusive *sp*-hybridised allotropes of carbon have been synthetic targets for many years. Two modern stabilisation approaches are discussed that may provide the opportunity to finally prepare and study these molecules. Primarily, this thesis focuses on the stabilisation of *sp*-hybridised carbons by encapsulation with protective macrocycles. The concept of on-surface synthesis is also introduced and a method to prepare polyynes on surfaces using scanning probe microscopy is developed. These distinct approaches have simultaneously made significant progress in approaching cyclocarbons while enriching our understanding of polyynes.

Chapter 1 reviews the history of carbon-rich molecules, experimental and theoretical studies of cyclocarbons and the concept of stabilising carbon chains *via* encapsulation.

Chapter 2 explores the strategy of templating polyynes around a central core by preparing porphyrin-polyyne [3]- and [5]rotaxanes. There is also a photophysical investigation of excited state energy donation properties of polyynes.

Chapter 3 details the synthesis of cobalt-masked polyynes and their mild unmasking. This unmasking process yields pristine polyynes in unprecedented yields and offers significant promise for the use of this method in cyclocarbon catenane synthesis.

Chapter 4 summarises the synthesis of small macrocycles and dibromoolefin rotaxanes. These dibromoolefin rotaxanes have their protective silyl groups removed, yet remain interlocked.

Chapter 5 introduces scanning probe microscopy and developments in on-surface synthesis. Furthermore, we develop the controlled synthesis of polyynes from dibromoolefins, using the Fritsch-Buttenberg-Wiechell rearrangement by atomic manipulation.

Chapter 6 summarises the key results in this thesis and contains proposals for future work in this area.

Acknowledgements

First of all, I would like to thank my supervisor Professor Harry Anderson, who trusted me with a project in his group and for his support and encouragement throughout my time in Oxford. The work presented here would not have been possible without contributions from collaborators in our group and elsewhere. Ideas have always flown freely in this project, which has been to its great credit. Dr Levon Movsisyan, Dr Przemyslaw Gawel, Dr Steffen Woltering and Ms Lorel Scriven have been part of a formidable team at various stages of my DPhil. Particular thanks must go to Levon, for showing me the ropes in the lab and Przemek, for two years of companionship and advice amidst many failed reactions. I would like to thank our collaborators at IBM Zurich: Dr Niko Pavlicek and Dr Leo Gross, for being part of such an exciting project with us. I would also like to express my gratitude to Dr. Amber Thompson, Dr Kirsten Christensen (Oxford Crystallography) and Yaoyao Xiong for help with many crystal structures. Finally, the NMR service have spent an extraordinarily long time recording carbon NMRs for me, for which I am very grateful.

I would like to thank Dr Martin Grossel for recommending Harry's group to me and encouraging me to go to that fateful DPhil open day. Thank you to everyone in the group, past and present (in vaguely chronological order): Arjen, Julien, Rene, Ludovic, Levon, Cécile, Nun, Renee, Jonathan, Anjul, Yaoyao, Isa, Sabine, Takayuki, Przemek, James, Bart, Will, Michael, Pernille, Steffen and Lorel. The lab chats, coffee breaks and 'the market' have been a great distraction from challenging chemistry, thank you to all of you. A special thanks must go to my dedicated proofreaders: Lauren, Przemek, Steffen, James and Harry for their hours of patient corrections.

Finally, I would like to thank those most special to me. To my family, thank you for for your love and support. I am incredibly grateful. Lastly, to Lauren. You have helped me finish this DPhil and made these three years the most unforgettable of my life.

Contents

List of Abbreviations iii

1. Introduction 1

1.1. Carbon allotropes and carbon-rich compounds 2

1.2. Cyclo[*n*]carbons 7

1.2.1. Theoretical studies of cyclo[*n*]carbons 7

1.2.2. Synthetic attempts towards cyclo[*s*]carbons 10

1.3. Stabilisation of acetylenic carbons 13

1.4. References 23

2. Porphyrin-polyyne [3]- and [5]rotaxanes 27

2.1. Introduction 28

2.2. Synthesis of polyynes 30

2.3. Attempted synthesis of porphyrin-polyyne [5]rotaxane P5Ra 32

2.4. Synthesis of porphyrin-polyyne [5]rotaxane P5Rb 41

2.5. Photophysical studies 44

2.5.1. Absorption and emission spectra 45

2.5.2. Absorption and excitation spectra 48

2.5.3. Methodology for determining EET, absorption spectra 49

2.5.4. Methodology for determining EET, excitaton spectra 52

2.6. Conclusions 55

2.7. Experimental data for known compounds 57

2.8. Experimental data for novel compounds 64

2.9. References 77

3. Synthesis of polyynes using dicobalt masking groups 79

3.1. Introduction 80

3.2. Synthesis of dicobalt and tetracobalt complexes 82

3.3. Unmasking polyynes from cobalt complexes 87

3.4. Attempted rotaxane synthesis 89

3.5. Reactivity of terminal acetylene 92

3.6. Electronic absorption spectra and molecular orbitals 95

3.7. Crystallography 100

3.8. Conclusions 104

3.9. Experimental data for known compounds 105
3.10. Experimental data for novel compounds 110
3.11. References 118

4. Dibromoolefin rotaxanes **121**
4.1. Introduction 122
4.2. Synthesis of macrocycles 124
4.3. Synthesis of TIPS-D1 and rotaxane formation 128
4.4. Synthesis of TIPS-D2 and rotaxane formation 133
4.5. Attempted synthesis of catenanes 134
4.6. Template-directed approaches towards dibromoolefin catenanes 137
4.7. Conclusions 140
4.8. Experimental data for known compounds 141
4.9. Experimental data for novel compounds 148
4.10. References 161

5. Preparing polyynes on surfaces **163**
5.1. Introduction 164
5.2. Synthesis of linear dibromoolefins 169
5.3. Crystallography 173
5.4. Generation and imaging of polyynes from dibromoolefins 176
5.5. Synthesis of linear dichloroolefins 181
5.6. Conclusions 183
5.7. Experimental data for known compounds 184
5.8. Experimental data for novel compounds 192
5.9. References 194

6. Conclusions and future work **197**
6.1. Conclusions 198
6.2. Future Work 199
6.3. References 203

List of abbreviations and symbols

Å – Angstroms
δ – Chemical shift
ε – Molar absorption coefficient
λ – Wavelength
μ – Micro
Θ – Angle
aq – Aqueous
AFM – Atomic force microscopy
Ar – Aryl
BLA – Bond length alternation
Bu – Butyl
CCDC – Cambridge crystallographic data centre
cm – Centimetre(s)
d – Doublet
DDQ – 2,3-dichloro-5,6-dicyano-*para*-benzoquinone
DFT – Density functional theory
DMF – N,N,dimethylformamide
DMSO – dimethylsulfoxide
DPM – Dipyromethane
EI MS – Electron impact mass spectrometry
ESI – Electrospray ionisation
Et – Ethyl
EtOAc – Ethyl acetate
Eq. – Equivalent(s)
EET – Excited state energy transfer
FBW – Fritsch-Buttenberg-Wiechell
FTIR – Fourier transform infra red
FVP – Flash vacuum pyrolysis
g – Grams
GPC – Gel permeation chromatography
h – Hours
HOMO – Highest occupied molecular orbital
HRMS – High resolution mass spectrometry
Hz – Hertz
i – Iso
IC – Internal conversion
IET – Inelastic electron transfer
ISC – Intersystem crossing
J – Coupling constrant
L – Litre
LDA – Lithium diisopropylamine
LUMO – Lowest unoccupied molecular orbital
m – Multiplet
M – Molar
MALDI – Matrix-assisted laser desorption ionisation
Me – Methyl
mg – Milligram(s)
MHz – Megahertz
MM – Molecular mechanics
n-BuLi – n-butyl lithium
NBS – N-bromosuccinimide
NIR – Near-infrared
Nm – Nanometre(s)
NMR – Nuclear magnetic resonance

NOE – Nuclear Overhauser effect
ns – Nanosecond
p – Para
PCC – Pyridinium chlorochromate
Ph – Phenyl
ppm – Parts per million
Py – Pyridine
q – quartet
quin – quintet
R_f – Retention factor
SEC – Size exclusion chromatography
STM – Scanning tunnelling microscopy
STS – Scanning tunnelling spectroscopy
t – Triplet
t – Tertiary
TBAF – Tetrabutylammonium fluoride
TFA – Trifluoroacetic acid
THF – Tetrahydrofuran
TIPS – Triisopropylsilyl
TLC – Thin layer chromatography
TMEDA –tetramethylethylenediamine
TMS – Trimethylsilyl
TOF – Time of flight
tol – Tolyl
Tr* – [tris(3,5-di-*t*-butylphenyl)methyl]
UV – Ultraviolet
UV-vis – Ultraviolet-visible
w – Weak

Chapter 1

Introduction

1.1. Carbon allotropes and carbon-rich compounds 2

1.2. Cyclo[*n*]carbons 7

1.2.1. Theoretical studies of cyclo[*n*]carbons 7

1.2.2. Synthetic attempts towards cyclo[*n*]carbons 10

1.3. Stabilisation of acetylenic carbons 13

1.4. References 23

Chapter 1 – Introduction

1.1– Carbon allotropes and carbon-rich compounds

Carbon is the foundation of life on Earth. We live in a carbon-based world and as we master this humble atom its importance only grows. Carbon's unique significance is a consequence of its physical properties and chemical behaviour. It has astonishing bonding diversity due to the four valence electrons located in its outer shell. Global research efforts guarantee that the prominence of carbonaceous materials will only increase[1–4]; forthcoming materials have the potential to push the limits of conductivity, stiffness and thermal stability. Researchers have accomplished impressive natural product syntheses[5] and are approaching atomic control of surface reactivity.[6] Yet, there are structurally simple, theoretical allotropes of carbon that continue to elude us.[7]

Graphite and diamond are allotropes of carbon that are abundant due to their high stability.[8,9] These carbon allotropes have many applications: graphite (sp^2) is strongly conductive and self-lubricating and diamond (sp^3) is the hardest known natural material. Theoretically, it is possible to form multiple networks and structures of *sp*, sp^2 and sp^3 carbon atoms in less thermodynamically stable ways.[1,10] Diamond and graphite were the only known carbon allotropes until 1985. Since then, there have been many discoveries of new sp^2-based carbon allotropes with extraordinary and useful properties (**Figure 1.1** i,ii,iii). Researchers are beginning to discover and develop a vast range of applications for these revolutionary carbonaceous materials.

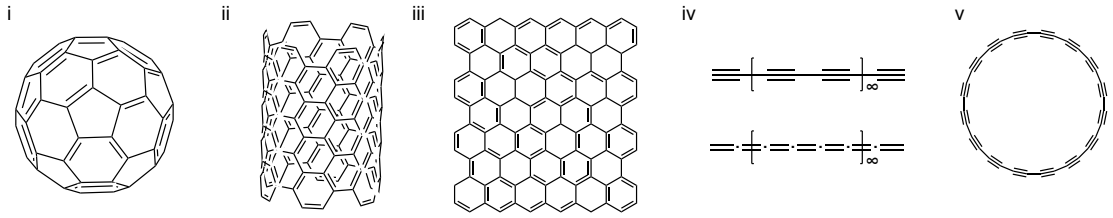

Figure 1.1. New carbon allotropes: i) fullerene C_{60} (1985)[11], ii) (6,6) armchair single-walled carbon nanotube (1993).[12] iii) graphene sheet (2004).[13] iv) carbyne v) cyclo[32]carbon.

In 1985, in a seminal paper, Kroto *et al.* initiated the 'new allotrope revolution' by discovering a C_{60} cluster.[11] The authors vaporised carbon from graphite, using laser irradiation, expanded by a molecular beam and detected C_{60} *via* time-of-flight mass

spectrometry. Careful tuning of clustering conditions optimised the clustering to favour C_{60} formation. However, it was not until 1990 that fullerenes could be prepared in macroscopic quantities after a pivotal publication from Huffman and coworkers.[14] This led to the realisation that chemical functionalisation was the key to unlocking the potential of fullerenes. Functional groups can solubilise fullerenes and work cooperatively with their extraordinary properties. To date, fullerenes have applications as electron acceptors in photovoltaic devices,[15] liquid crystals,[16] HIV drugs[17] and superconductors,[18] amongst others.

The concept of nanotubes made from carbon long predated their isolation. In 1889 a patent proposed the idea of growing carbon filaments by methane deposition. However, it was over 100 years until the first single walled carbon nanotube was prepared by Iijima *et al.* in 1993.[12] Carbon nanotubes are tubular networks of sp^2 carbons that are defined by their length:width ratio. Their lengths can reach the millimetre magnitude or above, despite having a diameter of only one or two nanometres. Carbon nanotubes are generally prepared *via* chemical-vapour deposition methods. Depending on the preparation conditions, either single-walled (SWCNTs) or multi-walled carbon nanotubes (MWCNTs) are obtained. However, modern synthetic approaches are concentrated on the greater level of control that is promised by bottom-up synthetic methods (**Figure 1.2**).[19–21]

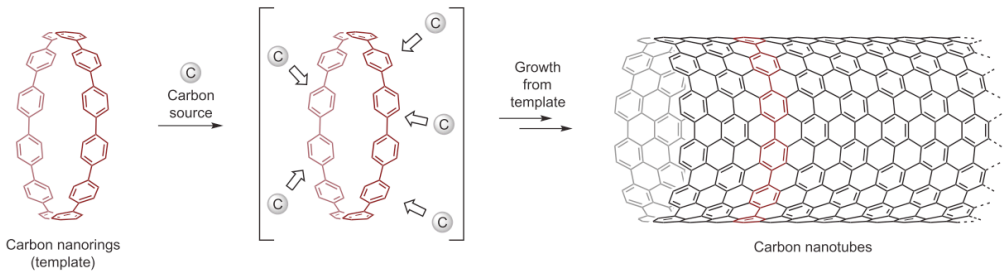

Figure 1.2. A'growth-from-template' strategy for the bottom-up synthesis of structurally uniform CNTs. General strategy for CNT growth using a carbon nanoring as a template. Cycloparaphenylene (CPP) is shown as an example. Figure adapted from reference 19 with permission from Nature Publishing Group.

The most recently discovered allotrope of carbon is graphene, which is a single sheet of graphite.[13] In 2004, single layers of graphene were removed from graphite *via* mechanical exfoliation with Scotch tape and were manufactured into field-effect

transistors. The discovery and subsequent characterisation of graphene was awarded the 2010 Nobel Prize in Physics (Konstanti Novoselov and Andre Geim). Since then, the field has exploded and over 20,000 articles have been published in peer-reviewed journals. Graphene can be prepared in many different ways, including liquid exfoliation,[22,23] chemical vapour deposition,[24] intercalative expansion of graphite,[25] thermal annealing of SiC[26] and bottom up methods.[27]

Meanwhile, there have been spurious claims that *sp* carbon allotropes exist in interstellar dust and meteorites.[28] However, carbon allotropes built exclusively from *sp* carbon atoms (carbyne and cyclo[*n*]carbons) have never been isolated by researchers, despite evidence of gas-phase formation (**Figure 1.1** iv, v).[29–31] There are many unanswered questions about these furtive allotropes, particularly concerning the ground state structure of carbyne and cyclo[*n*]carbons, which could be polyynic (alternating triple and single bonds) or cumulenic (consecutive double bonds). Investigating the fundamental properties of *sp* carbon allotropes is not only of academic interest but is of pressing practical importance; band structure, most notably the band gap, strongly depends on the bond length alternation (BLA). The potential use of these allotropes in molecular electronics hinges on these electronic properties, for example, in novel field-effect transistors or molecular wires.[32,33] Additionally, linear carbon is expected to possess intriguing physical properties, including exceptionally high tensile strength and Young's modulus (due to its directional strong bonding), making it very interesting for niche mechanical applications.[32]

Pioneering research from over 50 years ago yielded our first insights into the nature of carbyne by preparing short acetylenic oligomers.[34,35] Thereafter, synthetic developments and enlargement of bulky stopper groups progressively delivered longer polyynes (**Figure 1.3**). The extrapolation of trends was used to gain some insight into carbyne in later efforts.[36–38] In 2010, Tykwinski and coworkers synthesised the longest known polyyne, containing 44 *sp*-carbon atoms capped on both ends with bulky tris(3,5-di-*t*-butylphenyl)methyl (known as supertrityl) groups (**Figure 1.3**).[2] At this limit (44 *sp* carbons), the stoppers reach the limit of their ability to stabilise the *sp*-carbon chain, as they are a large distance from the centre of the

chain. An alternative source of protection that could shield the full length of the chain would allow even longer chains to be stabilised.

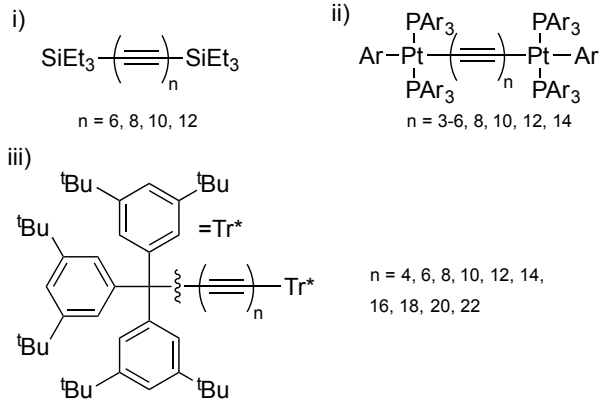

Figure 1.3. Synthetic approaches to long polyynes: i) Triethylsilyl polyynes (1972).[36] ii) Platinum capped polyynes (2006).[38] iii) Supertrityl polyynes (2010).[2]

In 2010, Tykwinski and coworkers predicted properties of carbyne with far more reliability than previous studies due to the length of the synthesised polyynes.[2] Crystal structures of long polyynes maintained BLA and implied carbyne would possess polyynic character. Additionally, a persistent HOMO-LUMO gap was deduced based on the absorption trends of the series of long polyynes. A similar analysis on curved π-systems would provide an extremely interesting comparison, to determine if aromaticity affects the bond length alternation and HOMO-LUMO gap. Although carbon allotropes represent the most celebrated examples of carbon-rich materials, there are many other materials that exhibit similar properties. The acetylene motif plays an essential role in bottom-up synthesis of these materials. Indeed, the development of acetylene chemistry and exploration of synthetic methods has led to an enormous variety of *sp* carbon-based compounds in the last 25 years.[39–42]

Bottom-up synthesis of carbon-rich networks and cage-like structures is desirable - particularly if it could lead directly to new carbon allotropes. It was long believed that carbon allotropes and networks would undergo facile conversion to the more thermodynamically stable diamond or graphite.[7] However, the isolation of fullerenes, nanotubes and graphene demonstrates that high kinetic inertness can inhibit thermodynamic equilibration. If there is no facile mechanism for interconversion to a more stable allotrope it is reasonable to assume thermodynamically unstable carbonaceous compounds could be long-lived. Hence, small acetylene building blocks have been synthesised to prepare acetylenic networks and scaffolds in one, two and

three dimensions.[43] 1,2-Diethynylethenes (DEEs)[44], geminal diethynylethenes,[45] 1,4 tetraethynylethenes (TEEs)[46] and tetraethynylmethane (TEM)[47] have all been utilised to prepare well-defined carbonaceous molecular architectures and advanced materials **(Figure 1.4).**

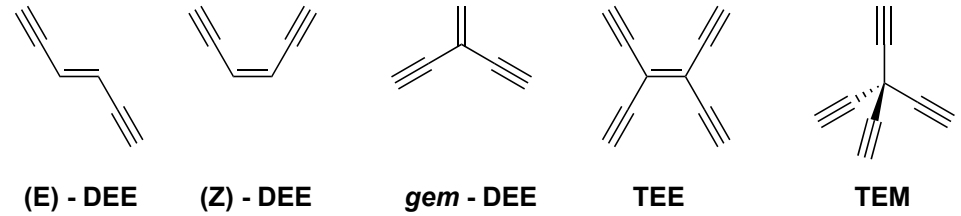

Figure 1.4. Carbon rich acetylenic building blocks.

Researchers had been attempting to prepare TEM for many years for use as a precursor to three-dimensional carbon networks. In 1993, it was successfully synthesised *via* a ten-step synthesis.[47] It was believed that networks formed from TEM may self-assemble more effectively than other acetylenic building blocks because oligomerisetion of tetraethynylmethane to yield two-dimensional 'graphitic' sheets would not be possible on energetic grounds (**Scheme 1.1**).

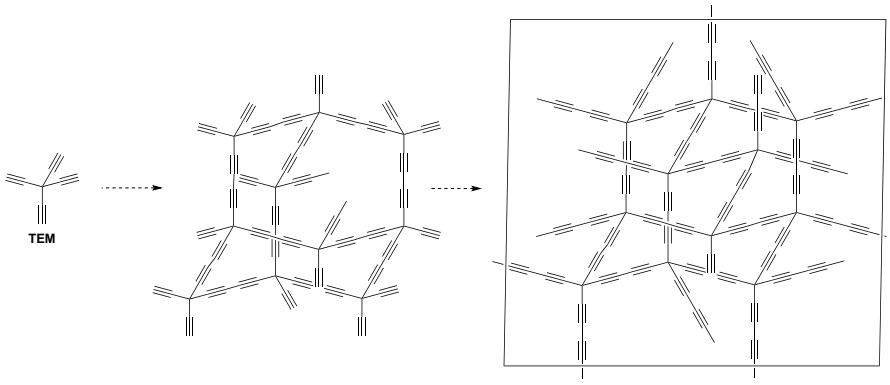

Scheme 1.1. Hypothesised formation of a superdiamond network *via* hexadecaethynyladamantane from TEM.[7]

One important category of carbon-rich materials are the [*n*]annulenes. [*n*]Annulenes are fully conjugated cyclic polyenes and their ring size is indicated by a number in brackets. Similarly, dehydroannulenes possess some triple bonds in place of double bonds and benzannulenes feature a phenyl ring that is fused into the annulene system. Dehydroannulenes and benzannulenes have potential applications as optoelectronic,[48] electrochromic,[49] liquid-crystalline,[50] and sensing materials.[51] Sondheimer and coworkers were pioneers in the aforementioned field and made many contributions to the scope of carbon-rich macrocycles using acetylenic coupling as a powerful bond-

forming technique.[44,52] One of the most noteworthy examples was the preparation of dodecadehydro[18]annulene **1.1** (**Scheme 1.2**). [n]Annulenes have played a very important role in synthetic approaches to cyclo[*n*]carbons (**Section 1.2.2**).

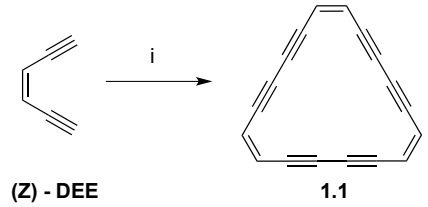

Scheme 1.2. – Synthesis of dodecadehydro[18]annulene **1.1**.[44] i) $Cu(OAc)_2$, pyridine, 20%.

Another important family of carbon-rich molecules are radialenes, a series of cycloalkanes containing exocyclic cross-conjugated double bonds with a general molecular formula of C_nH_n. It is possible to insert ethynediyl or buta-1,3-diynediyl moieties into the cyclic framework to make two carbon-rich analogous series of expanded radialenes (with the molecular formulas $C_{2n}H_n$ and $C_{3n}H_n$, respectively) (**Figure 1.5**). Geminal diethynylethene (***gem* – DEE**) is a precursor for these aforementioned carbon-rich radialenes. Carbon-rich radialenes themselves are precursors towards cyclo[*n*]carbons if used with an appropriate removable group (**Section 1.2.2**).

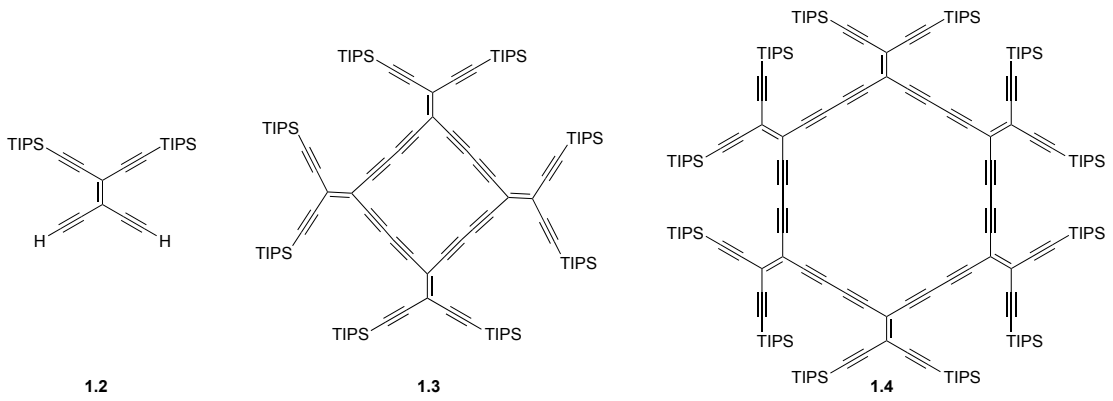

Figure 1.5. *gem* – DEE starting material and expanded radialene products **1.3** and **1.4**.[53]

1.2 – Cyclo[*n*]carbons

1.2.1 – Theoretical studies of cyclo[*n*]carbons

In 1966, Hoffman theorised that some cyclo[*n*]carbons such as cyclo[18]carbon would benefit from additional stabilisation compared to their linear analogues as a result of two orthogonal (4n+2) π-electrons.[54] Cyclo[*n*]carbons, or 'cyclocarbons' are monocyclic molecules composed of *sp*-hybridised carbon atoms (**Figure 1.6**). Like [*n*]annulenes, *n* defines the number of carbon atoms that are connected to form the

monocyclic structure. Early theoretical approaches using extended Hückel[54] and semi-empirical MNDO[55] calculations predicted an energetic preference for a cyclic structure of C_{18} over a linear one.

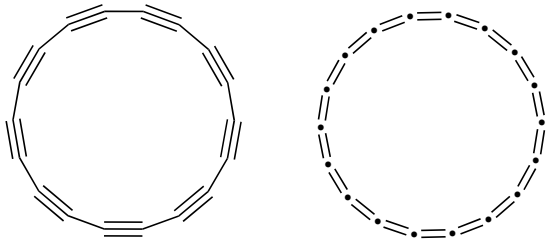

Figure 1.6. Possible ground state geometries of cyclo[18]carbons.

Most recent calculations suggest that, analogously to polyacetylene, infinite linear carbon is expected to experience a 'Peierls distortion'. Therefore, a polyynic structure with BLA would be favoured over a cumulenic structure. A Peierls distortion is a distortion of the periodic lattice of a one-dimensional crystal; atomic positions oscillate, hence the perfect order of the 1-D crystal is broken to lower the overall energy of the system.

The amount of BLA that is predicted is highly dependent on the computational method used. The Hartree-Fock (HF) method predicts a large BLA of approximately 20 pm.[56] However, generalised gradient (GGA) approximated density functional theory (DFT) calculations result in BLA of approximately 2-4 pm.[57] These results illustrate the tendency of HF methods to localise bonds and the tendency of GGA density functionals to generate more electronically delocalised structures.[58] It is important to note that although cyclocarbons serve as models for infinite length carbyne, the different magnitude of length between them has a pronounced effect.

In 2014, Neiss *et al.* published a more detailed study on cyclocarbons at a higher level of theory. This study considered BLA in different length regimes and the effect of vibrational modes.[58] The authors modelled cyclocarbons within periodic boundary conditions with N_k units. Each N_k unit contained two carbon atoms to allow for two separate bond lengths, so the BLA could be studied. This approximation should give identical results to a ring of $2N_k$ carbon atoms if the effect of curvature of the ring can

be disregarded. This experiment resulted in a fascinating observation of the effect of aromaticity on BLA (**Figure 1.7**).

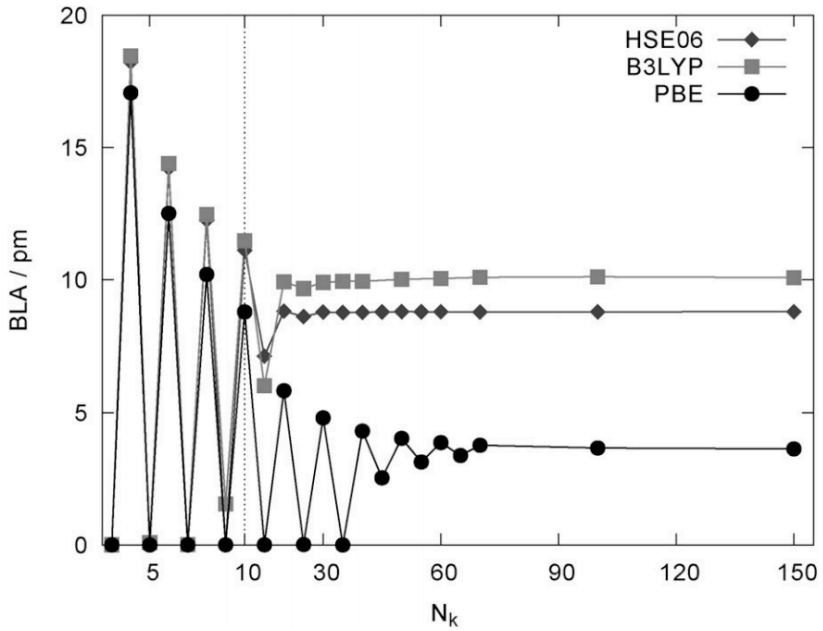

Figure 1.7. Bond length alternation (BLA) for different numbers N_k of unit cells (with two carbon atoms each). The scale on the abscissa changes at N_k=10 as indicated by the dotted line. All values are taken at the equilibrium geometries. Figure from reference 58 with permission from Wiley Publishing Group.

Figure 1.7 demonstrates that all three functionals exhibit the same trends upon first inspection. The GGA functional PBE[59] exhibits the behaviour most prominently: cyclocarbons with odd 'N_k' numbers, describing rings with (4n+2) carbon atoms, exhibit no BLA, whereas cyclocarbons with even 'N_k' numbers, describing rings with 4n carbon atoms, exhibit a strong alternation pattern. For $35<N_k<80$ (70–160 atoms) BLA occurs in all cases but its magnitude oscillates depending on whether N_k is even or odd. Finally, for $80<N_k$ (greater than 160 atoms) the BLA assumes an almost constant value that is independent of even or odd values of N_k.

BLA in small rings is dominated by the effect of aromaticity. Following Huckel's rule, rings with (4n+2) carbon atoms are aromatic and do not exhibit BLA. Whereas, antiaromatic rings of 4n atoms do exhibit BLA. Surprisingly, even in the aromatic systems, the driving force for a Peierls distortion is present but is too weak to result in an observed BLA. However, as the ring size increases the effect of aromaticity wanes. In the range $35<N_k<80$ there are a large number of π-levels and there are

always electrons close to the Fermi level that can strongly interact upon Peierls distortion. In this intermediate regime, BLA always occurs because the driving force for Peierls distortion is sufficiently strong, but its magnitude oscillates depending on whether the ring contains (4n+2) or 4n atoms. As the ring increases in size, this effect is enhanced further until total independence from number of electrons is achieved; this is the Peierls regime.

To further complicate this picture, zero BLA structures were also predicted throughout when the calculations were made more complex by factoring in zero point vibrations. This discrepancy highlights the challenges that face chemists when the molecule is still entirely theoretical. The presence or absence of BLA has enormous implications for the electronic properties of cyclocarbons. The successful isolation of cyclocarbons would allow these unanswered questions to finally be resolved. Additionally, the information obtained could be used for parameterising future computational studies and making predictions with a higher degree of confidence.

1.2.2 – Synthetic attempts towards cyclo[*n*]carbons

We are not the first group of organic chemists to study the cyclo[*n*]carbons; there have been multiple synthetic endeavours towards cyclo[*n*]carbons of various sizes. Until now, all known synthetic routes utilised dehydroannulene derivatives or extended radialenes as direct precursors to the final cyclocarbon (**Scheme 1.3**). These synthetic strategies used a variety of masked alkyne equivalent (MAE) groups that possessed facile methods for extrusion of the desired alkyne-containing cyclocarbon. Many of these MAEs yield the alkyne after a cycloreversion. However, one MAE designed by Tobe and coworkers (**1.10-1.13**) utilised a vinylidene-acetylene rearrangement.

In their groundbreaking work in 1989, just before the isolation of C_{60}, Diederich and coworkers kickstarted efforts at synthesising and isolating cyclocarbons. Their synthetic route used dodecahydro[18]annulene **1.4** as a precursor towards cyclo[18]carbon.[29] This unusually stable dehydroannulene contained three dibenzobicyclo[2.2.2]octatriene groups as MAEs (**Scheme 1.3**). The anticipated

elimination of three anthracene molecules, *via* [4 + 2] cycloreversion to release cyclo[18]carbon, was unsuccessful and the desired cyclo[18]carbon was only observed in the gas phase in laser-desorption time-of-flight (LD–TOF) mass spectra after flash heating to 800 K. Unfortunately, flash vacuum pyrolysis (FVP) of dehydroannulene **1.4** only yielded anthracene and polymeric material. Cyclo[18]carbon was highly reactive and either polymerised or formed C_{60} clusters.

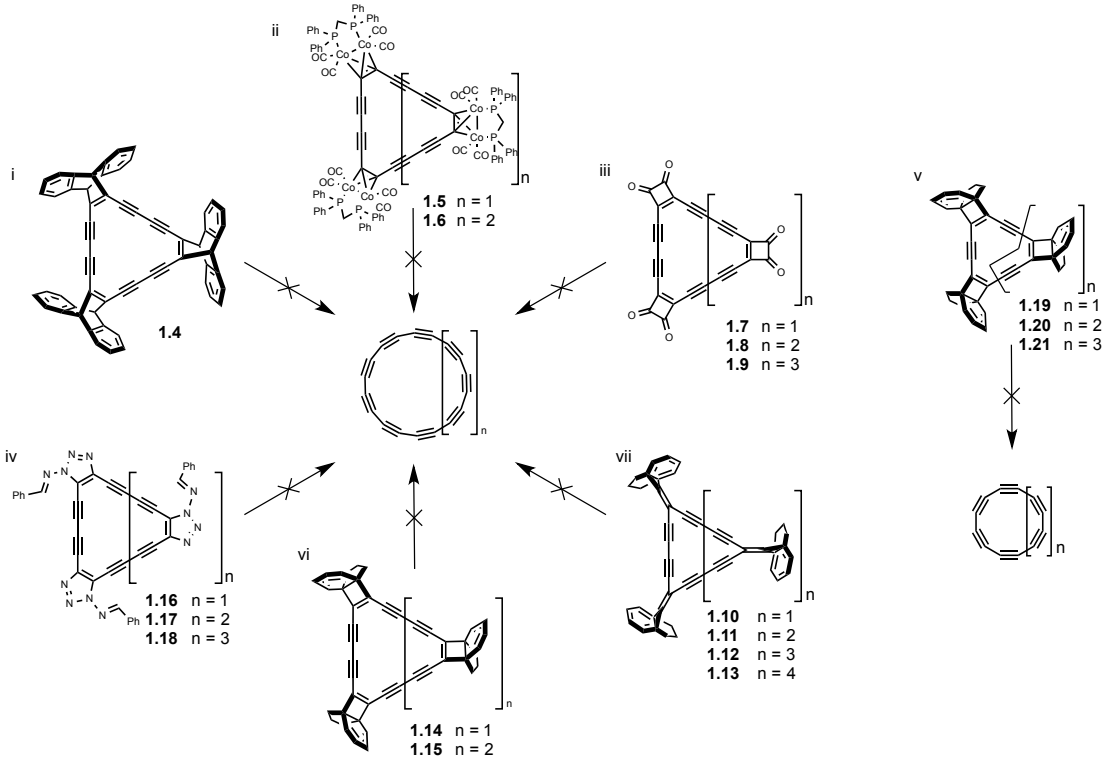

Scheme 1.3. Synthetic attempts towards cyclo[n]carbons. i) Diederich and coworkers (1989)[29]. ii) Diederich and coworkers (1990)[60]. iii) Diederich and coworkers (1989-1991)[29,31,61]. iv) Rees and coworkers (1996)[62]. v, vi) Tobe and coworkers (1994-2000)[63–65] vii) Tobe and coworkers (2003).[66]

Diederich and coworkers also prepared stable cobalt complexes of cyclocarbons, **1.5** and **1.6**.[60] These complexes showed excellent stability and were characterised *via* X-ray crystallography. The oxidative decomplexation of these complexes should have yielded unmasked cyclocarbons. However, no suitable conditions were found to successfully remove the dicobalt MAE. This precursor was of interest to us as conditions for removing the dicobalt MAE had been described since the original publication (**Chapter 3)**.[67]

In Diederich and coworkers' most recent attempt at preparing cyclocarbons, cyclobutadienone served as the MAE (**1.7–1.9)**.[30,61] The reactive conjugated ketones

required masking as ketal groups and subsequent unmasking in order to prepare the desired dehydroannulenes. All intermediates, formed after successive decarbonylations, together with the desired cyclocarbons, were detected in the gas phase. However, once again, the isolation of cyclocarbons could not be achieved.
Importantly, in the cyclobutadienone examples, C_{60}^+ and C_{70}^+ ions were observed in the mass spectra, suggesting these cyclocarbons could be intermediates in fullerene formation. Previously, cyclocarbons have been proposed as precursors to many carbon-rich structures.[68] Additional evidence for the production of cyclo[l8]carbon was also obtained upon irradiation of the precursor **1.7** at a suitable wavelength (>338 nm) to induce the removal of the alkyne masking groups in a low temperature glass.[40] Under continued irradiation, IR detection showed the disappearance of a carbonyl band in the starting material and the appearance of a ketene band. Further irradiation at a different wavelength (>280 nm) revealed the disappearance of the ketene band and appearance of a carbon monoxide band. The cyclo[18]carbon is expected to only show weak IR absorption due to its high symmetry and lack of polar groups, so the failure to directly observe it is not unexpected.

In 1994, Tobe and coworkers developed the [2 + 2] cycloreversion of [4.3.2]propella-1,3,11-trienes as a convenient method of polyyne synthesis.[63] Later, they recognised the wider utility of this rearrangement and synthesised the analogous dehydroannulenes as cyclocarbon precursors (**Scheme 1.3**, **1.14-1.15** and **1.19-1.21**).[64,65,69] This MAE was the first that could be extruded by irradiation with UV light; UV irradiation has the potential to be milder than reagents or extreme heating and is promising for isolation of an unstable cyclocarbon. However, similarly to previous attempts, the desired cyclocarbons could only be detected in LD–TOF mass spectrometry. Isolation was not possible.

In 1996, Rees and coworkers applied the 1-amino-1,2,3-triazole moiety as a MAE.[62] Their rationale for using this group was the extremely mild deprotection conditions ($Pb(OAc)_4$, CH_2Cl_2, -78 °C) that could liberate the cyclocarbon with little chance of other side reactions occurring. However, all attempts to unveil the cyclocarbons from aminotriazole-substituted dehydroannulenes **1.16-1.18** were unsuccessful.

Finally, Tobe and coworkers tried a different route. In 2003, they reported a novel approach based on the chelotropic fragmentation of radialenes.[66] These radialenes were composed of bicyclo[4.3.1]deca-1,3,5-triene derivatives, which were shown to yield polyynes upon irradiation with UV light in a model system (**Scheme 1.4**). Expanded [3]-, [4]-, [5]-, and [6]radialenes with exocyclic bicyclo[4.3.1]decatrienes **1.10-1.13** were prepared as precursors for cyclocarbons. LD–TOF mass spectra of radialenes **1.10-1.13** gave peaks of the desired cyclocarbons, but once again isolation was not possible.

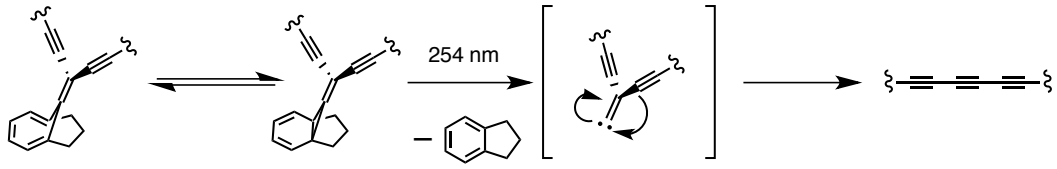

Scheme 1.4. UV irradiation of bicyclo[4.3.1]deca-1,3,5-triene derivatives yields polyynes.[63]

Ultimately, these comprehensive studies demonstrate that synthesis of pristine cyclocarbons is extremely difficult and potentially impossible. It is conceivable that many of these syntheses yielded cyclocarbons. However, they participated in subsequent reactions so quickly that it was impossible to identify them. Conceptually, we believe that another approach is required in order to isolate these elusive molecules and probe their properties. The exciting developments in supramolecular and surface chemistry that have occurred since the 'golden age' of cyclocarbon synthesis open new avenues to finally isolate and study the mysterious cyclocarbons.

1.3 – Stabilisation of acetylenic carbons

Conjugated acetylenic materials have attracted great interest for a variety of applications (**Section 1.1**). However, these highly unsaturated compounds are often unstable, particularly in concentrated solutions, because they have a tendency to polymerise. This is particularly common in polyynes. Polymerisation can be prevented by bulky substituents, but there are other methods of stabilisation that could permit a linear *sp* carbon chain to remain completely intact without functionalisation. In 1994, mechanical insulation was proposed as an alternative method of protecting fragile chains of *sp*-hybridised carbons.[7] Threading chains inside macrocycles to form rotaxanes or pseudorotaxanes could prevent them from adopting the required close-contact conformation for polymerisation.[70] It was periodically acknowledged by a

range of chemists that topological protection could provide additional stabilisation of polyynes[71,72] and conclusively proved in our group in 2016.[73]

Crucially, in mechanically locked architectures, molecules are linked together through their topology, rather than a covalent bond, and this kind of link is often referred to as a "mechanical bond".[74,75] The mechanical bond is defined in *The Nature of the Mechanical Bond: From Molecules to Machines* as 'an entanglement in space between two or more molecular entities (component parts) such that they cannot be separated without breaking or distorting chemical bonds between atoms'.[76] The mechanical bond and the molecular machines that were subsequently developed were awarded the Nobel Prize in Chemistry in 2016. A catenane is a molecule that consists of two or more interlocked ring components. The rotaxane is another type of interlinked structure that consists of a macrocycle threaded on a linear axle or 'dumbbell', with stoppers that prevent it from unthreading (**Figure 1.8**).

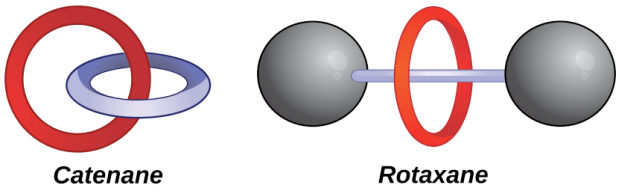

Figure 1.8. Mechanically interlocked architectures. Figure from reference 76 with permission from Wiley and Sons Publishing Group.

Rotaxanes can be synthesised *via* two general approaches which each contain significant diversity: statistical synthesis and template directed synthesis. The first reported synthesis of a rotaxane was performed in 1967 by Harrison *et al.*[77] and relied on the probability that if two halves of a dumbbell-shaped molecule reacted in the presence of a macrocycle, a small percentage of the reaction would take place directly through the ring (**Scheme 1.5**). The macrocycle was attached to a solid-phase support **1.22** and treated with both halves of the dumbbell 70 times in order to obtain a reasonable quantity of the rotaxane. Despite this monumental effort, when removed from the support, the yield of rotaxane **1.23** was only 6%. Since this report, the synthesis of rotaxanes has progressed considerably and excellent yields can be obtained by preorganising components using hydrogen bonding,[78,79] anions,[80,81] hydrophobic forces[82] and most importantly for our purposes, metal coordination.

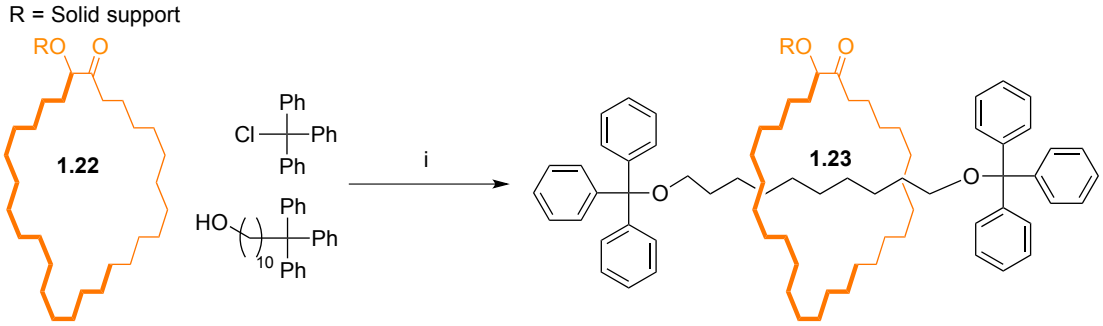

Scheme 1.5. The first example of statistical rotaxane synthesis. i) Pyridine, DMF, toluene, 6%.[77]

Metal-templated rotaxane synthesis can be categorised into two approaches which each have wide-ranging applications: passive-metal template (PMT) synthesis and the more recently discovered active-metal template (AMT) synthesis.[83] Early examples of metal coordination rotaxane synthesis utilised passive-metal template synthesis, while more recent rotaxane syntheses often use active-metal template synthesis. PMT synthesis was first envisaged to synthesise catenanes and was reported in a formative paper by the Nobel Prize-winning Jean-Pierre Sauvage in 1983.[84] He recognised that the shape and orthogonal arrangement of bidentate ligands in a tetrahedral Cu(I) complex **1.25** could generate the desired geometry and necessary cross-over points for catenane formation (**Scheme 1.6**). The subsequent ether formation generated the [2]catenane copper complex **1.26** in 27% yield. This represented an astounding breakthrough given that the statistical and directed catenane synthesis routes of the period typically took 6–20 steps to complete and frequently resulted in a less than 1% overall yield of the interlocked product. Critically, this approach comprised of two independent steps: (i) coordination of the ligands to the metal (passive-metal templating) (ii) covalent capture.

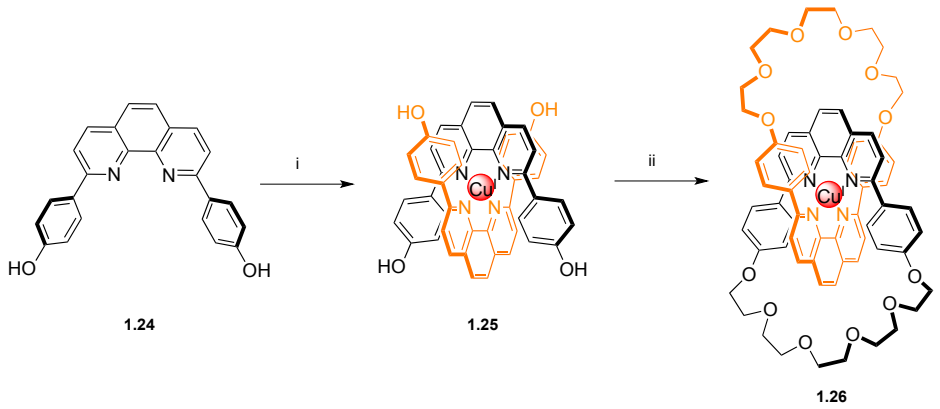

Scheme 1.6. The first example of metal-templated catenane synthesis. i) $Cu(CH_3CN)_4$ ii) 1,14-diiodo-3,6,9,12-tetraoxatetradecane, Cs_2CO_3, DMF, 27%.[84]

Since these revolutionary results a number of other PMT systems have been established, spanning octahedral,[85,86] square planar[87,88] and linear[89] metal coordination sites. All PMT systems have two shared features: (i) permanent coordination sites on each of the components are necessary to assemble the structure and (ii) they require a stoichiometric quantity of the metal template as a minimum.[90] The same two-step strategy has also been utilised to synthesise other interlocked molecules: knots and links,[91–93] molecular shuttles[94] and most crucially for our purposes, rotaxanes.[95,96] The coordination geometries of transition metals are well understood and can be used with ingenious molecular design for exquisite control of self-assembly. One of the most impressive examples of rational design was Leigh and coworkers' molecular knot with eight crossings **1.30**, which was systematically assembled by the octahedral passive-metal template effect of a Fe(II) ion and a well-designed precursor (**Scheme 1.7**).[93]

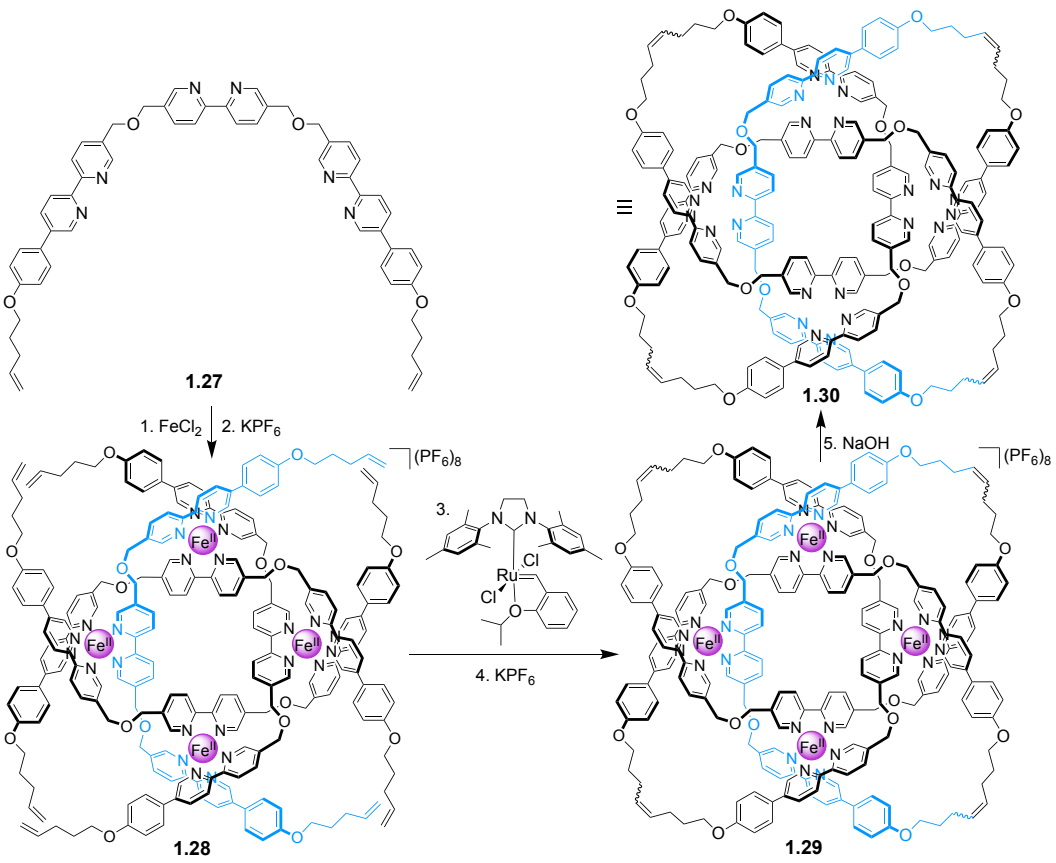

Scheme 1.7. Synthesis of 8 crossing molecular knot using passive-metal template synthesis. Reaction conditions: (1) 1 (1.0 equiv.), $FeCl_2$ (1.0 equiv.), DMF, 130 °C, 24 h; (2) KPF_6, MeOH, 60% (two steps); (3) Hoveyda-Grubbs second-generation catalyst (25 mol % per olefin metathesis reaction), $MeNO_2$/1,2-dichloroethane 1:1, 60°C, 24 hours; (4) KPF_6, H_2O, 62% (two steps); (5) NaOH (aq) (1 M)/MeCN 1:1, 70 °C, 30 min, 38%. Figure adapted with permission from reference 93 with permission from the Science publishing group.

Despite these impressive achievements, PMT synthesis does not fully utilise the properties of the metal itself. Rather, passive-metal template methods merely use the metal as a molecular adhesive to hold the reactive parts of molecules together in a desired orientation to favour interlocking. Building on the strategy of transition metal catalysis, a new approach was forged by Leigh and coworkers in 2006 where the metal template ions could play an additional active role in promoting the decisive, concluding covalent bond forming reaction.[97] In this case - 'active metal template synthesis' - the metal has a twofold function, acting as a template for interweaving the precursors and also catalysing the essential covalent bond formation between the reactants (**Figure 1.9**).

Figure 1.9. General scheme illustrating the principle of active-metal template synthesis. Bond formation between blue and green dumbbell units to generate the rotaxane is catalysed by a metal (shown in red) and orientated through the the macrocycle's cavity (shown in orange) by the metal's coordination requirements.

In 2006, the first example of an active-metal template alkyne coupling was performed by Saito and coworkers, by synthesising [2]rotaxanes *via* a copper catalysed Glaser coupling through a macrocyclic Cu(I)-phenanthroline complex.[98] The catalytic site was located inside the macrocycle **1.32** so that the rotaxane **1.33** could be efficiently formed and only a small excess of the substrate was required for the synthesis of the rotaxane in a good yield of 72% (**Scheme 1.8**).

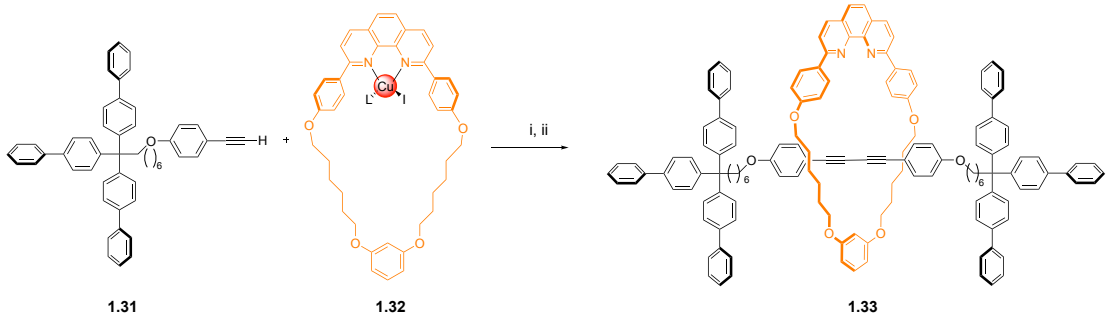

Scheme 1.8. Saito's [2]rotaxane synthesis. i) K_2CO_3, I_2, toluene, 110 °C, 48 h, 72%. ii) KCN (aq), CH_2Cl_2, MeCN.[98]

Analogously to polyyne synthesis, the use of palladium as the catalyst for alkyne–alkyne bond formation can be used in rotaxane preparation. AMT synthesis has the potential to execute catalytic metal couplings. This was first reported by the Leigh group in 2007, who described Pd(II) catalyzed homocoupling of alkynes using catalytic amounts of the active-template metal ion using relatively mild conditions (**Scheme 1.9**).[99] Conditions which employ 5-10 mol% of Pd(II) and iodine to oxidise Pd(0) back to Pd(II) resulted in higher yields of [2]rotaxane **1.41** compared to the stoichiometric reaction. According to the proposed reaction mechanism, transmetallation takes place between copper-acetylide complex **1.36** and macrocycle-Pd(II) complex **1.35**. A concerted trans–cis isomerisation in which the ligands do not detach from the Pd^{II} centre maintains the geometry. This allows for C-C bond formation by reductive elimination of *cis*-complex **1.39**, forming the [2]rotaxane-palladium complex **1.40**, which subsequently loses palladium and liberates [2]rotaxane **1.41**.

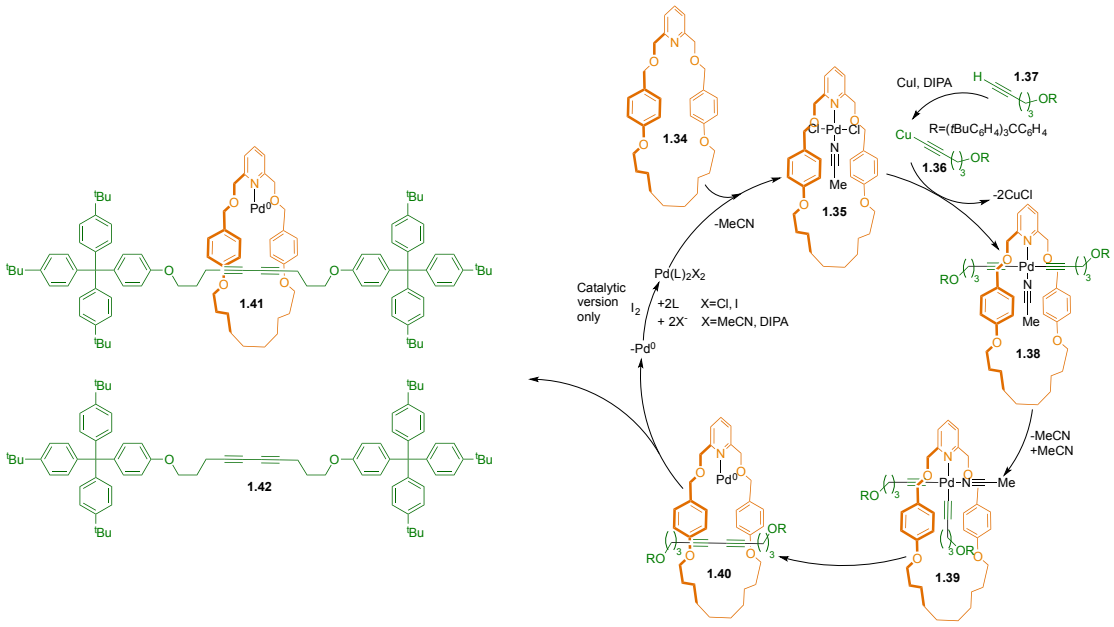

Scheme 1.9. Pd(II)-mediated active-metal template synthesis of [2]rotaxane **1.41** by Leigh and coworkers.[99]

After these successful rotaxane formations our group's interest was piqued by the prospect of using similar approaches to form rotaxanes incorporating polyynes. We aimed to test Anderson's 1994 hypothesis[7], that rotaxanation could stabilise fragile π-systems and *sp* carbons and that the macrocycle could prevent undesired polymerisation. Polyynes are more fragile than single alkynes and sometimes differ in

reactivity due to their extended conjugation. The first polyyne rotaxane **1.45** synthesis was reported by our group in collaboration with the Tykwinski group in 2012 (**Scheme 1.10**)[100] and was very closely followed by a similar approach yielding polyyne rotaxane **1.47** from Gladysz and coworkers (**Scheme 1.10**).[101] Both synthetic procedures were based on the conditions and macrocycle that was used by Saito and coworkers in 2006.[98] The polyyne remained intact and was relatively isolated from the macrocycle, exhibiting little change in absorption, chemical shift and solid state structure.

In 2015, the collaboration between our group and the Tykwinski group reported a significant piece of evidence supporting our 'stabilisation by encapsulation' theory.[102] [*n*]Cumulenes are the other family of *sp*-hybridised linear carbon chains and are even more unstable than polyynes.[103] The use of sterically shielding end groups to stabilise cumulenes has seemingly reached a practical limit and an alternative method was required to pursue longer [*n*]cumulenes. In this report, we outlined a new method for the kinetic stabilisation of [9]cumulenes through the synthesis of rotaxanes. The additional stability conferred by the macrocycle allowed a study of the properties of highly reactive [9]cumulenes for the first time (**Scheme 1.11**).

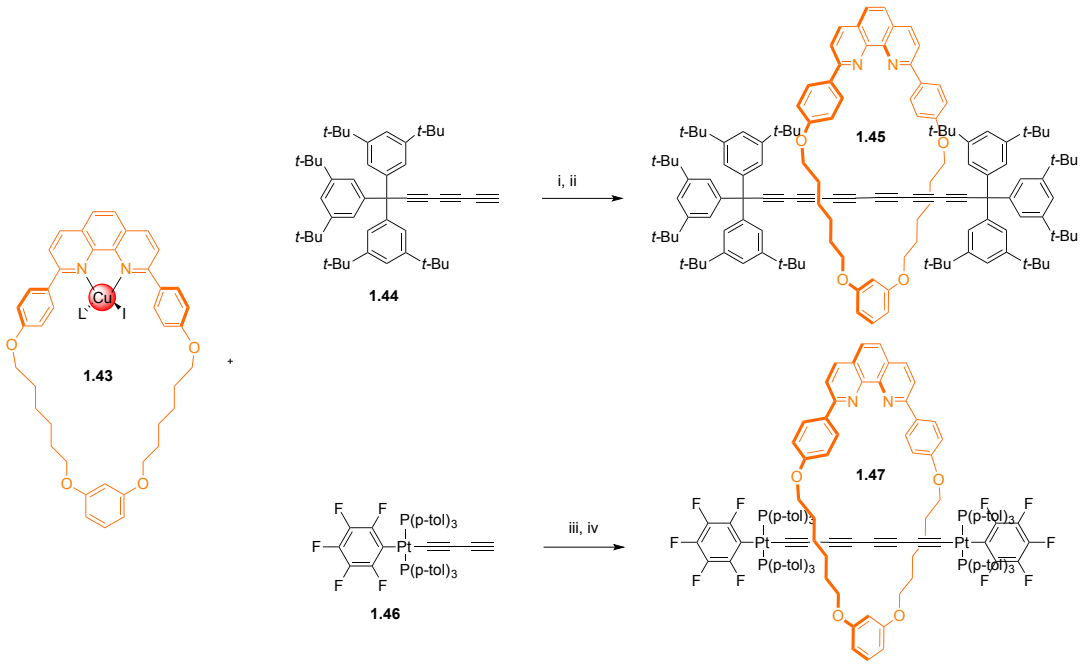

Scheme 1.10. Synthesis of polyyne rotaxanes **1.45** and **1.47**. i) Anderson and coworkers, K_2CO_3, I_2, THF, 60 °C ii) KCN (aq), 32% (two step yield).[100] iii) Gladysz and coworkers, K_2CO_3, I_2, THF, 55 °C. iv) KCN (aq), 9% (two step yield).[101]

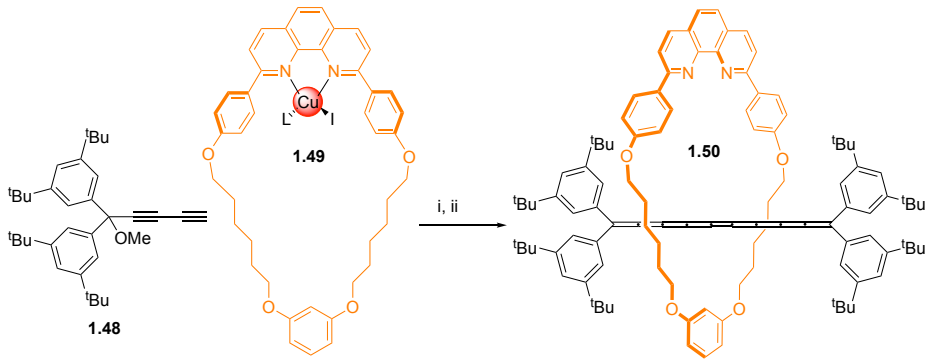

Scheme 1.11. Synthesis of [9]cumulene rotaxane **1.50**. i) K_2CO_3, I_2, THF, 60°C. 67% ii) $SnCl_2$ (anhydrous), HCl (1 M in Et_2O), Et_2O, Ar, 25 °C, 33%.

A more detailed study was subsequently performed by our group, investigating the effect of polyyne length and size of macrocycle on rotaxane yield and stability.[73] This series of rotaxanes consisted of polyynes, with up to 24 contiguous *sp*-hybridised carbon atoms, threaded through a variety of macrocycles (**Figure 1.10**). The highest yields of rotaxanes were reported in the intermediate sized macrocycles. Cadiot−Chodkiewicz cross-coupling afforded higher yields of rotaxanes than homocoupling throughout this study. This report also demonstrated a flagship [3]rotaxane **1.54** with two polyyne chains locked through the same macrocycle (**Figure 1.11**). This highlights the power of mechanical insulation as the polyynes could not adopt the required geometry to polymerise and the molecule was stable.

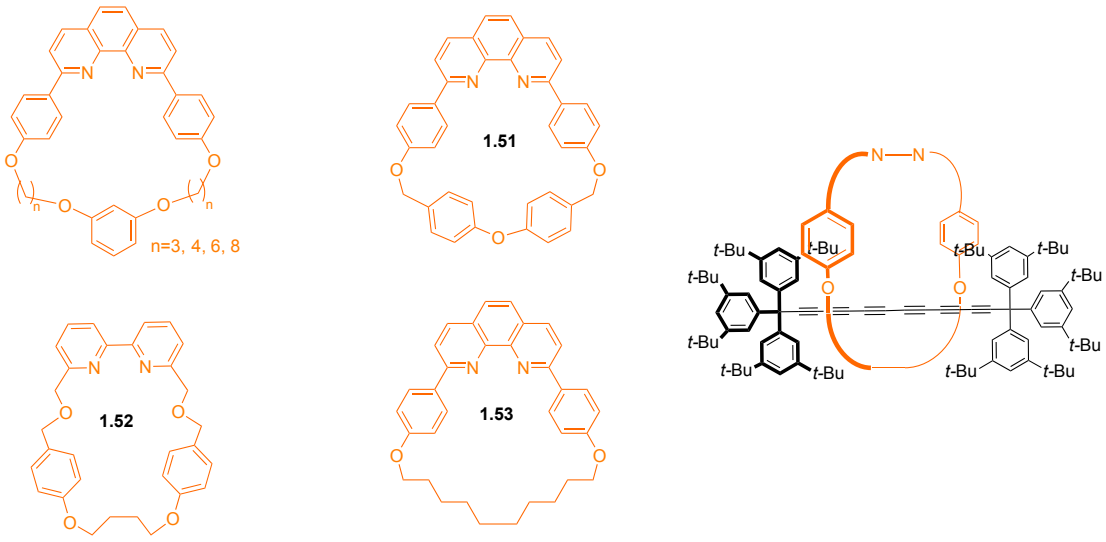

Figure 1.10. Various macrocycles were used to prepare a range of polyyne rotaxanes.[73]

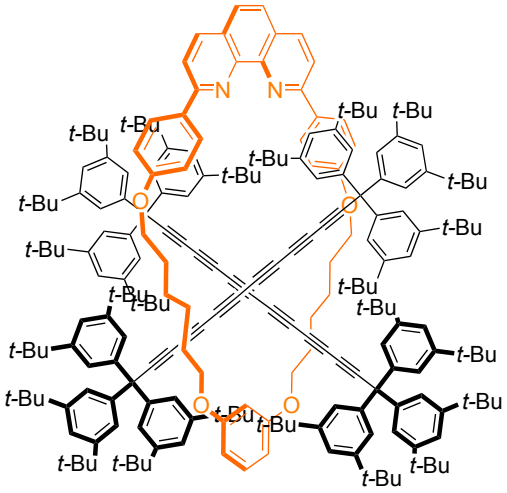

Figure 1.11. [3]rotaxane **1.54**, the polyynes cannot crosslink due to enforced diagonal arrangement.[73]

Finally, in 2016, the stabilising effect of the macrocycle was demonstrated using differential scanning calorimetry (DSC) and our theory of 'stabilisation of encapsulation' was strongly supported.[73] Longer polyynes underwent thermal decomposition without melting and the rotaxanes were more stable than the corresponding naked dumbbells; the difference in stability widens with increasing polyyne chain length. The greatest enhancement in thermal stability was observed in the longest polyyne measured, as DSC showed a marked difference in decomposition temperature (**Figure 1.12**). As the polyyne chain gets longer, steric shielding of the carbon chain by the supertrityl groups decreases, providing an opportunity for the macrocycle to act as an additional shield for the centre of the polyyne chain and suppress a reactive orientation of the polyynes and subsequent degradation.

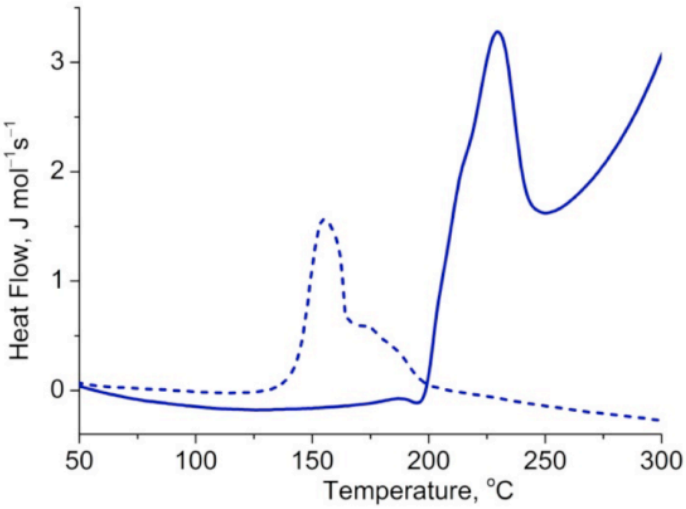

Figure 1.12. DSC traces of supertrityl dodecayne (dashed line) and the corresponding rotaxane (solid line). Heating: 10 °C/min. Figure adapted from reference 73 with permission from the ACS.

The conclusive proof of stabilisation by encapsulation offered us hope that the same strategy could be utilised to prepare cyclocarbons. Rotaxanation helped protect the fragile π-system of polyynes, hence, by extension, we believe that catenation could protect the fragile π-system of cyclocarbons. In our view, encapsulation of cyclocarbons is the most promising new method for their preparation.

In this thesis we will focus on encapsulation as a strategy to macroscopically prepare rotaxanes and catenanes for investigation of their properties. However, there is an alternative strategy: molecules too elusive to be studied in traditional ways have been stabilised on surfaces using a decoupling layer of NaCl and imaged at low temperatures using a combination of atomic force microscopy (AFM) and scanning tunnelling microscopy (STM). This approach also holds promise for the synthesis and observation of cyclocarbons, this will be discussed in **Chapter 5**.

1.4 - References

(1) Diederich, F.; Rubin, Y. *Angew. Chem. Int. Ed. Eng.* **1992**, *31*, 1101.
(2) Chalifoux, W.; Tykwinski, R. R. *Nat. Chem.* **2010**, *2*, 967.
(3) Neenan, T. X.; Whitesides, G. M. *J. Org. Chem.* **1988**, *53*, 2489.
(4) Hirsch, A. *Nat. Mater.* **2010**, *9*, 868.
(5) Nicolaou, K. C.; Yang, Z.; Liu, J. J.; Ueno, H.; Nantermet, P. G.; Guy, R. K.; Claiborne, C. F.; Renaud, J.; Couladouros, E. A.; Paulvannan, K.; Sorensen, E. J. *Nature* **1994**, *367*, 630.
(6) Pavliček, N.; Gross, L. *Nat. Rev. Chem.* **2017**, *1*.
(7) Diederich, F. *Nature* **1994**, *369*, 199.
(8) Bundy, F. P.; Bassett, W. A.; Weathers, M. S.; Hemley, R. J.; Mao, H. K.; Goncharov, A. F. *Carbon* **1996**, *34*, 141.
(9) Grochala, W. *Angew. Chem. Int. Ed.* **2014**, *53*, 3680.
(10) Karfunkel, H. R.; Dressler, T. *J. Am. Chem. Soc.* **1992**, *114*, 2285.
(11) Kroto, H. W.; Heath, J. R.; O'Brien, S. C.; Curl, R. F.; Smalley, R. E. *Nature* **1985**, *318*, 162.
(12) Iijima, S.; Ichihashi, T. *Nature* **1993**, *363*, 603.
(13) Novoselov, K. S.; Geim, A. K.; Morozov, S. V; Jiang, D.; Zhang, Y.; Dubonos, S. V; Grigorieva, I. V; Firsov, A. A. *Science* **2004**, *306*, 666.
(14) Kratschmer, W.; Lamb, L.; Fostiropoulos, K.; Huffmann, D. *Nature* **1990**, *347*, 354.
(15) Dennler, G.; Scharber, M. C.; Brabec, C. J. *Adv. Mater.* **2009**, *21*, 1323.
(16) Campidelli, S.; Brandmüller, T.; Hirsch, A.; Saez, I. M.; Goodby, J. W.; Deschenaux, R. *Chem. Commun.* **2006**, *41*, 4282.
(17) Friedman, S. H.; Decamp, D. L.; Sijbesma, R. P.; Srdanov, G.; Wudl, F.; Kenyon, G. L. *J. Am. Chem. Soc.* **1993**, *115*, 6506.
(18) Holczer, K.; Klein, O.; Huang, S.-M.; Kaner, R. .; Fu, K.-J.; Whetten, R. L.; Diederich, F. *Science* **1991**, *252*, 1154.
(19) Hitosugi, S.; Nakanishi, W.; Yamasaki, T.; Isobe, H. *Nat. Commun.* **2011**, *2*, 492.
(20) Omachi, H.; Nakayama, T.; Takahashi, E.; Segawa, Y.; Itami, K. *Nat. Chem.* **2013**, *5*, 572.
(21) Sisto, T. J.; Zakharov, L. N.; White, B. M.; Jasti, R. *Chem. Sci.* **2016**, *7*, 3681.
(22) De, S.; King, P. J.; Lotya, M.; O'Neill, A.; Doherty, E. M.; Hernandez, Y.; Duesberg, G. S.; Coleman, J. N. *Small* **2010**, *6*, 458.
(23) Cai, M.; Thorpe, D.; Adamson, D. H.; Schniepp, H. C. *J. Mater. Chem.* **2012**, *22*, 24992.
(24) Dedkov, Y.; Fonin, M.; Rudiger, U.; Laubschat, C. *Phys. Rev. Lett.* **2008**, *100*, 1.
(25) Li, X.; Wang, X.; Zhang, L.; Lee, S.; Dai, H. *Science* **2008**, *319*, 1229.
(26) Berger, C.; Wu, X.; Brown, N.; Naud, C.; Li, X.; Song, Z.; Mayou, D.; Li, T.; Hass, J.; Marchenkov, A.; Conrad, E. H.; First, P. N.; De Heer, W. A. *Science* **2006**, *312*, 1191.
(27) Turchanin, A.; Beyer, A.; Nottbohm, C. T.; Zhang, X.; Stosch, R.; Sologubenko, A.; Mayer, J.; Hinze, P.; Weimann, T.; Golzhauser, A. *Adv. Mater.* **2009**, *21*, 1233.
(28) R. Hayatsu, R. G. Scott, M. H. Studier, R. S. Lewis, E. A. *Science* **1980**, *209*, 1515.
(29) Rubin, Y.; Diederich, F. *J. Am. Chem. Soc.* **1989**, *11*, 6870.

(30) Li, Y.; Rubin, Yves; Diederich, François; Houk, K. *J. Am. Chem. Soc.* **1990**, *112*, 1618.
(31) Rubin, Y.; Knobler, C. B.; Diederich, F. *J. Am. Chem. Soc.* **1990**, *16*, 1607.
(32) Baughman, R. H. *Science* **2006**, *312*, 1009.
(33) Akdim, B.; Pachter, R. *ACS Nano* **2011**, *5*, 1769.
(34) Bohlmann, F. *Angew. Chem.* **1953**, *65*, 385.
(35) Jones, E. *Proc. Chem. Soc.* **1960**, 199.
(36) Eastmond, R.; Johnson, T. R.; Walton, D. R. M. *Tetrahedron* **1972**, *28*, 4601.
(37) Chalifoux, W. A.; McDonald, R.; Ferguson, M. J.; Tykwinski, R. R. *Angew. Chem. Int. Ed.* **2009**, *48*, 7915.
(38) Zheng, Q.; Bohling, J. C.; Peters, T. B.; Frisch, A. C.; Hampel, F.; Gladysz, J. A. *Chem. Eur. J* **2006**, *12*, 6486.
(39) Sprafke, J. K.; Kondratuk, D. V.; Wykes, M.; Thompson, A. L.; Hoffmann, M.; Drevinskas, R.; Chen, W. H.; Yong, C. K.; Kärnbratt, J.; Bullock, J. E.; Malfois, M.; Wasielewski, M. R.; Albinsson, B.; Herz, L. M.; Zigmantas, D.; Beljonne, D.; Anderson, H. L. *J. Am. Chem. Soc.* **2011**, *133*, 17262.
(40) Diederich, F. *Helv. Chim. Acta* **1994**, *77*, 1441.
(41) Anthony, J.; Boldi, A. M.; Rubin, Y.; Knobler, C. B.; Hobi, M.; Diederich, F. *Synth.* **1995**, *78*, 13.
(42) Siemsen, P.; Livingston, R. C.; Diederich, F. *Angew. Chem. Int. Ed.* **2000**, *39*, 2632.
(43) Nielsen, M. B.; Diederich, F. *Chem. Rev.* **2005**, *105*, 1837.
(44) Okamura, W. H.; Sondheimer, F. *J. Am. Chem. Soc.* **1967**, *89*, 5991.
(45) Alberts, A. H. *J. Am. Chem. Soc.* **1989**, *8*, 3093.
(46) Anthony, J.; Boldi, A. M.; Rubin, Y.; Hobi, M.; Gramlich, V.; Knobler, C. B.; Seiler, P.; Diederich, F. *Helv. Chim. Acta* **1995**, *78*, 13.
(47) Feldman, K. S.; Kraebel, C. M. *J. Am. Chem. Soc.* **1993**, *115*, 3846.
(48) Kivala, M.; Mitzel, F.; Boudon, C.; Gisselbrecht, J. P.; Seiler, P.; Gross, M.; Diederich, F. *Chem. Asian J.* **2006**, *1*, 479.
(49) Lincke, K.; Floor Frellsen, A.; Parker, C. R.; Bond, A. D.; Hammerich, O.; Nielsen, M. B. *Angew. Chem. Int. Ed.* **2012**, *51*, 6099.
(50) Moore, J. S. *Acc. Chem. Res.* **1997**, *30*, 402.
(51) Ajami, D.; Oeckler, O.; Simon, A.; Herges, R. *Nature* **2003**, *426*, 819.
(52) Sondheimer, F. *Acc. Chem. Res.* **1972**, *1975*, 81.
(53) Boldi, A. M.; Diederich, F. *Angew. Chem. Int. Ed. Engl.* **1994**, *33*, 468.
(54) Hoffmann, R. *Tetrahedron* **1966**, *22*, 521.
(55) Bernholc, J.; Phillips, J. C. *J. Chem. Phys.* **1986**, *85*, 3258.
(56) Kertesz, M.; Koller, J.; Afman, A. *J. Chem. Phys.* **1978**, *68*, 2779.
(57) Durgun, E.; Tongay, S.; Ciraci, S. *Phys. Rev. B* **2005**, *72*, 1.
(58) Neiss, C.; Trushin, E.; Görling, A. *ChemPhysChem* **2014**, *15*, 2497.
(59) Perdew, J. P.; Burke, K.; Ernzerhof, M. *J. Chem. Phys.* **1996**, *22*, 9982.
(60) Rubin, Y.; Knobler, C. B.; Diederich, F. *J. Am. Chem. Soc.* **1990**, *12*, 4966.
(61) Rubin, Y.; Kahr, M.; Knobler, C. B.; Diederich, F.; Wilkins, C. L. *J. Am. Chem. Soc.* **1991**, *113*, 495.
(62) Adamson, G. A.; Rees, C. W. *J. Chem. Soc. Perkin Trans* **1996**, *2*, 1535.
(63) Tobe, Y.; Fujii, T.; Naemura, K. *J. Org. Chem.* **1994**, *59*, 1236.
(64) Tobe, Y.; Matsumoto, H.; Naemura, K.; Achiba, Y.; Wakabayashi, T. *Angew. Chem. Int. Ed. Engl.* **1996**, *35*, 1799.
(65) Tobe, Y.; Fujii, T.; Matsumoto, H.; Naemura, K.; Achiba, Y.; Wakabayashi, T. *J. Am. Chem. Soc.* **1996**, *118*, 2758.

(66) Tobe, Y.; Umeda, R.; Iwasa, N.; Sonoda, M. *Chem. Eur. J* **2003**, *9*, 5549.
(67) Haley, M. M.; Langsdorf, B. L. *Chem. Commun.* **1997**, *2*, 1121.
(68) Diederich, F.; Kivala, M. *Adv. Mater.* **2010**, *22*, 803.
(69) Tobe, Y.; Fujii, T.; Matsumoto, H.; Tsumuraya, K.; Noguchi, D.; Nakagawa, N.; Sonoda, M.; Naemura, K. *J. Am. Chem. Soc.* **2000**, *122*, 1762.
(70) Huuskonen, J.; Buston, J. E. H.; Scotchmer, N. D.; Anderson, H. L. *New J. Chem.* **1999**, *23*, 1245.
(71) Weller, M. D.; Kariuki, B. M.; Cox, L. R. *J. Org. Chem.* **2009**, *74*, 7898.
(72) Shir, I. Ben; Sasmal, S.; Mejuch, T.; Sinha, M. K.; Kapon, M.; Keinan, E. *J. Org. Chem.* **2008**, *73*, 8772.
(73) Movsisyan, L. D.; Franz, M.; Hampel, F.; Thompson, A. L.; Tykwinski, R. R.; Anderson, H. L. *J. Am. Chem. Soc.* **2016**, *138*, 1366.
(74) Stoddart, J. F. *Chem. Soc. Rev.* **2009**, *38*, 1802.
(75) Fang, L.; Olson, M. A.; Benítez, D.; Tkatchouk, E.; Goddard III, W. A.; Stoddart, J. F. *Chem. Soc. Rev.* **2010**, *39*, 17.
(76) Bruns, C. J.; Stoddart, J. F. *The Nature of the Mechanical Bond: From Molecules to Machines*, 1st ed.; John Wiley & Sons, 2017.
(77) Eaton, E, P.; Stubbs, E, C. *J. Am. Chem. Soc.* **1967**, *2756*, 1966.
(78) Rowan, S. J.; Cantrill, S. J.; Stoddart, J. F. *Org. Lett.* **1999**, *1*, 1294.
(79) Leigh, D. A.; Murphy, A.; Smart, J. P.; Slawin, A. M. Z. *Angew. Chem. Int. Ed. Engl.* **1997**, *36*, 728.
(80) Wisner, J. A.; Beer, P. D.; Drew, M. G. B.; Sambrook, M. R. *J. Am. Chem. Soc.* **2002**, *124*, 12469.
(81) Spence, G. T.; Beer, P. D. *Acc. Chem. Res.* **2013**, *46*, 571.
(82) Ogini, H. *J. Am. Chem. Soc.* **1981**, *103*, 1303.
(83) Lewis, J. E. M.; Beer, P. D.; Loeb, S. J.; Goldup, S. M. *Chem. Soc. Rev.* **2017**, *46*, 2577.
(84) Dietrich-Buchecker, C. O.; Sauvage, J. P.; Kintzinger, J. P. *Tetrahedron Lett.* **1983**, *24*, 5095.
(85) Belfrekh, N.; Dietrich-Buchecker, C.; Sauvage, J. P. *Inorg. Chem.* **2000**, *39*, 5169.
(86) Leigh, D. A.; Lusby, P. J.; Teat, S. J.; Wilson, A. J.; Wong, J. K. Y. *Angew. Chem. Int. Ed.* **2001**, *40*, 1538.
(87) Fuller, A. M.; Leigh, D. A.; Lusby, P. J.; Oswald, I. D. H.; Parsons, S.; Walker, D. B. *Angew. Chem. Int. Ed.* **2004**, *43*, 3914.
(88) Fuller, A. M. L.; Leigh, D. A.; Lusby, P. J. *Angew. Chem. Int. Ed.* **2007**, *46*, 5015.
(89) Goldup, S. M.; Leigh, D. A.; Lusby, P. J.; McBurney, R. T.; Slawin, A. M. Z. *Angew. Chem. Int. Ed.* **2008**, *47*, 6999.
(90) Crowley, J. D.; Goldup, S. M.; Lee, A.-L.; Leigh, D. A.; McBurney, R. T. *Chem. Soc. Rev.* **2009**, *38*, 1530.
(91) Dietrich‐Buchecker, C. O.; Sauvage, J. ‐P. *Angew. Chem. Int. Ed. Engl.* **1989**, *28*, 189.
(92) Leigh, D. A.; Pritchard, R. G.; Stephens, A. J. *Nat. Chem.* **2014**, *6*, 978.
(93) Danon, J. J.; Krüger, A.; Leigh, D. A.; Lemonnier, J.; Stephens, A. J.; Vitorica-Yrezabal, I. J.; Woltering, S. L. *Science* **2017**, *355*, 159.
(94) Gaviña, P.; Sauvage, J. P. *Tetrahedron Lett.* **1997**, *38*, 3521.
(95) Wu, C.; Lecavalier, P. R.; Shen, Y. X.; Gibson, H. W. *Chem. Mater.* **1991**, *3*, 569.
(96) Solladié, N.; Chambron, J. C.; Sauvage, J. P. *J. Am. Chem. Soc.* **1999**, *121*,

3684.
(97) Aucagne, V.; Hänni, K. D.; Leigh, D. A.; Lusby, P. J.; Walker, D. B. *J. Am. Chem. Soc.* **2006**, *128*, 2186.
(98) Saito, S.; Takahashi, E.; Nakazono, K. *Org. Lett.* **2006**, *8*, 5133.
(99) Berná, J.; Crowley, J. D.; Goldup, S. M.; Hänni, K. D.; Lee, A. L.; Leigh, D. A. *Angew. Chem. Int. Ed.* **2007**, *46*, 5709.
(100) Movsisyan, L. D.; Kondratuk, D. V.; Franz, M.; Thompson, A. L.; Tykwinski, R. R.; Anderson, H. L. *Org. Lett.* **2012**, *14*, 3424.
(101) Weisbach, N.; Baranová, Z.; Gauthier, S.; Reibenspies, J. H.; Gladysz, J. A. *Chem. Commun.* **2012**, *48*, 7562.
(102) Franz, M.; Januszewski, J. A.; Wendinger, D.; Neiss, C.; Movsisyan, L. D.; Hampel, F.; Anderson, H. L.; Görling, A.; Tykwinski, R. R. *Angew. Chem. Int. Ed.* **2015**, *54*, 6645.
(103) Januszewski, J. A.; Tykwinski, R. R. *Chem. Soc. Rev.* **2014**, *43*, 3184.

Chapter 2

Porphyrin-polyyne [3]- and [5]rotaxanes

2.1. Introduction 28

2.2. Synthesis of polyynes 30

2.3. Attempted synthesis of porphyrin-polyyne [5]rotaxane P5Ra 32

2.4. Synthesis of porphyrin-polyyne [5]rotaxane P5Rb 41

2.5. Photophysical studies 44

2.5.1. Absorption and emission spectra 45

2.5.2. Absorption and excitation spectra 48

2.5.3. Methodology for determining EET, analysis spectra 49

2.5.4. Methodology for determining EET, excitaton spectra 52

2.6. Conclusions 55

2.7. Experimental data for known compounds 57

2.8. Experimental data for novel compounds 64

2.9. References 77

Part of this chapter has been published: Kohn, D. R.; Movsisyan, L. D.; Thompson, A. L.; Anderson, H. L. *Org. Lett.* **2017**, *19*, 348–351. Crystallography was performed by Amber. L. Thompson.

Chapter 2 - Porphyrin-polyyne [3]- and [5] rotaxanes

2.1 – Introduction

In supramolecular chemistry, molecular structures held together by mechanical interactions have attracted widespread attention.[1] These complex molecular topologies often require creative synthetic strategies and novel templating methods.[2] Advances in active metal template synthesis[3,4] provide access to a growing diversity of interlocked molecules, including threaded polyynes.[3,5–10] Linear chains of *sp*-hybridised carbon atoms (both polyynes and cumulenes) can be stabilised by threading them through macrocycles to form rotaxanes.[11,12] The combination of additional stability and lack of covalent bonding makes interlocking a very attractive prospect for stabilising extended systems of *sp*-carbons whilst keeping the π-system intact.

In polyyne rotaxanes, the macrocycle stabilises the polyyne, but can also force it into a certain spatial arrangement. Geometry control is an exciting strategy for linking polyynes and preparing cyclic acetylenic structures. Template synthesis has been integral in preparing some of the most elaborate nanostructures, favouring defined products over polymers.[8,13] As part of a project directed toward the synthesis of cyclocarbon catenanes, we are exploring strategies for positioning several polyyne rotaxane units around a central molecular hub, so the polyynes can be linked together to form a threaded cyclocarbon. We believe the development of this methodology and the combination of this approach with masked alkyne equivalents (MAEs) could lead to confined polyynes with the potential for subsequent deprotection and linkage, forming a cyclocarbon catenane.

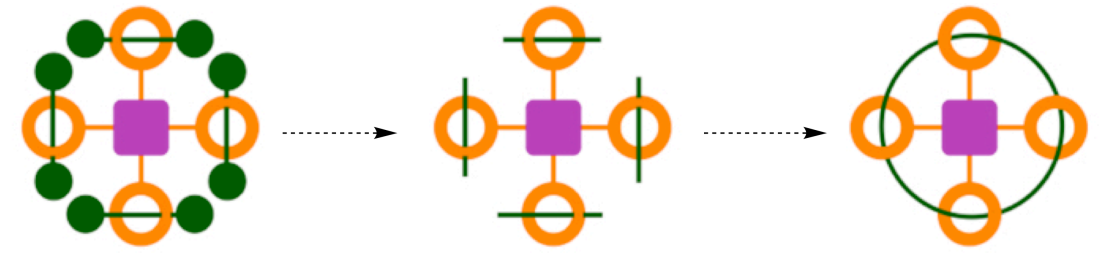

Figure 2.1. Positioning polyynes around a central core, removing stoppers and subsequent cyclisation.

Porphyrins are a family of heterocyclic macrocycles consisting of four pyrrole units linked by unsaturated =CH- groups through their α-positions (**Figure 2.2**).[14] The two other types of position on the porphyrin periphery are known as the *meso* and β

positions (**Figure 2.2**); these positions have the potential for extraordinarily diverse functionalisation. Porphyrins, metalloporphyrins and many related molecules are enormously important due to their metal binding and photophysical properties.[15–18] Porphyrins are the biological colours of life, giving haemoglobin its distinctive red colour and chlorophyll its green colour.[18]

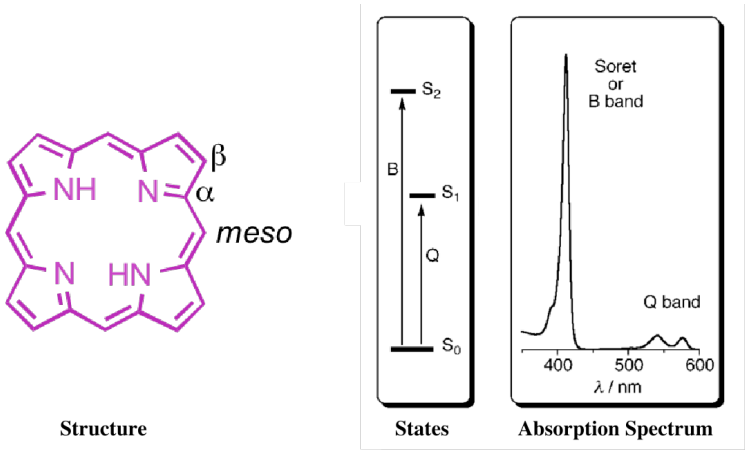

Figure 2.2. Structure, electronic excited states and absorption spectra of porphyrins (adapted with permission from reference 18. Copyright 2017 Royal Society of Chemistry).

A typical porphyrin electronic absorption spectrum contains a weak transition to the first excited state ($S_0 \rightarrow S_1$) at approximately 550 nm (the Q band) and a strong transition to the second excited state ($S_0 \rightarrow S_2$) at approximately 400 nm (the Soret or B band). Internal conversion ($S_2 \rightarrow S_1$) is rapid so fluorescence is only detected from the S_1 state.[18] The B and the Q bands both arise from $\pi - \pi^*$ transitions and can be explained by configurational interaction, resulting in two bands with very different intensities and wavelengths. Constructive interference leads to the intense short-wavelength B band, while the weak long-wavelength Q band results from destructive combinations.[19] The photophysical behavior of porphyrins is very well understood because of their variety of applications. This makes them an excellent chromophore to combine with a less studied chromophore such as a polyyne for investigation.

It has been shown that polyynes exhibit unusual photophysical behaviour. However, there is a limit to our understanding. Polyynes show absorption into higher S_n states and rapid formation of a dark S_1 state.[20–22] They also undergo a rapid ($S_1 \rightarrow T_1$) transition, as proved conclusively by our group through characterisation with time resolved infra-red spectroscopy (TRIR).[23] This study was the most detailed of its type

and uncovered the first direct evidence of excited state energy transfer from phenanthroline macrocycles to hexayne chains in polyyne rotaxanes (**Figure 2.3**). The TRIR spectra show that this energy-transfer process directly populates the vibrationally equilibrated S_1 state of the hexayne. In contrast, internal conversion ($S_n \rightarrow S_1$) creates a hot vibrational state, which cools over about 5 ps. Combining polyyne rotaxanes with an additional chromophore could provide a fascinating system to investigate excited state energy transfer further. Although polyynes are non-emissive, if singlet or triplet energy could be transferred to an emissive group this could be observed as luminescence. Observing fluorescence from a porphyrin while selectively exciting a polyyne would allow the opportunity to observe polyynes acting as excited state energy donors.

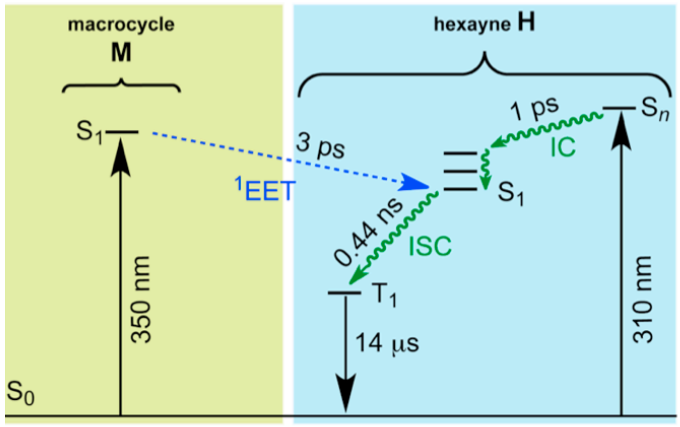

Figure 2.3. Energy diagram summarising excited-state processes in (a) dumbbell H and rotaxane H⊂M (adapted with permission from reference 23. Copyright 2017 American Chemical Society).

Our aim was to prepare a series of polyrotaxanes, with the most prized compound being a [5]rotaxane. These compounds were prepared for two reasons. Firstly, the insulation of the macrocycle stabilises the polyyne, probing the compatibility of synthetic methods with these systems and arranging them could provide useful insight for our long-term goal of preparing insulated cyclocarbon. Secondly, combining the porphyrin and polyyne moieties will lead to an interesting series of compounds for probing the excited state interactions of polyynes and porphyrins.

2.2 - Synthesis of polyynes

Tykwinski *et al.* recognised that large, sterically demanding end groups prevented crosslinking and allowed access to longer polyynes.[24] This led to them utilising the

tris(3,5-di-*tert*-butylphenyl)methyl (supertrityl) end group.[25] The supertrityl end group is a perfect building block for our research objectives due to its stability and large size. Supertrityl groups are very large (approximately 14 Å in diameter), which means we can discount unthreading of rotaxanes as an issue. Additionally, the purpose of synthesising the triyne unit is that this molecule provides a good compromise between rotaxane yield, stability and ease of synthesis.

In order to prepare a stock of triyne **2.10** a large-scale polyyne synthesis was performed according to previous literature procedures. A three-fold Friedel Crafts alkylation of benzene under thermodynamic control at −20 °C with excess 2-chloro-2-methylpropane yielded 1,3,5-tri-*tert*-butylbenzene **2.2** in good yield.[26] Monosubstitution of one alkyl group with bromine was performed using Br_2 and iron turnings at 0 °C in good yield to afford **2.3**.[27] Magnesium turnings were activated and the Grignard reagent of **2.3** was formed; this was used in a double substitution-addition of diethyl carbonate to yield supertrityl alcohol **2.4** in excellent yield.[24] The alcohol **2.4** was converted to the supertrityl chloride using oxalyl chloride and the addition of excess ethynyl magnesium bromide afforded supertritylacetylene **2.5** in excellent yield over two steps (**Scheme 2.1**).[24]

From this crucial building block, a series of reactions were performed which will prove fundamental in this thesis for preparing many acetylenic building blocks (**Scheme 2.5**). Supertrityl acetylene **2.5** was lithiated using *n*-BuLi at −78 °C. This solution was subsequently added to a solution of triisopropylsilyl propargylic aldehyde **2.1** and after quenching yielded alcohol **2.6** in good yield.[24] This type of reaction can be used to prepare alcohols with many combinations of acetylenic substitutents (**Chapter 3, Chapter 4, Chapter 5**). Oxidation with pyridinium chlorochromate (PCC) occurred overnight to yield ketone **2.7** in excellent yield. Dibromoolefination using Ramirez's conditions furnished dibromoolefin **2.8** in excellent yield.[28] A Fritsch-Buttenberg-Wiechell (FBW) rearrangement using *n*-BuLi in hexane was used to transform dibromoolefin **2.8** into triyne **2.9** in excellent yield.[29] Desilylation of **2.9** using TBAF at 0 °C yielded terminal triyne **2.10** in average yield. Finally, bromination was performed to prepare brominated triyne **2.11** for Cadiot-Chodkiewicz coupling. This bromination was performed using NBS and $AgNO_3$ in acetone and yielded **2.11** as a slightly yellow unstable solid in quantitative yield

(**Scheme 2.1**).[24] Our stock of **2.10** was kept as a stable solid in the freezer and parts of it were converted to slightly unstable **2.11** as required. Supertrityl triyne **2.10** is an excellent model compound for the active-metal template rotaxane synthesis. It possesses a combination of reasonable stability, a large size and a long distance between the coupling point and the steric bulk of the stoppering group. Additionally, any rotaxanes synthesised from this precursor would contain a hexayne, which would make photophysical studies consistent with previous results.[23]

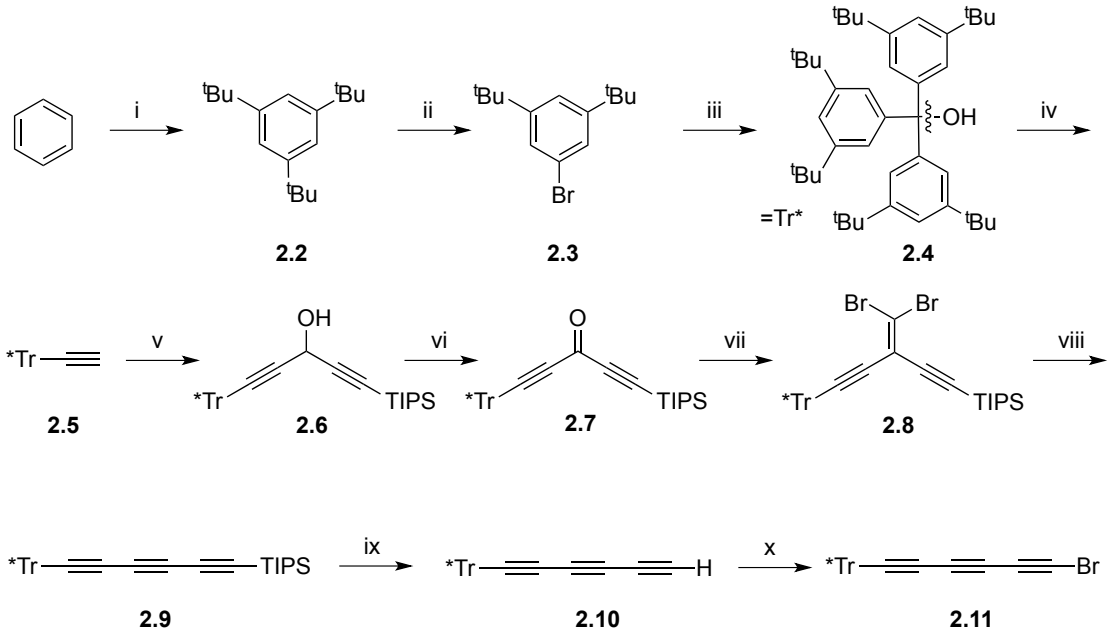

Scheme 2.1. Polyyne Synthesis. i) $AlCl_3$, *tert*-butyl chloride, −40 °C - −20 °C, 2 h, 77% ii) Bromine, Fe powder, $CHCl_3$, 0 °C, 4 h, 68% iii) Mg, diethyl carbonate, THF, RT, 3 d, 91% iv) Oxalyl chloride, 4 h, ethynylmagnesium bromide (1.0 M in THF), 4 d, 92% v) a) *n*-BuLi, THF, −78 °C, 30 min b) Aldehyde **2.1**, THF, 1 h, 25 °C, 71% vi) PCC, celite, mol. sieves, CH_2Cl_2, 20 h, 98% vii) PPh_3, CBr_4, CH_2Cl_2, 20 h, 93% viii) *n*-BuLi, hexane, −78 °C - 0 °C 30 mins, 91% ix) TBAF, THF, H_2O, 0 °C, 15 min, 60% x) NBS, $AgNO_3$, 25 °C, 2 h, acetone, 100%.

2.3 - Attempted synthesis of porphyrin-polyyne [5]rotaxane **P5Ra**

The initial target of this work was the porphyrin [5]rotaxane **P5Ra** (**Figure 2.4)**. [5]rotaxane **P5Ra** is comprised of a porphyrin core with four macrocycles at its *meso* positions. These macrocycles are all threaded with a supertrityl capped hexayne. This particular molecular design was chosen because we believed the molecule would provide evidence that we could arrange polyynes around a central core and would also provide an opportunity to investigate the behaviour of polyyne excited states in the close presence of both phenanthrolines and a porphyrin. We also chose this molecule

due to the literature precedent for many intermediates. Sauvage and coworkers synthesised a similar phenanthroline macrocycle with an aldehyde on the single aryl moiety.[30] They also reported a similar porphyrin with four phenanthroline macrocycles substituted attached at the *meso* positions which was prepared from the aforementioned aldehyde.[30,31] Our group had prepared polyyne rotaxanes with very similar macrocycles. We believed by combining methods from both approaches that we could synthesise porphyrin [5]rotaxane **P5Ra**.

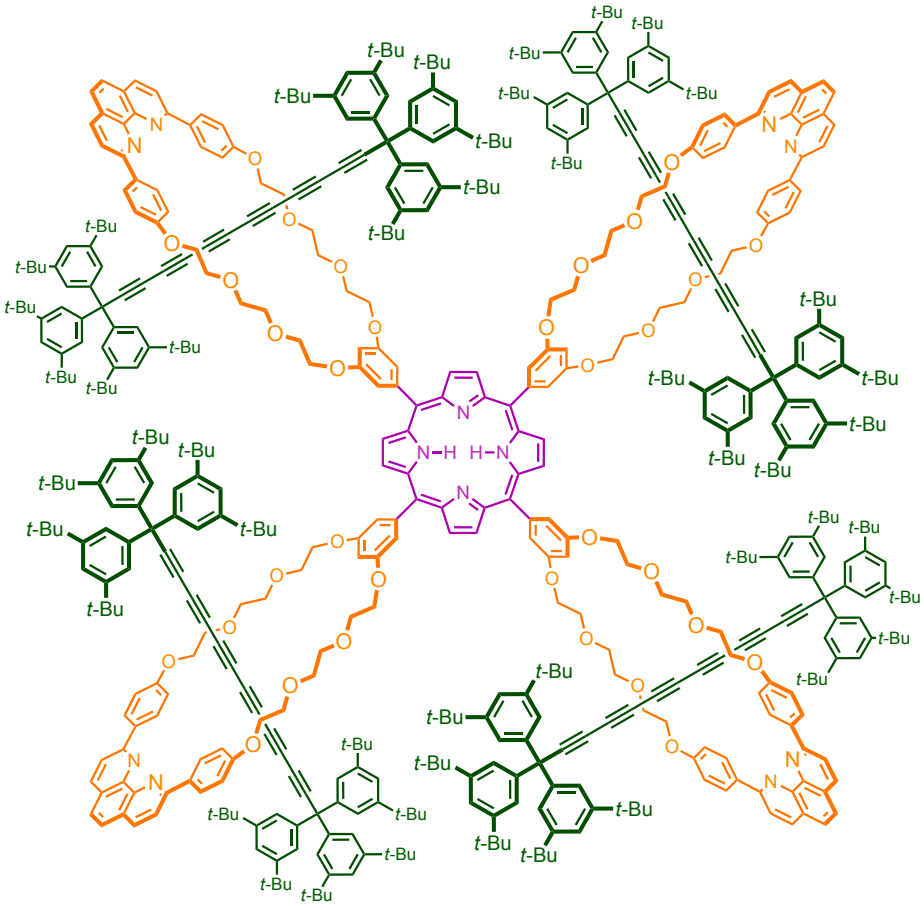

Figure 2.4. Structure of target [5]rotaxane **P5Ra**.

There are two primary synthetic pathways towards porphyrin [5]rotaxane **P5Ra**. One route (a) was to first prepare a phenanthroline-containing macrocyclic aldehyde **Ma**; from this macrocycle, a hexayne rotaxane **2Ra** could be prepared using an active-metal template coupling. A condensation reaction from this [2]rotaxane aldehyde with pyrrole would then be performed to isolate the desired [5]rotaxane **P5Ra (Scheme 2.2a)**. If route (a) was unsuccessful there is an alternative strategy. Route (b): form a macrocycle-substituted porphyrin **PM4a** from macrocycle **Ma** and attempt a multiple rotaxanation to afford the desired product (**Scheme 2.2b**). We did not

anticipate that the final step in route (a) or route (b) would be particularly high yielding. However, we suspected that the multiple-rotaxanation in route (b) would be particularly poor. A typical rotaxanation does not give a yield of higher than 50%. Therefore, this reaction occurring four times would give an estimated yield of: $0.5^4 = 6.25\%$. The separation of partially threaded products could also be challenging. For this reason route (a) was favoured, but we were prepared to use the second route if necessary.

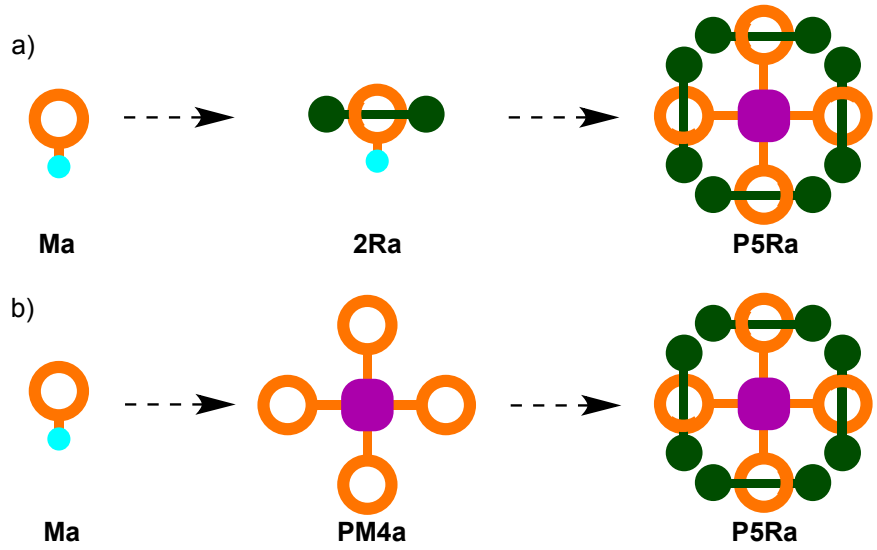

Scheme 2.2. Synthetic routes a) and b) towards porhyrin [5]rotaxane **P5Ra.**

In order to form rotaxanes we had to synthesise a phenanthroline-containing macrocycle. The chosen framework had been synthesised previously and had been used to form polyyne rotaxanes.[5,9] First, lithiation of 4-bromoanisole was performed at low temperature and the lithiated species was added to 1,10-phenanthroline. After 48 h the reaction mixture was quenched and oxidised *in situ* with MnO_2.[32] After recrystallisation from toluene, **2.12** was isolated in good yield. Substituted phenanthroline **2.12** was demethylated with pyridinium hydrochloride and diol **2.13** precipitated in excellent yield (**Scheme 2.3**).[32]

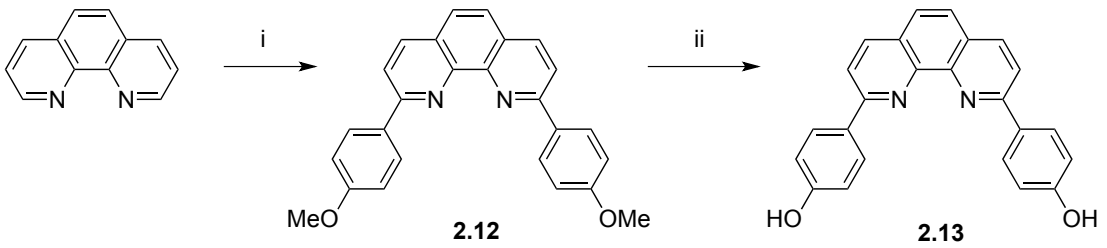

Scheme 2.3. Synthesis of diol **2.13**. i) a) 4-Bromoanisole, *t*-BuLi, Et_2O, -78 °C, 1.5 h b) 1,10-phenanthroline, Et_2O, 25 °C, 48 h c) MnO_2, 25 °C, 36 h, 58% ii) HCl.py, 200 °C, 2 h, 99%.

Porphyrins are synthesised in a condensation reaction from aldehydes and pyrrole or dipyrromethanes. Therefore, an aldehyde-substituted macrocycle was essential to this synthetic target. There has been one similar synthetic attempt by Sauvage and workers where a macrocycle-bearing porphyrin was synthesised.[31] However, we intended to use a slightly larger macrocycle than previously used. A larger cavity could give the hexayne more space to orient itself in a less sterically demanding conformation in the final [5]rotaxane. Diol **2.13** was reacted with chlorinated ethylene glycol derivative 2-(2-chloroethoxy)ethoxyethanol and K_2CO_3 to yield diol **2.14** in good yield. Diol **2.14** was tosylated using tosyl chloride, DMAP and NEt_3 and furnished **2.15** in good yield. Finally, macrocyclisation was performed in high dilution using Cs_2CO_3 and 3,5-dihydroxybenzaldehyde at 60 °C to yield macrocyclic aldehyde **Ma** in good yield (**Scheme 2.4**).

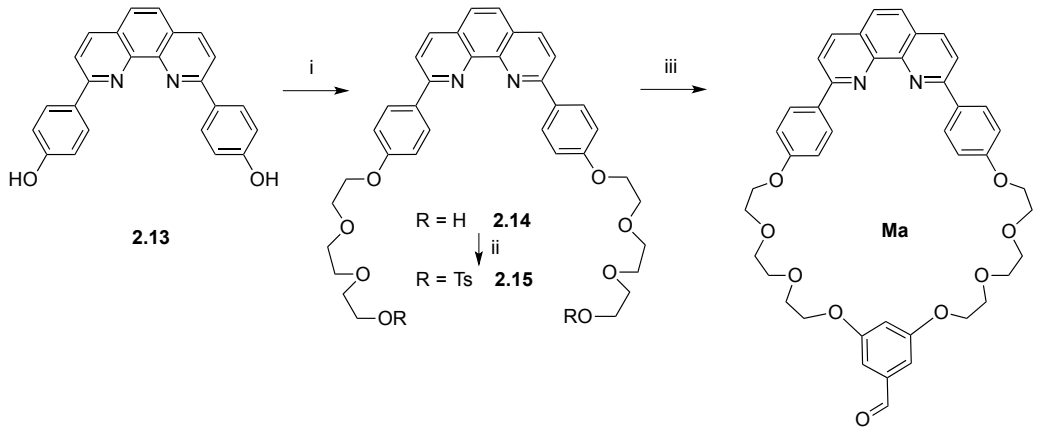

Scheme 2.4. Synthesis of macrocycle **Ma**. i) K_2CO_3, 2-(2-chloroethoxy)ethoxyethanol, acetone, 60 °C, 36 h, 76% ii) NEt_3, DMAP, TsCl, CH_2Cl_2, 0 °C- 25 °C, 20 h, 78% iii) 3,5-dihydroxybenzaldehyde, Cs_2CO_3, DMF, 60 °C, 24 h, 68%.

Active metal template Cadiot-Chodkiewicz coupling of supertrityl triyne **2.10** and bromotriyne **2.11** in the presence of the copper(I) complex of **Ma** gave the [2]rotaxane aldehyde **2Ra** in 58% yield (**Scheme 2.5)**. The Cadiot-Chodkiewicz coupling gave considerably better yields than the analogous homocoupling with I_2 (26%). A wide variety of conditions were tested for the reaction of **2Ra** with pyrrole in our attempts to prepare the desired porphyrin [5]rotaxane **P5Ra**, but they all failed to give even a trace of this target [5]rotaxane. Conditions that were used to attempt **P5Ra** synthesis included Lindsey's conditions,[33] modified equilibrium controlled conditions from Anderson and coworkers,[13] Adler-Longo conditions[34] and microwave synthesis from Sauvage and coworkers.[31] In contrast, reaction of the [2]rotaxane

aldehyde **2Ra** with dipyrromethane gave the porphyrin [3]rotaxane **P3Ra** in 62% yield (**Scheme 2.5**). The different result in these porphyrin formations suggest that a steric clash between the supertrityl groups in **P5Ra** could be what is preventing porphyrin formation. The formation of imine bonds is reversible and many of these conditions are equilibrium controlled; if steric clashes form high energy intermediate this could prevent formation of the desired product.

The porphyrins **PM2a** and **PM4a** are both novel compounds and are important compounds for our planned photophysical experiments (**Scheme 2.5**). **PM2a** was synthesised *via* Lindsey's conditions. In contrast, attempts to prepare **PM4a** were very low yielding with these conditions.[33] However, we managed to isolate **PM4a** in 24% yield when using Sauvage and coworkers' microwave conditions.[31] These conditions may help to solubilise the planar charged intermediates. We also attempted the multiple rotaxanation of porphyrin **Zn-PM4a** with a large excess of supertrityl triyne **2.10**. MALDI mass spectrometry showed a mixture of products with between 1 and 4 threaded dumbbells. Although we resubjected the reaction mixture to more copper and supertrityl triyne **2.10**, we could not force this reaction to completion. These products proved impossible to separate *via* silica chromatography, size exclusion chromatography (SEC) or numerous cycles of recycling gel permeation chromatography (GPC).

All free-base porphyrins **PM2a**, **PM4a** and **P3Ra** were immediately metallated with $Zn(OAc)_2$ in $CHCl_3$/MeOH at 60 °C, metallation often made purification more facile. All photophysical experiments were performed with metallated porphyrins. Porphyrin [3]rotaxane **P3Ra** is the first compound that has been prepared by further functionalisation of a polyyne rotaxane. The macrocycle's protective effect means a fragile hexayne can remain intact in a strongly acidic reaction mixture. This molecule is very large and is characterised conclusively by ^{1}H NMR, ^{13}C NMR, MALDI mass spectrometry, UV-vis spectrometry and single crystal X-ray crystallography.

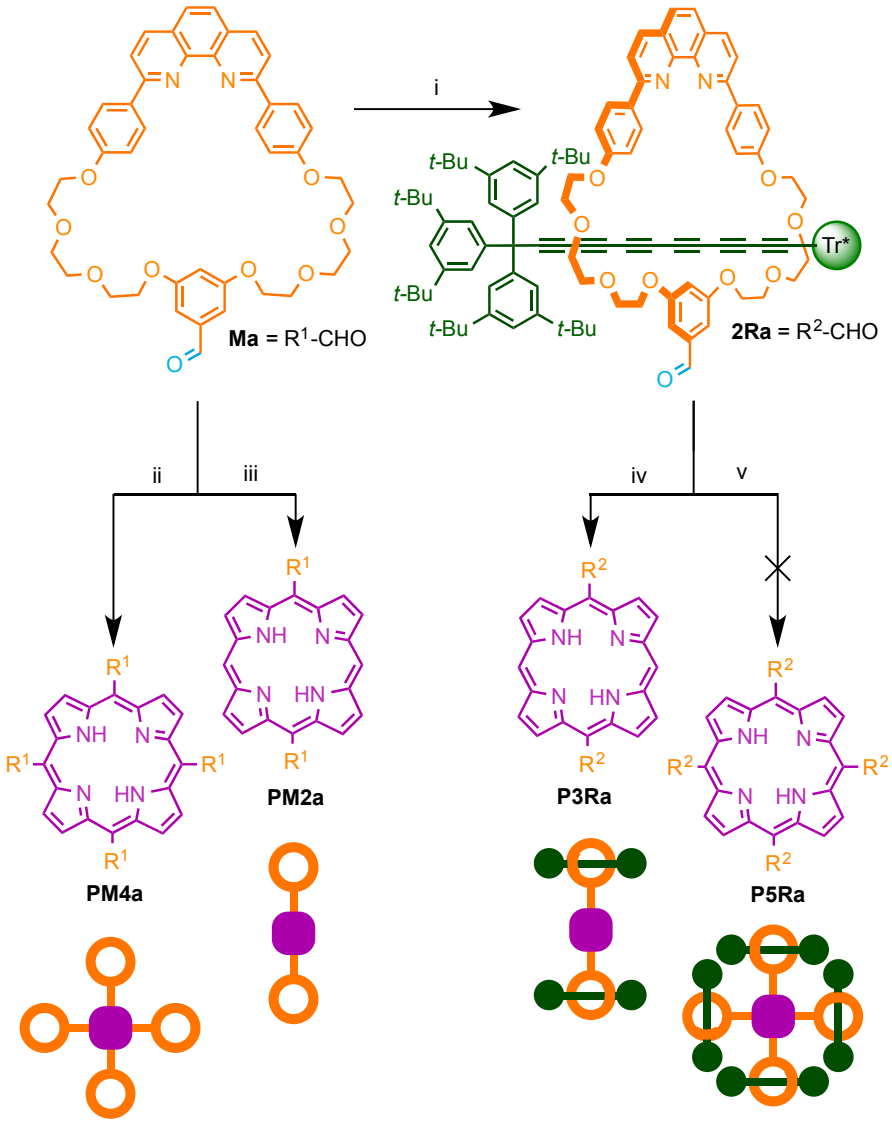

Scheme 2.5. Porphyrin formation from **Ma** and **2Ra**. i) a) CuI, CH_2Cl_2, MeCN, 30 min, 25 °C b) triyne **2.10**, bromotriyne **2.11**, K_2CO_3, THF, 60 °C, 2 d, 58%. ii) Pyrrole, Nitrobenzene, propionic acid, microwave irradiation, 140 °C, 15 min, 24%. iii) a) Dipyrromethane, TFA, CH_2Cl_2, 25 °C, 1 h b) DDQ, 25 °C, 3 h, 18%. iv) Dipyrromethane, TFA, CH_2Cl_2, 25 °C, 1 h b) DDQ, 25 °C, 3 h, 62%. v) Various conditions, 0%.

Protons could be clearly assigned *via* ^{1}H NMR from their original shifts in macrocycle **Ma**, to rotaxanes **2Ra** and **Zn-P3Ra**. In rotaxane **2Ra** the protons from the hexayne's supertrityl stopper are clearly visible and integrate correctly in the aromatic region. There is a marked shift of the proton signals in the phenanthroline macrocycle upon threading. This has been observed previously in polyyne rotaxanes.[9,12] The anisotropic effect of the polyyne causes a shift in the local magnetic field of nearby protons in rotaxane **2Ra**. This shift is particularly pronounced in protons *i* and *j*, which could suggest the hexayne sits close to this phenyl ring. It is

also possible that the aromatic ring currents from the supertrityl group could be influencing macrocycle protons from an anisotropic effect (**Figure 2.5)**.

In **P3Ra** there are also clear shifts in the ^{1}H NMR spectrum. All protons are shifted downfield in comparison to **Ma**, which could be caused by ring currents in the aromatic porphyrin. Once again, the most pronounced changes are seen in protons *i* and *j*, which could suggest a significant change in conformation in order to prevent a steric clash. The porphyrin protons are also highly characteristic. Protons *a* are highly deshielded due to their position on the outside of an aromatic ring current. Protons *b* and *c* are coupled and appear as two doublets. These signals were assigned by observing an NOE between protons *c* and *j*. (**Figure 2.5**).

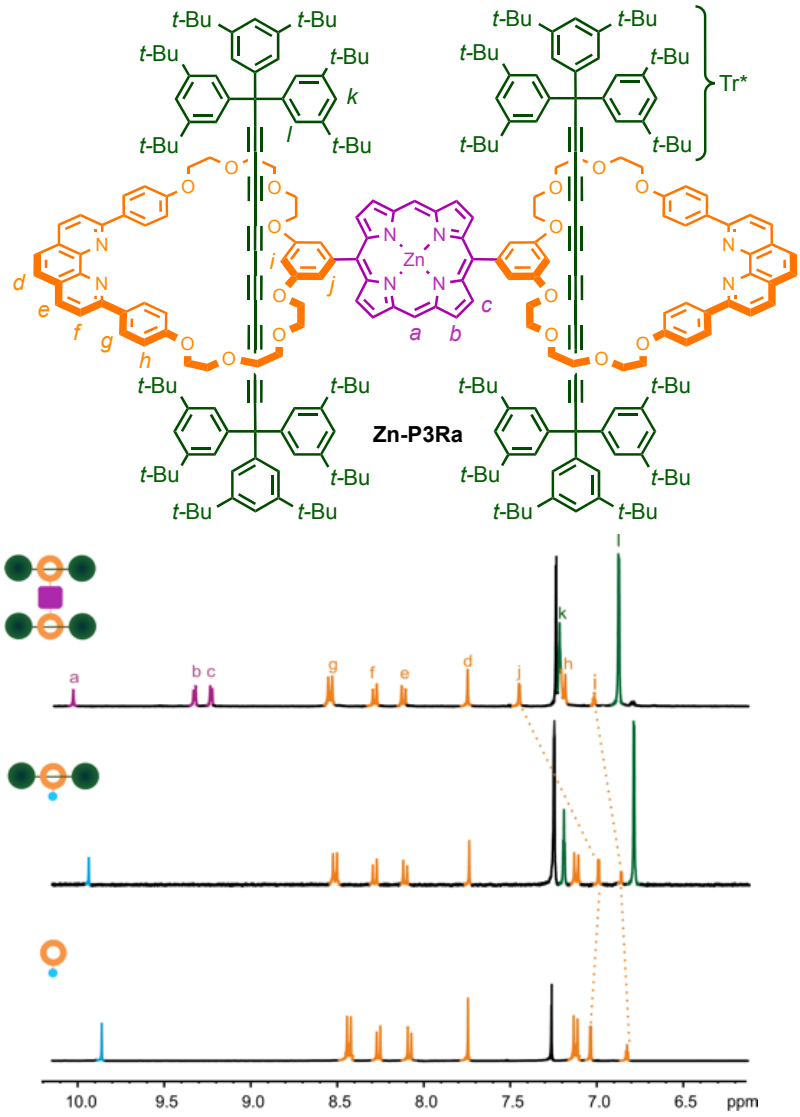

Figure 2.5. ^{1}H NMR of **Ma**, **2Ra** and **Zn-P3Ra** ($CDCl_3$, 500 MHz, 298 K).

Crystals of [3]rotaxane **Zn-P3Ra** were grown by diffusion of methanol vapour into a solution in chloroform and analysed by single crystal X-ray diffraction. Diffraction data were collected with synchrotron radiation using I19 (EH1) at Diamond Light Source ($\lambda = 0.6889$ Å[35]). Cell parameters were determined and refined and raw frame data were integrated using CrysAlisPro (Agilent Technologies, 2010) by Amber L. Thompson.

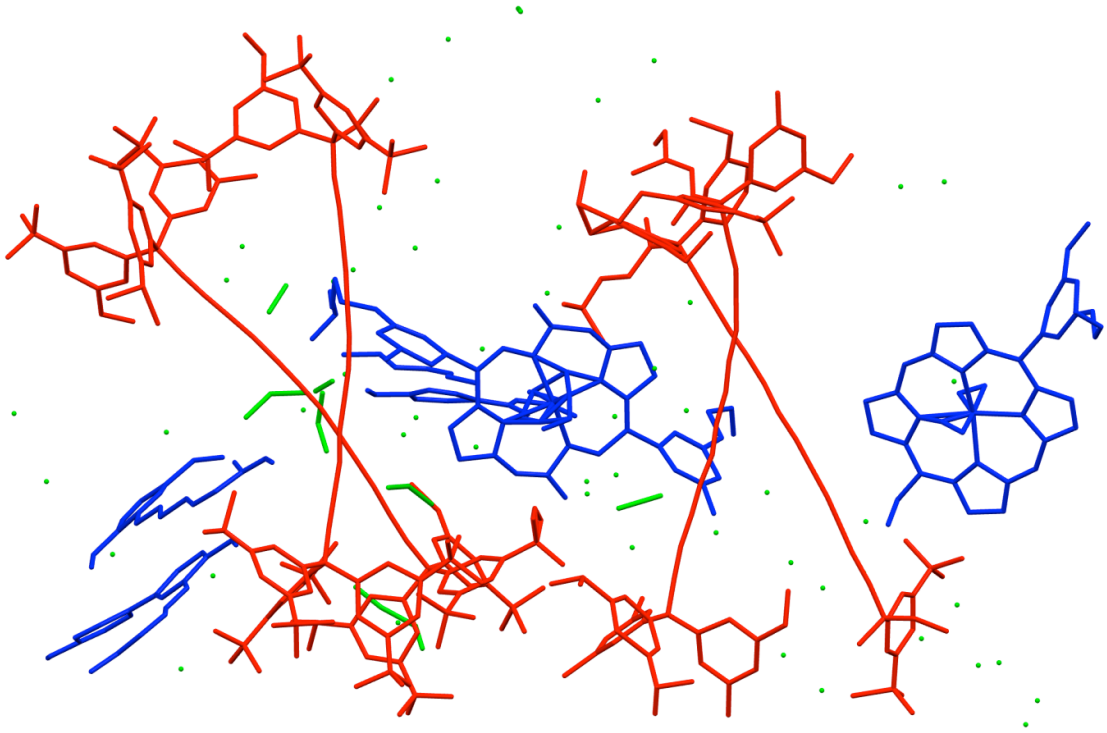

Figure 2.6. The structure as solved using charge-flipping: the threads are clearly visible (shown in red), as are parts of the macrocycle (in blue). However, there are many unconnected atoms (in green) and missing atoms.

The structure was solved with SuperFlip[36] by Amber L. Thompson, but was incomplete. Atoms were missing – particularly from the oligoethyleneglycol chains and the tertiary butyl groups of the stoppers (**Figure 2.6**). Fourier refinement and examination of the difference Fourier maps using CRYSTALS[37,38] revealed the location of many of the missing atoms. However, the poor resolution of the data and the fact that atoms in these regions were poorly resolved (due to disorder) meant that the location of some of these atoms had to be inferred. Distance, angle and thermal restraints were applied to ensure the geometry and displacement ellipsoids remained sensible on refinement, and efforts were made to model the disorder in the oligoethyleneglycol chains. The difference maps indicated the presence of diffuse

electron density in the void spaces, believed to be disordered solvent. The discrete Fourier transform of the void region were treated as contributions to the A and B parts of the calculated structure factors using PLATON/SQUEEZE,[39,40] effectively leaving voids from which the electron density had been removed (**Figure 2.7**).

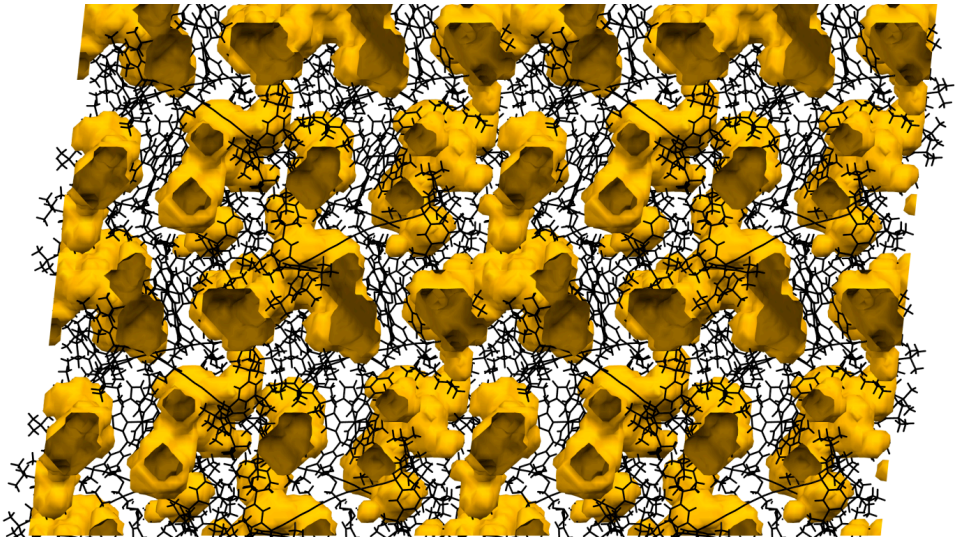

Figure 2.7. The structure is shown in black with the voids, which occupy approximately 20% of the unit cell shown in yellow.

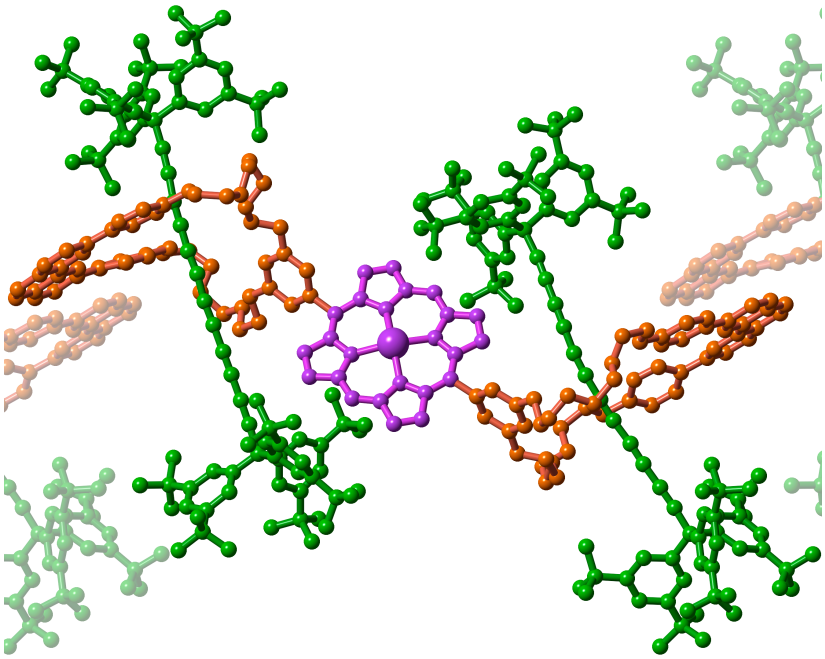

Figure 2.8. A projection of the solid-state structure of the [3]rotaxane **Zn-P3Ra** from X-ray crystallography. This figure only shows one of the two molecules in the asymmetric unit (coordinated methanol and hydrogen atoms omitted for clarity).

The crystal structure has two molecules of **Zn-P3Ra** in the asymmetric unit (**Figure 2.8**). Both rotaxane molecules have similar conformations with methanol

coordinated to the zinc centres. The phenanthroline units of each rotaxane form intermolecular π-stacked dimers with crystallographically equivalent rotaxanes, forming infinite strands of interactions (**Figure 2.8**). The oligoethyleneglycol chains of the macrocycles adopt compact conformations and are mostly gauche (O-CH_2CH_2-O torsional angle 40–80°) with the polyyne chains held close to the porphyrin units. Thus all four polyyne chains make close van der Waals contacts with the β-pyrrole protons of the porphyrins (*sp*-C···H distance: 2.9–3.1 Å). The four hexayne chains have slightly curved geometries, similar to those reported in crystal structures of other polyynes.[9,12,23,41,42]

2.4 - Synthesis of porphyrin-polyyne [5]rotaxane **P5Rb**

We concluded in **Section 2.3** that the primary reason we could not synthesise porphyrin [5]rotaxane **P5Ra** was because of steric interactions between the bulky supertrityl groups. We decided to synthesise elongated aldehyde-substituted macrocycle **Mb** to try and realise the direct formation of **P5Rb**. Increasing the distance between the hub and the macrocycles could allow the dumbbells to adopt a more relaxed conformation. We synthesised a macrocyclic aryl bromide **2.16** and then performed a Suzuki coupling to yield macrocyclic aldehyde **Mb (Scheme 2.6).**

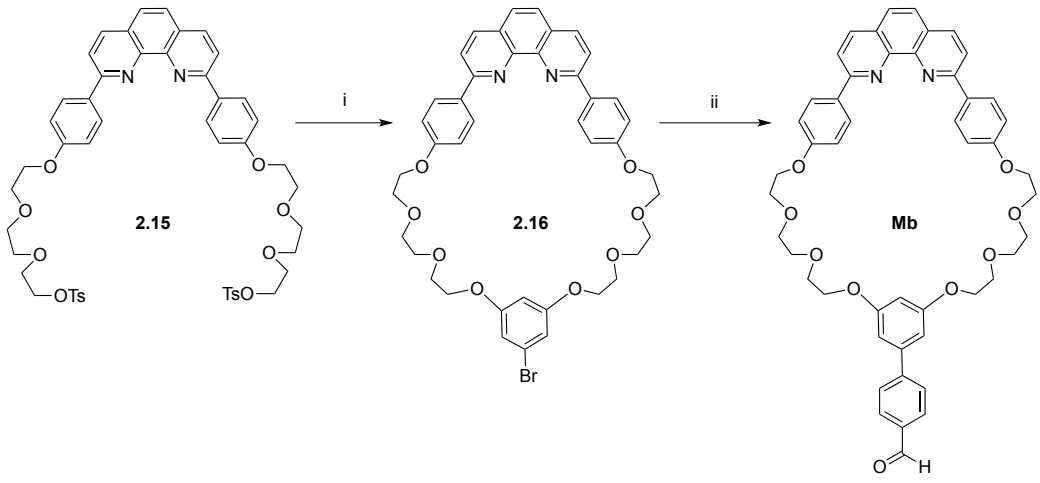

Scheme 2.6. Synthesis of Macrocycle **Mb**. i) 3,5-Dihydroxybenzaldehyde, Cs_2CO_3, DMF, 60 °C, 24 h, 68% ii) 4-(4,4,5,5-tetramethyl-1,3,2-dioxaborolan-2-yl)benzaldehyde, $PdCl_2$(dppf) (0.05 equiv.), Na_2CO_3, THF:H_2O 2:1, 80 °C, 20 h, 93%.

Active metal template Cadiot-Chodkiewicz coupling of supertrityl triyne **2.10** and bromotriyne **2.11** in the presence of the copper(I) complex of **Mb** gave the [2]rotaxane aldehyde **2Rb** in 50% yield (**Scheme 2.7)**. A wide variety of conditions

were tested for the reaction of **2Rb** with pyrrole in attempts to prepare porphyrin [5]rotaxane **P5Rb**; stirring **2Rb** in CH_2Cl_2 with freshly distilled pyrrole and TFA and subsequent oxidation with DDQ gave desired porphyrin [5]rotaxane **P5Rb** in fairly low yield. Additionally, reaction of the [2]rotaxane aldehyde **2Rb** with dipyrromethane gave the porphyrin [3]rotaxane **P3Rb** in 33% yield. The elongation of the macrocycle has provided sufficient steric relief to synthesise the porphyrin, but not enough relief to synthesise the desired compound in a good yield.

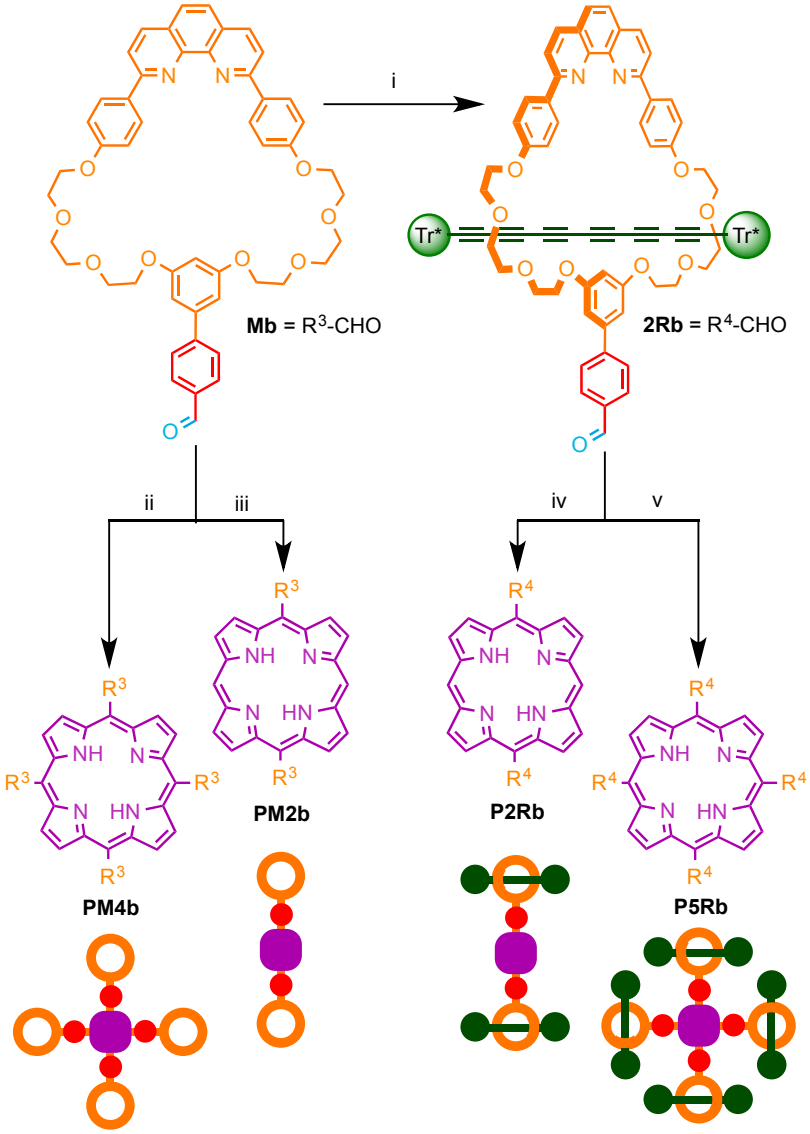

Scheme 2.7. Porphyrin formation from macrocycle **Mb** and rotaxane **2Rb**. i) a) CuI, CH_2Cl_2, MeCN, 25 °C, 30 min, b) triyne **2.10**, bromotriyne **2.11**, K_2CO_3, THF, 60 °C, 2 d, 50% ii) Pyrrole, nitrobenzene, propionic acid, 140 °C, 15 min, microwave irradiation, 12% iii) Dipyrromethane, TFA, CH_2Cl_2, 25 °C, 1 h b) DDQ, 25 °C, 3 h, 31% iv) Dipyrromethane, TFA, CH_2Cl_2, 25 °C, 1 h b) DDQ, 25 °C, 3 h, 33% v) a) Pyrrole, TFA, CH_2Cl_2, 25 °C, 1 h b) DDQ, 25 °C, 3 h, 10%.

All free base porphyrins **PM2b**, **PM4b** and **P3Rb, P5Rb** were immediately metallated with $Zn(OAc)_2$ in $CHCl_3$/MeOH at 60 °C. Metallation often made purification more facile. Porphyrin [3]rotaxane **P5Ra** is the first ever polyyne [5]rotaxane. The hexaynes are arranged around the central hub in a cyclic shape. This molecule is very large and is characterised conclusively by ^{1}H NMR (**Figure 2.9**), ^{13}C NMR, MALDI mass spectrometry and UV-vis spectrometry.

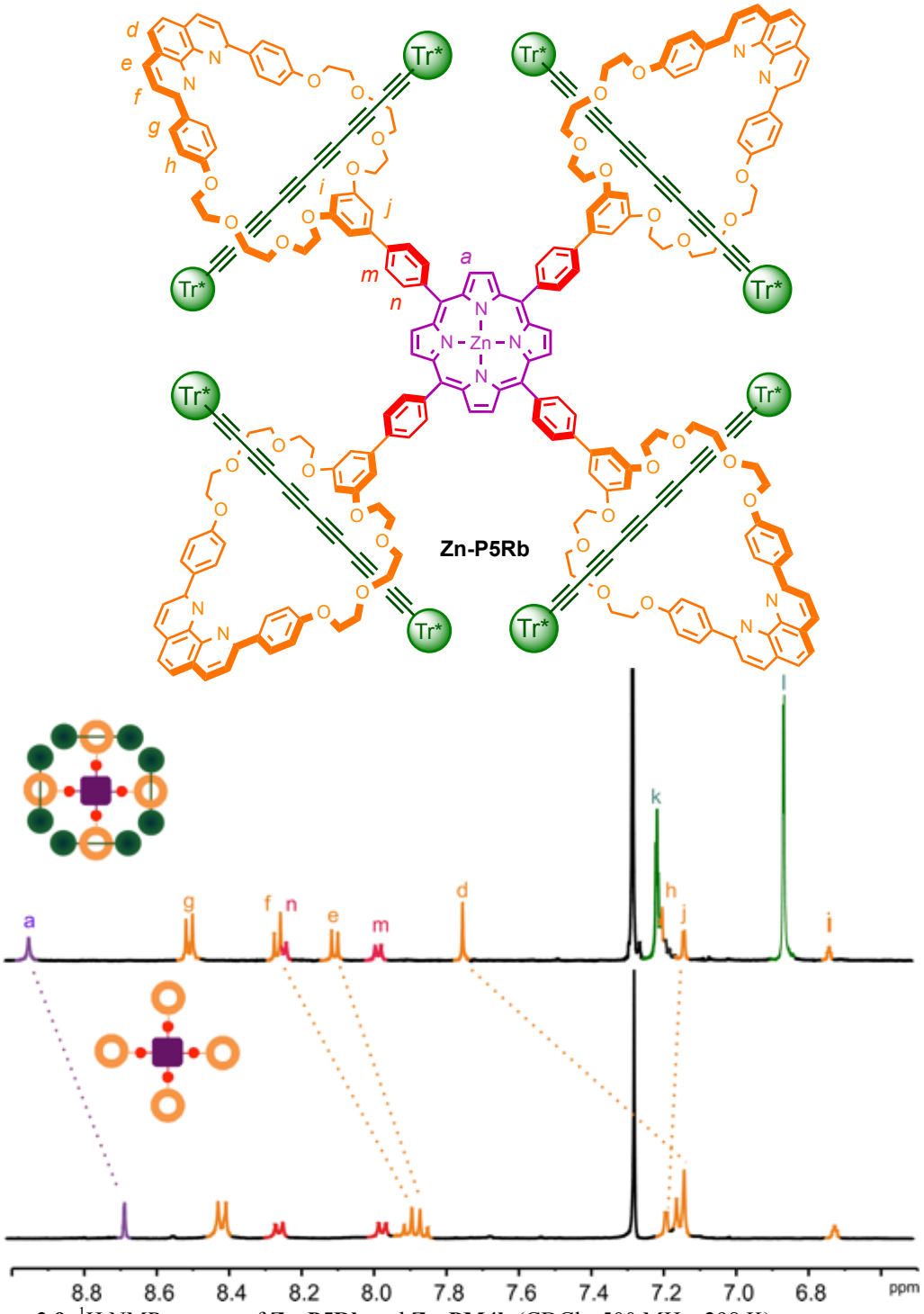

Figure 2.9. ^{1}H NMR spectra of **Zn-P5Rb** and **Zn-PM4b** ($CDCl_3$, 500 MHz, 298 K).

In **Section 2.3** we observed the marked effect of rotaxanation and conformational change on chemical shift. In **Figure 2.9** these pronounced changes in chemical shift that threading in **Zn-P5Rb** causes are revealed. In rotaxane **Zn-P5Rb** the protons from the hexayne's supertrityl stopper are clearly visible and integrate correctly in the aromatic region. There is a marked shift in protons in the phenanthroline macrocycle upon threading. This has been observed previously in polyyne rotaxanes.[9,12] It is interesting to note that the protons that are most affected by threading are quite different in this example to **Zn-P3Ra**. Proton *d* shows an extremely large downfield shift upon threading, protons *e* and *f* are also changed notably. This suggests that the hexayne may be positioned more closely to this part of the macrocycle. This would be a logical observation as the molecule is highly sterically congested and the dumbbells are likely to need to get as far from one another as possible.

We also performed NOE experiments to attempt to gain further insight into the conformation of **Zn-P5Rb**. The NOE experiment provided assignment for the protons *m* and *n* from the additional phenyl linker. Protons *n* showed a strong correlation with protons *a*. However, conformational information was difficult to infer from the spectrum. We had hoped to see NOE correlations between protons *k* and *l* from the supertrityl group and phenanthroline protons, but did not observe any. Additionally, there were no well-defined NOE correlations from the tertiary-butyl groups. Despite our best efforts, we could not grow single crystals of this compound to confirm our conformational hypothesis. Nonetheless, our characterisation is still conclusive.

2.5 - Photophysical studies

The family of rotaxanes synthesised during this study provides a unique opportunity to investigate photophysical interactions between the excited states of polyyne and porphyrin chromophores. The photophysical behavior of polyynes is particularly interesting because their absorption spectra are dominated by strong transitions to higher excited states at 280–320 nm ($S_0 \rightarrow S_n$, $\varepsilon \approx 3 \times 10^5$ M^{-1} cm^{-1}); absorption into the first excited state is dipole-forbidden and can occasionally be observed as a very weak band at 350-450 nm ($S_0 \rightarrow S_1$, $\varepsilon \approx 500$ M^{-1} cm^{-1}).[23,24] We hope that excited state energy transfer (EET) will allow us to observe luminescence despite the remarkably

fast intersystem crossing ($S_1 \rightarrow T_1$), which usually prevents observation of fluorescence from polyynes. We previously observed the polyyne acting as a sink for excited state energy.[23] In this study we hope to investigate whether polyynes can act as a donor of excited state energy.

2.5.1 - Absorption and emission spectra

A Perkin-Elmer Lambda 25 UV-vis spectrometer was used to record absorption spectra in the range 250–600 nm in CH_2Cl_2. Molar absorption coefficients were measured by taking three samples of different concentrations; each sample was made by weighing out approximately 1 mg of the compound with an accuracy of ±0.01 mg.

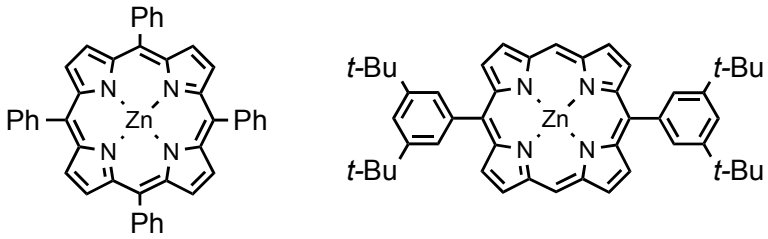

Figure 2.10. Model porphyrin compounds **Zn-TPP** and **Zn-TBP**.

A Fluoromax LS55 was used to record emission and excitation spectra. The reference compounds **Zn-TPP** and **Zn-TBP** were used to estimate the absorption contribution of the porphyrin component of the more complex synthesised diaryl and tetraaryl porphyrins. First, all compounds were excited at the Soret band to record emission spectra. The concentrations of the samples used to measure emission and excitation spectra were adjusted to give a peak optical density of 0.1 to avoid intermolecular fluorescence quenching, reabsorption effects and saturation of the detector.

The absorption spectra of rotaxanes **Zn-P3Ra**, **Zn-P3Rb** and **Zn-P5Rb** demonstrate that threading causes very little perturbation to the electronic structure of the component chromophores, this observation was also made in previous studies of polyyne rotaxanes.[9,12] Thus, the absorption bands of the polyyne (280–320 nm), the phenanthroline macrocycle (250–380 nm) and porphyrin (400–450 nm Soret band and 530–560 nm Q band) are readily identified in the rotaxanes (**Figure 2.11**, **Figure 2.12**, **Figure 2.13**).

Comparison with simple reference porphyrin derivatives *meso*-tetraphenyl porphyrin (**Zn-TPP**) for **Zn-P5Rb** and **Zn-PM4a**; 5,15-diaryl porphyrin (**Zn-TBP**) for **Zn-P3Ra**, **Zn-P3Rb**, **Zn-PM2a** and **Zn-PM2b**) shows that the polyyne and phenanthroline-macrocycle units have no effect on the fluorescence quantum yield, measured on excitation of the porphyrin Soret band at around 415 nm (**Table 2.1**). This demonstrates that there is no significant energy migration from the porphyrin to the polyyne or to the macrocycle. This is expected as previous reports suggest the excited states of the polyyne and the macrocycle are higher in energy than the porphyrin's S_2 state. Additionally, the emission bands adopt a similar shape in all comparable compounds.

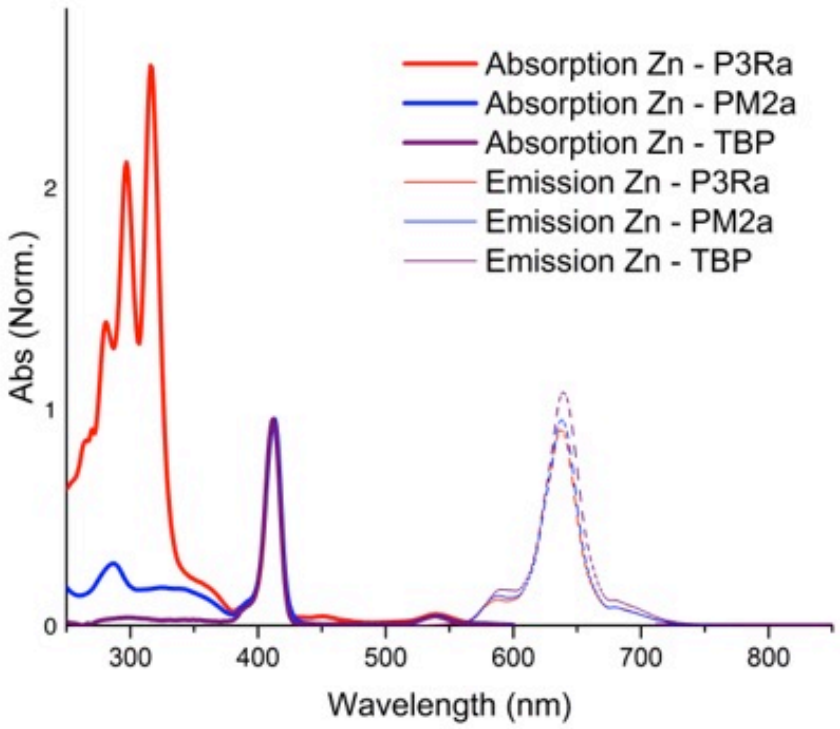

Figure 2.11. Absorption and emission spectra of **Zn-P3Ra**, **Zn-PM2a**, **Zn-TBP** (absorption normalised at the Soret band; emission on arbitrary vertical scale; solvent: CH_2Cl_2, 298K).

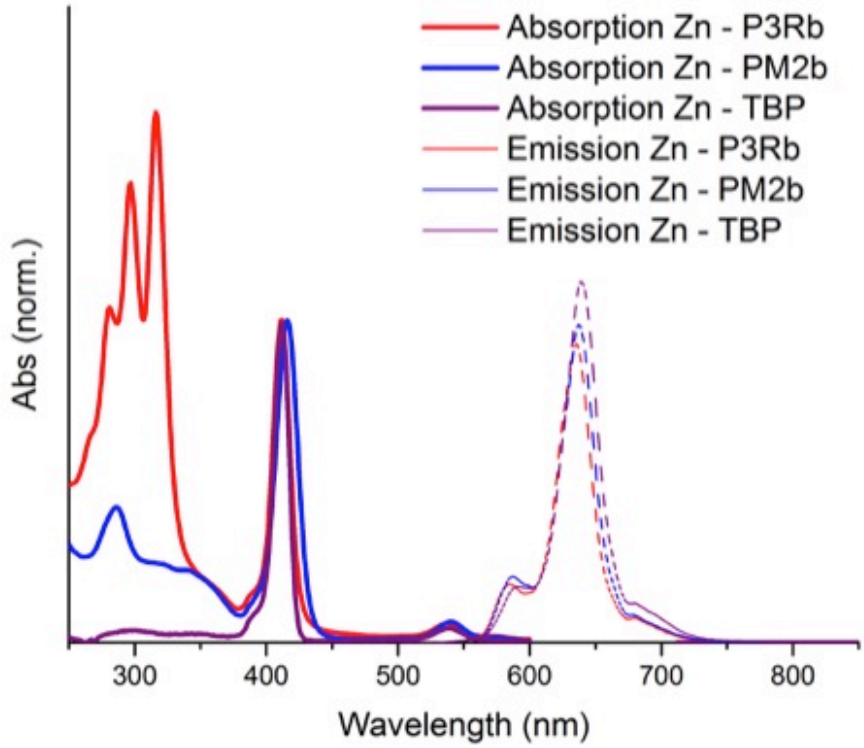

Figure 2.12. Absorption and emission spectra of **Zn-P3Rb**, **Zn-PM2b**, **Zn-TBP** (absorption normalised at the Soret band; emission on arbitrary vertical scale; solvent: CH_2Cl_2, 298K).

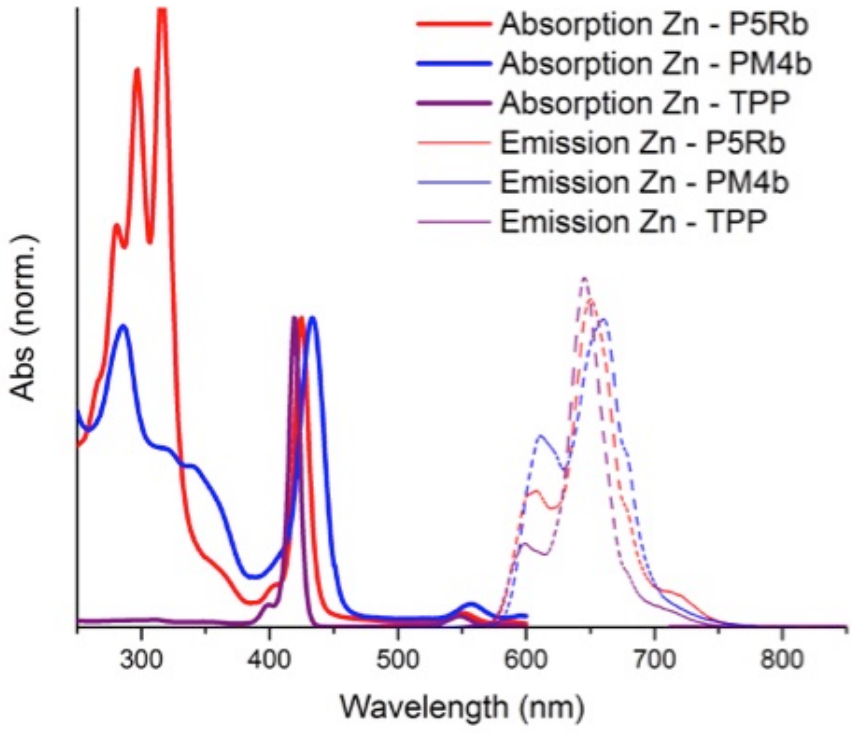

Figure 2.13. Absorption and emission spectra of **Zn-P5Rb**, **Zn-PM4b**, **Zn-TPP** (absorption normalised at the Soret band; emission on arbitrary vertical scale; solvent: CH_2Cl_2, 298K).

Compound	ϕ_X
Zn-TPP	0.030[43]
Zn-P5Rb	0.038
Zn-PM4b	0.041
Zn-TBP	0.021[44]
Zn-P3Ra	0.017
Zn-PM2a	0.018
Zn-P3Rb	0.017
Zn-PM2b	0.017

Table 2.1. Fluorescence quantum yields measured in air-saturated CH_2Cl_2 for excitation at the peak of the Soret band (λ_{max} for each compound, about 415 nm) using Zn-TPP and Zn-TBP as standards.[43,44]

$$\Phi_X = \Phi_{ST}\left(\frac{Grad_X}{Grad_{ST}}\right)\left(\frac{\eta_X^2}{\eta_{ST}^2}\right)$$

Equation 2.1. X = sample, ST = standard, Φ = Quantum yield of sample, Grad = gradient of fluorescence integral, η = refractive index.

Equation 2.1 was used experimentally to determine the quantum yields reported in **Table 2.1**. The right hand bracket corrects for different refractive indices of solvents. The left hand term is comparing the gradients of the straight line obtained for the sample and the standard in order to determine the value for the sample. The standard used was **Zn-TPP**.

2.5.2 - Absorption and excitation spectra

Fluorescence excitation spectra of the porphyrin rotaxanes, measured by recording emission from the porphyrin Q-band at around 640 nm, show clear features from excitation into the polyyne and phenanthroline macrocycle components, as illustrated for **Zn-P3Ra** and **Zn-PM2a** (**Figure 2.14a**), indicating that both these chromophores

transfer energy to the porphyrin. The excited state energy transfer processes that have been observed in these experiments are illustrated in a Jablonski diagram **(Figure 2.14b)**. A detailed examination of the absorption spectra, fluorescence spectra and excitation spectra of the whole family of compounds allowed us to determine the quantum yields of excited state energy transfer (EET) from the polyyne to the porphyrin, and from the phenanthroline macrocycle to the porphyrin (**Table 2.2**), this methodology is explained further in **Section 2.5.3** and **Section 2.5.4**.

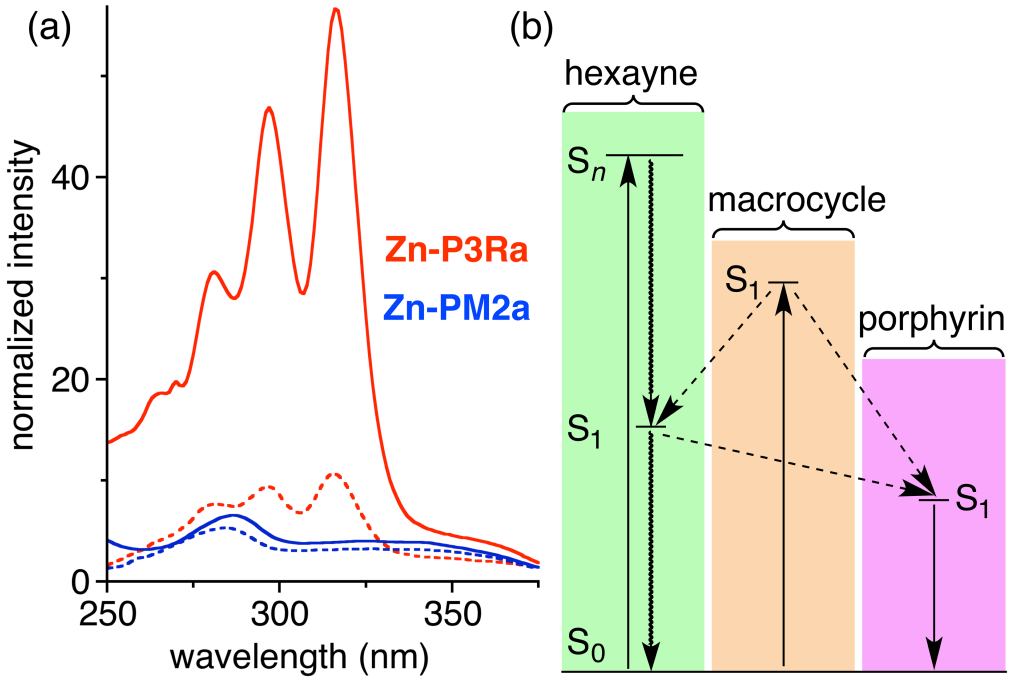

Figure 2.14. (a) Absorption spectra (continuous line) and excitation spectra (dashed line) of **Zn-P3Ra** (red) and **Zn-PM2a** (blue); the spectral intensities are normalised to 1.0 at the Q-band and the excitation spectra are recorded for emission at 639 nm (porphyrin Q-band); solvent: CH_2Cl_2. (b) Jablonski diagram showing the energy transfer processes.

2.5.3 -Methodology for determining EET, analysis of absorption spectra

To facilitate the comparison of the absorption spectra of **Zn-PM4a**, **Zn-PM2a**, **Zn-P3Ra**, **Zn-PM4b**, **Zn-PM2b**, **Zn-P3Rb** and **Zn-P5Rb**, all these spectra, and those of **Zn-TPP** and **Zn-TBP**, were normalised to a value of 1.0 at the Q-band maximum (at around 550 nm). Comparison of the absorption spectra of this family of compounds shows that there is only weak ground-state electronic coupling between the three types of connected chromophore units: the polyyne, the phenanthroline and the porphyrin; i.e. the absorption bands due to the polyyne at around 300 nm are

essentially identical in **Zn-P3Ra**, **Zn-P3Rb** and **Zn-P5Rb**; the absorption bands due to the phenanthroline at around 275–375 nm are essentially identical in **Zn-PM4a**, **Zn-PM2a**, **Zn-P3Ra**, **Zn-PM4b**, **Zn-PM2b, Zn-P3Rb** and **Zn-P5Rb**; the absorption bands due to the porphyrin at around 410 nm and 540 nm in **Zn-PM4b** and **Zn-P5Rb** closely resemble those of **Zn-TPP**; the absorption bands due to the porphyrin at around 410 nm and 540 nm in **Zn-PM2a**, **Zn-P3Ra**, **Zn-PM2b** and **Zn-P3Rb** closely resemble those of **Zn-TBP**. Thus the absorption spectrum of the polyyne component can be calculated in three ways:

(a) Subtraction of the absorption spectrum of **Zn-PM4b** from that of **Zn-P5Rb**.
(b) Subtraction of the absorption spectrum of **Zn-PM2b** from that of **Zn-P3Rb**.
(c) Subtraction of the absorption spectrum of **Zn-PM2a** from that of **Zn-P3Ra**.

These three difference-spectra are compared with the absorption spectrum of the isolated hexayne dumbbell Tr*-C_{12}-Tr* in **Figure 2.15**. This subtraction demonstrates that the absorption spectra of the macrocycle, porphyrin and polyyne components are essentially identical in these compounds. A bathochromic shift of 2 nm is observed in all of the polyyne vibronic bands in the rotaxanes, in comparison to free Tr*C_{12}Tr*, this has been consistently observed in other polyyne rotaxanes.[12] All of these experiments confirm the validity of our approach to attributing components of absorption to different parts of the molecule. Similarly the absorption spectrum of the phenanthroline component can be calculated by:

(a) Subtraction of the absorption spectrum of **Zn-TPP** from that of **Zn-PM4a**.
(b) Subtraction of the absorption spectrum of **Zn-TBP** from that of **Zn-PM2a**.
(c) Subtraction of the absorption spectrum of **Zn-TPP** from that of **Zn-PM4b**.
(d) Subtraction of the absorption spectrum of **Zn-TBP** from that of **Zn-PM2b**.

These four difference-spectra are compared with the absorption spectra of **Ma** and **Mb** in **Figure 2.16**, showing that the absorption spectra of the macrocycle are essentially identical in all these complexes. These absorption spectra demonstrate that it is valid to split the absorption and excitation into components originating individually from each type of chromophore.

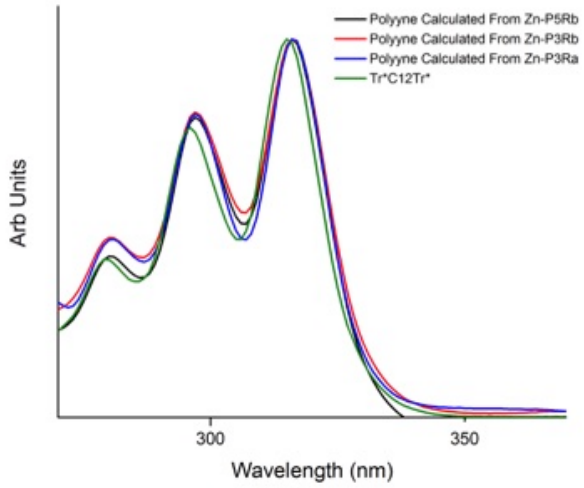

Figure 2.15. Calculation of the polyyne contribution to absorbance of different porphyrin rotaxanes and free Tr*C_{12}Tr* dumbbell. Normalised at maximum intensity (solvent: CH_2Cl_2).

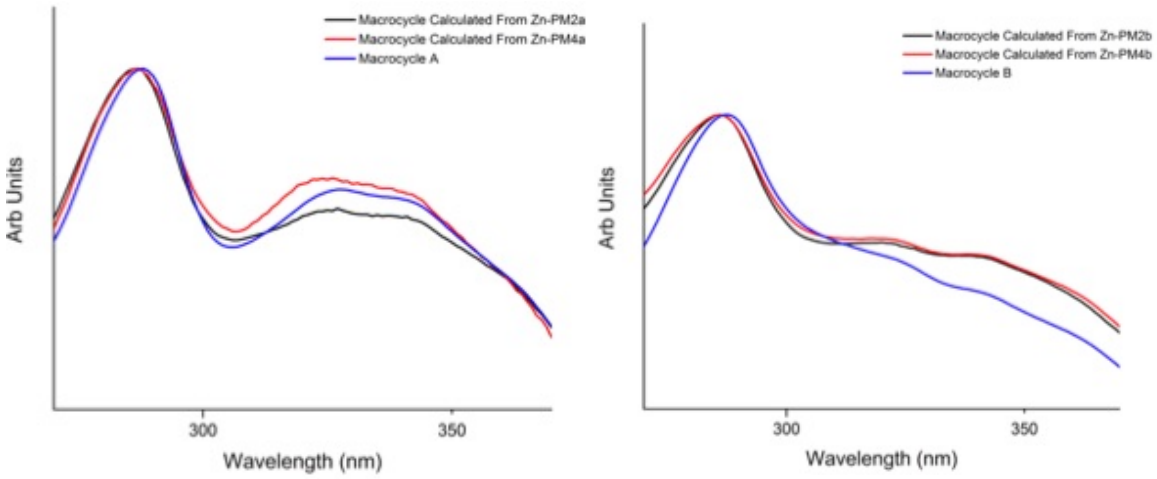

Figure 2.16. Calculation of the macrocycle contribution to the absorption spectra of different macrocycle-substituted compounds. Left: normalised absorptions of the macrocycle components in **Zn-PM2a** and **Zn-PM4a** compared with the UV spectrum of macrocycle **Ma**. Right: normalised absorptions of the macrocycle components in **Zn-PM2b** and **Zn-PM4b** compared with the UV spectrum of macrocycle **Mb** (solvent: CH_2Cl_2).

Figure 2.17 demonstrates that this approach can be used to resolve the complex absorption of porphyrin[5]rotaxane **P5Rb** into its components. This approach will become particularly important when considering excitation spectra (**Section 2.5.4**). The same type of analysis was performed for **Zn-PM4a**, **Zn-PM2a**, **Zn-P3Ra**, **Zn-PM4b**, **Zn-PM2b** and **Zn-P3Rb**.

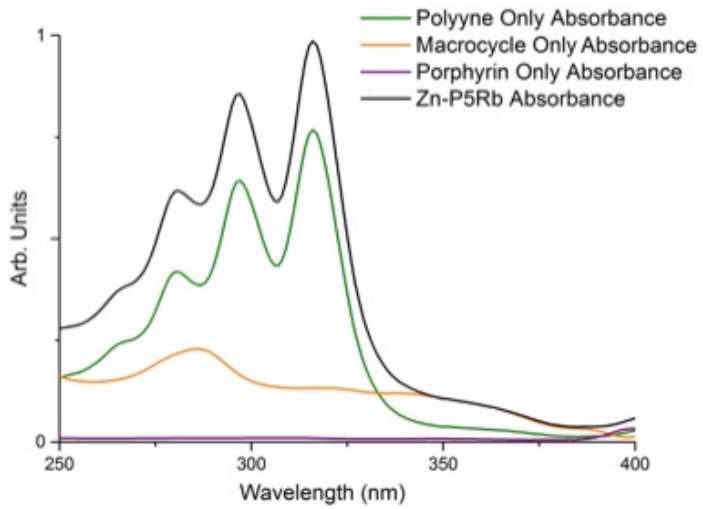

Figure 2.17. Resolution of the UV absorption spectrum of **Zn-P5Rb** into three components (solvent: CH_2Cl_2).

2.5.4 -Methodology for determining EET, analysis of excitation spectra

To facilitate the analysis of the absorption and excitation spectra of **Zn-PM4a**, **Zn-PM2a**, **Zn-P3Ra**, **Zn-PM4b**, **Zn-PM2b**, **Zn-P3Rb** and **Zn-P5Rb**, all these spectra, and those of **Zn-TPP** and **Zn-TBP**, were normalised to a value of 1.0 at the Q-band maximum (at around 550 nm).

We assume that direct excitation of the Q-band of each porphyrin derivative generates the S_1 excited state of the porphyrin unit with 100% efficiency. Thus if the excitation spectrum of a given compound is divided by its absorption spectrum, then the value of the normalised excitation/absorption spectrum at any wavelength provides an estimate of the efficiency with which excitation at that wavelength generates the S_1 excited state of the porphyrin unit. The interaction between the chromophore components is weak in the ground state (as demonstrated above), but the interaction between the components is stronger in the excited states, which makes it more complicated to calculate of the EET efficiency from a specific component of the molecule, because one component can affect the EET efficiency of another component. This means that we need to split the contributions of the components to the excitation spectra, as discussed above for absorption spectra.

Comparison of the excitation spectra of **Zn-P5Rb** and **Zn-PM4b** (**Figure 2.18**) illustrates the fact that the effect of one component on another cannot be ignored.

These excitation spectra would be identical at 350 nm if the components acted independently, as the polyyne component has negligible absorption at this wavelength. However the excitation spectra (normalised at the Q-band) have very different intensities at 350 nm. The excitation spectrum of the rotaxane (**Zn-P5Rb**) is less intense than that of the polyyne-free compound (**Zn-PM4b**) because of the quenching effect of the polyyne. The absorption and excitation spectra of **Zn-P5Rb**, **Zn-PM4b** and **Zn-TPP** (normalised at the Q band) are compared in **Figure 2.19a).**

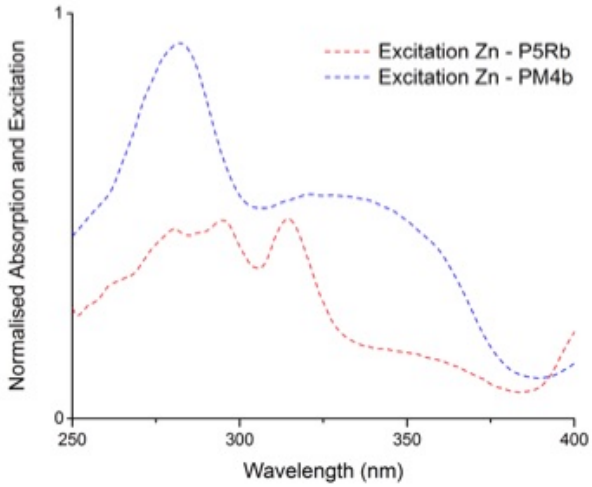

Figure 2.18. Comparison of excitation spectra of **Zn-P5Rb** and **Zn-PM4b** (normalised at the Q band; solvent: CH_2Cl_2)

The absorption coefficient of **Zn-TPP** is negligible compared to those of **Zn-P5Rb** and **Zn-PM4b** in the wavelength range 250–375 nm (**Figures 2.13**, **2.17** and **2.19a**), which leads to the following two conclusions:

(a) The intensity of the excitation spectrum of **Zn-PM4b** in this region (250–375 nm) can be attributed entirely to fluorescence originating from absorption by the phenanthroline macrocycle followed by energy transfer to the porphyrin.

(b) The intensity of the excitation spectrum of **Zn-P5Rb** in this region can be attributed to two components:

(i) fluorescence originating from absorption by the phenanthroline macrocycle followed by energy transfer to the porphyrin

(ii) fluorescence originating from absorption by the polyyne followed by energy transfer to the porphyrin

The absorption coefficient of the polyyne (and isolated Tr*C_{12}Tr* hexayne) is negligible compared to those of **Zn-P5Rb** and **Zn-PM4b** in the wavelength range 350–400 nm (**Figures 2.15** and **2.17**). Thus the excitation spectrum of **Zn-P5Rb** in

this region (350–400 nm) is entirely caused by fluorescence originating from absorption by the phenanthroline macrocycle followed by energy transfer to the porphyrin, in competition with energy transfer to the polyyne. We assume that the ratio of energy transfer macrocycle → porphyrin and energy transfer macrocycle → polyyne is constant across the wavelength region 250–375 nm. A scaling factor was calculated by dividing the value of excitation spectrum intensity for **Zn-P5Rb** at 350 nm by that of **Zn-PM4b.** The excitation spectrum of **Zn-PM4b** was multiplied by this scaling factor to give a new spectrum for the macrocycle contribution to the excitation spectrum of **Zn-P5Rb** (**Figure 2.19b**). The area under this curve is marked "*macrocycle*" in **Figure 2.19b**; this area represents the contribution of the macrocycle to the excitation spectrum of **Zn-PM4b**. Subtraction of this area "*macrocycle*" from the excitation spectrum of **Zn-P5Rb** yields the area marked "*polyyne*", which is attributed to polyyne → porphyrin energy transfer.

Quantum yields for excited-state energy transfer (EET) were calculated from the ratios of excitation spectra divided by absorption spectra, for macrocycle-specific or polyyne-specific spectral components, according to **Equations 2.2** and **2.3**, after dissecting absorption and excitation spectra as described in **Section 2.5.3** and **Section 2.5.4** respectively. Excitation/absorption rations were integrated across the absorption bands: 275–375 nm in **Zn-PM2a**, **Zn-PM2b** and **Zn-PM4b**; 350–370 nm for ϕ_{EET} (macrocycle → porph) in **Zn-P3Ra**, **Zn-P3Rb** and **Zn-P5Rb** and 280–330 nm for ϕ_{EET} (polyyne → porph) in **Zn-P3Ra**, **Zn-P3Rb** and **Zn-P5Rb**.

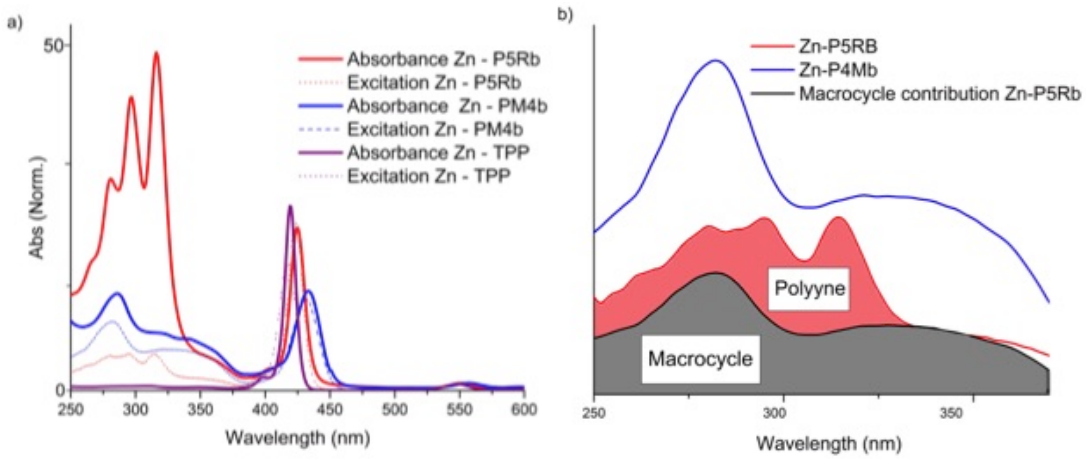

Figure 2.19. (a) Absorption and excitation spectra of **Zn-P5Rb**, **Zn-PM4b**, **Zn-TPP** (all spectra normalised at the Q band; solvent: CH_2Cl_2; same data as **Figure 2.13**) and (b) the resolution of **Zn-P5Rb** excitation spectrum into different components (solvent: CH_2Cl_2).

$$\phi_{EET}\ (\text{macrocycle} \rightarrow \text{porph}) = \frac{macrocycle\text{–}specific\ excitation\ intensity}{macrocycle\text{–}specific\ \ absorption\ intensity} \qquad \textbf{Equation 2.2}$$

$$\phi_{EET}\ (\text{polyyne} \rightarrow \text{porph}) = \frac{polyyne\text{–}specific\ excitation\ intensity}{polyyne\text{–}specific\ \ absorption\ intensity} \qquad \textbf{Equation 2.3}$$

Table 2.2. EET efficiency of each component

Compound	ϕ_{EET} (macrocycle → porph)	ϕ_{EET} (polyyne → porph)
Zn-PM2a	0.67 ± 0.08	–
Zn-P3Ra	0.32 ± 0.03	0.16 ± 0.02
Zn-PM2b	0.88 ± 0.11	–
Zn-P3Rb	0.22 ± 0.03	0.10 ± 0.03
Zn-PM4b	0.68 ± 0.06	–
Zn-P5Rb	0.25 ± 0.02	0.09 ± 0.02

There are several key conclusions from this excited state energy transfer data. Firstly, the polyyne quenches the macrocycle's S_1 state, thus diminishing the efficiency of the EET. This is observed by comparing the (macrocycle → porph) EET efficiency in **Zn-PM2a, Zn-P3Ra** and **Zn-PM2b, Zn-P3Rb**.

Secondly, the polyyne can participate in an EET to the porphyrin, this is not very efficient, probably because of the competing formation of a triplet state. This can be observed in all of the porphyrin rotaxanes when an appropriate excitation wavelength is used.

Thirdly, the distance between the components affects the EET (**Zn-P3Ra** has a more efficient EET from the polyyne than the compounds derived from macrocycle **Mb** due to the shorter distance between these components).

2.6 – Conclusions

In conclusion, we have prepared a series of porphyrin-polyyne [3]- and [5]rotaxanes that comprise multiple chromophores in a unique interlocked architecture by condensing aldehyde-[2]rotaxanes with pyrrole or dipyrromethane. The prepared compounds successfully arrange polyynes around a central core for the first time. This

work paves the way for a template-directed synthesis of polycatenane cyclocarbons. Using this approach with a masked alkyne equivalent (MAE) group, the template effect of the central hub could be used to dramatically favour cyclisation.

The crystal structure of a [3]rotaxane shows that the macrocycles adopt compact conformations, holding the hexaynes near the porphyrin core, and that the phenanthroline units form intermolecular π-stacked dimers in the solid. This crystal structure comprises multiple polyyne chains in one structure and demonstrates the different conformations they can adopt, even within one molecule.

An analysis of the absorption, fluorescence and excitation spectra of the rotaxanes reveals three types of energy transfer processes (a) from the phenanthroline macrocycle to the porphyrin, (b) from the phenanthroline macrocycle to the polyyne, and (c) from the polyyne to the porphyrin. The comparison of macrocycle → porphyrin EET efficiencies in the presence and absence of polyyne show that the polyyne acts as a sink for singlet excited state energy from the phenanthroline macrocycle, even though it does not quench the porphyrin.[18] The excited state energy of the macrocycle is split between the porphyrin and the polyyne. The higher efficiency of polyyne→porphyrin EET in [3]rotaxane **Zn-P3Ra**, compared with **Zn-P3Rb** and **Zn-P5Rb**, reflects the shorter polyyne-porphyrin distance. The polyyne → porphyrin EET must be very rapid to compete with intersystem crossing ($\tau \approx 0.5$ ns).[18] Furthermore, the S_1 of the polyyne is a dark state with negligible oscillator strength, so that Förster type energy transfer is expected to be very inefficient, implying that the observed EET occurs via a Dexter mechanism.

2.7 – Experimental data for known compounds

1-(Triisopropylsilyl)-1-propynal – **2.1**[24]

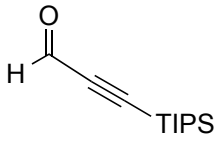

To a stirred solution of TIPS-acetylene (2.00 g, 2.45 mL, 11.0 mmol) in Et_2O (15 mL) at 0 ºC was added *n*-BuLi (4.80 mL, 2.5 M in hexane, 12.1 mmol) dropwise over 5 min. Then dry DMF (2.01 mL, 0.032 mmol) was added at –78 ºC. The reaction mixture was allowed to warm up to 0 ºC over a period of 2 h. The reaction mixture was quenched at 0 °C by pouring it into a solution of water/ice, HCl (aq) (10 %, 15 mL). After stirring for 1 h, the organic phase was separated and the aqueous phase was extracted with Et_2O. The organic layers were combined, dried over $MgSO_4$, filtered and concentrated under reduced pressure. The residual oil was purified by column chromatography (silica, pentane/Et_2O 10:1 → 5:1) to afford aldehyde **2.1** (1.83 g, 79%) as a light yellow oil. R_f = 0.51 (hexanes/CH_2Cl_2 2:1). As in lit.[24]

^{1}H NMR (400 MHz, $CDCl_3$) δ 9.20 (s, 1H), 1.13–1.07 (m, 21H).
^{13}C NMR (100 MHz, $CDCl_3$) δ 176.6, 104.4, 100.8, 18.4, 10.9.

1,3,5-Tri-*tert*-butylbenzene – **2.2**[26]

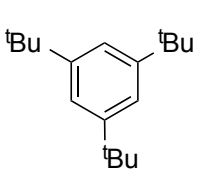

To a mixture of *tert*-butylchloride (207.6 g, 247.0 mL, 2.243 mol) and benzene (17.52 g, 20.00 mL, 0.224 mol) cooled to –40 °C, $AlCl_3$ (14.95 g, 0.112 mol) was added in small portions and the reaction mixture was slowly warmed to –20 °C and stirred for 2 h while keeping the temperature below –10 °C. The reaction was quenched *via* slow addition of a water/ice-mixture (80 mL) at –20 °C. The reaction mixture was warmed to 20 °C and the layers were separated, the organic phase washed with $NaHCO_3$ (aq) (3 × 40 mL), brine (3 × 40 mL), dried over $MgSO_4$ and filtered. The solvent was removed under reduced pressure and the reaction crude was precipitated from cold CH_3OH to yield the product **2.2** as a white solid (42.50 g, 77%). R_f = 0.8 (hexanes). As in lit.[26]

^{1}H NMR (400 MHz, $CDCl_3$) δ 7.42 (s, 3H), 1.50 (s, 27H).
^{13}C NMR (100 MHz, $CDCl_3$) δ 150.1, 119.7, 35.2, 31.8.

1-Bromo-3,5-di-*tert*-butylbenzene – **2.3**[27]

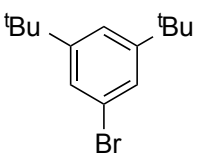

To a solution of 1,3,5-tri-*tert*-butylbenzene **2.2** (34.16 g, 0.1385 mol) in dry $CHCl_3$ (150 mL), Fe powder (9.365 g, 0.167 mol) was added at 0 °C. A solution of Br_2 (46.50 g, 15.00 mL, 0.291 mol in 10 mL $CHCl_3$) was added over 30 min through a dropping funnel, and the mixture was stirred for 4 h at 0 °C. The reaction was quenched *via* the addition of NaOH (aq) (10 %, 50 mL). The mixture was warmed to 20 °C, filtered through a filter paper, and the layers were separated. The organic phase was washed with saturated Na_2SO_3 (aq) (75 mL), saturated $NaHCO_3$ (aq) (75 mL), brine (75 mL) and dried over $MgSO_4$. The solvent was removed *in vacuo* and the crude product purified by fractional distillation (75−85 °C at $P \approx 3.0 \times 10^{-2}$ mbar) to yield the product **2.3** as a white solid (24.92 g, 68%). R*f* = 0.85 (hexanes). As in lit.[27]

^{1}H NMR (400 MHz, $CDCl_3$) δ 7.37 (s, 3H), 1.35 (s, 18H).
^{13}C NMR (100 MHz, $CDCl_3$) δ 153.0, 125.8, 122.3, 121.1, 35.1, 31.4.

Tris(3,5-di-*tert*-butylphenyl)methanol - **2.4**[24]

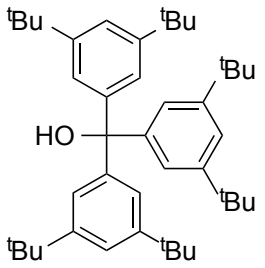

To a mixture of activated (stirring overnight *in vacuo*) Mg turnings (3.68 g, 149 mmol) in dry THF (40 mL), a solution of 1-bromo-3,5-di-*tert*-butylbenzene **2.3** (35.0 g, 130 mmol) in THF (40 mL) was slowly added under N_2. A crystal of I_2 was added to aid Grignard reagent formation at reflux. The reaction was maintained at a gentle reflux for 4 h. The reaction mixture was cooled to 20 °C, a solution of freshly distilled diethyl carbonate (4.56 g, 2.25 mL, 37.2 mmol) in THF (100 mL) was slowly added, and the resulting mixture was stirred at 20 °C for 3 days under N_2. After this period the reaction mixture was cooled to 0 °C, quenched *via* the addition of saturated NH_4Cl (aq) (100 mL) and Et_2O (150 mL) was added. The layers were separated, and the organic phase was washed with H_2O (150 mL), brine (150 mL), and dried using $MgSO_4$. The solvent was removed *in vacuo* and the crude product was purified by column chromatography (silica, pentane → pentane/EtOAc 98:2) yielding the product **2.4** (20.1 g, 91%) as a white solid. As in lit.[24]

^{1}H NMR (400 MHz, $CDCl_3$) δ 7.28 (t, J = 1.8 Hz, 3H), 7.04 (d, J = 1.8 Hz, 6H), 2.80 (bs, 1H), 1.23 (s, 54H).
^{13}C NMR (100 MHz, $CDCl_3$) δ 149.6, 146.7, 122.6, 120.4, 83.4, 34.9, 31.5.

Tris(3,5-di-*tert*-butylphenyl)methyl-acetylene – **2.5**[24]

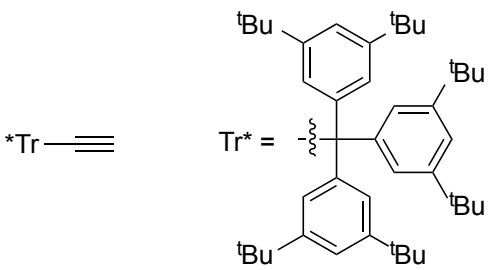

To a solution of tris(3,5-di-*tert*-butylphenyl)methanol **2.4** (10.0 g, 16.8 mmol) in dry THF (35 mL) at 20 °C was slowly added oxalyl chloride (10.6 g, 7.19 mL, 83.9 mmol). The mixture was left under vigorous stirring for 4 h before the solvent was removed *in vacuo* overnight. The pale yellow crude product was redissolved in the minimum amount of THF (10 mL). To this solution, ethynylmagnesium bromide (0.5 M in THF, 167.5 mL, 83.75 mmol) was added and the mixture stirred at 20 °C for 4 days under N_2. The reaction mixture was cooled to 0 °C, quenched via the addition of saturated NH_4Cl (aq) (100 mL), and Et_2O was added (150 mL). The layers were separated, the organic phase was washed with brine (3 × 100 mL), dried using $MgSO_4$ and filtered. The solvent was removed *in vacuo* and the crude product was purified by column chromatography (silica, hexanes/CH_2Cl_2 10:1) to yield the product **2.5** (9.35 g, 92 %) as a white solid. As in lit.[24]

^{1}H NMR (400 MHz, $CDCl_3$) δ 7.29 (t, J = 1.8 Hz, 3H), 7.05 (d, J = 1.8 Hz, 6H), 2.65 (s, 1H), 1.25 (s, 54H).
^{13}C NMR (100 MHz, $CDCl_3$) δ 149.7, 144.8, 123.8, 119.9, 90.7, 72.0, 56.1, 34.9, 31.4.

6,6,6-Tris(3,5-di-*tert*-butylphenyl)-1-[tri(propan-2-yl)silyl]hexa-1,4-diyn-3-ol - **2.6**[24]

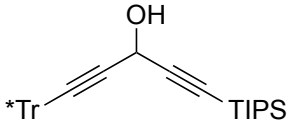

A solution of supertrityl acetylene **2.5** (0.896 g, 1.48 mmol) in THF (50 mL) was cooled to –78 °C under a N_2 atmosphere and *n*-BuLi (0.61 mL, 2.5 M in hexanes, 1.51 mmol) was added and the reaction mixture was stirred for 15 min. A solution of aldehyde **2.1** (332 mg, 1.48 mmol) in THF (5 mL) was added over 5 min, the resulting mixture warmed to 20 °C and stirred for 1 h. The reaction was cooled to 0

°C, quenched with saturated NH_4Cl (aq) (50 mL), and the mixture was extracted with Et_2O (50 mL). The organic phase was washed with saturated NH_4Cl (aq) (50 mL), H_2O (50 mL), brine (50 mL), and dried over $MgSO_4$. The solvent was removed *in vacuo* and the crude product purified by column chromatography (silica, pentane/EtOAc 100:1) to yield alcohol **2.6** (0.837 g, 71 %) as a pale yellow oil that solidified upon standing. As in lit.[24]

^{1}H NMR (400 MHz, $CDCl_3$) δ 7.25 (t, J = 2 Hz, 3H), 6.97 (d, J = 2 Hz, 6H), 5.32 (d, J = 8 Hz), 2.14 (d, J = 8 Hz), 1.2 (s, 54H), 1.05 (s, 21H).
^{13}C NMR (100 MHz, $CDCl_3$) δ 149.8, 144.7, 123.8, 119.9, 104.6, 91.9, 85.4, 80.9, 56.2, 53.2, 34.8, 31.4, 18.6, 11.2.

6,6,6-Tris(3,5-di-tert-butylphenyl)-1-[tri(propan-2-yl)silyl]hexa-1,4-diyn-3-one - **2.7**[24]

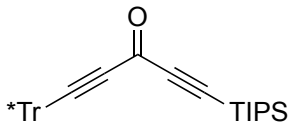

To a solution of **2.6** (4.34 g, 5.92 mmol) in CH_2Cl_2 (200 mL) celite (4.68 g), molecular sieves (4.68 g) and pyridinium chlorochromate (PCC) (2.34 g, 10.84 mmol) were added in that order and the reaction mixture was stirred at 20 °C under N_2 atmosphere for 20 h. The mixture was passed through a silica plug (CH_2Cl_2) and the solvents were removed *in vacuo* to yield ketone **2.7** (4.22 g, 98%) as a yellow solid. As in lit.[24]

^{1}H NMR (400 MHz, $CDCl_3$) δ 7.29 (t, J = 2 Hz, 3H), 6.96 (d, J = 2 Hz, 6H), 1.21 (s, 54H), 1.11-1.06 (m, 21H).
^{13}C NMR (100 MHz, $CDCl_3$) δ 160.8, 150.3, 143.3, 123.9, 120.5, 105.4, 100.1, 95.6, 85.2, 56.9, 35.0, 31.5, 18.6, 11.2.

[3-(Dibromomethylidene)-6,6,6-tris(3,5-di-tert-butylphenyl)hexa-1,4-diyn-1-yl]tri(propan-2-yl)silane - **2.8**[24]

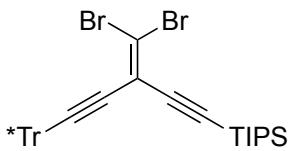

A solution of CBr_4 (1.80 g, 5.42 mmol) in CH_2Cl_2 (8 mL) was transferred to a flask containing PPh_3 (2.84 g, 10.84 mmol) under an N_2 atmosphere and the resulting mixture stirred at 20 °C for 1 h. A solution of **2.7** (2.21 g, 2.71 mmol) in CH_2Cl_2 (10 mL) was cannulated to the solution of ylid and the reaction mixture was stirred for 20 h. The reaction mixture was concentrated to ca. 30 mL and hexanes were added to precipitate

the Ph_3PO as a white solid along with an oily residue. The supernatant was decanted and filtered through a silica plug. The oily residue left in the flask was dissolved in the minimum amount of CH_2Cl_2 and hexanes were added. The heterogeneous mixture was then decanted and the supernatant filtered through a silica plug (this procedure was repeated three times). The solvent was removed *in vacuo* and the crude product was purified by passing through a silica plug (EtOAc/hexanes 1:20) to yield dibromoolefin **2.8** (2.45 g, 93%) as a white solid: *Rf* = 0.9 (EtOAc/hexanes 1:25). As in lit.[24]

^{1}H NMR (400 MHz, $CDCl_3$) δ 7.23 (t, *J* = 2 Hz, 3H), 6.99 (d, *J* = 2 Hz, 6H), 1.19 (s, 54H), 1.09–1.05 (m, 21H).
^{13}C NMR (100 MHz, $CDCl_3$) δ 150.1, 143.1, 123.8, 120.4, 115.1, 108.2, 103.6, 102.4, 98.4, 81.1, 57.4, 34.9, 31.4, 18.5, 11.0.
FTIR 3070 (w), 2958, 2900, 2866, 2229, 1593, 1462 cm^{-1}. As in lit.[1]

Tri(propan-2-yl)[7,7,7-tris(3,5-di-tert-butylphenyl)hepta-1,3,5-triyn-1-yl]silane - **2.9**[24]

To a solution of **2.8** (0.97 g, 1.00 mmol) in hexanes (50 mL) at –78 °C, *n*-BuLi was added (0.50 mL, 2.5M in hexanes, 1.25 mmol) dropwise under a N_2 atmosphere. The reaction mixture was warmed to 20 °C over 30 min and the reaction was quenched by the addition of saturated NH_4Cl (aq) (20 mL). The layers were separated and the organic layer dried over $MgSO_4$. The solvent was removed *in vacuo* and the crude product was purified by column chromatography (silica, hexanes) to yield polyyne **2.9** (0.735 g, 91%) as a white solid: *Rf* = 0.6 (CH_2Cl_2/hexanes 1:20). As in lit.[24]

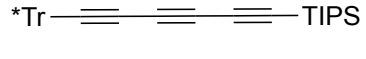

^{1}H NMR (400 MHz, $CDCl_3$) δ 7.25 (t, *J* = 2 Hz, 3H), 6.91 (d, *J* = 2 Hz, 6H), 1.19 (s, 54H), 1.09-1.06 (m, 21H).
^{13}C NMR (100 MHz, $CDCl_3$) δ 150.0, 143.8, 123.7, 120.2, 90.2, 85.0, 83.6, 69.0, 62.5, 61.6, 57.1, 34.8, 31.4, 18.5, 11.3.

1,1',1''-(Hepta-1,3,5-triyne-7,7,7-triyl)tris(3,5-di-tert-butylbenzene) - **2.10**[24]

To a solution of **2.9** (0.340 g, 0.420 mmol) in wet THF (10 mL THF and 5 μL H_2O) was added TBAF (0.462 mL, 1.0 M in THF,

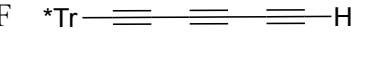

0.462 mmol). The solution was stirred at 20 °C for 15 min. The reaction was quenched with saturated NH_4Cl (aq) (10 mL) and extracted with hexanes (20 mL). The organic phase was washed with H_2O (10 mL), and dried over $MgSO_4$. The solvent was removed *in vacuo* and the crude product purified by slurry washing with Et_2O (×2) to yield polyyne **2.10** (0.162 g, 60%) as a white solid. As in lit.[24]

^{1}H NMR (400 MHz, $CDCl_3$) δ 7.26 (t, J = 2 Hz, 3H), 6.90 (d, J = 2 Hz, 6H), 2.07 (s, 1H), 1.19 (s, 54H).
^{13}C NMR (100 MHz, $CDCl_3$) δ 150.1, 143.6, 123.7, 120.3, 84.8, 68.9, 68.5, 66.6, 61.6, 61.3, 57.0, 34.8, 31.4.

1,1',1''-(1-Bromohepta-1,3,5-triyne-7,7,7-triyl)tris(3,5-di-*tert*-butylbenzene) - **2.11**[24]

To a mixture of **2.10** (75 mg, 0.115 mmol) in acetone (25 mL) was added *N*-bromosuccinimide (24.8 mg, 0.138 mmol) and $AgNO_3$ (3.90 mg, 0.023 mmol). The reaction was stirred at 20 ºC for 10 h and monitored by TLC (hexanes). The reaction mixture was quenched by adding water (5 mL) and then extracted with a CH_2Cl_2 (3 × 20 mL). The organic layers were combined, washed with brine (10 mL), and dried over $MgSO_4$. The solvent was removed *in vacuo* and the crude product purified by passing through a silica plug (CH_2Cl_2/hexanes 1:5) to yield **2.11** (79 mg, 100%) as a slightly yellow solid. *Rf* = 0.4 (hexanes). As in lit.[24]

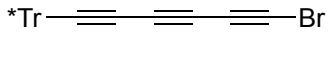

^{1}H NMR (400 MHz, $CDCl_3$) 7.26 (t, J = 2 Hz, 3H), 6.91 (d, J = 2 Hz, 6H), 1.19 (s, 54H).
^{13}C NMR (100 MHz, $CDCl_3$) 150.1, 143.6, 123.7, 120.3, 84.5, 68.5, 66.4, 62.4, 60.0, 57.1, 40.0, 34.8, 31.4.

2,9-Bis(4-methoxyphenyl)-1,10-phenanthroline – **2.12**[45]

A solution of bromoanisole (2.40 mL, 5.55 g, 29.7 mmol) in dry Et_2O (80 mL) was freeze-pump-thaw degassed, then was cooled to –30 °C and *t*-BuLi (1.7 M in pentane, 42.0 mL, 71.4 mmol) was added

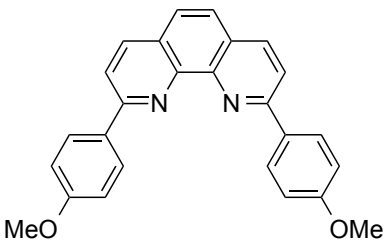

by cannula. The reaction was allowed to warm to 20 °C and stirred for 1.5 h. The solution was transferred by cannula to a suspension of 1,10-phenanthroline (1.50 g, 7.57 mmol, dried overnight *in vacuo*) in dry toluene which had been freeze-pump-thaw degassed. The reaction mixture was stirred at 20 °C for 48 h. The reaction was quenched by the addition of *i*-PrOH (1 mL), then MeOH (1 mL) and finally water (10 mL). The organic layer was decanted and the aqueous layer extracted with CH_2Cl_2. To the combined organic layers was added MnO_2 (30.0 g, 345 mmol) and the resulting suspension stirred for 36 h. The suspension was filtered and the filtrate concentrated. Recrystallisation of the crude from toluene yielded derivatised phenanthroline **2.12** as a yellow solid (1.64 g, 55%). As in lit.[45]

^{1}H NMR (400 MHz, $CDCl_3$) δ 8.43-8.46 (m, 4H), 8.27 (d, J = 8.5 Hz, 2H), 8.09 (d, J = 8.5 Hz, 2H), 7.75 (s, 2H), 7.13 (m, 4H), 3.93 (s, 6H).

2,9-Bis(4-hydroxyphenyl)-1,10-phenanthroline – **2.13**[45]

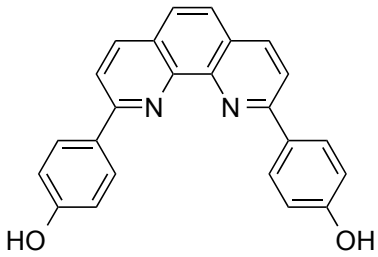

Hydrochloric acid (33%, 16.5 mL) and pyridine (15 mL) were added to a flask equipped for distillation. Water was distilled from the mixture until the internal temperature reached 200 °C. The reaction mixture temperature was lowered to 140 °C and **2.12** (1.50 g, 3.88 mmol) was added. After 3 h refluxing under N_2 at 190 °C the reaction mixture was cooled to room temperature and water (15 mL) was added. The bright yellow precipitate was filtered and the crude product was suspended in an ethanol/water mixture (4:1, 100 mL), neutralised with $NaHCO_3$ (aq) and the yellow-orange precipitate was filtered and dried *in vacuo* to yield diol **2.13** (1.40 g, 99%) as a dark yellow powder. As in lit.[45]

^{1}H NMR (400 MHz, DMSO-d_6) δ 10.30 (s, 2H), 8.78 (d, J = 8.7 Hz, 2H), 8.46 (d, J = 8.5 Hz, 2H), 8.35 (d, J= 8.7 Hz, 4H), 8.12 (s, 2H), 7.08 (d, J = 8.5 Hz, 4H).

2.8 – Experimental data for novel compounds

Diol **2.14**

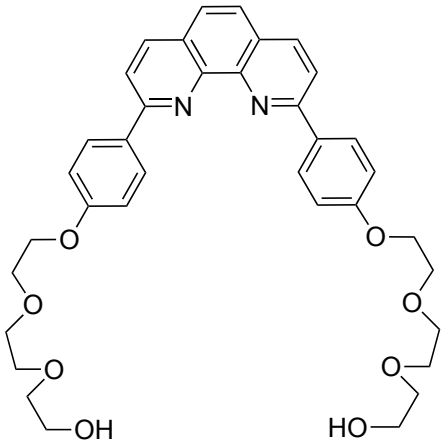

As reported in a similar procedure,[30] **2.13** (764 mg, 2.10 mmol) was added to a suspension of K_2CO_3 (2.90 g, 21 mmol) in DMF (70 mL) under N_2. 2-(2-Chloroethoxy)ethoxyethanol (0.83 mL, 7.90 mmol) was then added and the mixture was stirred at 90 °C under argon. After 12 h, more 2-(2-chloroethoxy)ethanol (0.41 mL, 3.9 mmol) was added. The solution was stirred at 90 °C for 4 h. After filtration and evaporation of the solvent, the remaining solid was dissolved in CH_2Cl_2/MeOH 1:1 (100 mL). The solution was washed with water (3 × 100 mL). The organic layer was dried over $MgSO_4$ and concentrated *in vacuo*. The product was purified by column chromatography (silica, CH_2Cl_2/MeOH 100:2) to yield the diol **2.14** as a yellow solid (1.00 g, 76%).

^{1}H NMR (400 MHz, $CDCl_3$): δ 8.43 (d, ^3J = 9.0 Hz, 4H), 8.27 (d, ^3J = 8.8 Hz, 2H), 8.10 (d, ^3J = 8.8 Hz, 2H), 7.76 (s, 2H), 7.15 (d, ^3J = 9.0 Hz, 4H), 4.29 (t, ^3J = 5.1 Hz, 4H), 3.95 (t, ^3J = 4.8 Hz, 4H), 3.76 (m, 12H), 3.65 (m, 4H), 2.46 (s, br, 2H).
^{13}C NMR (100 MHz, $CDCl_3$): δ 160.1, 156.3, 146.1, 136.8, 132.5, 129.0, 127.6, 125.6, 119.4, 114.9, 72.5, 70.9, 70.5, 69.8, 67.5, 61.8.
ESI-MS: $C_{36}H_{40}N_2O_8$ Calc – 628.28 Found *m/z* – 629.2 $(M+H)^+$.

Ditosylate **2.15**

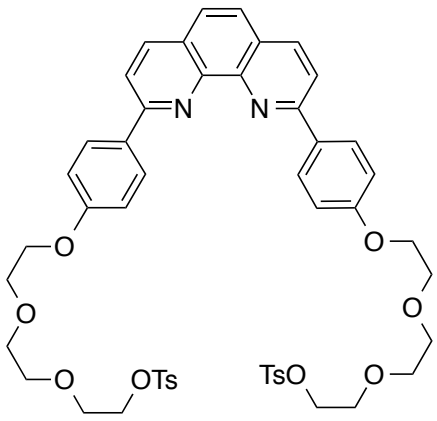

Diol **2.14** (1.00 g, 1.85 mmol) was suspended in dry CH_2Cl_2 (70 mL). The solution was cooled to 0 °C in an ice-bath under nitrogen. Triethylamine (1.20 mL, 9.00 mmol) and 4-dimethylaminopyridine (DMAP, 18.3 mg, 0.149 mmol) were added to the cooled mixture. Tosyl chloride (1.55 g, 8.16 mmol) was slowly added. The solution was stirred under

nitrogen at 0 °C for 2 h, then at room temperature for 12 h. Further tosyl chloride (0.35 g, 1.84 mmol) was added to the reaction mixture and the solution was stirred at room temperature overnight. The solution was then poured onto a mixture of ice (300 g) and hydrochloric acid (1% aq., 10 mL). The aqueous layer was neutralized to pH 7 with aqueous NaOH. The organic layer was separated and the aqueous layer was washed with CH_2Cl_2 (2 × 50 mL). The organic layers were combined, washed with water (20 mL), and dried with $MgSO_4$. The solvent was removed *in vacuo*. The resulting yellow oil was purified by chromatography (silica, CH_2Cl_2/MeOH 100:1) to yield the ditosylate **2.15** (1.35 g, 78%) as a yellow solid.

^{1}H NMR (400 MHz, $CDCl_3$): δ 8.42 (d, ^3J = 9.0 Hz, 4H), 8.28 (d, ^3J = 8.8 Hz, 2H), 8.10 (d, ^3J = 8.8 Hz, 2H), 7.81 (s, 2H), 7.15 (d, ^3J = 9.0 Hz, 4H), 4.24 (t, ^3J = 5.1 Hz, 4H), 4.19 (t, ^3J = 4.8 Hz, 4H), 3.90 (t, 4H), 3.72 (m, 8H), 3.65 (m, 4H), 2.42 (s, 6H).
^{13}C NMR (100 MHz, $CDCl_3$): δ 160.1, 156.3, 145.9, 144.8, 136.8, 133.0, 132.3, 130.1, 129.8, 128.9, 127.9, 127.6, 125.6, 119.4, 114.9, 70.8, 70.8, 69.8, 69.3, 68.7, 67.5.
ESI-MS: $C_{50}H_{52}N_2O_{12}S_2$ Calc – 936.30 Found *m/z* – 937.3 $(M+H)^+$.

Macrocycle **Ma**

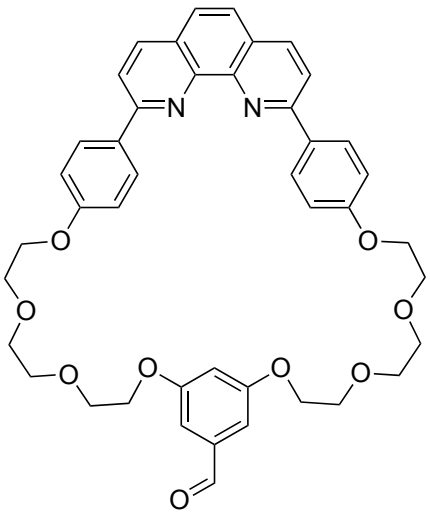

As reported in a similar procedure,[31] a solution of the ditosylate **2.15** (1.32 g, 1.41 mol) and 3,5-dihydroxybenzaldehyde (195 mg, 1.41 mol) in DMF (130 mL) was degassed, transferred to an addition funnel, and added dropwise to a suspension of Cs_2CO_3 (2.30 g, 7.10 mmol) in DMF (200 mL) over a period of 4 h. The mixture was then heated to 60 °C and stirred under argon for 16 h. The warm mixture was filtered and the solid residue was washed with DMF (50 mL). After evaporation of the solvent, the remaining solid was dissolved in CH_2Cl_2 (100 mL), washed with water (3 × 100 mL) and dried over $MgSO_4$. The organic layer was evaporated, and the crude product was purified by column chromatography (silica, CH_2Cl_2/MeOH 100:1) to yield the macrocycle **Ma** as a pale yellow solid (695 mg, 68%).

^{1}H NMR (400 MHz, $CDCl_3$): δ 9.87 (s, 1H), 8.42 (d, ^3J = 9.0 Hz, 4H), 8.28 (d, ^3J = 8.8 Hz, 2H), 8.10 (d, ^3J = 8.8 Hz, 2H), 7.81 (s, 2H), 7.15 (d, ^3J = 9.0 Hz, 4H), 7.05 (d, ^3J = 2.2 Hz), 6.83 (d, ^3J = 2.2 Hz, 1H), 4.27 (t, ^3J = 5.1 Hz, 4H), 4.21 (t, ^3J = 4.8 Hz, 4H), 3.93 (m, 8H), 3.80 (m, 8H).

^{13}C NMR (100 MHz, $CDCl_3$): δ 192.1, 160.7, 160.4, 156.4, 146.1, 138.6, 137.1, 132.5, 129.2, 127.8, 125.9, 119.5, 115.1, 108.3, 108.3, 71.3, 71.3, 70.0, 70.0, 68.3, 67.7.

ESI-MS: $C_{43}H_{42}N_2O_9$ Calc – 730.2 Found - 731.2 [M+H]

Macrocycle **2.16**

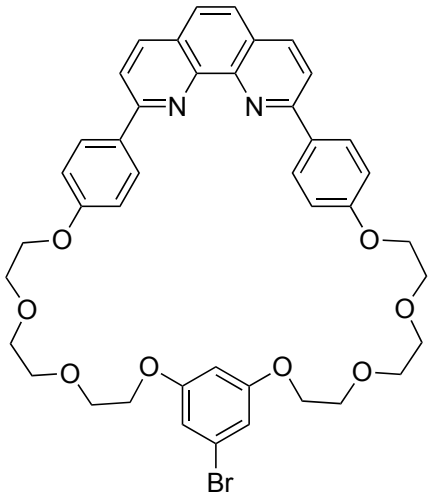

A solution of the ditosylate **2.15** (500 mg, 0.531 mmol) and 3,5-dihydroxybromobenzene (101 mg, 0.531 mmol) in DMF (100 mL) was degassed, transferred to an addition funnel, and added dropwise to a suspension of Cs_2CO_3 (0.87 g, 2.67 mmol) in DMF (150 mL) over a period of 4 h. The mixture was then heated to 60 °C and stirred under argon for 16 h. The warm mixture was filtered and the solid residue was washed with DMF (50 mL). After evaporation of the solvent, the remaining solid was dissolved in CH_2Cl_2 (100 mL), washed with water (3 × 100 mL) and dried over $MgSO_4$. The organic layer was evaporated, and the crude product was purified by column chromatography (silica, CH_2Cl_2/MeOH 100:1) to yield the macrocycle **2.16** as a pale yellow solid (315 mg, 75%).

^{1}H NMR (400 MHz, $CDCl_3$): δ 8.44 (d, ^3J = 8.9 Hz, 4H), 8.25 (d, ^3J = 8.4 Hz, 2H), 8.07 (d, ^3J = 8.4 Hz, 2H), 7.73 (s, 2H), 7.13 (d, ^3J = 8.9 Hz, 4H), 6.73 (d, ^3J = 2.0 Hz, 2H), 6.48 (d, ^3J = 2.0 Hz, 1H), 4.26 (t, ^3J = 5.1 Hz, 4H), 4.12 (t, ^3J = 4.8 Hz, 4H), 3.93 (t, ^3J = 4.8 Hz, 4H), 3.88 (t, ^3J = 4.8 Hz, 4H), 3.78 (m, 8H).

^{13}C NMR (100 MHz, $CDCl_3$): δ 160.4, 160.1, 156.2, 145.9, 136.8, 132.3, 129.0, 127.5, 125.6, 122.9, 119.2, 114.9, 110.9, 100.7, 71.1, 71.0, 69.7, 69.7, 67.9, 67.5.

ESI MS: $C_{42}H_{41}BrN_2O_9$ – Calc - 780.2 Found *m/z* – 781.2 $(M+H)^+$.

Macrocycle **Mb**

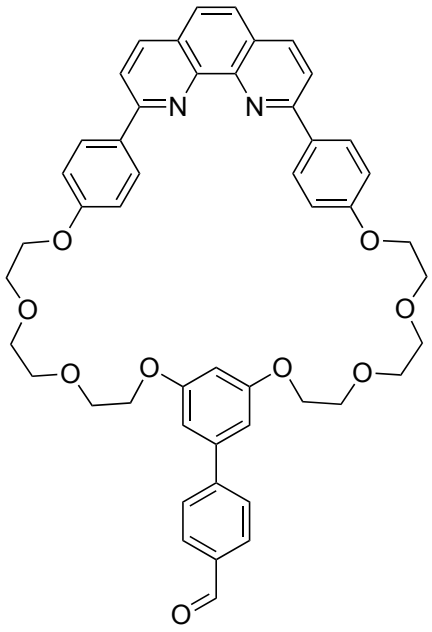

Macrocycle **2.16** (50 mg, 64 μmol), B_2Pin_2 (22.5 mg, 96 μmol), $PdCl_2$(dppf) (2.6 mg, 3.2 μmol, 0.05 equiv.) and Na_2CO_3 (13.5 mg, 128 μmol) were loaded into a Schlenk tube and dried *in vacuo* for 10 min. THF/water 2:1 (4.5 mL) was added. The mixture was pump-purge degassed three times and then heated to 80 °C for 18 h. The reaction mixture was added to CH_2Cl_2 (30 mL), washed with water (3 × 10 mL) and dried over $MgSO_4$. The organic layer was evaporated, and the crude product was purified by column chromatography (silica, CH_2Cl_2/MeOH 100:1) to yield the macrocycle **Mb** as a white solid (48 mg, 93%).

^{1}H NMR (400 MHz, $CDCl_3$): δ 9.88, (s, 1H), 8.41 (d, ^3J = 8.5 Hz, 4H), 8.26 (d, ^3J = 8.4 Hz, 2H), 8.08 (d, ^3J = 8.4 Hz, 2H), 7.83 (d, ^3J = 8.3 Hz, 2H), 7.75 (s, 2H), 7.68 (d, ^3J = 8.3 Hz, 2H), 7.11 (d, ^3J = 8.5 Hz), 6.82 (d, ^3J = 2.0 Hz, 2H), 6.63 (d, ^3J = 2.0 Hz, 1H), 4.26 (t, ^3J = 5.1 Hz, 4H), 4.23 (m, 8H), 3.94 (m, 8H), 3.80 (m, 8H).

^{13}C NMR (100 MHz, $CDCl_3$): δ 192.2, 160.8, 160.4, 156.4, 147.2, 146.3, 142.1, 137.0, 132.6, 130.5, 129.2, 127.9, 125.9, 119.5, 115.2, 107.0, 101.4, 71.4, 71.4 70.2, 70.1, 68.2, 67.8.

ESI MS: $C_{49}H_{46}N_2O_9$ – Calc – 806.32 Found *m/z* – 807.2 $(M+H)^+$.

Polyyne [2]Rotaxane **2Ra**

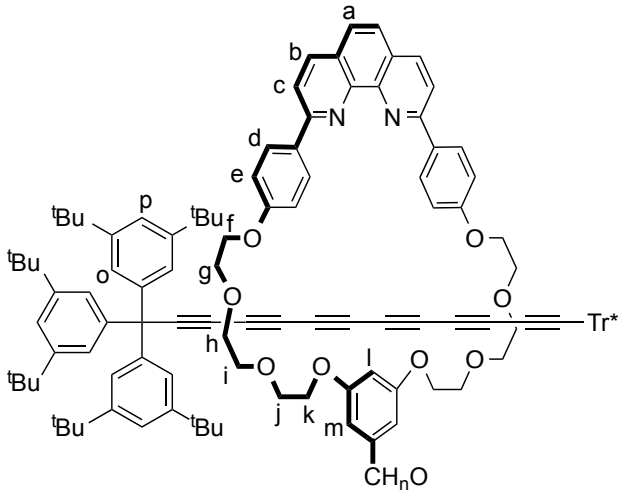

A solution of CuI (3.4 mg, 18 μmol) in MeCN (2.5 mL) was added to a solution of **Ma** (13 mg, 18 μmol) in CH_2Cl_2 (2.5 mL) and the mixture was stirred for 1.5 h at 20 °C. The solvent was removed *in vacuo* and the residue redissolved in $CHCl_3$

(10 mL). This solution was then added to a mixture of polyyne **2.10** (12.8 mg, 19.6 µmol), bromopolyyne **2.11** (19.5 mg, 26.7 µmol), and K_2CO_3 (9.8 mg, 71 µmol). The mixture was degassed through pump-freeze-thaw cycles, flushed with nitrogen, and stirred at 60 °C for 2 d. After cooling to 20 °C, the reaction was quenched by the addition of EDTA (20 mg, 0.3 mmol) in H_2O (1 mL) and stirred at 20 °C for 2 h. CH_2Cl_2 (10 mL) was added, the organic phase separated, washed with H_2O (10 mL), brine (10 mL), dried with $MgSO_4$ and the solvents were removed. Column chromatography (silica, hexanes/EtOAc 5:1 → 5:2) afforded the polyyne rotaxane **2Ra** as a yellow solid (21 mg, 58%).

^{1}H NMR (500 MHz, $CDCl_3$): δ 9.81 (s, 1H H_n), 8.47 (d, ^3J = 8.6 Hz, 4H, H_d), 8.25 (d, ^3J = 8.4 Hz, 2H, H_c), 8.08 (d, ^3J = 8.4 Hz, 2H, H_b), 7.73 (s, 2H, H_a), 7.22 (t, 6H, ^3J = 1.6 Hz, H_p), 7.13 (d, 4H, J = 8.9 Hz, H_e), 6.98 (d, ^3J = 2.2 Hz, 2H, H_m), 6.84 (d, 12H, ^3J =1.6 Hz, H_o), 6.81 (t, 1H, ^3J = 2.2 Hz, H_l), 4.27 (t, ^3J = 5.0 Hz, 4H, H_f), 4.19 (t, ^3J = 4.8 Hz, 4H, H_k), 3.90-3.94 (m, 8H, $H_{g,i}$), 3.79 (s, $H_{h,i}$), 1.14 (s, 108H, $H_{t\text{-}Bu}$).
^{13}C NMR (125 MHz, $CDCl_3$): δ 191.9, 160.5, 160.1, 156.3, 150.1, 146.0, 143.2, 138.2, 136.5, 132.5, 132.2, 130.9, 128.9, 128.8, 127.3, 125.5, 123.6, 120.4, 119.0, 114.9, 108.3, 107.5, 86.3, 71.0, 69.7, 69.6, 68.1, 67.4, 63.2, 63.1, 62.7, 62.5, 57.2, 34.8, 31.3.
UV λ_{max} $CHCl_3$ (log ε): 317 (5.33), 298 (5.24), 282 (5.08).
MALDI-TOF MS: $C_{141}H_{168}N_2O_9$ Calculated – 2034.90, Found *m/z* – 2035.89 $(M+H)^+$.

Polyyne Rotaxane **2Rb**

A solution of CuI (31.7 mg, 166 µmol) in MeCN (5 mL) was added to a solution of macrocycle **Mb** (135 mg, 166 µmol) in CH_2Cl_2 (5 mL) and the mixture was stirred for 1.5 h at 20 °C. The solvent was removed *in vacuo* and the residue redissolved in $CHCl_3$ (25 mL). This solution was then added to a mixture of polyyne **3.10** (130 mg,

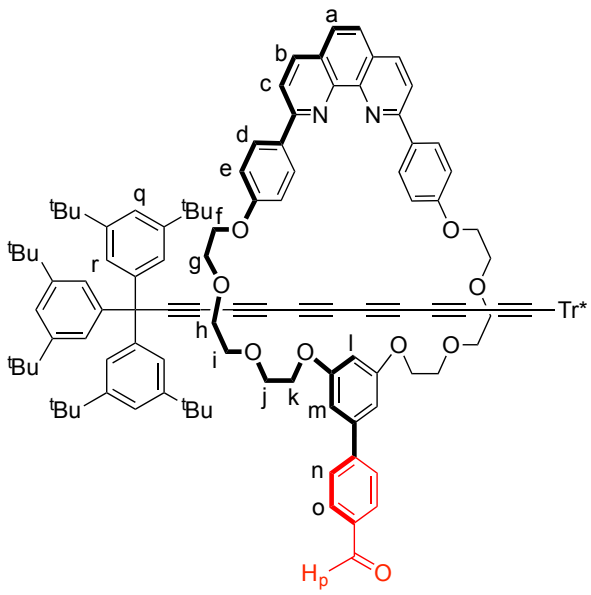

199 μmol), bromopolyyne **3.11** (195 mg, 265 μmol), and K_2CO_3 (91.7 mg, 664 μmol). The mixture was degassed through pump-freeze-thaw cycles, flushed with nitrogen, and stirred at 60 °C for 24 h. After cooling to 20 °C, the reaction was quenched by the addition of EDTA (50 mg, 0.75 mmol, in 1 mL H_2O) and stirred at 20 °C for 2 h. CH_2Cl_2 (30 mL) was added, the organic phase separated, washed with H_2O (30 mL), brine (30 mL), dried with $MgSO_4$ and the solvents were removed. Column chromatography (silica, hexanes/EtOAc 5:1 → 5:2) afforded the polyyne rotaxane **2Rb** as a yellow solid (176 mg, 50%).

^{1}H NMR (400 MHz, $CDCl_3$): δ 9.78, (s, 1H, H_p), 8.46 (d, ^3J = 8.5 Hz, 4H, H_d), 8.24 (d, ^3J = 8.4 Hz, 2H, H_c), 8.07 (d, ^3J = 8.4 Hz, 2H, H_b), 7.75 (m, 6H, $H_{a,n,o}$), 7.23 (t, ^3J = 2.0 Hz, 6H, H_q), 7.14 (d, ^3J = 8.5 Hz, 4H, H_e), 6.85 (d, ^3J = 2.0 Hz, 12H, H_r), 6.81 (d, ^3J = 2.0 Hz, 2H, H_m), 6.64 (d, ^3J = 2.0 Hz, 1H, H_l), 4.24-4.28 (m, 8H, $H_{f,k}$), 3.89-3.95 (m, 8H, $H_{g,j}$), 3.77-3.81 (m, 8H, $H_{h,i}$), 1.13 (s, 108H, $H_{t\text{-}Bu}$).
^{13}C NMR (100 MHz, $CDCl_3$): δ 192.1, 160.7, 160.4, 156.5, 150.4, 147.6, 146.2, 143.5, 143.4, 141.7, 136.7, 135.4, 132.4, 130.3, 129.1, 127.9, 127.6, 125.6, 123.9, 123.8, 120.6, 119.2, 115.1, 107.2, 101.0, 86.6, 71.3, 70.0, 69.8, 68.1, 67.7, 63.4, 63.0, 62.7, 62.5, 57.5, 34.9, 31.5.
UV λ_{max} $CHCl_3$ (log ε): 317 (5.31), 297 (5.29), 283 (5.13).
MALDI TOF MS: $C_{147}H_{172}N_2O_9$ Calc - 2110.31, Found *m/z* – 2111.11 $(M+H)^+$

Porphyrin Zn-PM2a

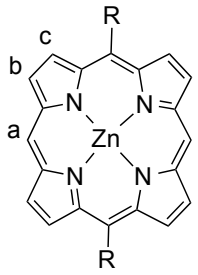

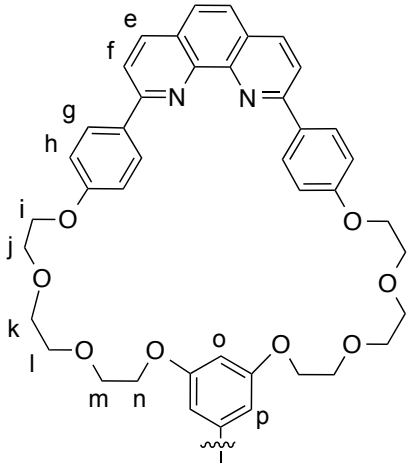

TFA (31 μL, 0.41 mmol) was added to a solution of macrocycle **Ma** (50 mg, 68 μmol) and 2,2'-dipyrromethane (10 mg, 68 μmol) in dry CH_2Cl_2 (15 mL). The flask was protected from light and stirred under N_2 for 2 h. DDQ (31 mg, 137 μmol) was added and stirred for a further 1 h. NEt_3 (50 μL, 0.36 mmol) was added to neutralise the reaction mixture and it was passed through a silica plug (CH_2Cl_2) to yield free-base porphyrin **PM2a** as a red

solid (12 mg), this was immediately dissolved in $CHCl_3$ (5 mL) and treated with a solution of $Zn(OAc)_2.2H_2O$ (20 mg) in MeOH (3 mL). The solution was heated to reflux for 2 h under N_2. Solvents were evaporated and the solid taken up in CH_2Cl_2 and washed with water. The organic layer was separated, washed with water and dried with $MgSO_4$. This yielded zinc porphyrin **Zn-PM2a** as a purple solid (10 mg, 5.6 μmol. Two step yield = 18%).

^{1}H NMR (400 MHz, $CDCl_3$): δ 10.11 (s, 2H, H_a), 9.28 (d, ^3J = 4.7 Hz, 4H, H_b), 9.12 (d, ^3J = 4.7 Hz, 4H, H_c), 8.48 (d, ^3J = 8.6 Hz, 8H, H_h) 8.22 (d, ^3J = 8.5 Hz, 4H, H_e), 8.10 (d, ^3J = 8.5 Hz, 4H, H_f), 7.72 (s, 4H, H_d), 7.44 (t, ^3J = 2.0 Hz, 4H, H_p), 7.14 (d, ^3J = 8.5 Hz, 8H, H_g), 6.81 (d, ^3J = 2.0 Hz, 2H, H_o), 4.35 (t, ^3J = 5.1 Hz, 8H, H_i), 4.26 (t, ^3J = 5.1 Hz, 8H, H_n), 3.98 (t, ^3J = 5.1 Hz, 8H, H_j), 3.93 (t, ^3J = 5.1 Hz, 8H, H_m), 3.83 (m, 16H, $H_{k,l}$).

^{13}C NMR (100 MHz, $CDCl_3$): δ 159.1, 156.8, 155.2, 148.6, 148.4, 145.0, 144.2, 135.7, 131.3, 131.0, 130.4, 127.9, 126.5, 124.6, 118.2, 117.9, 114.1, 113.9, 104.5, 99.4, 70.0, 70.0, 68.9, 68.7, 66.9, 66.4.

UV-vis λ_{max} $CHCl_3$ (log ε): 539 (4.09), 414 (5.41), 288 (4.89), 243 (4.84).

MALDI-TOF MS $C_{104}H_{92}N_8O_{16}Zn$ Calc - 1774.59, Found *m/z* 1775.39 $(M+H)^+$.

Porphyrin Zn-PM4a

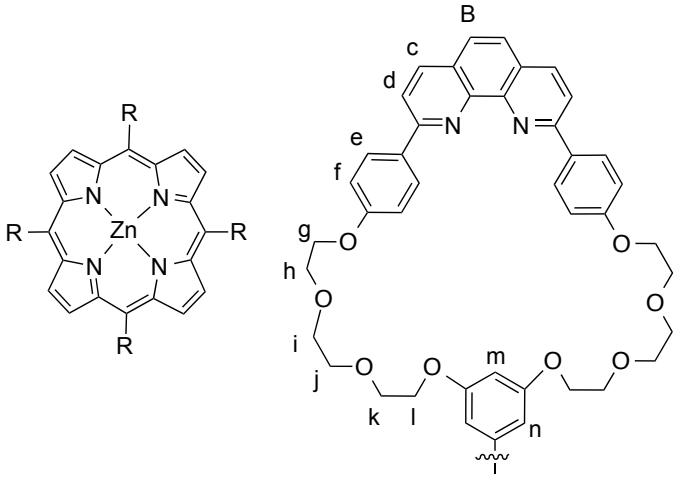

Macrocycle **Ma** (175 mg, 0.239 mmol) was dissolved in 7:3 propionic acid:nitrobenzene (1.2 mL). Pyrrole (16.6 μL, 0.239 mmol) was added and the mixture was heated in the microwave at 140 °C for 15 min, then diluted with $CHCl_3$, washed with water and dried with $MgSO_4$. The product was purified by column chromatography (99:1 CH_2Cl_2 : MeOH) to yield free-base porphyrin **PM4a** as a purple solid, which was not completely pure so was immediately taken forward to metallation to aid further purification. Free-base porphyrin **PM4a** was dissolved in $CHCl_3$ (15 mL). A solution of $Zn(OAc)_2.2H_2O$ (20 mg, 91 μmol) in MeOH (3 mL)

was added. The solution was heated to reflux and stirred for 2 h under N_2, then evaporated; the residue was dissolved in CH_2Cl_2 and washed with water. An aqueous solution of EDTA (0.10 M, 12.5 mL) was added to the organic layer and the biphasic mixture was stirred for 24 h. The organic layer was separated, washed with water and dried with $MgSO_4$. This yielded zinc porphyrin **Zn-PM4a** as a purple solid (44 mg, 24%).

^{1}H NMR (400 MHz, $CDCl_3$): δ 8.98 (s, 8H, H_a) 8.43 (d, ^3J = 9.2 Hz, 16H, H_f), 8.20 (d, ^3J = 8.8 Hz, 8H, H_c), 8.05 (d, ^3J = 8.8 Hz, 8H, H_d), 7.67 (s, 8H, H_b), 7.39 (d, ^3J = 2.3 Hz, 8H, H_n), 7.13 (d, 16H, ^3J = 8.8 Hz, H_e), 6.93 (t, ^3J = 2.3 Hz, 4H, H_n), 4.27 (t, ^3J = 5.1 Hz, 16H, H_g), 4.23 (t, ^3J = 4.8 Hz, 16H, H_l), 3.93 (m, 32H, $H_{h,k}$), 3.80 ppm, 32H, $H_{i,j}$).

^{13}C NMR (125 MHz, $CDCl_3$): δ 159.1, 156.8, 155.1, 148.8, 144.9, 143.6, 135.7, 131.2, 130.9, 127.9, 126.4, 124.5, 119.6, 118.1, 113.9, 113.6, 99.9, 70.0, 69.9, 68.9, 68.6, 66.8, 66.5.

UV-vis λ_{max} $CHCl_3$, (log ε): 551 (4.25), 425 (5.48), 323 (5.08), 288 (5.25).

MALDI-TOF MS: $C_{188}H_{174}N_{12}O_{32}$ Calculated - 3113.24, Found *m/z* - 3118.89.

Porphyrin Zn-PM2b

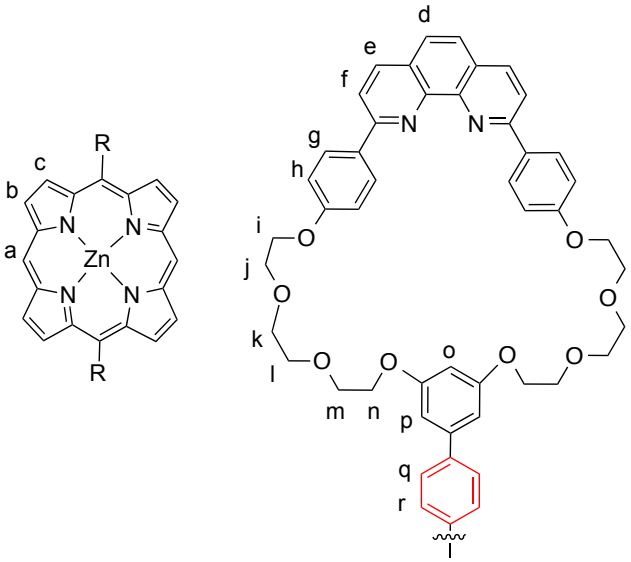

TFA (26 µL, 0.34 mmol) was added to a solution of macrocycle **Mb** (46 mg, 57 µmol) and 2,2'-dipyrromethane (8.3 mg, 57 µmol) in dry CH_2Cl_2 (15 mL). The flask was protected from light and stirred under N_2 for 2 h. DDQ (25.7 mg, 0.113 mmol) was added and stirred for a further 1 h. NEt_3 (50 µL, 0.36 mmol) was added to neutralise the reaction mixture and it was passed through a silica plug (CH_2Cl_2) to yield free-base porphyrin **PM2b** as a red solid (18 mg), which was immediately metallated. Free-base porphyrin **PM2b** was dissolved in $CHCl_3$ (5 mL). A solution of $Zn(OAc)_2.2H_2O$ (20 mg, 91 µmol) in MeOH (3 mL) was added. The solution was heated to reflux and stirred for 2 h under N_2, then evaporated; the residue

was dissolved in CH_2Cl_2 and washed with water. An aqueous solution of EDTA (0.10 M, 12.5 mL) was added to the organic layer and the biphasic mixture was stirred for 24 h. The organic layer was separated, washed with water and dried with $MgSO_4$. This yielded zinc porphyrin **Zn-PM2b** as a purple solid (15 mg, 31%).

^{1}H NMR (400 MHz, $CDCl_3$): δ 10.09 (s, 2H, H_a), 9.25 (d, ^3J = 4.7 Hz, 4H, H_b), 9.00 (d, ^3J = 4.7 Hz, 4H, H_c), 8.43 (d, ^3J = 8.6 Hz, 8H, H_h) 8.37 (d, ^3J = 8.5 Hz, 4H, H_e), 8.00 (d, ^3J = 8.5 Hz, 4H, H_f), 7.89 (d, ^3J = 8.5 Hz, 4H, H_q), 7.73 (d, ^3J = 8.5 Hz, 4H, H_r), 7.15 (m, 12H, $H_{d,g}$), 6.88 (d, ^3J = 2.2 Hz, 4H, H_p) 6.81 (d, ^3J = 2.0 Hz, 2H, H_o), 4.39 (t, ^3J = 5.1 Hz, 8H, H_i), 4.31 (t, ^3J =5.1 Hz, 8H, H_n), 4.02 (m, 16H, $H_{j,m}$), 3.89 (m, 16H, $H_{k,l}$).

^{13}C NMR (100 MHz, $CDCl_3$): δ 160.8, 160.4, 155.9, 150.0, 145.6, 145.6, 143.7, 142.9, 139.9, 136.4, 135.8, 132.6, 132.3, 131.5, 129.2, 127.0, 125.4, 125.0, 119.1, 118.9, 115.1, 107.0, 105.8, 100.6, 71.4, 71.4, 70.2, 70.0, 68.1, 67.8.

UV-vis λ_{max} $CHCl_3$ (log ε): (539, 4.09), (414, 5.41), (288, 4.89), (243, 4.84).

MALDI-TOF MS: $C_{116}H_{100}N_8O_{16}Zn$ Calc – 1930.69, Found *m/z* 1930.69 $(M)^+$.

Porphyrin Zn-PM4b

Macrocycle **Mb** (50 mg, 64 µmol) was dissolved in 7:3 propionic acid:nitrobenzene (0.5 mL). Pyrrole (4.4 µL, 64 µmol) was added. The mixture was heated in the microwave at 140 °C for 15 min, then diluted with $CHCl_3$, washed with water and dried with $MgSO_4$. The product was purified by column chromatography (99:1 CH_2Cl_2:MeOH) to yield free-base porphyrin **PM4b** as a purple solid. The crude free-base porphyrin **PM4b** was dissolved in $CHCl_3$ (15 mL). A solution of $Zn(OAc)_2.2H_2O$ (20 mg, 91 µmol) in MeOH (3 mL) was added. The solution was heated to reflux and stirred for 2 h under N_2, then evaporated; the residue was dissolved in CH_2Cl_2 and washed with water. An

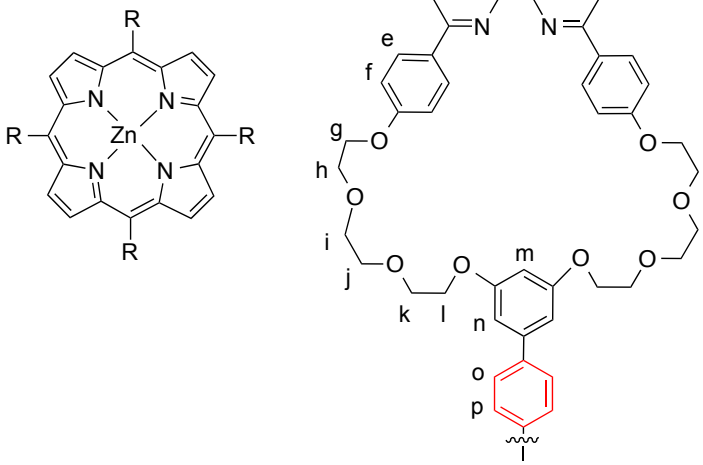

aqueous solution of EDTA (0.10 M, 12.5 mL) was added to the organic layer and the biphasic mixture was stirred for 24 h. The organic layer was separated, washed with water and dried with $MgSO_4$. This yielded zinc porphyrin **Zn-PM4b** as a purple solid (6 mg, 1.72 µmol; two step yield: 11%).

^{1}H NMR (400 MHz, $CDCl_3$): δ 8.68 (s, 8H H_a) 8.41 (d, ^3J = 9.2 Hz, 16H, H_f), 8.24 (d, ^3J = 8.6 Hz, 8H, H_c), 7.96 (d, ^3J = 8.6 Hz, 8H, H_d), 7.86 (m, 16H, $H_{o,p}$), 7.17 (m, 32H, $H_{b,e,n}$), 6.71 (t, ^3J = 2.3 Hz, 4H, H_m), 4.36 (t, ^3J = 5.1 Hz, 16H, H_g), 4.28 (t, ^3J = 4.8 Hz, 16H, H_l), 4.00 (m, 32H, $H_{h,k}$), 3.86 ppm (m, 32H, $H_{i,j}$).
^{13}C NMR (125 MHz, $CDCl_3$): δ 160.8, 160.4, 156.2, 150.1, 145.9, 143.6, 143.2, 139.8, 136.7, 136.2, 132.6, 129.3, 127.3, 125.3, 124.0, 120.1, 119.3, 115.1, 107.7, 100.7, 71.4, 71.4, 70.3, 70.1, 68.2, 67.8.
UV-vis λ_{max} CH_2Cl_2 (log ε): 557 (4.16), 434 (5.28), 287 (5.27).
MALDI-TOF MS: $C_{212}H_{188}N_{16}O_{32}Zn$ Calc – 3480.28, Found *m/z* 3483.72.

[3]Rotaxane **P3Ra**

TFA (3.2 µL, 41 µmol) was added to a solution of rotaxane aldehyde **2Ra** (14 mg, 6.9 µmol) and 2,2'-dipyrromethane

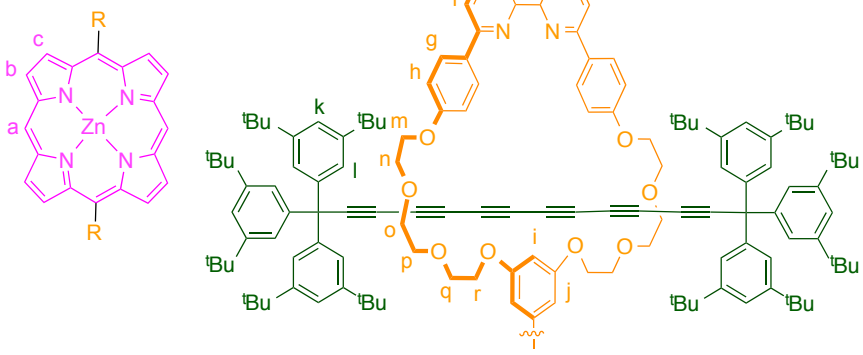

(1.0 mg, 6.9 µmol) in dry CH_2Cl_2 (2 mL). The flask was protected from light and stirred under N_2 for 2 h. DDQ (3.1 mg, 14 µmol) was added and stirred for a further 1 h. NEt_3 (20 µL, 0.14 mmol) was added to neutralise the reaction mixture and it was passed through a silica plug (CH_2Cl_2) to yield free-base [3]rotaxane **P3Ra** as a red solid (10 mg, 2.3 µmol, 67%). Free-base [3]rotaxane **P3Ra** was dissolved in $CHCl_3$ (5 mL). A solution of $Zn(OAc)_2.2H_2O$ (20 mg, 91 µmol) in MeOH (3 mL) was added. The solution was heated to reflux and stirred for 2 h under N_2, then evaporated; the residue was dissolved in CH_2Cl_2 and washed with water. An aqueous solution of EDTA (0.10 M, 2.5 mL) was added to the organic layer and the biphasic mixture was

stirred for 24 h. The organic layer was separated, washed with water and dried with $MgSO_4$. This yielded zinc [3]rotaxane **Zn-P3Ra** as a purple solid (9.1 mg, 2.0 μmol; two step yield: 62%).

^{1}H NMR (400 MHz, $CDCl_3$): δ 10.07 (s, 2H H_a), 9.28 (d, ^3J = 4.6 Hz , 4H, H_b), 9.19 (d, ^3J = 4.6 Hz, 4H, H_c) 8.52 (d, ^3J = 8.6 Hz, 8H, H_g), 8.27 (d, J = 8.4 Hz, 4H, H_f), 8.11 (d, ^3J = 8.4 Hz, 4H, H_e), 7.76 (s, 4H, H_d), 7.47 (d, ^3J = 1.8 Hz, 4H, H_j), 7.25 (t, 12H, ^3J = 1.6 Hz, H_k), 7.06 (d, ^3J = 2.2 Hz, 2H, H_i), 6.92 (d, 24H, ^3J =1.6 Hz, H_l), 4.38 (t, ^3J = 4.6 Hz, 8H, H_m), 4.35 (t, ^3J = 4.6 Hz, 8H, H_r), 3.98-4.00 (m, 16H, $H_{n,q}$) 3.85-3.89 (m, 16H, $H_{o,p}$), 1.14 (s, 216H, H_{tBu}).

^{13}C NMR (125 MHz, $CDCl_3$): δ 160.3, 158.4, 156.4, 150.2, 146.9, 146.1, 145.2, 143.3 136.6, 132.5, 132.2, 131.5, 131.2, 130.9, 129.0, 127.4, 125.5, 123.7, 120.4, 119.1, 118.8, 115.2, 114.9, 105.1, 100.4, 96.1, 86.4, 71.2, 71.1, 70.0, 69.7, 68.9, 68.2, 68.0, 67.5, 57.4, 34.8, 31.3.

UV vis λ_{max} $CHCl_3$, (log ε): 280 (5.29), 297 (5.50), 316 (5.58), 410 (5.39).

MALDI-TOF MS: $C_{300}H_{344}N_8O_{16}Zn$ Calculated – 4380.57, Found *m/z* 4366.23

Biphenyl [3]rotaxane **Zn-P3Rb**

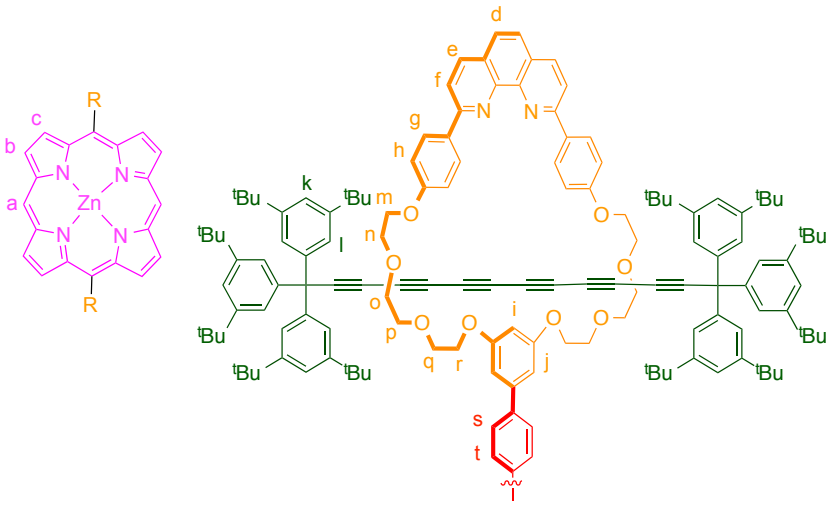

TFA (4.0 μL, 41 μmol) was added to a solution of rotaxane aldehyde **2Rb** (20 mg, 9.0 μmol) and 2,2'-dipyrromethane (1.3 mg, 9.0 μmol) in dry CH_2Cl_2 (3 mL). The flask was protected from light and stirred under N_2 for 2 h. DDQ (4.1 mg, 18 μmol) was added and stirred for a further 1 h. NEt_3 (20 μL, 0.14 mmol) was added to neutralize the reaction mixture and it was passed through a silica plug (CH_2Cl_2) to yield free-base [3]rotaxane **P3Rb** as a red solid (7 mg, 34%), which was immediately metallated. Free-base [3]rotaxane **P3Rb** was dissolved in $CHCl_3$ (5 mL). A solution

of $Zn(OAc)_2.2H_2O$ (20 mg, 91 µmol) in MeOH (3 mL) was added. The solution was heated to reflux and stirred for 2 h under N_2, then evaporated; the residue was dissolved in CH_2Cl_2 and washed with water. An aqueous solution of EDTA (0.10 M, 2.5 mL) was added to the organic layer and the biphasic mixture was stirred for 24 h. The organic layer was separated, washed with water and dried with $MgSO_4$. This yielded zinc [3]rotaxane **Zn-P3Rb** as a purple solid (6.7 mg; two step yield: 33%).

^{1}H NMR (500 MHz, $CDCl_3$): δ 10.30 (s, 2H, H_a), 9.44 (d, ^3J = 4.7 Hz , 4H, H_b), 9.21 (d, ^3J = 4.7 Hz, 4H, H_c) 8.48 (d, ^3J = 8.6 Hz, 8H, H_h), 8.26 (d, ^3J = 8.3 Hz, 4H, H_f), 8.16 (d, ^3J = 8.5 Hz, 4H, H_s), 8.05 (d, ^3J = 8.5 Hz, 4H, H_t), 8.00 (d, ^3J = 8.3 Hz, 4H, H_e), 7.59 (s, 4H, H_d), 7.21 (t, 12H, ^3J = 1.7 Hz, H_k), 7.16 (d, ^3J = 1.8 Hz, 4H, H_j), 6.87 (d, 24H, ^3J =1.7 Hz, H_l), 6.74 (t, ^3J = 1.7 Hz, 2H, H_i), 4.36 (t, 8H, H_r), 4.32 (t, 8H, H_m), 4.02 (m, 16H $H_{n,q}$), 3.86 (m, 16H, $H_{o,p}$), 1.13 (s, 216H, H_{tBu}).

^{13}C NMR (125 MHz, $CDCl_3$): δ 160.9, 160.5, 156.6, 150.5, 149.8, 146.3, 143.6, 143.2, 142.0, 140.7, 136.8, 135.3, 133.0, 132.5, 132.1, 129.3, 127.6, 125.8, 125.6, 124.0, 120.7, 120.1, 119.4, 116.7, 115.3, 107.4, 106.6, 100.4, 86.7, 71.5, 71.4, 70.3, 70.0, 69.1, 68.3, 67.8, 63.6, 63.6, 63.2, 63.0, 57.6, 35.1, 31.6.

UV-vis λ_{max} $CHCl_3$, (log ε): 539 (4.18), 412 (5.39), 317 (5.59), 298 (5.53), 282 (5.39).

MALDI TOF MS: $C_{312}H_{352}N_8O_{16}Zn$ Calc – 4533.63, Found *m/z* – 4527.98.

[5]Rotaxane Zn-P5Rb

TFA (14.7 µL, µmol) was added to a solution of rotaxane aldehyde **2Rb** (68 mg, 32 µmol) and freshly distilled pyrrole (2.0 µL, 32 µmol) in dry CH_2Cl_2 (2 mL). The flask was protected from light and stirred under N_2 for 2 h. DDQ (14.6 mg, 64.4 µmol) was added and stirred for a further 1 h. NEt_3 (20 µL, 0.14 mmol) was added to neutralise the reaction mixture and it was passed through a silica plug (CH_2Cl_2). The crude

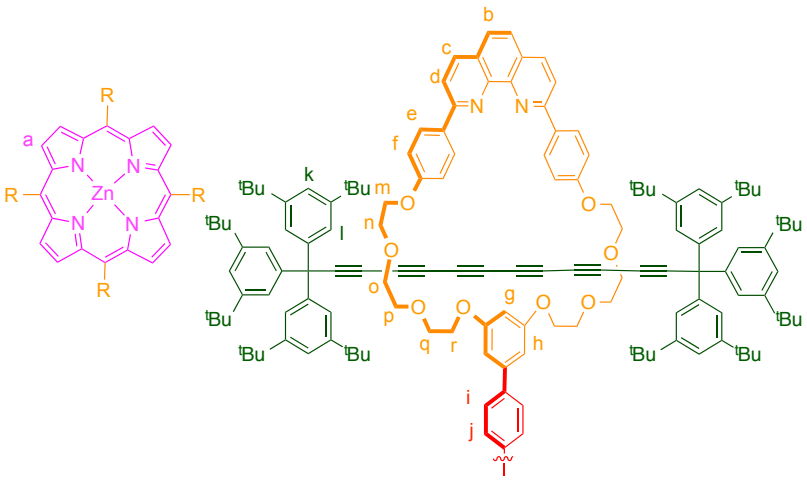

product was passed through a SEC column in toluene/pyridine 99:1, then purified further via recycling GPC to yield [5]rotaxane **P5Rb** as a red solid (7 mg, 10%).

^{1}H NMR (500 MHz, $CDCl_3$): δ 8.93 (s, 8H, H_a), 8.48 (d, ^3J = 8.8 Hz, 16H, H_e), 8.24 (d, ^3J = 8.3 Hz, 8H, H_d), 8.23 (d, ^3J = 8.5 Hz, 8H, H_i), 8.08 (d, ^3J = 8.5 Hz, 8H, H_c), 7.97 (d, ^3J = 8.3 Hz, 8H, H_j), 7.74 (s, 8H, H_b), 7.19 (t, 24H, ^3J =1.7 Hz, H_k), 7.18 (d, ^3J = 8.8 Hz, 16H, H_f), 7.12 (d, 8H, ^3J = 1.8 Hz, H_g), 6.85 (d, 48H, ^3J = 1.7 Hz, H_l), 6.72 (t, ^3J = 1.7 Hz, 2H, H_h), 4.32 (m, 32H, $H_{m,r}$), 3.99 (t, 32H, $H_{n,q}$), 3.84 (m, 32H, $H_{o,p}$), 1.13 (s, 432H, H_{tBu}), –2.70 (s, 2H, $H_{internal}$).
^{13}C NMR (125 MHz, $CDCl_3$): δ 160.9, 160.5, 156.6, 150.4, 146.4, 143.5, 143.1, 141.6, 140.8, 136.8, 135.3, 132.5, 129.4, 129.3, 128.5, 127.7, 125.7, 125.6, 124.2, 123.9, 120.7, 120.2, 119.3, 115.2, 107.4, 100.2, 86.7, 71.5, 71.4, 70.3, 70.0, 69.1, 68.2, 67.8, 63.6, 63.6, 63.1, 62.9, 57.6, 35.1, 31.6.

Metallation was performed by addition of $Zn(OAc)_2.2H_2O$ (10 mg, 46 μmol) in MeOH (2 mL) to a solution of free-base [5]rotaxane **P5Rb** in $CHCl_3$ and heating to 60 °C for 1 h, yielding a red-brown solid **Zn-P5Rb** (5 mg, 7% over two steps).

^{1}H NMR (500 MHz, $CDCl_3$): δ 8.94 (s, 8H, H_a), 8.48 (d, ^3J = 8.6 Hz, 16H, H_e), 8.24 (d, ^3J = 8.3 Hz, 8H, H_d), 8.23 (d, ^3J = 8.5 Hz, 8H, H_i), 8.08 (d, ^3J = 8.5 Hz, 8H, H_c), 7.97 (d, ^3J = 8.3 Hz, 8H, H_j), 7.74 (s, 8H, H_b), 7.20 (t, 24H, ^3J =1.7 Hz, H_k), 7.18 (d, ^3J = 8.5 Hz, 16H, H_f), 7.13 (d, 8H, ^3J = 1.8 Hz, H_g), 6.85 (d, 48H, ^3J =1.7 Hz, H_l), 6.72 (t, ^3J = 1.7 Hz, 2H, H_h), 4.32 (m, 32H, $H_{m,r}$), 3.99 (t, 32H, $H_{n,q}$), 3.85 (m, 32H, $H_{o,p}$), 1.13 (s, 432H, H_{tBu})
^{13}C NMR (125 MHz, $CDCl_3$): δ 160.8, 160.5, 156.6, 150.4, 146.3, 143.5, 143.2, 140.1, 138.2, 136.8, 135.3, 132.4, 132.0, 129.3, 129.3, 128.5, 127.7, 125.7, 125.6, 125.3, 123.9, 120.7, 120.2, 119.3, 115.2, 107.3, 86.7, 71.4, 71.4, 70.2, 70.0, 69.0, 68.1, 67.8, 63.6, 63.6, 63.1, 62.9, 57.6, 35.1, 31.6.
UV-vis λ_{max} CH_2Cl_2 (log ε): 551 (4.00), 425 (5.32), 317 (5.64), 298 (5.57), 282 (5.43).
MALDI TOF MS: $C_{604}H_{692}N_{16}O_{32}Zn$ Calc – 8697.24, Found *m/z* – 8699.69 (broad).

2.9 - References

(1) Breault, G. A.; Hunter, C. A.; Mayers, P. C. *Tetrahedron* **1999**, *55*, 5265–5293.
(2) van Dongen, S. F. M.; Cantekin, S.; Elemans, J. A. A. W.; Rowan, A. E.; Nolte, R. J. M. *Chem. Soc. Rev.* **2014**, *43*, 99–122.
(3) Berná, J.; Crowley, J. D.; Goldup, S. M.; Hänni, K. D.; Lee, A. L.; Leigh, D. A. *Angew. Chemie - Int. Ed.* **2007**, *46*, 5709–5713.
(4) Crowley, J. D.; Goldup, S. M.; Lee, A.-L.; Leigh, D. A.; McBurney, R. T. *Chem. Soc. Rev.* **2009**, *38*, 1530–1541.
(5) Saito, S.; Takahashi, E.; Nakazono, K. *Org. Lett.* **2006**, *8*, 5133–5136.
(6) Saito, S.; Takahashi, E.; Wakatsuki, K.; Inoue, K.; Orikasa, T.; Sakai, K.; Yamasaki, R.; Mutoh, Y.; Kasama, T. *J. Org. Chem.* **2013**, *78*, 3553–3560.
(7) Hayashi, R.; Mutoh, Y.; Kasama, T.; Saito, S. *J. Org. Chem.* **2015**, *80*, 7536–7546.
(8) Langton, M. J.; Matichak, J. D.; Thompson, A. L.; Anderson, H. L. *Chem. Sci.* **2011**, *2*, 1897.
(9) Movsisyan, L. D.; Kondratuk, D. V.; Franz, M.; Thompson, A. L.; Tykwinski, R. R.; Anderson, H. L. *Org. Lett.* **2012**, *14*, 3424–3426.
(10) Weisbach, N.; Baranová, Z.; Gauthier, S.; Reibenspies, J. H.; Gladysz, J. A. *Chem. Commun.* **2012**, *48*, 7562.
(11) Franz, M.; Januszewski, J. A.; Wendinger, D.; Neiss, C.; Movsisyan, L. D.; Hampel, F.; Anderson, H. L.; Görling, A.; Tykwinski, R. R. *Angew. Chem. Int. Ed.* **2015**, *54*, 6645–6649.
(12) Movsisyan, L. D.; Franz, M.; Hampel, F.; Thompson, A. L.; Tykwinski, R. R.; Anderson, H. L. *J. Am. Chem. Soc.* **2016**, *138*, 1366–1376.
(13) Hoffmann, M.; Wilson, C. J.; Odell, B.; Anderson, H. L. *Angew. Chem. Int. Ed.* **2007**, *46*, 3122–3125.
(14) Kadish, K. M.; Smith, K. M.; Guilard, R. World Scientific Publishing 2010.
(15) Karolczak, J.; Kowalska, D.; Lukaszewicz, A.; Maciejewski, A.; Steer, R. P. *J. Phys. Chem. A* **2004**, *108*, 4570–4575.
(16) Du, B.; Fortin, D.; Harvey, P. D. *Inorg. Chem.* **2011**, *50*, 11493–11505.
(17) Wagner, R. W.; Lindsey, J. S. *J. Am. Chem. Soc.* **1994**, *116*, 9759–9760.
(18) Anderson, H. L. *Chem. Commun.* **1999**, *23*, 2323–2330.
(19) Gouterman, M. *J. Mol. Spectrosc.* **1961**, *127*, 138–163.
(20) Saltiel, J.; Kumar, V. K. R. *J. Phys. Chem. A* **2012**, *116*, 10548–10558.
(21) Nagano, Y.; Ikoma, T.; Akiyama, K.; Tero-Kubota, S. *J. Am. Chem. Soc.* **2003**, *125*, 14103–14112.
(22) Deperasińska, I.; Szemik-Hojniak, A.; Osowska, K.; Rode, M. F.; Szczepanik, A.; Wiśniewski, Ł.; Lis, T.; Szafert, S. *J. Photochem. Photobiol. A Chem.* **2011**, *217*, 299–307.
(23) Movsisyan, L. D.; Peeks, M. D.; Greetham, G. M.; Towrie, M.; Thompson, A. L.; Parker, A. W.; Anderson, H. L. *J. Am. Chem. Soc.* **2014**, *136*, 17996–18008.
(24) Chalifoux, W.; Tykwinski, R. R. *Nat. Chem.* **2010**, *2*, 967–971.
(25) Khuong, T. A. V; Zepeda, G.; Ruiz, R.; Khan, S. I.; Garcia-Garibay, M. A. *Cryst. Growth Des.* **2004**, *4*, 15–18.
(26) Ditto, S, R.; Card, R, J.; Davis, P, D.; Neckers, D, C. *J. Am. Chem. Soc.* **1971**, *93*, 731–737.
(27) Bartlett, P. D.; Roha, M.; Stiles, R. M. *J. Am. Chem. Soc.* **1953**, *76*, 2349–2353.

(28) Ramirez, F.; Desai, N. B.; McKelvie, N. *J. Am. Chem. Soc.* **1962**, *84*, 1745–1747.
(29) Jahnke, E.; Tykwinski, R. R. *Chem. Commun.* **2010**, *46*, 3235–3249.
(30) Roche, C.; Sour, A.; Niess, F.; Heitz, V.; Sauvage, J. P. *Eur. J. Org. Chem* **2009**, *17*, 2795–2800.
(31) Roche, C.; Sauvage, J.-P.; Sour, A.; Strutt, N. L. *New J. Chem.* **2011**, *35*, 2820.
(32) Amabilino, D. B.; Sauvage, J.; Pascal, B. *New J. Chem.* **1998**, 395–409.
(33) Lindsey, J. S.; Schreiman, I. C.; Hsu, H. C.; Kearney, P. C.; Marguerettaz, A. M. *J. Org. Chem.* **1987**, *52*, 827–836.
(34) Adler, A. D.; Longo, F. R.; Shergalis, W. *J. Am. Chem. Soc.* **1964**, *86* (15), 3145–3149.
(35) Nowell, H.; Barnett, S. A.; Christensen, K. E.; Teat, S. J.; Allan, D. R. *J. Synchrotron Radiat.* **2012**, *19*, 435–441.
(36) Palatinus, L.; Chapuis, G. *J. Appl. Crystallogr.* **2007**, *40*, 786–790.
(37) Betteridge, P. W.; Carruthers, J. R.; Cooper, R. I.; Prout, K.; Watkin, D. J. *J. Appl. Crystallogr.* **2003**, *36*, 1487–1487.
(38) Cooper, R. I.; Thompson, A. L.; Watkin, D. J. *J. Appl. Crystallogr.* **2010**, *43*, 1100–1107.
(39) Van Der Sluis, P.; Spek, A. L. *Acta Crystallogr. Sect. A* **1990**, *46*, 194–201.
(40) Spek, A. L. *J. Appl. Crystallogr.* **2003**, *36*, 7–13.
(41) Chalifoux, W. A.; McDonald, R.; Ferguson, M. J.; Tykwinski, R. R. *Angew. Chem. Int. Ed.* **2009**, *48*, 7915–7919.
(42) Szafert, S.; Gladysz, J. A. *Chem. Rev.* **2006**, *106*, 1–33.
(43) Strachan, J. P.; Gentemann, S.; Seth, J.; Kalsbeck, W. A.; Lindsey, J. S.; Holten, D.; Bocian, D. F. *J. Am. Chem. Soc.* **1997**, *119*, 11191–11201.
(44) Jiang, H. W.; Kim, T.; Tanaka, T.; Kim, D.; Osuka, A. *Chem. - A Eur. J.* **2016**, *22*, 83–87.
(45) Amabilino, D. B.; Sauvage, J.; Pascal, B. *New J. Chem.* **1998**, *1998*, 395–409.

Chapter 3

Synthesis of polyynes using dicobalt masking groups

3.1. Introduction 80

3.2. Synthesis of dicobalt and tetracobalt complexes 82

3.3. Unmasking polyynes from cobalt complexes 87

3.4. Attempted rotaxane synthesis 89

3.5. Reactivity of terminal acetylene 92

3.6. Electronic absorption spectra and molecular orbitals 95

3.7. Crystallography 100

3.8. Conclusions 104

3.9. Experimental data for known compounds 105

3.10. Experimental data for novel compounds 110

3.11. References 118

Parts of this chapter have been submitted to the *Journal of Organic Chemistry*. (D.R. Kohn, P. Gawel, Y. Xiong, K. Christensen, H.L. Anderson). DFT was performed by Dr Przemyslaw Gawel. Crystallography was performed by myself, Yaoyao Xiong and Dr Kirsten Christensen.

Chapter 3 – Synthesis of polyynes using dicobalt masking groups

3.1 - Introduction

Polyynes are fragile molecules and they readily undergo cross-linking reactions, leading to decomposition and sometimes even explosions.[1] One method of circumventing this undesired reactivity is to mask the alkyne as a 'masked alkyne equivalent' (MAE). The alkyne-dicobalt carbonyl moiety is a potential MAE, as it can reversibly complex a triple bond (**Figure 3.1a**).[2,3] Dicobalt octacarbonyl consists of a cobalt(0)-based structure that forms a butterfly-shaped complex with alkynes.[4] The affinity of cobalt(0) carbonyl complexes for alkynes is utilised in many important reactions. The cobalt(0) acts as a catalytic centre, facilitating beta substitution of alkynes in the Nicholas reaction[5] and preparing α,β-cyclopentenones in the Pausson-Khand reaction[6,7] amongst others. Cobalt clusters have also been used as electrochemical probes in acetylenic molecular wires.[8–10]

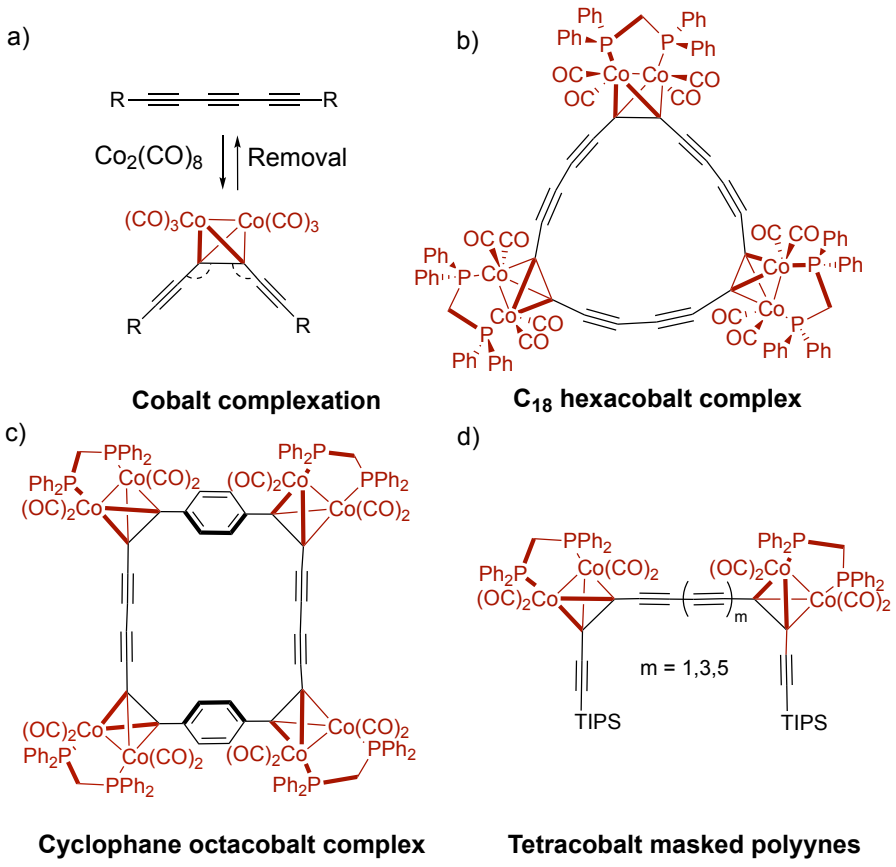

Figure 3.1. a) Dicobalt complexation of an alkyne, b) C_{18} hexacobalt complex,[11] c) [8,8]paracyclophaneoctayne octacobalt complex,[12] d) tetracobalt masked polyynes (this work).

The high demand for functional organic materials has led to increasing interest in carbon-rich materials.[9–11] Alkynes play an essential role in bottom-up synthesis in this field.[15,17] The dicobalt carbonyl MAE group is particularly interesting for synthesising acetylene-based structures because it can stabilise conjugated alkynes in two ways. Firstly, its steric bulk prevents close contacts between *sp*-chains, blocking crosslinking reactions.[1] Secondly, it breaks the conjugation of the polyyne by changing the hybridisation of the complexed carbon atoms from *sp* to sp^3. Additionally, it induces significant bending between the attached groups, aiding formation of curved structures.[12,18] A search in the Cambridge Structural Database (CSD) revealed the maximum observed bending was 133.3 °, other parameters were also determined (**Figure 3.2**). The pristine dicobalt carbonyl group can be removed by oxidation,[19] alkyne-ligand exchange[20] or flash vacuum pyrolysis.[21] However, it is more useful when modified to incorporate a *bis*-(diphosphinomethane) ligand, which improves the stability of the complexes due to its basicity and chelating effect.[22–24]

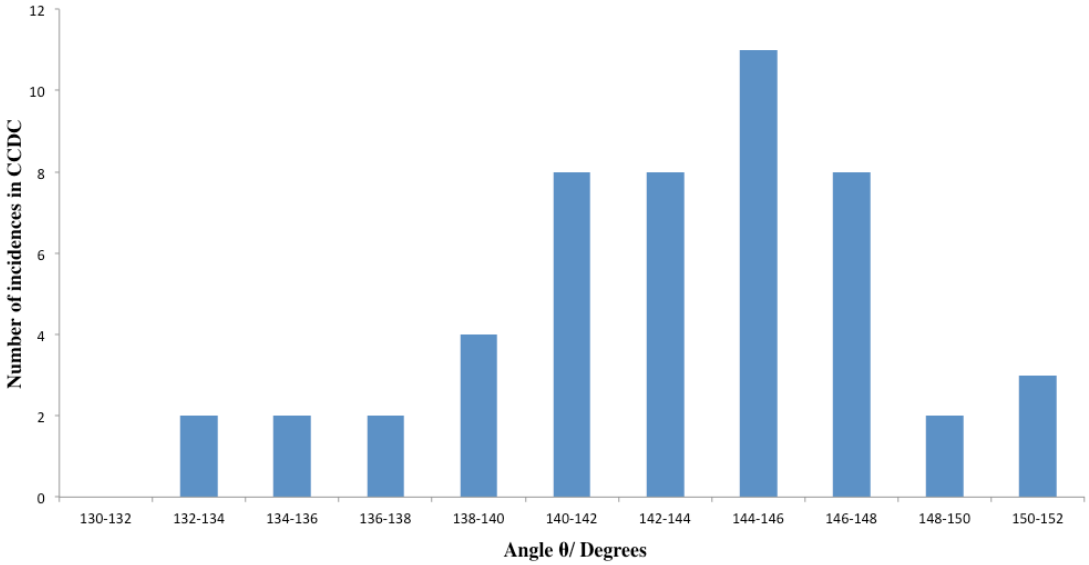

Figure 3.2. Frequency of angle θ in the CSD. Average = 141.2 °, standard deviation = 4.1 °; these parameters have been determined from a sample of 52 crystal structures from the CSD.

Previously, two carbon-rich compounds with curved acetylenic π-systems have been approached by preparing their masked cobalt complexes. In the first example by Diederich and coworkers, a cobalt-masked triyne was used to assemble the corresponding hexacobalt masked cyclo[18]carbon macrocycle (**Figure 3.1b**).[11] Haley *et al.* also prepared an octacobalt complex of a cyclophane with a curved tetrayne bridges (**Figure 3.1c**).[12] Both studies failed to unmask the desired curved π-

systems from the corresponding cobalt complex. However, Haley *et al.* successfully removed the dicobalt carbonyl moieties with excess I_2 in diyne model compounds, but this could not be reproduced on the octacobalt cyclophane complex. We believe the origin of these failures is the inherent reactivity of the desired curved polyynes rather than the unmasking of the dicobalt group itself.

Polyyne synthesis *via* MAEs, such as dibromoolefins, dialkynyl-3-cyclobutene-1,2-diones and dialkynylmethylenebicyclo[4.3.1]deca-1,3,5-triene, offer high yields in relatively short systems.[25–27] Further development of masking groups would be useful for the synthesis of longer polyynes. Several other MAEs have been developed and used in efforts to unmask cyclocarbons from the corresponding precursors. These MAEs require relatively harsh unmasking conditions, including high temperatures,[28] flash vacuum pyrolysis,[29] *n*-BuLi[25,30] or intense UV light.[31–33] The use of harsh unmasking conditions limits the use of these MAEs when unmasking long polyynes and other fragile alkynes.

The aim of this work was to prepare cobalt-masked acetylenic building blocks and cobalt-masked long polyynes (**Figure 3.1d**), as part of an effort towards carbon-rich supramolecular structures.[34,35] Further understanding of the effect of the dicobalt moiety on conjugated polyynes is obtained from analysis of NMR, IR, UV-vis spectroscopies, density functional theory (DFT) and X-ray crystallography.

3.2 – Synthesis of dicobalt and tetracobalt complexes

Three dicobalt-masked building blocks containing terminal oligoynes of different length were prepared in order to access a series of tetracobalt-masked polyynes and as substrates for attempted rotaxane formation. Firstly, TIPS-protected cobalt complex **3.5** was prepared as previously reported[11] in order to prepare **3** (**Scheme 3.1**). Synthesis of a dibromo compound **3.3**[36], followed by the FBW rearrangement was used to prepare the bis-TIPS triyne **3.4**, in contrast to the flash vacuum pyrolysis method used by Diederich *et al.*[11] Triyne **3.4** was transformed into bis-TIPS cobalt complex **3.5** by refluxing in toluene with $Co_2(CO)_8$ and dppm. As expected, there was total selectivity for the central acetylene in C_2 symmetric polyyne **3.4** due to the large bulk of the TIPS groups; no other isomers were observed. Hereafter, from the bis-

TIPS compound **3.5**, we hoped it would be possible to utilise a statistical deprotection in order to yield the desired compound **3**. However, in wet THF (1 µL per 1 mL) with 0.1 equiv of TBAF, full deprotection occurred within 5 minutes. In contrast, portionwise addition of TBAF in CH_2Cl_2 (0.1 equiv. until 1 equiv. was added) did permit a statistical deprotection. However, it was very slow and decomposition appeared to compete with deprotection. The maximum isolated yield of the mono-deprotected complex **3** was 10% when utilising this approach. This was unfeasible for scaling up and an alternative retrosynthetic route was explored.

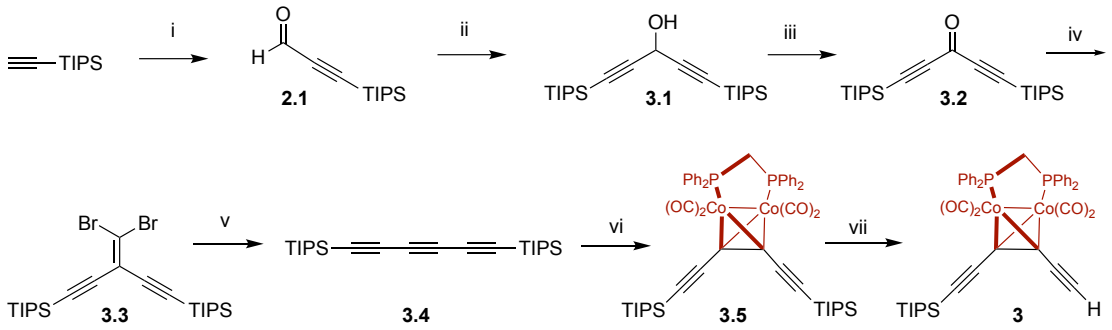

Scheme 3.1. Synthesis of known compound **3.5** and novel compound **3**. i) a) *n*-BuLi, THF, -78 °C, 30 min. b) DMF, -78 °C, 88% ii) a) TIPS-acetylene, *n*-BuLi, THF, -78 °C, 30 min. b) Aldehyde **2.1**, -78 °C, 1 h, 71% iii) PCC, Celite, mol Sieves, CH_2Cl_2, 25 °C, 86% iv) PPh_3, CBr_4, CH_2Cl_2, 25 °C, 100 % v) *n*-BuLi, hexane, -78 °C, 30 min., 85% vi) a) $Co_2(CO)_8$, hexane, 25 °C, 12 h. b) dppm, toluene, 110 °C, 1 h, 84% vii) TBAF, CH_2Cl_2, $CHCl_3$, 25 °C, 15 min., 10%.

TIPS,TMS-protected triyne **3.10**[30] (**Scheme 3.2**) was synthesised because the TMS group can be selectively removed whilst leaving the TIPS group untouched using K_2CO_3 in THF/MeOH at room temperature.[37,38] Our expectation was that dicobalt complex formation with TIPS,TMS-triyne **3.10** would occur at the central alkyne to give **2** (analogously to the reported bis-TIPS complex[11]) and that regioisomer **2b** would be a minor byproduct. However, the major product was the undesired product **2b**, where the dicobalt group is adjacent to the less bulky TMS group (45% yield) (**Scheme 3.2**). The desired product **2** was isolated in 27% yield. The identities of **2** and **2b** were confirmed by NMR spectroscopy (**Figure 3.3**, **Figure 3.4**) and X-ray crystallography (**Figure 3.14**). Despite the large amount of undesired regioisomer that is formed, this is a more efficient synthetic route than statistical deprotection of a bis-TIPS complex (**Scheme 3.1**).

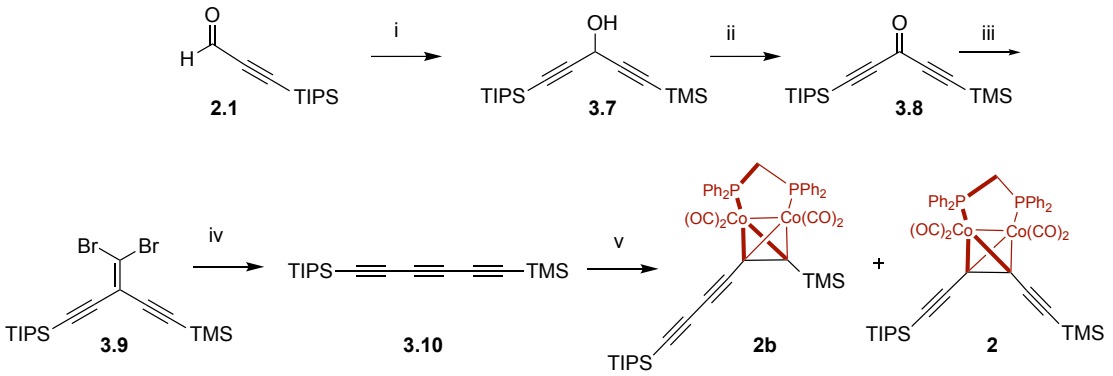

Scheme 3.2. i) TMS-acetylene, *n*-BuLi, aldehyde **2.1**, THF, −78 °C, 1 h, 88% ii) PCC, celite, mol. sieves, CH_2Cl_2, 25 °C, 20 h, 96% iii) PPh_3, CBr_4, CH_2Cl_2, 25 °C, 16 h, 93% iv) *n*-BuLi, hexane, −78 °C, 30 min, 80% v) a) $Co_2(CO)_8$, hexane, 25 °C, 12 h b) diphenylphosphinomethane, toluene, 110 °C, 30 min., 45% (**2b**) and 27% (**2**).

The ^{1}H NMR spectra of the regioisomers **2** and **2b** are similar because the variance between them is remote from any hydrogen atoms (**Figure 3.3**). The two geminal protons from the diphosphine bridge are inequivalent, as observed in both spectra ($\delta_H \approx 3.5$ ppm). There is a greater splitting of signals in the regioisomer **2b** because the proton environments are more different. The chemical shift of the trimethylsilyl group supports the assignment as the signal comes at an unusual chemical shift of 0.40 ppm in **2b**. This reflects the unusual environment of the adjacent carbon atom. The TMS signal in **2** has a chemical shift of 0.25 ppm, which is in the typical range for a TMS group attached to an alkyne.

The NMR spectra of **2** and **2b** contain the expected number of signals. In both compounds the carbon atoms that are directly connected to cobalt are observed at 69-80 ppm in ^{13}C NMR spectra, although they are broader and less well resolved in **2** (**Figure 3.4**). The chemical shifts are as expected for each isomer, two acetylenic carbons with satellites are observed in **2**, in contrast to **2b**. In **2**, carbon atoms 1 and 2 from the TIPS-acetylene have distinctive chemical shifts that are also observed in the ^{13}C NMR of compounds **3-7**. These signals are also crucial in confirming the identies of each isomer.

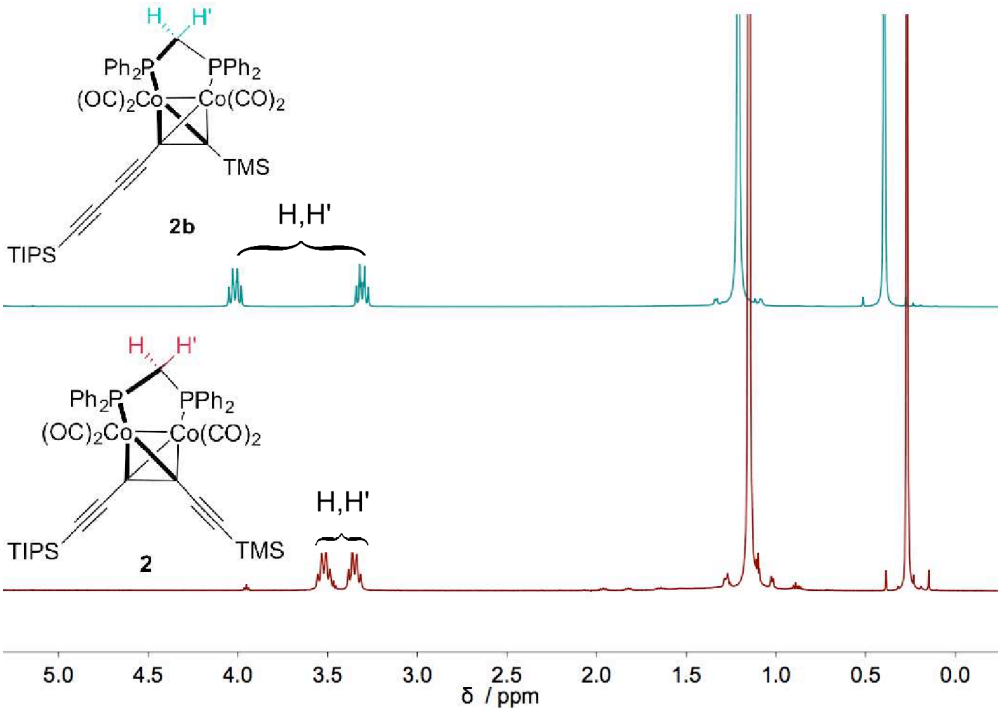

Figure 3.3. ^{1}H NMR signals differentiating isomer **2b** from **2** (500 MHz, $CDCl_3$).

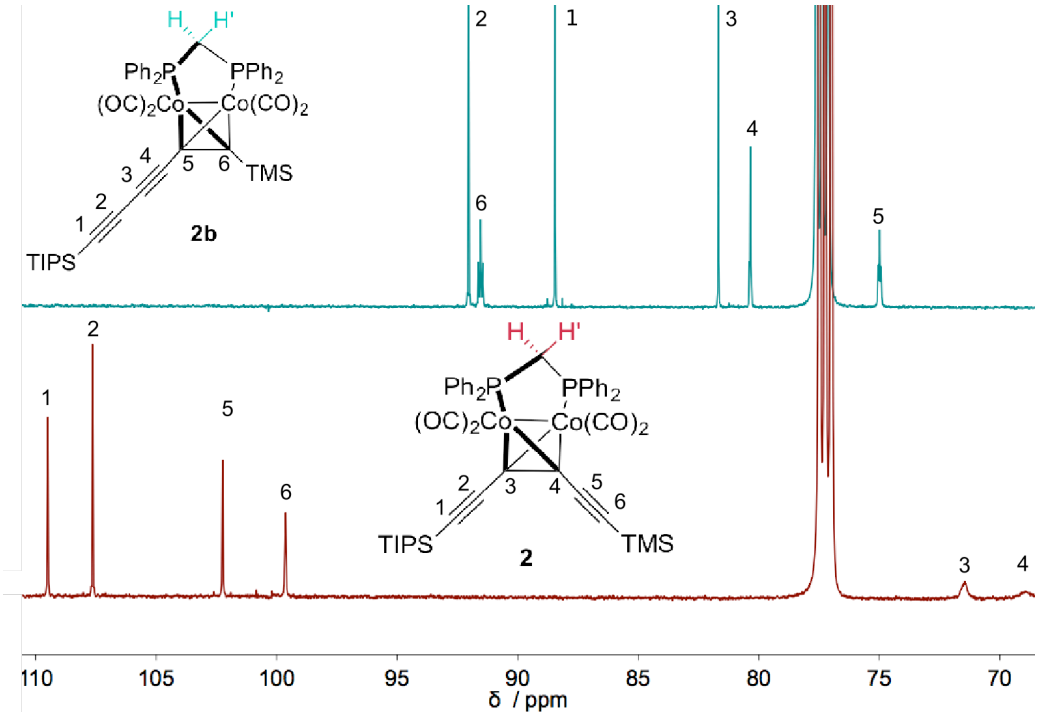

Figure 3.4. ^{13}C NMR signals differentiating isomer **2b** from **2** (125 MHz, $CDCl_3$).

Deprotection of **2** with K_2CO_3 in MeOH/THF yielded the desired cobalt complex **3** quantitatively (**Scheme 3.3**). The acetylenic chain in cobalt complex **3** can be readily extended *via* a Glaser coupling with TMS-acetylene.[39] Use of an excess of TMS-acetylene, CuCl and TMEDA gave the desired butadiyne **4** in 82% yield (with bis

TMS-butadiyne as a side product, **Scheme 3.3**). The large excess of reagents was required to avoid homocoupling of **3**. The structure of **4** was confirmed by single crystal X-ray diffraction (**Figure 3.16**). Deprotection of **4** using K_2CO_3 in THF/MeOH yielded the desired **5** in a quantitative yield. The acetylene chain extension methodology was used again to furnish **6** in 84% yield and the following deprotection gave terminal triyne **7** (**Scheme 3.3**). Complex **7** must be handled with care, as it is relatively unstable when dry and particularly whilst at elevated temperatures. However, it is notably more stable than the corresponding unmasked terminal pentayne.

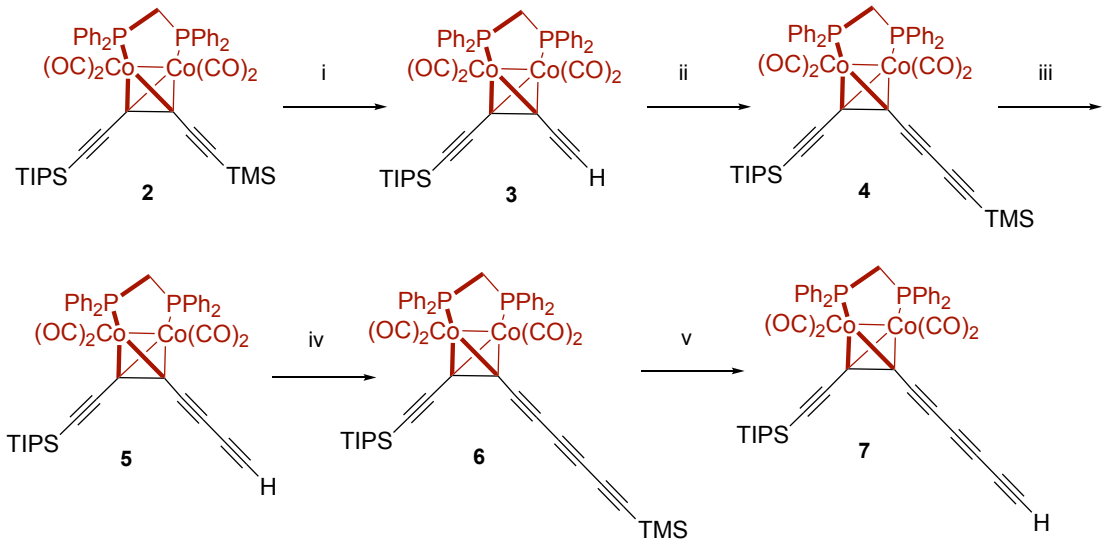

Scheme 3.3. i) K_2CO_3, THF/MeOH, 25 °C, 30 min. ii) TMS-acetylene, CuCl, TMEDA, CH_2Cl_2, 25 °C, 2 h. iii) K_2CO_3, THF/MeOH, 25 °C, 30 min. iv) TMS-acetylene, CuCl, TMEDA, CH_2Cl_2, 25 °C, 2 h. v) K_2CO_3,THF/MeOH, 25 °C, 30 min.

The oxidative homocoupling reaction of **3** using Eglinton coupling conditions[40] with $Cu(OAc)_2$ in pyridine gave two separable products. The expected isomer **8** was the major product but a small quantity of regiosiomer **8b** was also isolated (**Scheme 3.4**). The structures of these compounds were confirmed by analysis of single crystals (**Figure 3.15**). Repeating the reaction using different coupling conditions did not change the outcome of this reaction; a small amount of rearranged product **8b** was always formed. A partially rearranged product was never isolated. The reason for this unexpected isomerisation is not clear. Isomerisation experiments were performed with **2**, **2b**, **8** and **8b.** We hypothesised that the reaction conditions could be facilitating cobalt decomplexation and recomplexing in a different position. To test this theory we subjected the regioisomers individually to the reaction conditions and monitored the

reaction by TLC and NMR spectroscopy. Additionally, we tried heating in the presence of excess bis(diphenylphosphinomethane). None of these processes led to rearrangement.

The analogous tetracobalt complex **9** was also prepared *via* Eglinton coupling. Once again, two products were observed by TLC; however, the higher R_f spot decomposed during silica column chromatography. By analogy to **8b** we presume that the unexpected byproduct contains a hexayne. The stable product was identified as **9** by ^{13}C NMR spectroscopy through observation of the characteristic signals from acetylene carbons adjacent to the TIPS group. The analogous complex **10** was also formed from **7** using Eglinton coupling conditions (**Scheme 3.3**). The loss of terminal acetylene peaks in ^{1}H and ^{13}C NMR, increased symmetrisation of the alkyl diphosphinomethane signal and presence of the expected ^{13}C acetylene signals for the tetracobalt complex confirmed the successful formation of tetracobalt complex **10**.

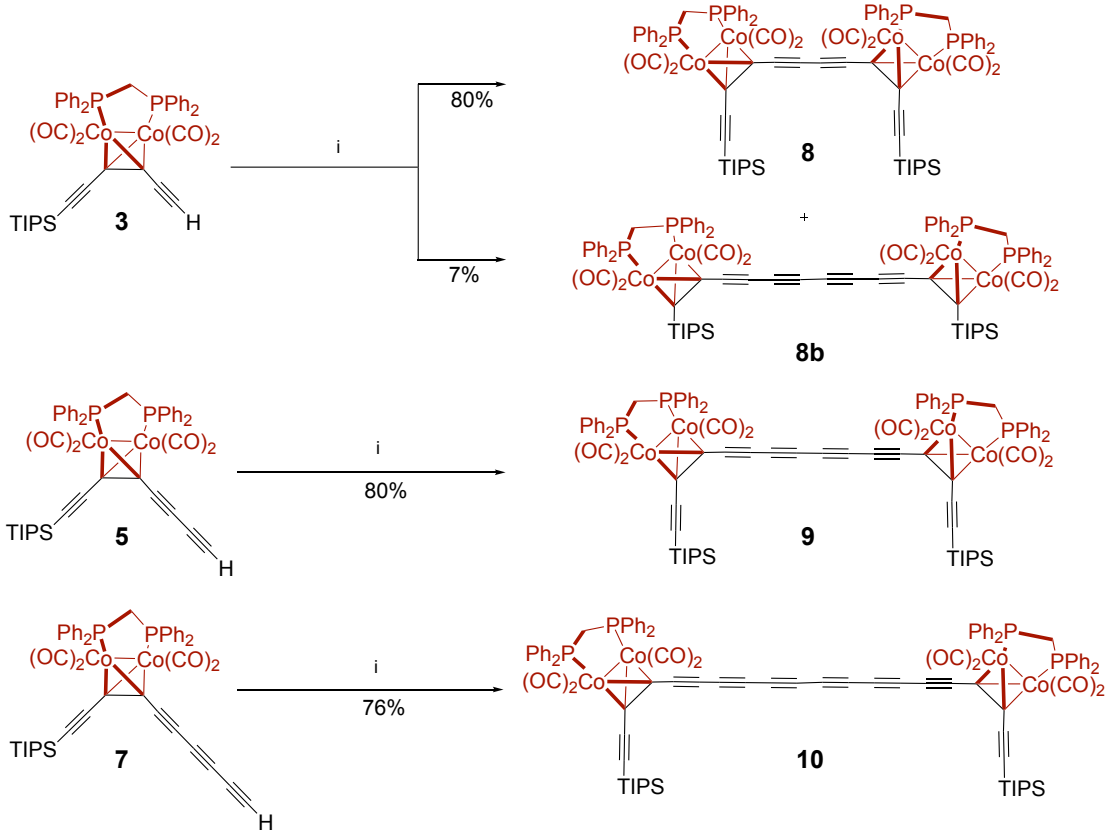

Scheme 3.4. i) $Cu(OAc)_2$, pyridine, 20 h.

3.3 – Unmasking polyynes from cobalt complexes

The removal of the $Co_2(CO)_4$dppm masking group was first tested on simple cobalt complexes. Both **2** and **2b** were used as model systems for optimisation of the

removal of the reaction conditions. Decomplexing of the dicobalt group is possible using the conditions reported previously on diynes by Haley *et al.* (I_2 in THF) (**Scheme 3.5**).[12] The successful removal of the masking group on simple systems resulted in our investigation of extended polyynes.

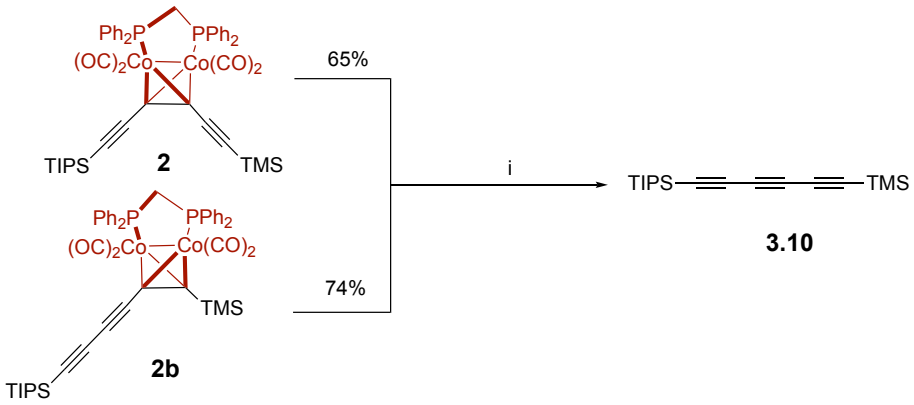

Scheme 3.5. i) I_2 (5 eq.), THF, 20 °C, 3 h.

The tetracobalt complexes **8, 9** and **10** were unmasked using the conditions described above to give the corresponding polyynes in 39-55% yields (**Scheme 3.6**). The unmasked polyynes were purified easily by silica chromatography with petroleum ether as the eluent. The desired non-polar TIPS end-capped polyyne was separated easily from the polar oxidised cobalt species. As expected, the longest polyyne was isolated in a slightly lower yield, reflecting its lower stability. UV-vis spectroscopy was invaluable in identifying the desired polyynes, due to the characteristic vibronically coupled absorption bands (**Figure 3.5**).[30] UV-vis spectroscopy is very sensitive to the presence of an incomplete reaction or other polyynic products, as both outcomes result in the presence of other strong chromophores with absorption bands that overlap with those of the desired polyynes in the visible region. The products were conclusively identified *via* ^{13}C NMR spectroscopy. This is the first time to the best of our knowledge that the dicobalt moiety has been used to synthesise polyynes.

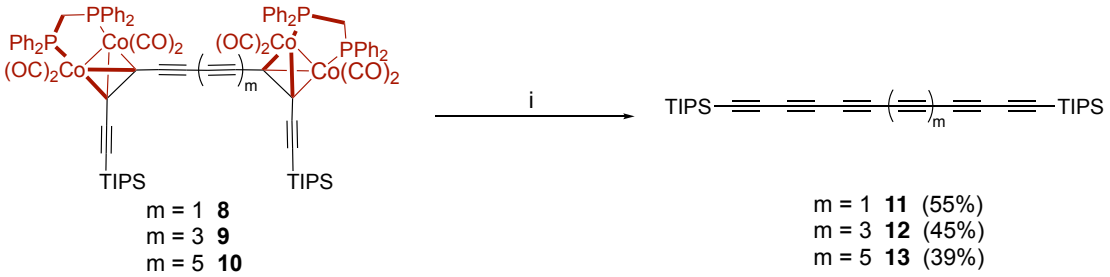

Scheme 3.6. i) I_2 (5 eq.), THF, 20 °C, 3 h.

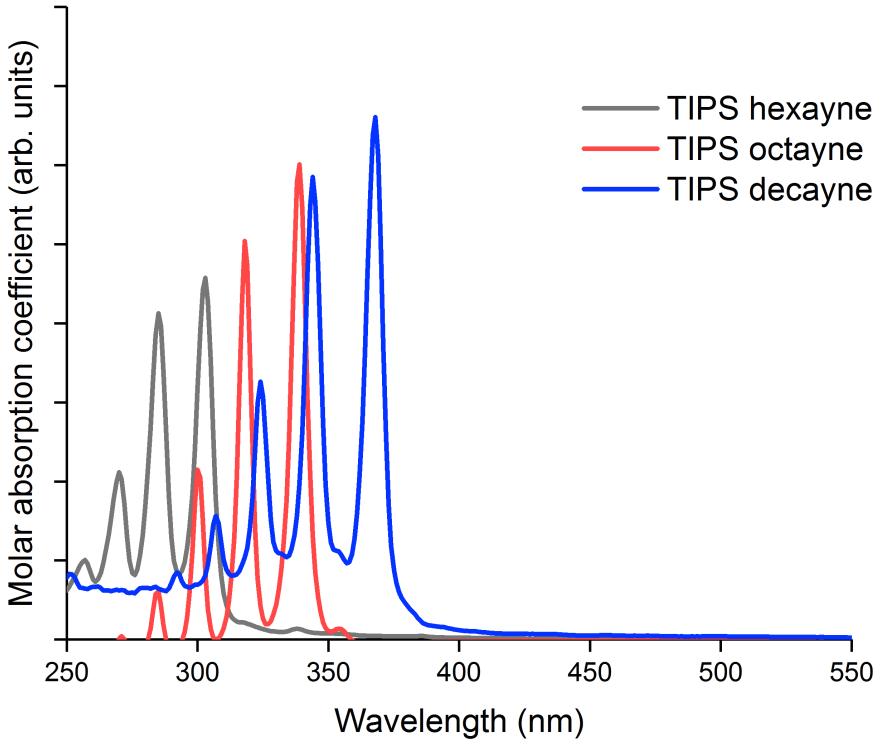

Figure 3.5. Absorption spectra of unmasked polyynes **11-13**.

The yields of polyyne unmasking (**Scheme 3.6**) were significantly higher than those for Fritsch-Buttenberg-Wiechell rearrangements that were reported by Tykwinski and coworkers in the synthessis of the same polyynes.[30] In this work, the octayne **12** is synthesised in 45% yield from a tetracobalt complex. The same octayne was isolated in only 10% yield from a dibromoolefin-masked precursor.[30] It was not previously possible to directly unmask a decayne from a masked precursor; Tykwinski and coworkers reported that this reaction led only to decomposition. In contrast, in this work the decayne **13** is isolated in 39% yield after simple purification from tetracobalt complex **10**. These results demonstrate that unmasking of the $Co_2(CO)_4$dppm MAE is a promising methodology in polyyne synthesis and offers great opportunities in carbon-rich chemistry.

3.4 – Attempted rotaxane synthesis

The successful unmasking experiments make the formation of rotaxanes from the cobalt oligoynes **3, 5** and **7** highly desirable. The successful formation of tetracobalt complexes **8-10** indicated that formation of rotaxanes should be synthetically possible. The hypothesised rotaxanes could be subjected to TIPS-deprotection and

further couplings in order to yield cyclic structures, realising our desire of masked cyclocarbon catenanes (**Scheme 3.7**). Furthermore, the mild unmasking conditions that were used to unmask long polyynes are likely to be compatible with the extended π-system of the cyclocarbon. However, all of our synthetic attempts to prepare rotaxanes were unsuccessful. Herein, the multiple different attempts towards these elusive rotaxanes are summarised **(Figure 3.6).** We also present our hypotheses for why these attempts were unsuccessful.

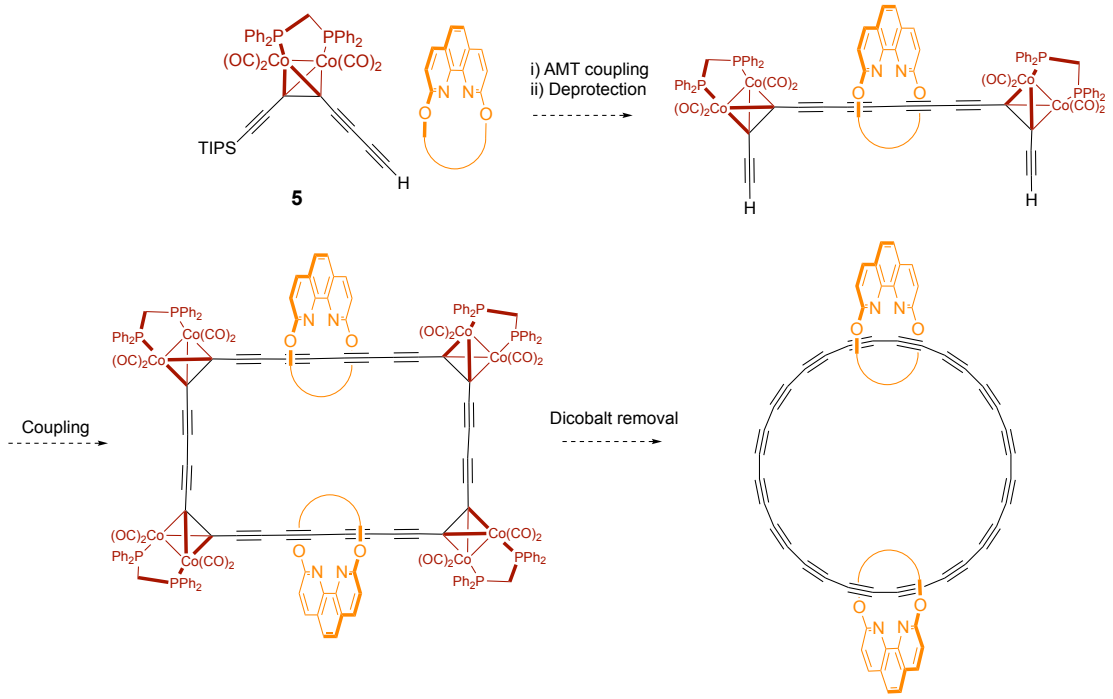

Scheme 3.7. Synthetic route towards cyclocarbons using the dicobalt MAE.

The two macrocycles chosen for screening represent the two main classes of macrocycles: alkyl straps and more rigid macrocycles. Both macrocycle **M1** and **M2** appeared to be small enough to prevent slippage over the very bulky dicobalt MAE when modelled using Hyperchem.[42] Active-metal template (AMT) homocoupling conditions as established by Saito[43] and then further developed by Anderson and coworkers were used for rotaxanation attempts.[44] Iodine is typically used as an oxidant in AMT homocouplings, which could be problematic for unmasking. However, iodine is used in a larger excess when used for cobalt decomplexation than in AMT couplings. Furthermore, we also attempted to use Cadiot-Chodciewicz cross-coupling with supertrityltriyne bromide **Tr*C$_6$Br** – another coupling partner that our group had successfully used in rotaxane forming reactions.[34] The aforementioned cross coupling usually gives a higher yield than the homocoupling reaction and also

circumvented any concerns about iodine as it does not require any oxidant. All of these efforts were unsuccessful. For this reason, we pursued an investigation of potential differences between dicobalt oligoynes **3**, **5**, **7** and their tris(3,5-di-t-butylphenyl)methyl (supertrityl, Tr*) end-capped oligoyne counterparts, which were previously used in the formation of polyyne rotaxanes (**Section 3.5**).[34,35,44]

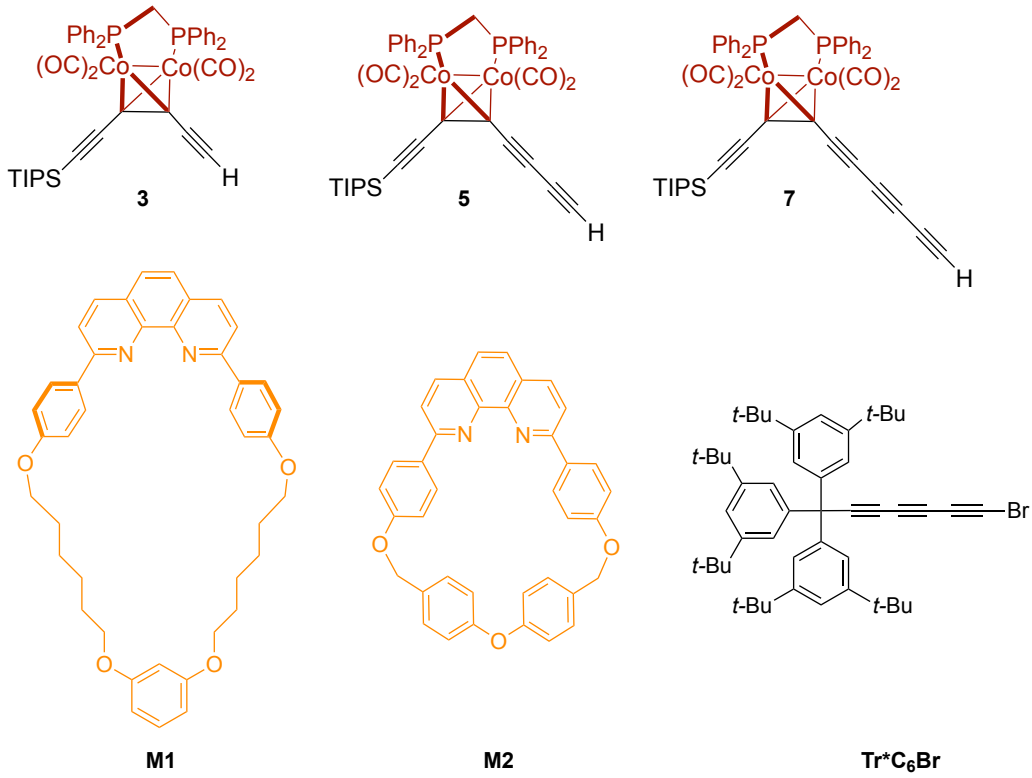

Reagent 1	Reagent 2	Macrocycle	Reaction Outcome
3	**3**	**M1**	No reaction
3	**3**	**M2**	No reaction
3	**Tr*C$_6$Br**	**M1**	Trace of **M1⊂Tr*C$_{12}$ Tr***
5	**5**	**M1**	No reaction
5	**Tr*C$_6$Br**	**M1**	Trace of **M1⊂Tr*C$_{12}$ Tr***
5	**5**	**M2**	No reaction
7	**Tr*C$_6$Br**	**M1**	Trace of **M1⊂Tr*C$_{12}$ Tr***

Figure 3.6. Attempted rotaxane formation reactions.

3.5 – Terminal acetylene reactivity

The most striking property of the dicobalt acetylenes **3**, **5**, **7** is the unusually high chemical shift of the terminal acetylene protons (**Table 3.1**). In **3**, this resonance appears at 3.63 ppm, which is 0.98 ppm further downfield than that of the supertrityl monoyne counterpart. However, this difference diminishes as the distance increases from the end-capping group in corresponding diyne and triyne. The same trend is reflected in the ^{13}C NMR. The chemical shift of the terminal carbon in **3** is shifted downfield 11.8 ppm more than the analogous supertrityl compound. In the longest analogues, this chemical shift change is reduced to 8.5 ppm (**7** vs Tr*-$(C\equiv C)_3$-H). This increase in chemical shift can be attributed to the electron-withdrawing effect of the cobalt carbonyl group or to deshielding by the phenyl substituents of the phosphine. In both cases, the ring currents from the aromatic systems in the bulky phosphine or supertrityl groups exert a magnetic field on the oligoyne chain, which diminishes with increased distance. The magnitude of this magnetic effect would be larger in the dicobalt complexes due to the proximity of the phenyl groups to the chain.

Table 3.1. Comparison of ^{1}H and ^{13}C chemical shifts ($CDCl_3$, 400 MHz) and acetylenic C-H stretch frequencies (deposited as thin film after CH_2Cl_2 evaporation) in cobalt and supertrityl oligoynes.[14]

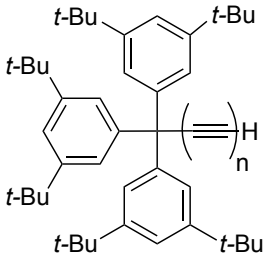

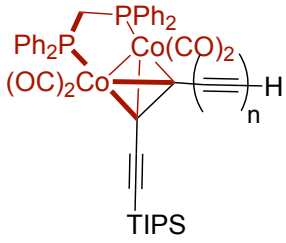

Compound	C≡C-*H* ^{1}H δ_H/ ppm	C≡*C*-H ^{13}C δ_C / ppm	C≡*C*-*H* stretch frequency / cm^{-1}
Tr*-C≡C-H	2.65	72.0	3306.0
Tr*-$(C\equiv C)_2$-H	2.10	66.7	3315.1*
Tr*-$(C\equiv C)_3$-H	2.07	61.3	3282.2
3	3.63	83.8	3306.4
5	2.81	73.0	3305.8
7	2.43	69.8	3296.6

The stretch frequency for Tr-$(C\equiv C)_2$-H is from reference 14.

Infra-red spectroscopy is useful for providing insight into bond strengths in acetylenes. A decrease in the C-H stretch frequency with increased number of acetylenes in the dicobalt oligoynes is observed (**Table 3.1**), which indicates a slightly weaker C-H bond in **7** than in **3**. However, the shift is small and a change this small in bond strength may not play a particularly large role in reactivity at room temperature. The same overall trend is repeated in both series of compounds (with the exception of Tr*-$(C\equiv C)_3$-H), which suggests a negligible reactivity difference between both series of compounds.

To support these experimental results, we performed computational studies on both types of terminal oligoynes. The electrostatic potential maps (ESP) on total density surfaces show significantly higher charge accumulation over the oligoyne chain in dicobalt complexes compared to supertrityl end-capped oligoynes (–0.04 vs 0.02 a.u, respectively). This is presumably due to the electronic communication between acetylene units and cobalt centers in **3**, **5**, **7**, which does not occur in supertrityl derivatives, where conjugation is broken by the quaternary carbon atom. However, the positive charge on the terminal hydrogen is similar in both cases, suggesting similar reactivity (**Figure 3.7**).

In order to get detailed charge distribution along the oligoyne chains, we calculated atomic charges using three different methods: Mulliken, Hirshfield, and Natural Population Analysis. In all three methods, the positive charge on the terminal hydrogen atom increases with increasing acetylenic chain length. In contrast, the charge difference between terminal carbon and hydrogen exhibits the reverse trend, as predicted by NPA and Hirshfield analysis. The latter parameter can be assumed as the more relevant for the reactivity. Nevertheless, the length-dependent changes and the value range are very similar in both cases, suggesting similar reactivity.

In general, the comparable size and electronic similarities between dicobalt and supertrityl oligoynes imply that initial incompatibility with the active metal template rotaxane formation is a result of incompatibility with oxidative coupling conditions, rather than reactivity differences in terminal acetylene. The successful formation of tetracobalt complexes *via* homocoupling supports this (**Scheme 3.4**).

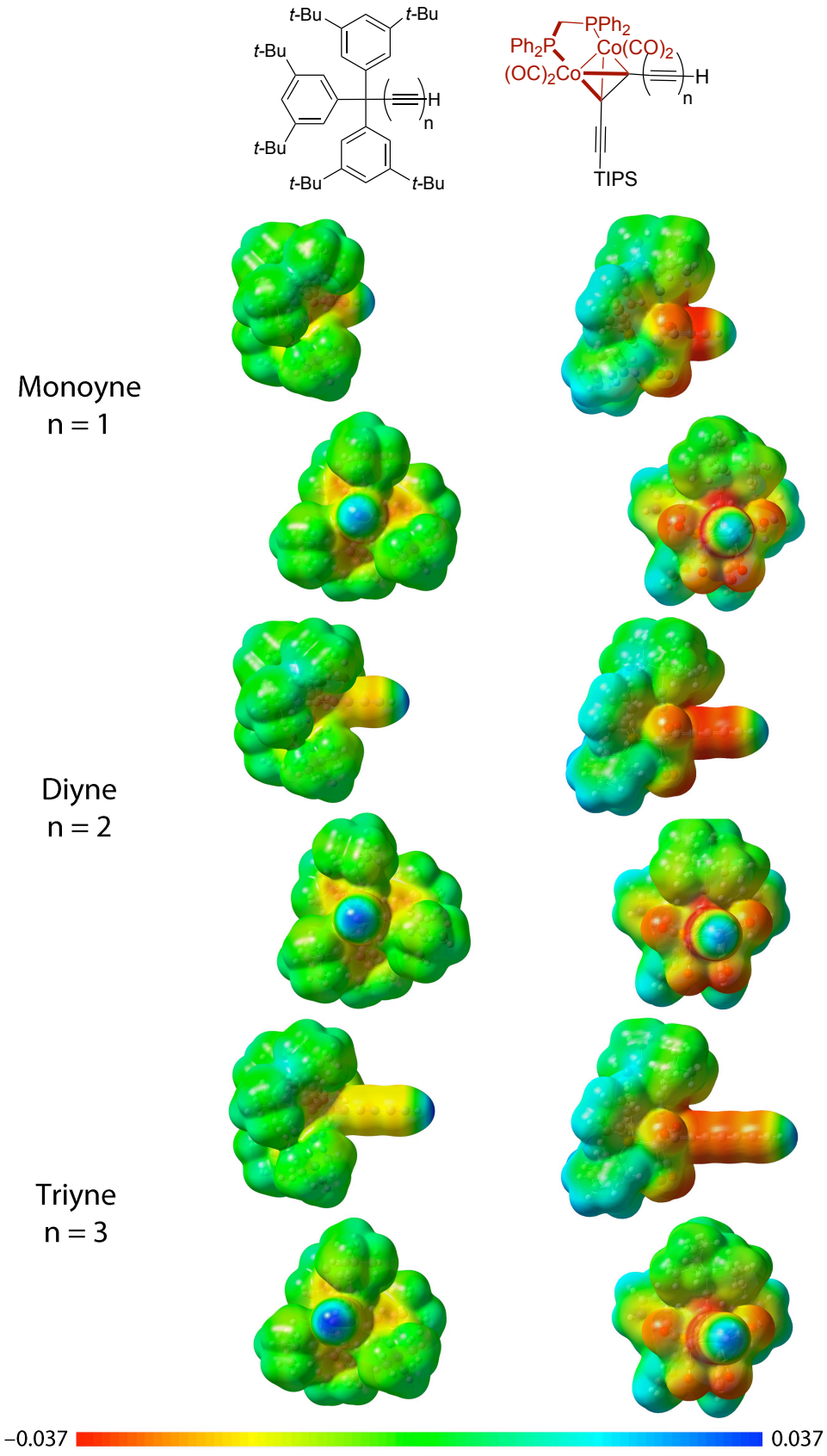

Figure 3.7. Electrostatic potential maps on total density surfaces of Supertrityl (left) and dicobalt (right, Conf1) mono-, di-, and triynes. The regions of positive and negative charges are depicted in blue and red, respectively.

3.6 – Electronic Absorption Spectroscopy and Molecular Orbitals

UV-vis absorption spectra were measured of all novel cobalt complexes (CH_2Cl_2, 298 K). The change in absorption upon cobalt complexation of triyne **3.10** is pronounced (**Figure 3.8**). After complexation, the fine vibronic band (280-330 nm) is inundated by a new broad absorption with a maxima at 290 nm and high molar extinction coefficient (25000 $M^{-1}cm^{-1}$). The solutions of **2-7** have an intense red colour. The very broad signals of the other TMS-protected dicobalt complexes (**4** and **6**) did not reveal any particularly unexpected behaviour (**Figure 3.9**).

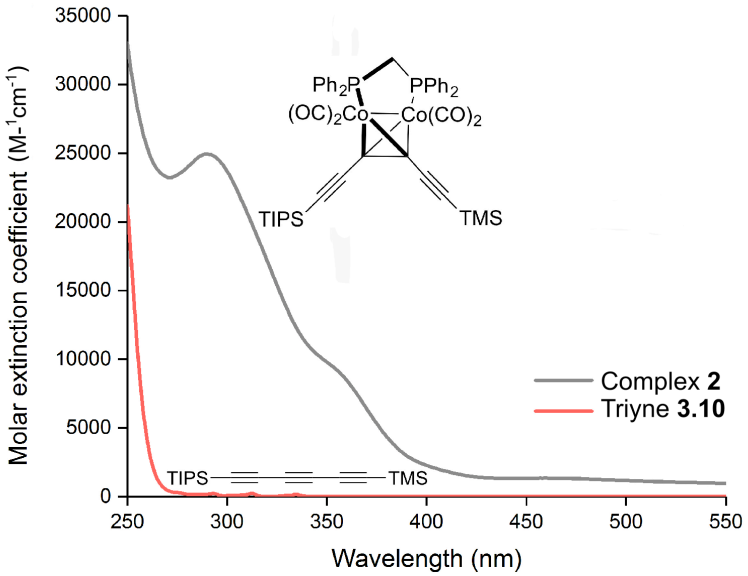

Figure 3.8. The effect of cobalt complexation on absorption (UV-vis spectra, CH_2Cl_2)

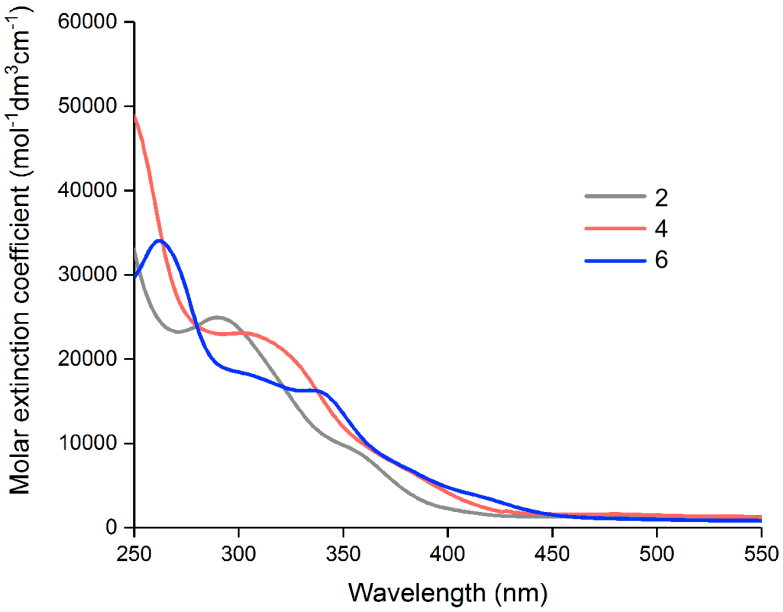

Figure 3.9. The effect of polyyne length on absorption in **2,4,6** (UV-vis spectra, CH_2Cl_2).

The absorption spectra of tetracobalt polyyne complexes were also measured. The maxima of these spectra are significantly red-shifted compared to the dicobalt oligoynes (**Figure 3.9**). Additionally, there is a bathochromic shift with increasing length of polyyne. The tetracobalt complexes (**Figure 3.10**) are considerably more red-shifted than the unmasked polyynes (**Figure 3.5**).

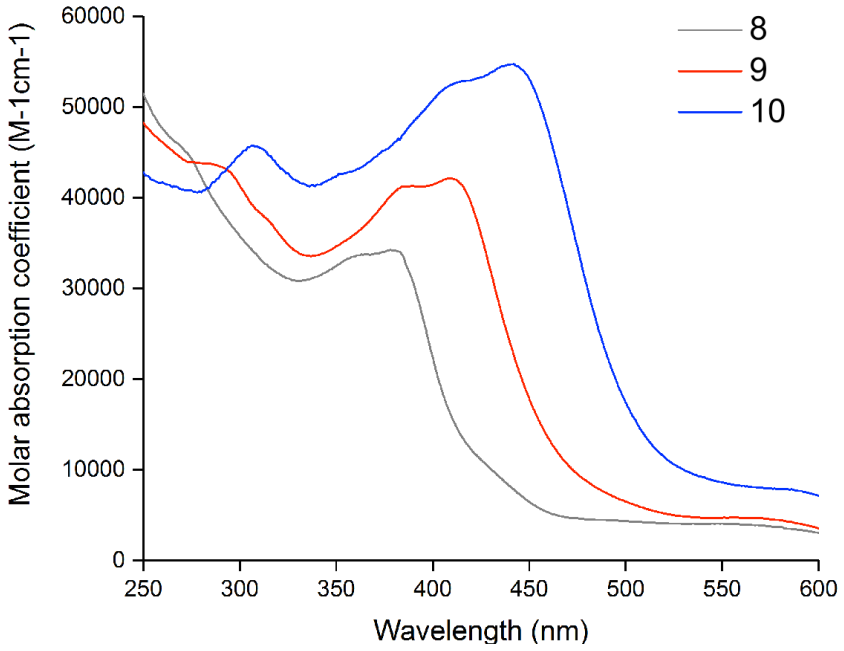

Figure 3.10. The effect of polyyne length on absorption in tetracobalt complexes **8, 9, 10** (UV-vis spectra, CH_2Cl_2).

Frontier molecular orbitals were calculated for **8**, **9**, **10** at the B3LYP/STO-3G level of theory (**Figure 3.11**). The crystal structures of complexes **2**, **4** and **6** were used as starting points for geometry optimisation (**Section 3.7**). These geometries were optimised and *E* and *Z* geometries were modelled, since it was not possible to determine what conformation the dimers would possess in solution. In all cases, the HOMO is localised predominantly on the polyyne core, whereas the LUMO delocalises into the cobalt and the electron withdrawing carbonyl ligands. This implies a HOMO-to-LUMO transition possesses significant charge transfer character, shifting electron density from the conjugated π-system to the metal carbonyl. This predicted charge transfer would explain the intense red colour of the cobalt complexes, why the colour is consistent between all complexes and the fact it dominates over any absorption from the polyyne itself.

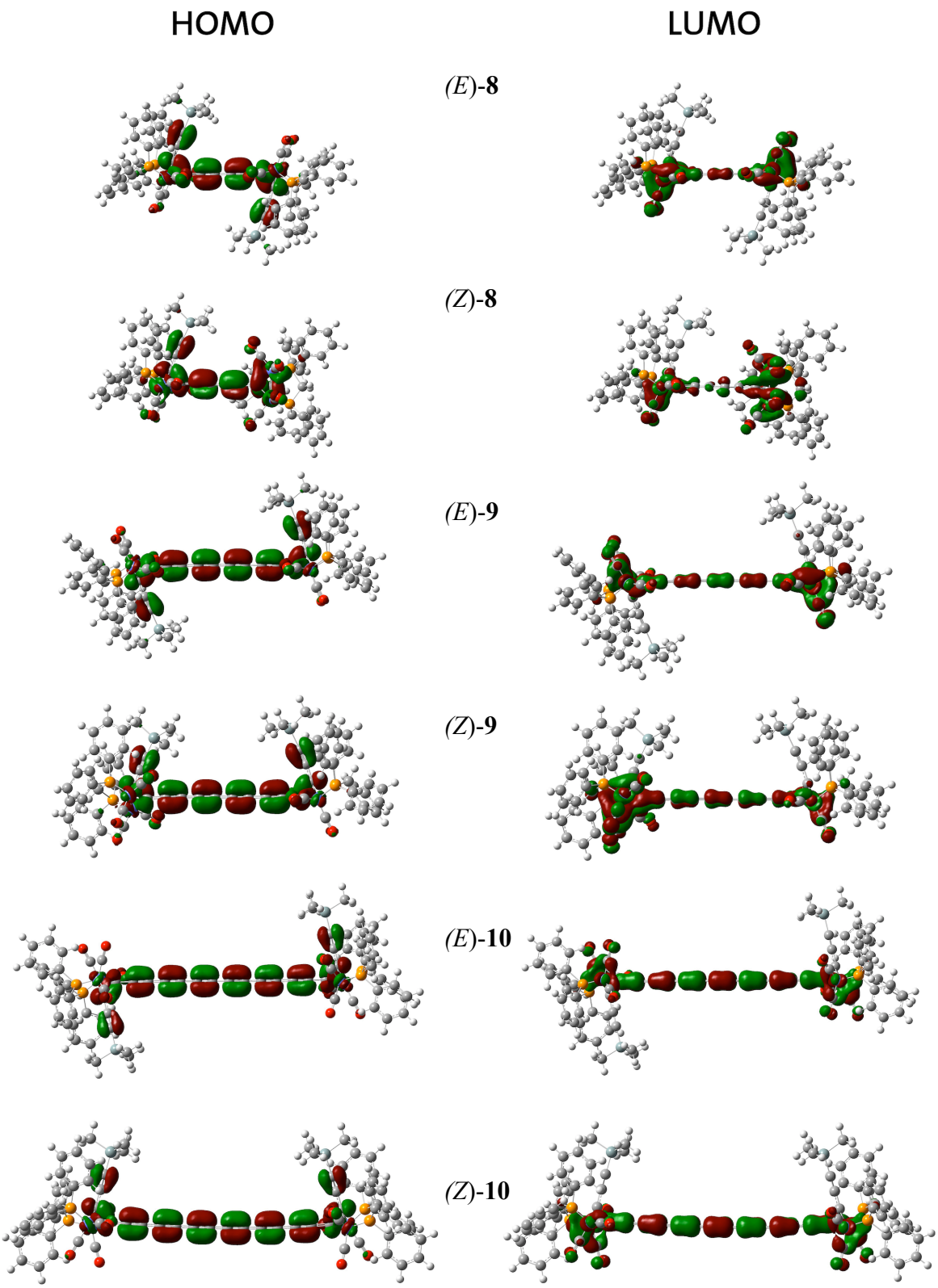

Figure 3.11. Calculated molecular orbitals of **8,9,10** in *E* and *Z* geometries (DFT/B3LYP/STO-3G)

We performed a solvatochromism experiment with complex **2** to confirm our hypothesis that a charge transfer is occurring. Solvatochromism is a dependence of absorption and emission spectra on solvent polarity.[45] Ground and excited states of chromophores have different polarities due to electronic redistribution. Therefore, solvent polarity changes can stabilise ground or excited states. This leads to a change in the energy gap between the two states and a subsequent change in the spectra. A series of absorption spectra were recorded with different polarity solvent mixtures to try and confirm our hypothesis of a charge transfer, a subtle solvatochromic shift can be observed in the absorption spectra (**Figure 3.12**).

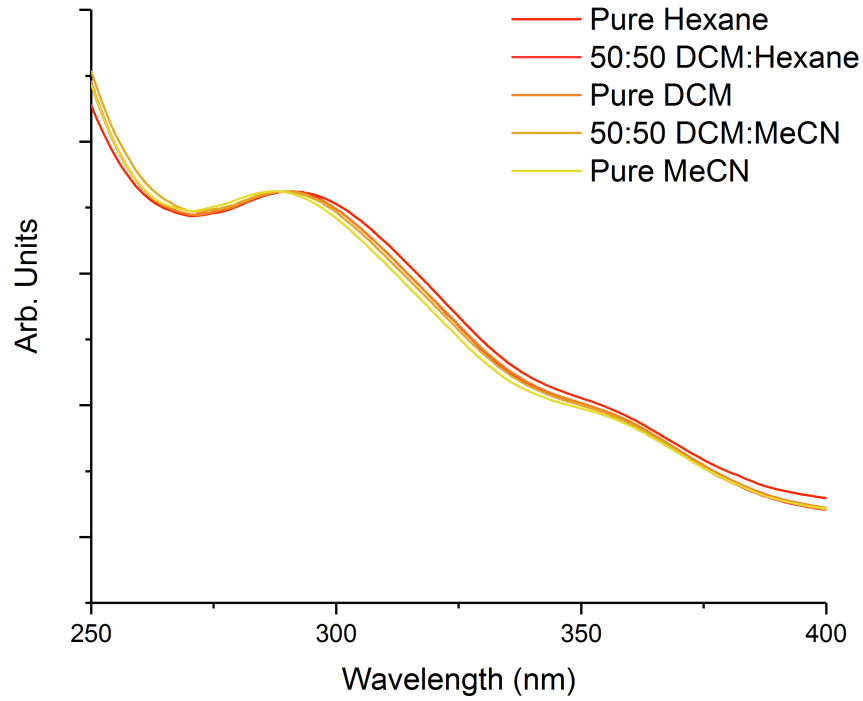

Figure 3.12. The effect of solvent polarity on absorption of **2** (All spectra recorded at 25 °C, at approximately 10^{-5} M, normalised at maxima).

In order to further investigate the perceived shift we plotted the maxima of the shifting peak against the solvent polarity. $E_T(30)$ values are a measure of solvent polarity based on the negatively solvatochromic pyridinium N-phenolate betaine dye as a probe molecule. They are defined as the molar electronic transition energies (ET) of dissolved dye, measured in kilocalories per mole (kcal/mol) at room temperature (25 °C) and normal pressure (1 bar), according to the following equation:

E_T (30) = $hc\nu_{max}N_A$

E_T (30) = 28591/ λ_{max} (nm)

Where λ_{max} = the wavelength of the maximum of the longest wavelength, intramolecular charge-transfer n-n* absorption band of the pyridinium N-phenolate betaine dye.

It appears that increased polarity causes negative solvatochromism; a hypsochromic shift is observed (**Figure 3.13**). This subtle solvatochromic shows there is be a charge transfer occurring in **2**, the trend was larger than the margin of error. This observation is consistent with the DFT and the large change in absorption spectrum upon complexation. We tentatively propose that there is a charge transfer from the π-orbitals of the alkyne to low-lying orbitals in the cobalt. The shift exhibited between hexane and MeCN solutions is 358 cm^{-1}. However, many known strongly solvatochromic systems exhibit shifts between 1000 cm^{-1} and 10000 cm^{-1}.[46] Nevertheless, this subtle solvatochromic shift implies there is a charge transfer occurring in **2**, which is consistent with the DFT.

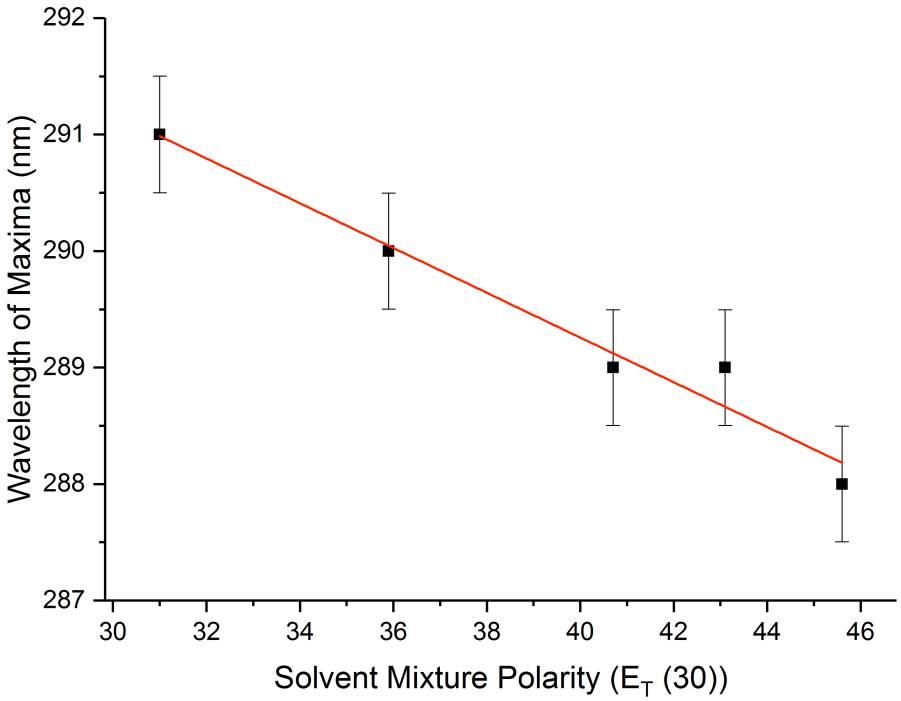

Figure 3.13. The effect of solvent polarity on absorption maxima of **2**. Red line shows linear fitting, error bars denote resolution limit of UV-vis spectrometer.

3.7 – Crystallography

Single crystal X-ray diffraction studies provide insight into the geometries of cobalt-polyyne complexes and the crystal structures act as an essential diagnostic tool for confirming the structure of these unusual compounds. This was particularly valuable because these structures possess very few hydrogen atoms, are challenging to characterise by mass spectrometry and their UV-vis absorption spectra are broad – lacking any characteristic bands. The crystal structures of polyynes can reveal the bond length alternation (BLA) and the degree of deviation from the expected linearity.[47] Bond length alternation is the difference between the carbon-carbon bond length of adjacent single and triple bonds. In polyynes, BLA is defined as the difference in length between the central-most single and triple bonds.[48,49] It can be described by the following equation: BLA = $Distance_{C\text{-}C}$ - $Distance_{C\equiv C}$.

Here, seven crystal structures of cobalt-polyyne complexes are presented: **2, 4, 6, 2b**, **8** and **8b** and bis-TIPS complex **3.5**. All crystals were grown by layer addition of MeOH to a solution of compound in $CHCl_3$. Diffraction data for **8** and **8b** were collected at 100 K using synchrotron radiation on beamline I19-1 at Diamond Light Source. The structures were solved using charge flipping[50,51] with SuperFlip[52] and refined using the full-matrix least-squares method within the CRYSTALS software package.[53,54] Crystallography proved to be an essential tool when distinguishing between the regioisomers **2** and **2b** (**Figure 3.14**). The bond angles are broadly similar in the two regioisomers. However, the dppm ligand is directed towards TMS group in **2** and towards TIPS group in **2b**, which may be a result of crystal packing.

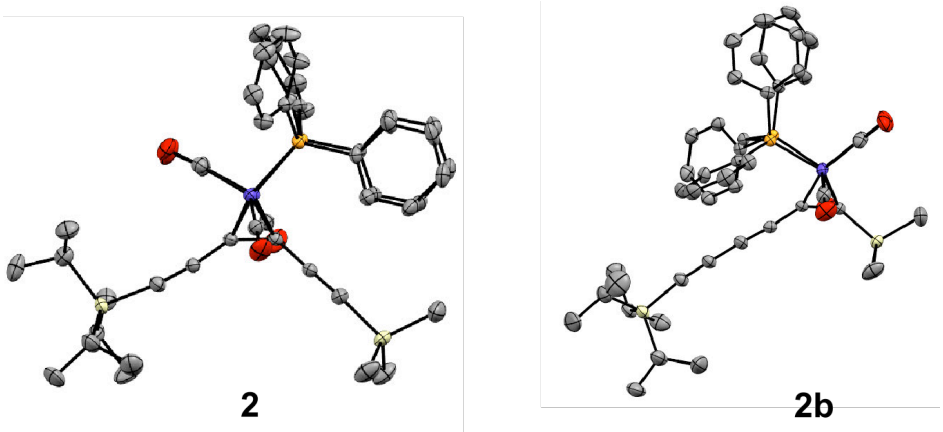

Figure 3.14. Displacement ellipsoid plots of **2** and **2b** (H atoms and solvent omitted for clarity, thermal ellipsoids drawn at 50% probability).

Single crystal X-ray diffraction led to the serendipitous discovery of an unexpected type of reactivity. As discussed in **Section 3.2**, when **3** was subjected to Eglinton coupling conditions, two products were observed (**8** and **8b**, **Scheme 3.4** and **Figure 3.15**). End groups in **8** are oriented in (*E*) fashion, where the TIPS groups are perfectly anti-periplanar to one another because the compound crystallises with a centre of symmetry. The diyne core is highly linear, while **8b** has a far more curved polyyne chain and a slightly twisted *syn*-periplanar geometry of the TIPS groups.

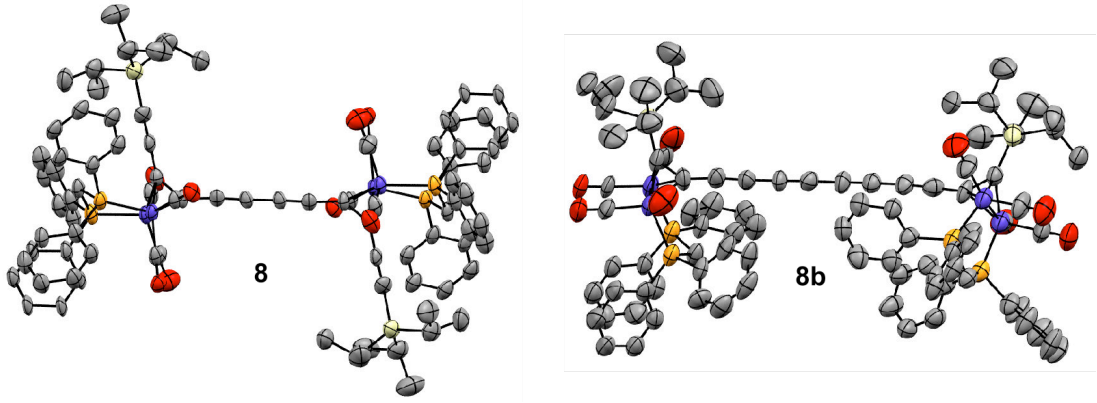

Figure 3.15. Displacement ellipsoid plots of regioisomers **8** and **8b** (H atoms and disorder omitted for clarity, thermal ellipsoids drawn at 50% probability).

Systematic analysis of the set of complexes **2**, **4**, **6** was performed (**Figure 3.16**, **Table 3.2**). We observed that the length of the $C_{sp3} - C_{sp}$ bond decreases as the polyyne gets longer. In **2**, this bond is markedly longer than in **6** (0.02 Å). In contrast, there appears to be no relationship between the length of the Co-C bond and the polyyne length. The average Co-C bond length was 1.95 Å in all of the compounds. This implies that the complexation of the dicobalt group is of similar strength in all cases. The BLA is lower in complex **6** than complex **4**.

One of the most attractive features of the dicobalt alkyne masking group is the angle that it infers on the polyyne system while masking it – particularly the angle between the coordinated alkyne and its adjacent carbons. As the chain lengthens, the angle θ_2 increases. It appears the angle is forced to widen in order to prevent a steric clash. In contrast, θ_1 reduces in size. These angles do fall within the range of angles for crystal structures of dicobalt-acetylene complexes that are currently deposited in the Cambridge Structural Database (**Figure 3.2**).[55]

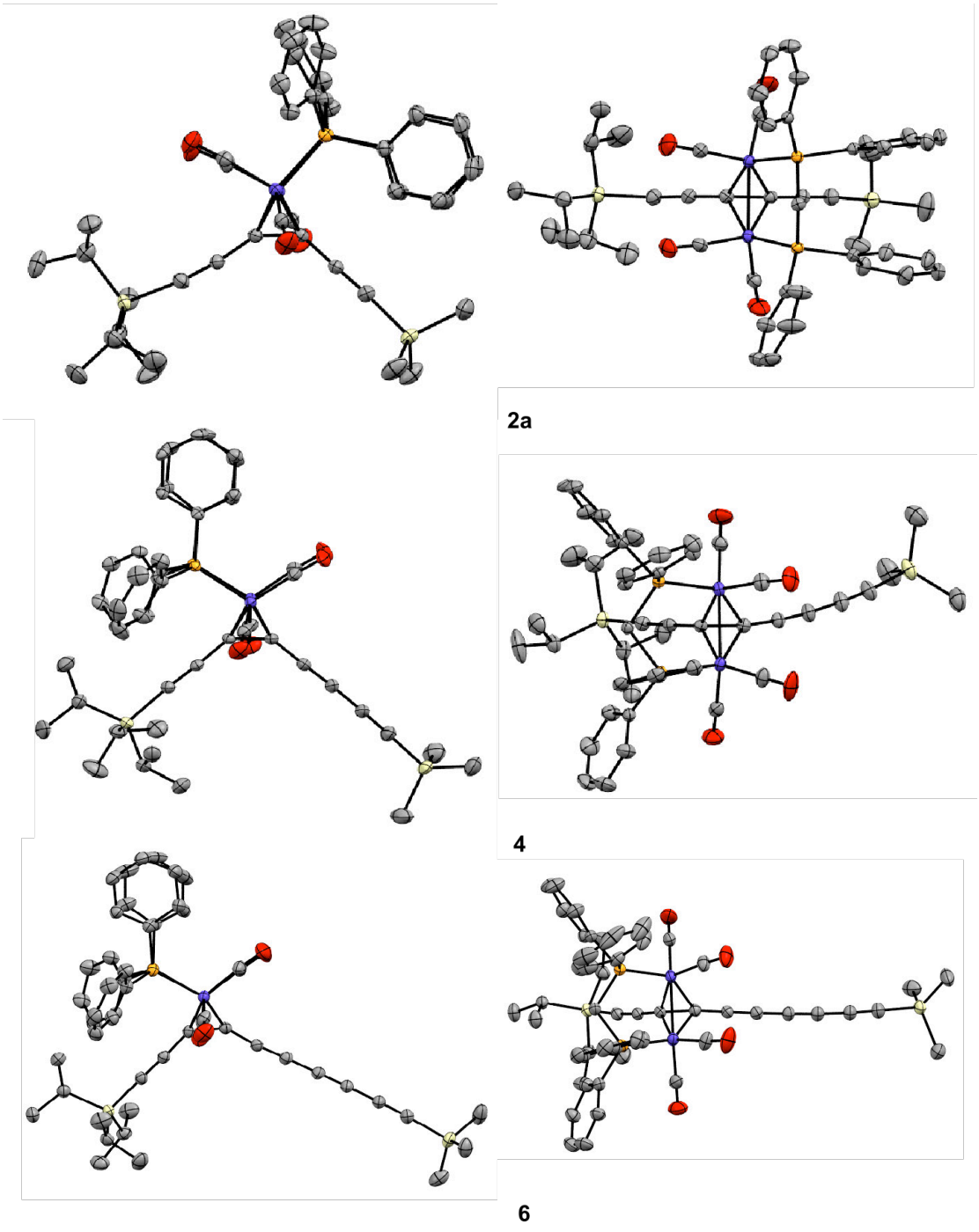

Figure 3.16. Displacement ellipsoid plots of **2**, **4** and **6** (H atoms omitted for clarity, thermal ellipsoids drawn at 50% probability).

Table 3.2. Bond lengths and angles of **2,4,6**.

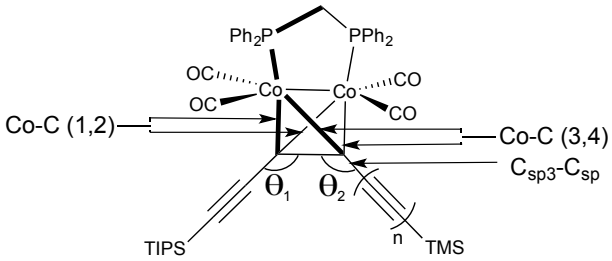

Complex	**2**	**4**	**6**
Co–C (1)/ Å	1.945	1.947	1.944
Co–C (2)/ Å	1.948	1.948	1.955
Co-C (3)/ Å	1.957	1.952	1.959
Co–C (4)/ Å	1.963	1.954	1.959
C_{sp}–C_{sp3} / Å	1.407	1.391	1.380
CC / Å	1.212	1.208	1.216
C–C / Å	N/A	1.372	1.358
C≡C / Å	N/A	1.208	1.215
C–C / Å	N/A	N/A	1.366
C≡C / Å	N/A	N/A	1.208
C–Si / Å	1.839	1.841	1.852
Avg. BLA / Å	N/A	0.164	0.149
Avg. Co-C / Å	1.953	1.950	1.954
θ_1 / º	146.27	137.50	138.03
θ_2 / º	136.75	139.10	143.55
∠ C_{Co} - C≡C / º	178.88	174.93	174.88
C≡C-C / º	N/A	175.58	178.10
C-C≡C / º	N/A	177.33	179.24
C≡C-C / º	N/A	N/A	177.40
C-C≡C / º	N/A	N/A	177.22
Avg. chain / º	178.88	175.96	177.37

3.8 – Conclusions

A series of cobalt complexes that mask an alkyne π-system have been synthesised. A synthetic route that yielded a series of dicobalt complexes with an exposed arm of one, two and three alkynes was designed. This series provided substrates for forming long masked polyynes and allowed a systematic investigation into optical and solid-state properties of these complexes. The absorption spectra of these complexes have been investigated. A charge transfer band between the polyyne and the dicobalt moiety is postulated, which was supported by DFT calculations and solvatochromism experiments.

Further chemistry on these cobalt complexes led to preparation, *via* Eglinton couplings, of tetracobalt masked TIPS-endcapped polyynes of lengths up to the decayne. An unexpected isomerisation during Eglinton coupling was discovered by crystallographic analysis. Most notably, these structures could be readily unmasked with elemental iodine, offering the most facile method of unmasking long polyynes yet reported. This method offers promise for mild unmasking of supramolecular carbon-rich structures and other extended π-systems.

3.9 – Experimental data for known compounds

1,5-Bis(triisopropylsilyl)penta-1,4-diyn-3-ol - **3.1**[56]

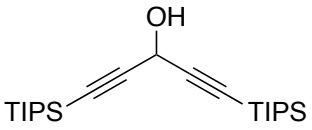

To a solution of TIPS-acetylene (2.82 mL, 2.24 g, 12.6 mmol) in THF (45 mL), *n*-BuLi (8.67 mL, 13.8 mmol, 1.6 M in hexanes) was added at –78 °C under N_2. The reaction mixture was warmed to –30 °C to promote lithiation. The mixture was then cooled to –78 °C and a solution of aldehyde **2.1** (2.83 g, 12.6 mmol) in THF (10 mL) was added. The reaction mixture was stirred for 1 h upon warming to 20 °C. The reaction mixture was quenched by saturated NH_4Cl (aq) (10 mL), washed with brine (100 mL) and the organic phase was dried over $MgSO_4$. Solvents were removed and the crude mixture was purified by column chromatography (hexanes/CH_2Cl_2 2:1) affording **3.1** (3.50 g, 71%) as a brown oil. As in lit.[56]

^{1}H NMR (400 MHz, $CDCl_3$) δ 5.11 (s, 1H), 2.16 (br. s, 1H), 1.08 (s, 42H).
^{13}C NMR (100 MHz, $CDCl_3$) δ 104.4, 86.4, 53.3, 18.8, 11.3.

1,5-Bis(triisopropylsilyl)penta-1,4-diyn-3-one - **3.2**[57]

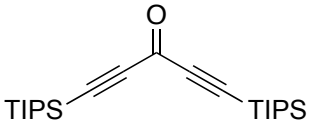

To a solution of alcohol **3.1** (3.50 g, 8.92 mmol) in CH_2Cl_2 (100 mL) celite (7.68 g), molecular sieves (7.68 g), and PCC (3.84 g, 17.8 mmol) were added in that order and the reaction mixture stirred at 20 °C overnight. The mixture was passed through a silica plug (CH_2Cl_2) and the solvent removed in *vacuo* to yield ketone **3.2** (3.05 g, 86%) as a pale brown oil. As in lit.[57]

^{1}H NMR (400 MHz, $CDCl_3$) δ 1.09 (s, 42H).
^{13}C NMR (100 MHz, $CDCl_3$) δ 160.2, 105.5, 97.9, 18.7, 11.2.

(3-(Dibromomethylene)penta-1,4-diyne-1,5-diyl)bis(triisopropylsilane) - **3.3**[57]

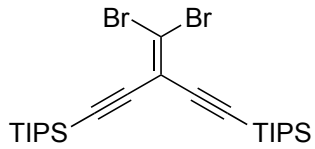

To a solution of CBr_4 (2.54 g, 7.68 mmol) in CH_2Cl_2 (10 mL) was added PPh_3 (4.03 g, 15.4 mmol) in CH_2Cl_2 (15 mL) and the resulting mixture stirred at 20 °C under N_2 for 1 h. A solution of ketone **3.2** (1.50 g, 3.84 mmol) in CH_2Cl_2 (30 mL) was

added and the reaction was stirred for 24 h. The reaction mixture was concentrated and hexanes were added to precipitate the Ph_3PO as a white solid along with an oily residue. The supernatant was decanted and passed through a silica plug (hexane). The oily residue left in the flask was dissolved in minimal CH_2Cl_2 and hexane was added; the heterogeneous mixture was then decanted and the supernatant passed through a silica plug (this procedure was repeated three times). The solvent was removed *in vacuo* yielding **3.3** (2.24 g, 100%) as a yellow solid. As in lit.[57]

^{1}H NMR (400 MHz, $CDCl_3$) δ 1.10 (s, 42H).
^{13}C NMR (100 MHz, $CDCl_3$) δ 115.1, 109.0, 102.6, 99.6, 18.8, 11.3.

1,6-Bis(triisopropylsilyl)hexa-1,3,5-triyne - **3.4**[29]

To a solution of **3.3** (2.16 g, 3.95 mmol) in hexane (70 mL) at –78 °C, *n*-BuLi was added (3.10 mL, 1.6 M in hexanes, 4.94 mmol) dropwise under a N_2 atmosphere. The reaction mixture was warmed to 20 °C over 30 min and the reaction mixture was quenched by the addition of saturated NH_4Cl (aq) (10 mL). The layers were separated and the organic layer dried over $MgSO_4$. The solvent was removed *in vacuo* and the crude product was purified by column chromatography (silica, hexanes) to yield triyne **3.4** (1.30 g, 85%) as an off-white solid. As in lit.[29]

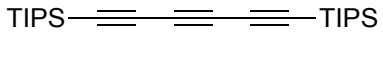

^{1}H NMR (400 MHz, $CDCl_3$) δ 1.08 (s, 21H).
^{13}C NMR (100 MHz, $CDCl_3$) δ 90.1, 85.4, 61.7, 18.8, 11.6.

Tetracarbonyl[μ^2-(3,4-η:3,4-η)-1,6-bis(triisopropylsilyl)hexa-1,3,5-triyne][μ-methylenebis(diphenylphosphine)-P:P']dicobalt – **3.5**[11]

A solution of triyne **3.4** (400 mg, 1.04 mmol) and $Co_2(CO)_8$ (390 mg, 1.13 mmol) in degassed hexane (25 mL) was stirred at 20 ºC under N_2 for 12 h. The hexane was evaporated and the residue redissolved in dry toluene (15 mL). Bis-diphenylphosphinomethane (406 mg, 1.06

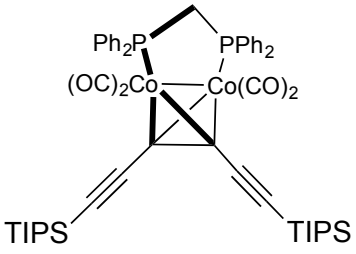

mmol) was added and the solution heated to reflux for 1 h. Evaporation and column chromatography (hexane/CH_2Cl_2 9:1 and 8:2) afforded intensely dark red crystals of **3.5** (872 mg, 84%) after recrystallisation with CH_2Cl_2/MeOH. As in lit.[11]

^{1}H NMR (400 MHz, $CDCl_3$) δ 7.30-7.40 *(*m*,* 8H, *H*–Ar), 7.23-7.30 *(*m*,* 4H, *H*–Ar), 7.11-7.22 *(*m*,* 8H, *H*–Ar), 3.40 *(*t*,* $^2J_{H\text{-}P}$ = 10.3 Hz, 2H, PC*H*$_2$P), 1.09-1.11 *(*m*,* 42H, *i*-Pr-*H*).
^{13}C NMR (100 MHz, $CDCI_3$) δ 203.2 (*br*), 135.9 *(br),* 132.0 (t, J ($J_{C\text{-}P}$ = 6.2 Hz), 129.9, 128.5 (t, $J_{C\text{-}P}$ = 4.9 Hz), 109.6, 98.8, 71.2 (*br*), 35.4 (t, $^1J_{C\text{-}P}$ = 22.1 Hz), 19.0, 11.7.

Tetracarbonyl[μ^2-(3,4-η:3,4-η)hexa-1,3,5-triyne][μ-methylenebis(diphenylphosphine)-P:P']dicobalt – **3.6**[11]

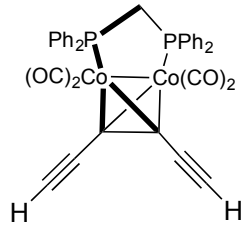

To a solution of **3.5** (200 mg, 0.224 mmol) in wet THF (20 μL of H_2O in 20 mL of THF) was added TBAF (1 M solution) in THF (0.472 mL, 0.472 mmol). After 5 min, the mixture was partitioned between hexane (40 mL) and NH_4Cl (aq). Drying of the organic phase over $MgSO_4$, evaporation, and washing of the residue with hexane afforded **3.6** (160 mg, 96%) as dark red prisms. As in lit.[11]

^{1}H NMR (400 MHz, $CDCl_3$) δ 7.32-7.40 *(*m*,* 8H, *H*–Ar), δ 7.26-7.31 *(*m*,* 4H, *H*–Ar), 7.19-7.25 *(*m*,* 8H, *H*–Ar), 3.73 (s, 2H, C≡*H*), 3.40 *(*t*,* $^2J_{H\text{-}P}$ = 10.3 Hz, 2H, PC*H*$_2$P).
^{13}C NMR (100 MHz, $CDCI_3$) δ 203.2 (*br*), 135.9 *(br),* 132.0 (t, $^2J_{C\text{-}P}$ = 6.4 Hz), 130.2, 128.6 (t, $^2J_{C\text{-}P}$ = 4.8 Hz), 85.8, 84.6, 36.0 (t, $^1J_{C\text{-}P}$ = 22.0 Hz),

1-(Triisopropylsilyl)-5-(trimethylsilyl)penta-1,4-diyn-3-ol **- 3.7**[36]

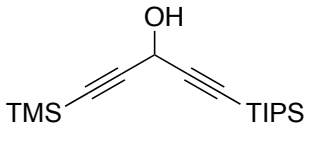

To a solution of TMS-acetylene (1.85 mL, 1.31 g, 13.4 mmol) in dry THF (35 mL), *n*-BuLi (9.20 mL, 14.7 mmol, 1.6 M in hexane) was added at –78 °C under a N_2 atmosphere. The reaction was warmed to –30 °C to promote lithiation. The mixture was then cooled to –78 °C and a solution of aldehyde **2.1** (3.00 g, 13.4 mmol) in THF (10 mL) was added. The reaction mixture was stirred for 1 h upon warming to 20 °C. The reaction was quenched by saturated NH_4Cl (aq) (10 mL), washed with

brine (100 mL) and the organic phase was dried over $MgSO_4$. The solvents were removed and the crude mixture was purified by column chromatography (hexanes/CH_2Cl_2 2:1) affording alcohol **3.7** (3.76 g, 88%) as a brown oil. As in lit.[36]

^{1}H NMR (400 MHz, $CDCl_3$) δ 5.09 (s, 1H), 2.16 (br. s, 1H), 1.08 (s, 21H), 0.18 (s, 9H).
^{13}C NMR (100 MHz, $CDCl_3$) δ 104.2, 102.3, 89.5, 86.5, 53.2, 18.7, 11.3, -0.2.

1-(Triisopropylsilyl)-5-(trimethylsilyl)penta-1,4-diyn-3-one - **3.8**[36]

To a solution of alcohol **3.7** (3.76 g, 11.7 mmol) in CH_2Cl_2 (300 mL) celite (10.06 g), molecular sieves (10.06 g), and PCC (5.03 g, 23.3 mmol) were added in that order and the reaction was stirred at 20 °C overnight. The mixture was filtered through a silica plug (CH_2Cl_2) and the solvent removed *in vacuo* to yield ketone **3.8** (3.58 g, 96%) as an orange oil. As in lit.[36]

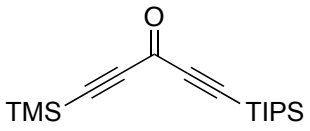

^{1}H NMR (400 MHz, $CDCl_3$) δ 1.11 (s, 21H), 0.25 (s, 9H).
^{13}C NMR (100 MHz, $CDCl_3$) δ 160.3, 105.2, 103.0, 99.6, 98.4, 18.6, 11.2, -0.8.

(3-(Dibromomethylene)-5-(triisopropylsilyl)penta-1,4-diyn-1-yl)trimethylsilane-**3.9**[36]

To a solution of CBr_4 (7.40 g, 22.3 mmol) in CH_2Cl_2 (15 mL) was added PPh_3 (11.3 g, 44.7 mmol) in CH_2Cl_2 (30 mL) and the resulting mixture stirred at 20 °C under a N_2 atmosphere for 1 h. A solution of ketone **3.8** (3.58 g, 11.2 mmol) in CH_2Cl_2 (80 mL) was added and the reaction was stirred for 24 h. The reaction mixture was concentrated and hexanes were added to precipitate the Ph_3PO as a white solid along with an oily residue. The supernatant was decanted and passed through a silica plug (hexane). The oily residue left in the flask was dissolved in ca. 30 mL of CH_2Cl_2 and hexane was added; the heterogeneous mixture was then decanted and the supernatant filtered through a silica plug (three times). The solvent was removed *in vacuo* yielding dibromoolefin **3.9** (4.97 g, 93%) as an orange oil. As in lit.[36]

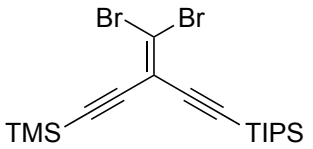

^{1}H NMR (400 MHz, $CDCl_3$) δ 1.10 (s, 21H), 0.22 (s, 9H).

^{13}C NMR (100 MHz, $CDCl_3$) δ 114.7, 109.7, 102.5, 102.4, 100.5, 99.9, 18.7, 11.3, –0.3.

l-(Triisopropylsilyl)-6-(trimethylsilyl)-l,3,5-hexatriyne - **3.10**[30]

To a solution of **3.9** (434 mg, 0.936 mmol) in hexanes (30 mL) at –78 °C, *n*-BuLi was added (0.733 mL, 1.6 M in hexanes, 1.17 mmol) dropwise under a N_2 atmosphere. The reaction mixture was warmed to 20 °C over 30 min and the reaction was quenched by the addition of saturated NH_4Cl (aq) (10 mL). The layers were separated and the organic layer dried over $MgSO_4$. The solvent was removed *in vacuo* and the crude product was purified by column chromatography (silica, hexanes) to yield **3.10** (0.227 g, 80%) as an orange oil. As in lit.[25]

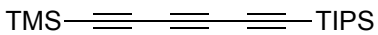

^{1}H NMR (400 MHz, $CDCl_3$) δ 1.10 (s, 21H), 0.22 ppm (s, 9H).
^{13}C NMR (100 MHz, $CDCl_3$) δ -0.6, 11.2, 18.5, 60.9, 62.4, 85.1, 87.0, 88.0, 89.6

(1,12-Bis(triisopropylsilyl)-1,3,5,7,9,11-dodecahexayne) - **11**[30]

Tetracobalt masked hexayne **8** (50 mg, 28.7 μmol) was dissolved in THF (3 mL), I_2 (37.0 mg, 144 μmol) was added and the reaction mixture was stirred for 3 h. After completion was observed *via* TLC chromatography, the reaction mixture was passed through a silica plug (Pet. Ether). The hexayne **11** was isolated as a yellow solid (8.0 mg, 17.4 μmol, 61%). As in lit.[30]

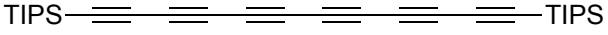

^{1}H NMR (500 MHz, $CDCl_3$) δ 1.09 (s, 42H).
^{13}C NMR (125 MHz, $CDCl_3$) δ 11.8, 18.7, 61.2, 62.5, 62.8, 63.0, 89.5, 87.9.

1,16-Bis(triisopropylsilyl)-1,3,5,7,9,11,13,15-hexadecaoctayne - **12**[30]

Tetracobalt masked octayne **9** (25 mg, 14.4 μmol) was dissolved in THF (10 mL), I_2 (18 mg, 69.8 μmol) was added and the reaction mixture was stirred for 3 h. After completion was observed *via* TLC

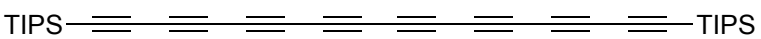

chromatography, the reaction mixture was passed through a silica plug (Pet. Ether). The octayne **12** was isolated as a yellow solid (3.2 mg, 6.4 μmol). As in lit.[30]

^{1}H NMR (500 MHz, $CDCl_3$) δ 1.08 (s, 42H).
^{13}C NMR (125 MHz, $CDCl_3$) δ 11.7, 18.7, 61.1, 62.3, 62.6, 63.1, 63.4, 63.4, 88.5, 89.4.

(1,20-Bis(triisopropylsilyl)-1,3,5,7,9,11,13,15,17,19-einacosadecayne) - **13**[30]

Tetracobalt masked 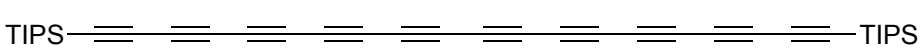

decayne **10** (50 mg, 28.0 μmol) was dissolved in THF (10 mL), I_2 (10 mg) was added and the reaction mixture was stirred for 3 h. After completion was observed *via* TLC chromatography, the reaction mixture was passed through a silica plug (Pet. Ether).. The decayne **13** was isolated as an orange solid (6.0 mg, 10.8 μmol, 39%). As in lit.[30]

^{1}H NMR (500 MHz, $CDCl_3$) δ 1.08 (s, 42H).
^{13}C NMR (125 MHz, $CDCl_3$) 11.7, 18.7, 61.0, 62.2, 62.9, 63.2, 63.5, 63.8, 88.8, 89.3.

3.10 – Experimental data for novel compounds

Tetracarbonyl[μ^2-(3,4-η:3,4-η*)*-triisopropyl((trimethylsilyl)hexa-1,3,5-triyn-1-yl)silane][μ-methylenebis(diphenylphosphine)-P:P']dicobalt - **2**

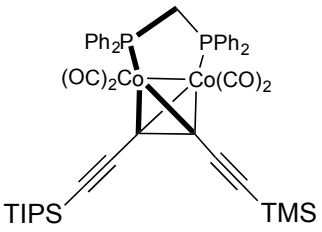

A solution of triyne **3.10** (1.22 g, 4.03 mmol) and $Co_2(CO)_8$ (1.52 g, 4.44 mmol) in degassed hexane (60 mL) was stirred at 20 °C under N_2 for 12 h. The hexane was evaporated and the residue dissolved in dry toluene (25 mL). Bis-diphenylphosphinomethane (1.60 g, 4.16 mmol) was added and the solution heated to reflux for 30 min. The crude reaction mixture contained two products. Evaporation and column chromatography (hexane/CH_2Cl_2 9:1 and 8:2) afforded intensely dark red crystals of **2**. R_f = 0.35 (Hexane), (0.98 g, 27%) after recrystallisation from CH_2Cl_2/MeOH.

^{1}H NMR (400 MHz, $CDCl_3$) δ 7.32-7.41 *(*m*,* 8H, *H*–Ar), 7.21-7.31 *(*m*,* 8H, *H*–Ar), 7.15-7.20 *(*m*,* 4H, *H*–Ar), 3.51 *(*q*,* $^2J_{H\text{-}P}$ = 10.9 Hz, 1H, PC*H'*P), 3.34 *(*q*,* $^2J_{H\text{-}P}$ = 10.9 Hz, 1H, PC*H*P), 1.12-1.16 *(*m*,* 21 H, *i*-Pr-*H*), 0.26 (s, 9H).

^{13}C NMR (100 MHz, $CDCI_3$) δ 203.8 (*br*), 202.3 *(br),* 136.5 (t, $J_{C\text{-}P}$ = 19.8 Hz), 135.1 (t, $J_{C\text{-}P}$ = 19.1 Hz), 132.4 (t, $^2J_{C\text{-}P}$ = 5.1 Hz), 131.8 (t, $^3J_{C\text{-}P}$ = 4.7 Hz), 130.0, 129.8, 128.4-128.6 (m), 109.6, 107.6, 102.3, 99.6, 71.5 (*br*), 68.9 (*br*), 35.1 (t, $^1J_{C\text{-}P}$ = 22.1 Hz), 19.0, 11.7, 0.5.

FTIR: 2105.1 (C≡C), 2026.5 (C=O), 1996.2 (C=O), 1973.2 (C=O), 1956.0 (C=O) cm^{-1}.

MALDI MS: 804.17 (Calc (–4 CO). $C_{43}H_{52}Co_2P_2Si_2$)), 804.16 (–4 CO).

Elemental: Calcd. for $C_{47}H_{52}Co_2O_4P_2Si_2$: C, 61.57; H, 5.72 Found: C, 61.56; H, 5.75.

UV-vis λ_{max}*:* CH_2Cl_2, 25 °C, (log ε) 290 (4.40), 350 (3.99).

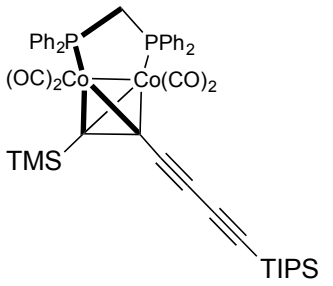

Additionally, a regioisomer Tetracarbonyl[μ^2-(5,6-η:5,6-η)-triisopropyl((trimethylsilyl)hexa-1,3,5-triyn-1-yl)silane][μ-methylenebis(diphenylphosphine)-P:P']dicobalt **2b** was isolated from the same reaction and was characterised as dark red crystals (1.63 g, 45%), R_f = 0.51 (Hexane). The structure of this regioisomer **2b** was confirmed *via* X-ray crystallographic analysis.

^{1}H NMR (400 MHz, $CDCl_3$) δ 7.39-7.49 *(*m*,* 4H, *H*–Ar), 7.27-7.34 *(*m*,* 10H, *H*–Ar), 7.21-7.24 *(*m*,* 2H, *H*–Ar), 7.12-7.16 *(*m*,* 4H, *H*–Ar), 3.94-4.03 *(*m, 1H, PC*H'*P), 3.27-3.32 *(*m, PC*H*P), 1.16-1.21 *(*m*,* 21 H, *i*-Pr-*H*), 0.37 (s, 9H).

^{13}C NMR (100 MHz, $CDCI_3$) δ 207.2 (*br*), 201.4 *(br),* 137.1 (t, $^1J_{C\text{-}P}$ = 22.6 Hz), 135.2 (t, $^1J_{C\text{-}P}$ = 17.8 Hz), 132.7 (t, $^2J_{C\text{-}P}$ = 6.1 Hz), 131.5 (t, $^2J_{C\text{-}P}$ = 6.4 Hz), 130.1, 129.8, 128.7 (t, $^3J_{C\text{-}P}$ = 4.7 Hz), 128.5 (t, $^3J_{C\text{-}P}$ = 4.8 Hz), 92.0, 91.5, 88.5, 81.7, 80.3 (*br*), 75.0 (*br*), 38.6 (t, $^1J_{C\text{-}P}$ = 19.5 Hz), 19.1, 11.8, 0.9.

FTIR: 2159.5 (C≡C), 2024.5 (C=O), 2001.2 (C=O), 1973.2 (C=O) cm^{-1}.

MALDI MS 804.17 (Calc. (–4 CO) $C_{43}H_{52}Co_2P_2Si_2$)), 804.16 (–4 CO).

Elemental: Calcd for $C_{47}H_{52}Co_2O_4P_2Si_2$: C, 61.57; H, 5.72 Found: C, 59.15; H, 5.79 (Fits with modelled CH_2Cl_2).

Tetracarbonyl[μ^2-(3,4-η:3,4-η)-triisopropyl(hexa-1,3,5-triyn-1-yl)silane][μ-methylenebis(diphenylphosphine)-P:P']dicobalt - **3**

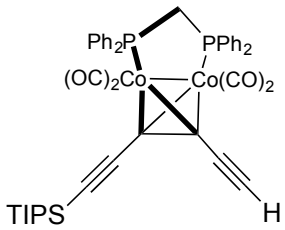

Cobalt complex **2** (67 mg, 0.073 mmol) was dissolved in 1:1 MeOH/THF mixture (6 mL). K_2CO_3 (100 mg, 0.73 mmol) was added in one portion. The reaction was stirred at 25 ºC and monitored *via* TLC, completion occurred after 30 min. The reaction mixture was evaporated and then dissolved in CH_2Cl_2/petroleum ether (1:1) and passed through a silica plug. Compound **3** was isolated as red crystals (57 mg, 96%).

^{1}H NMR (400 MHz, $CDCl_3$) δ 7.38-7.45 *(*m*,* 8 H, *H*–Ar). 7.21-7.33 *(*m*,* 8H, *H*–Ar), 7.11-7.18 *(*m*,* 4H, *H*–Ar), 3.71 *(*s, 1H, C≡C–*H*), 3.34-3.50 *(*m*,* 2H, PC*H*$_2$P), 1.09-1.15 *(*m, 21 H, *i*-Pr-*H*).

^{13}C NMR (100 MHz, $CDCl_3$) δ 204.0 (*br*), 202.2 *(br),* 136.8 (t, $^1J_{C\text{-}P}$ = 23.1 Hz), 134.6 (t, $^1J_{C\text{-}P}$ = 21.8 Hz), 132.5 (t, $^2J_{C\text{-}P}$ = 5.1 Hz), 131.7 (t, $^2J_{C\text{-}P}$ = 5.7 Hz), 130.2 (s), 130.0 (s), 128.7 (t, $^3J_{C\text{-}P}$ = 5.0 Hz), 128.4 (t, $^3J_{C\text{-}P}$ = 5.0 Hz), 109.0, 99.6, 86.4, 83.8, 70.4 (*br*), 69.8 (*br*), 35.5 (t, $^1J_{C\text{-}P}$ = 21.9 Hz), 19.1, 11.8.

FTIR: 3306.4 (C≡C-H), 2105.7 (C≡C), 2070.1 (C≡C), 2033.1 (C=O), 2008.6 (C=O), 1982.9 (C=O) cm^{-1}.

MALDI MS 732.13 (Calc. $C_{40}H_{44}Co_2P_2Si$), 732.90 (Found −4 CO).

Tetracarbonyl[μ^2-(3,4-η:3,4-η)-triisopropyl((trimethylsilyl)octa-1,3,5,7-tetrayn-1-yl)silane][μ-methylenebis(diphenylphosphine)-P:P']dicobalt - **4**

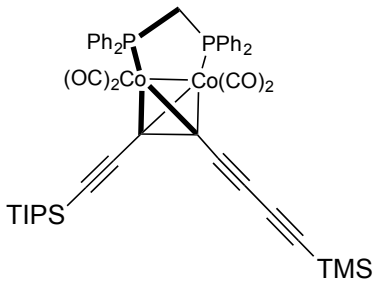

Cobalt complex **3** (50 mg, 0.059 mmol), TMS acetylene (0.29 g, 0.406 mL, 2.95 mmol), CuCl (3.01 g, 30.4 mmol) were dissolved in CH_2Cl_2 (400 mL) and stirred vigorously under dry air. TMEDA (3.22 g, 4.25 mL, 27.6 mmol) was added and the reaction was stirred vigorously for 20 min. The reaction was quenched with water (200 mL), organic phase separated and washed again with water to remove Cu salts. The organic phase was concentrated *in vacuo* and then passed through a silica plug to yield **4** as a red solid (42 mg, 82%)

^{1}H NMR (400 MHz, $CDCl_3$) δ 7.37-7.43 (m, 4H, *H*–Ar), 7.20-7.33 (m, 12H, *H*–Ar), 7.09-7.12 (m, 4H, *H*–Ar), 3.46 (q, $^{2}J_{H\text{-}P}$ = 10.9 Hz, 1H, PC*H*'P), 3.36 (q, $^{2}J_{H\text{-}P}$ = 10.5 Hz, 1H, PC*H*P), 1.08-1.12 (m, 21 H, i-Pr-*H*), 0.25 (s, 9H).

^{13}C NMR (100 MHz, $CDCI_3$) δ 204.0 (br), 201.6 (br), 136.9 (t, $^{1}J_{C\text{-}P}$ = 22.7 Hz), 134.0 (t, $^{1}J_{C\text{-}P}$ = 21.8 Hz), 132.6 (t, $^{2}J_{C\text{-}P}$ = 5.6 Hz), 131.6 (t, $^{2}J_{C\text{-}P}$ = 5.4 Hz), 130.2, 130.0, 128.8 (t, $^{3}J_{C\text{-}P}$ = 4.7 Hz), 128.6 (t, $^{3}J_{C\text{-}P}$ = 4.8 Hz), 108.8, 100.5, 88.3, 86.3, 81.2, 80.9, 70.6 (br), 67.9 (br), 35.8 (t, $^{1}J_{C\text{-}P}$ = 22.4 Hz), 19.1, 11.8, 0.2.

FTIR: 2156.0 (C≡C), 2105.8 (C≡C), 2038.3 (C=O), 2018.5 (C=O), 1986.5 (C=O), 1960.7 (C=O) cm^{-1}.

MALDI MS: 828.17 (Calc. (–4 CO) $C_{45}H_{52}Co_2P_2Si_2$)), 828.17 (–4 CO).

UV-vis λ_{max}: (CH_2Cl_2, 25 °C) (log ε) 304 (4.36), 372 (3.90).

Tetracarbonyl[μ^2-(3,4-η:3,4-η)-triisopropyl(octa-1,3,5,7-tetrayn-1-yl)silane][μ-methylenebis(diphenylphosphine)-P:P']dicobalt - **5**

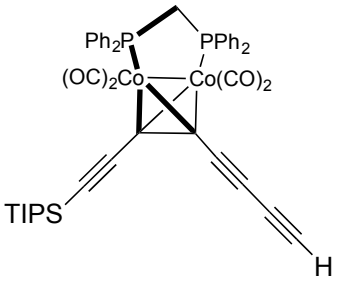

A solution of cobalt complex **4** (30 mg, 0.039 mmol) was dissolved in 1:1 MeOH/THF mixture (6 mL). K_2CO_3 (52.5 mg, 0.38 mmol) was added in one portion. The reaction was stirred at 25 °C and monitored *via* TLC, completion occurred after 30 min. The reaction mixture was evaporated and then dissolved in CH_2Cl_2/petroleum ether (1:1) and passed through a silica plug. Complex **5** was isolated as red crystals (26 mg, 100%).

^{1}H NMR (400 MHz, $CDCl_3$) δ 7.38-7.43 (m, 4H, *H*–Ar), 7.20-7.33 (m, 12H, *H*–Ar), 7.13-7.17 (m, 4H, *H*–Ar), 3.41 (m, 2H, PC*H*$_2$P), 2.80 (s, 1H, C≡C–*H*), 1.10-1.14 (m, 21 H, *i*-Pr-*H*).

^{13}C NMR (100 MHz, $CDCI_3$) δ 203.6 (*br*), 201.9 (*br*), 136.9 (*br*), 134.1 (*br*), 132.6 (t, $^{2}J_{C\text{-}P}$ = 5.6 Hz), 131.6 (t, $^{2}J_{C\text{-}P}$ = 5.4 Hz), 130.3, 130.1, 128.8 (t, $^{3}J_{C\text{-}P}$ = 4.7 Hz), 128.6 (t, $^{3}J_{C\text{-}P}$ = 4.8 Hz), 108.8, 100.6, 80.1, 79.6, 72.9, 70.7, 36.1 (t, $^{1}J_{C\text{-}P}$ = 22.4 Hz), 19.1, 11.8.

FTIR: 3305.1 (C≡C-H), 2161.3 (C≡C), 2102.0 (C≡C), 2034.8 (C=O), 2010.0 (C=O), 1985.0 (C=O) cm^{-1}.

Tetracarbonyl[μ^2-(3,4-η:3,4-η*)*-triisopropyl((trimethylsilyl)deca-1,3,5,7,9-pentayn-1-yl)silane][μ-methylenebis(diphenylphosphine)-P:P']dicobalt **6**

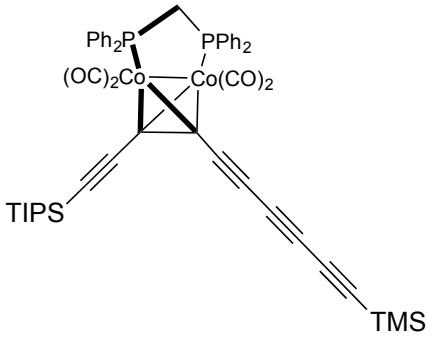

Cobalt complex **5** (100 mg, 0.12 mmol), TMS acetylene (0.580 g, 0.813 mL, 5.90 mmol), CuCl (1.17 g, 11.8 mmol) were dissolved in CH_2Cl_2 (400 mL) and stirred vigorously under dry air. TMEDA (1.68 mL, 11.7 mmol) was added and the reaction mixture was stirred for 40 min. The reaction was quenched with water (200 mL), organic phase separated and washed again with water (150 mL) to remove Cu salts. The organic phase was reduced *in vacuo* and purified by column chromatography (pet. ether:CH_2Cl_2 1:1) to yield **6** as a red solid (84 mg, 82%)

^{1}H NMR (400 MHz, $CDCl_3$) δ 7.37-7.43 (m, 4H, *H*–Ar), 7.22-7.33 (m, 12H, *H*–Ar), 7.11-7.19 (m, 4H, *H*–Ar), 3.35-3.42, m, 2H, PC***H*****$_2$**P), 1.08-1.13 (m, 21 H, i-Pr-*H*), 0.24 (s, 9H).

^{13}C NMR (100 MHz, $CDCI_3$) δ 203.3 (br), 201.8 (br), 136.9 (t, $^1J_{C-P}$ = 21.5 Hz), 134.1 (t, $^1J_{C-P}$ = 20.8 Hz), 132.5 (t, $^2J_{C-P}$ = 5.7 Hz), 131.7 (t, $^2J_{C-P}$ = 6.0 Hz), 130.4, 130.2, 128.8 (t, $^3J_{C-P}$ = 4.9 Hz), 128.7 (t, $^3J_{C-P}$ = 4.7 Hz), 108.9, 101.2, 89.8, 89.7, 82.1, 81.1, 72.3 (br), 68.9, 66.1 (br), 64.4, 36.3 (t, $^1J_{C-P}$ = 20.5 Hz), 19.1, 11.8, 0.0.

FTIR: 2126.4 (C≡C), 2054.6 (C=O), 2035.9 (C=O), 2014.9 (C=O), 1991.5 (C=O) cm^{-1}.

MALDI MS: 852.17 (Calc. $C_{47}H_{52}Co_2P_2Si_2$), 853.95 (–4 CO).

UV-Vis λ_{max} (CH_2Cl_2, 25 °C): (log ε) 342 (4.20), 417 (3.55).

Tetracarbonyl[μ^2-(3,4-η:3,4-η)-triisopropyl(deca-1,3,5,7,9-pentayn-1-yl)silane][μ-methylenebis(diphenylphosphine)-P:P']dicobalt - **7**

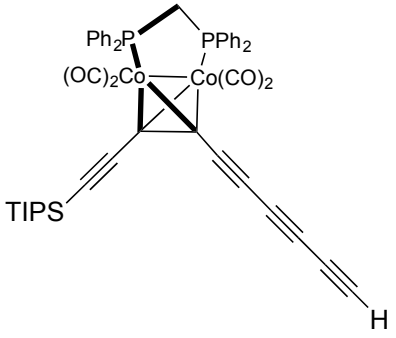

A solution of cobalt complex **6** (50 mg, 0.052 mmol) was dissolved in 1:1 MeOH/THF mixture (6 mL). K_2CO_3 (65 mg, 0.47 mmol) was added in one portion. The reaction was stirred at 25 °C and monitored *via* TLC, completion occurred

after 30 mins. The solvents were evaporated and the residue dissolved in CH_2Cl_2/petroleum ether (1:1) and passed through a silica plug (CH_2Cl_2/petroleum ether). Compound **7** was isolated as red crystals (40 mg, 90%).

^{1}H NMR (400 MHz, $CDCl_3$) δ 7.37-7.43 *(*m, 4H, *H*–Ar), 7.22-7.33 *(*m, 12H, *H*–Ar), 7.11-7.17 *(*m, 4H, *H*–Ar), 3.41 *(*q, $^2J_{H\text{-}P}$ = 10.9 Hz, 2H, PC*H*$_2$P), 2.43 (s, 1H, C≡C–*H*), 1.07-1.13 *(*m, 21 H, *i*-Pr-*H*).

^{13}C NMR (100 MHz, $CDCI_3$) δ 203.3 (*br*), 201.8 *(br),* 136.7 (br), 133.9 (br), 132.4 (t, $^2J_{C\text{-}P}$ = 5.7 Hz), 131.5 (t, $^2J_{C\text{-}P}$ = 6.0 Hz), 130.3, 130.0, 128.7 (t, $^3J_{C\text{-}P}$ = 4.9 Hz), 128.5 (t, $^3J_{C\text{-}P}$ = 4.7 Hz), 108.6, 101.1, 81.2, 80.6, 70.0, 69.7, 68.2, 62.9, 36.4 (t, $^1J_{C\text{-}P}$ = 20.5 Hz), 19.0, 11.7.

FTIR: 3296.6 (C≡C-H), 2131.8 (C≡C), 2033.0 (C=O), 2003.6 (C=O), 1988.9 (C=O), 1963.9 (C=O) cm^{-1}.

Octacarbonylbis[μ-methylenebis(diphenylphosphine)-P:P']$[\mu^4$-(3,4-η:3,4-η;9,10-η:9,10-η)-(1,12-Bis(triisopropylsilyl)-1,3,5,7,9,11-dodecahexayne)]tetracobalt - **8**

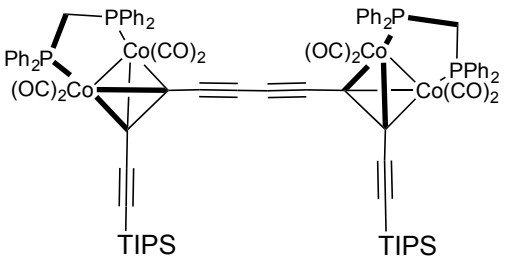

Mono-TIPS acetylene Co complex **3** (40 mg, 47.3 μmol) was dissolved in dry pyridine (3 mL). $Cu(OAc)_2$ (86 mg, 473 μmol) was added under N_2 and stirred overnight at 25 °C. Pyridine was removed *in vacuo*. This yielded two products, which were separated via column chromatography (CH_2Cl_2/petroleum ether 9:1). The higher R_f product **8** was isolated as a brown solid (32 mg, 80%).

^{1}H NMR (400 MHz, $CDCl_3$) δ 7.38-7.45 (m, 8H, *H*–Ar), 7.21-7.33 (m, 24H, *H*–Ar), 7.11-7.18 (m, 8H, *H*–Ar), 3.40 (t, $^2J_{H\text{-}P}$ = 10.3 Hz, 2H, PC*H*$_2$P), 1.09-1.13 (m, 42H, i-Pr-*H*).

^{13}C NMR (100 MHz, $CDCI_3$) δ 203.1 (br), 136.6 (t, $^1J_{C\text{-}P}$ = 23.1 Hz), 134.3 (t, $^1J_{C\text{-}P}$ = 21.8 Hz), 132.3 (t, $^2J_{C\text{-}P}$ = 5.1 Hz), 131.7 (t, $^2J_{C\text{-}P}$ = 5.7 Hz), 130.2, 129.9, 128.4-128.6 (m), 108.2, 100.5, 87.6, 84.4, 71.4 (br), 68.8 (br), 35.5 (t, $^1J_{C\text{-}P}$ = 21.9 Hz), 19.1, 11.8.

IR (ATR): 2169.9 (C≡C), 2079.5 (C≡C), 2034.5 (C=O), 2013.8 (C=O), 1989.5 cm^{-1} (C=O).

Elemental: Calcd for $C_{88}H_{86}Co_4O_4P_4Si_2$: C, 62.64; H, 5.14. Found: C, 62.57; H, 5.31.
UV-Vis λ_{max}: (log ε) 270 (4.65), 361 (4.52), 378 (4.53).

Octacarbonylbis[μ-methylenebis(diphenylphosphine)-P:P'][μ^4-1,2-η:1,2-η;11,12-η:11,12-η)-(1,12-Bis(triisopropylsilyl)-1,3,5,7,9,11-dodecahexayne)]tetracobalt - **8b**

The lower R_f product **8b** was also isolated as a red-brown solid (3 mg, 7%)

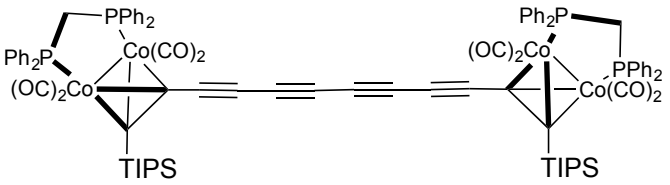

^{1}H NMR (400 MHz, $CDCl_3$) δ 7.38-7.45 (m, 8H, *H*–Ar), 7.21-7.33 (m, 24H, *H*–Ar), 7.11-7.18 (m, 8H, *H*–Ar), 3.40 (t, $^2J_{H-P}$ = 10.3 Hz, 4H, PC*H*$_2$P), 1.09-1.13 (m, 42H, i-Pr-*H*).
FTIR: 2169.9 (C≡C), 2079.5 (C≡C), 2034.5 (C=O), 2013.8 (C=O), 1989.5 (C=O) cm^{-1}.

Octacarbonylbis[μ-methylenebis(diphenylphosphine)-P:P'][μ^4-(3,4-η:3,4-η;13,14-η:13,14-η)-1,16-Bis(triisopropylsilyl)-1,3,5,7,9,11,13,15-hexadecaoctayne]tetracobalt - **9**.

Mono-TIPS butadiyne Co complex **5** (30 mg, 47.3 μmol) was dissolved in dry pyridine (3 mL). $Cu(OAc)_2$ (75 mg, 473 μmol) was added under N_2 and stirred overnight at 25 ºC. The pyridine was removed *in vacuo*. This yielded two products which were separated via column chromatography (CH_2Cl_2/petroleum ether 9:1). The lower R_f product **9** was isolated as a brown solid (23 mg, 77%).

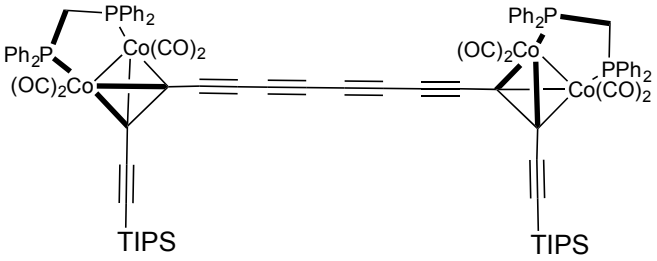

^{1}H NMR (400 MHz, $CDCl_3$) δ 7.38-7.42 (m, 8H, *H*–Ar), 7.23-7.36 (m, 24H, *H*–Ar), 7.13-7.18 (m, 8H, *H*–Ar), 3.36-3.43 (m, 4H, PC*H*$_2$P), 1.09-1.14 (m, 42H, i-Pr-*H*).
^{13}C NMR (100 MHz, $CDCl_3$) δ 202.9 (br), 201.7 (br), 136.3 (t, $^1J_{C-P}$ = 23.1 Hz), 134.1 (t, $^1J_{C-P}$ = 21.8 Hz), 132.3 (t, $^2J_{C-P}$ = 5.1 Hz), 131.6 (t, $^2J_{C-P}$ = 5.7 Hz), 130.2, 130.0, 128.5-128.8 (m), 108.7, 101.3, 83.3, 82.4, 70.8, 67.1, 36.3 (t, $^1J_{C-P}$ = 21.9 Hz), 19.1, 11.9.

FTIR: 2148.8 (C≡C), 2079.5, 2034.5 (C=O), 2013.8 (C=O), 1987.8 (C=O) cm^{-1}.

UV-Vis λ_{max}: (log ε) 285 (4.64), 385 (4.61), 409 (4.62).

Octacarbonylbis[μ-methylenebis(diphenylphosphine)-P:P'][μ^4-(3,4-η:3,4-η;17,18-η:17,18-η)-(1,20-Bis(triisopropylsilyl)-1,3,5,7,9,11,13,15,17,19-einacosadecayne)]tetracobalt **- 10**.

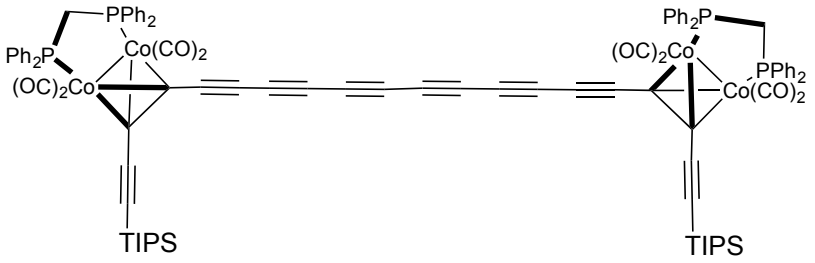

Mono-TIPS hexatriyne Co complex **7** (100 mg, 157 μmol) was dissolved in dry pyridine (12 mL). $Cu(OAc)_2$ (225 mg, 0.142 mmol) was added under N_2 and stirred overnight at room temperature. The pyridine was removed *in vacuo*. This yielded two products, which were separated via column chromatography (CH_2Cl_2/petroleum ether 9:1). The lower R_f product **10** was isolated as a brown solid (74 mg, 75%).

^{1}H NMR (400 MHz, $CDCl_3$) δ 7.10-7.40 (m, 40H, *H*–Ar), 3.40 (t, $^2J_{H-P}$ = 10.8 Hz, 4H, PC*H*$_2$P), 1.09-1.12 (m, 42H, *i*-Pr-*H*),

^{13}C NMR (100 MHz, $CDCI_3$) δ 203.1 (br). 200.5 (br), 136.2-136.3 (m), 133.6-134.2 (m), 132.2 (t, $^2J_{C-P}$ = 5.1 Hz), 131.5 (t, $^2J_{C-P}$ = 5.7 Hz), 130.3, 130.0, 128.4-128.8 (m), 108.5, 101.6, 83.3, 81.3, 69.9, 66.7, 65.6, 65.0, 36.4-36.6 (m), 19.0, 11.6.

FTIR: 2092.4 (C≡C), 2008.6 (C=O), 1991.9 (C=O), 1970.9 (C=O) cm^{-1}.

UV-vis λ_{max}: (log ε) 285 (4.64), 385 (4.61), 409 (4.62).

3.11 - References

(1) Hoye, T. R.; Baire, B.; Niu, D.; Willoughby, P. H.; Woods, B. P. *Nature* **2012**, *490*, 208.
(2) Greenfield, H.; Sternberg, H.; Friedel, R.; Wotiz, J.; Markby, R.; Wender, I. *J. Am. Chem. Soc.* **1956**, *78*, 120.
(3) Pearson, R.; Muir, W. *J. Am. Chem. Soc.* **1970**, *2*, 5520.
(4) Nicholas, K. M.; Pettit, R. *Tetrahedron Lett.* **1971**, *12*, 3475.
(5) Lockwood, R. F.; Nicholas, K. M. *Tetrahedron Lett.* **1977**, *18*, 4163.
(6) Khand, I. U.; Knox, G. R.; Pauson, P. L.; Watts, W. E. *J. Chem. Soc. D Chem. Commun.* **1971**, *1*, 36.
(7) Jeong, N.; Hwang, S. H.; Lee, Y.; Chung, Y. K. *J. Am. Chem. Soc.* **1994**, *116*, 3159.
(8) Low, P.; Rousseau, R.; Lam, P. *Organometallics* **1999**, *18*, 3885.
(9) Macazaga, M. J.; Marcos, M. L.; Moreno, C.; Benito-Lopez, F.; Gomez-González, J.; González-Velasco, J.; Medina, R. M. *J. Organomet. Chem.* **2006**, *691*, 138.
(10) Bruce, M. I.; Smith, M. E.; Zaitseva, N. N.; Skelton, B. W.; White, A. H. *J. Organomet. Chem.* **2003**, *670*, 170.
(11) Rubin, Y.; Knobler, C. B.; Diederich, F. *J. Am. Chem. Soc.* **1990**, *12*, 4966.
(12) Haley, M. M.; Langsdorf, B. L. *Chem. Commun.* **1997**, *2*, 1121.
(13) Diederich, F.; Rubin, Y. *Angew. Chem. Int. Ed. Eng.* **1992**, *31*, 1101.
(14) Chalifoux, W.; Tykwinski, R. R. *Nat. Chem.* **2010**, *2*, 967.
(15) Neenan, T. X.; Whitesides, G. M. *J. Org. Chem.* **1988**, *53*, 2489.
(16) Hirsch, A. *Nat. Mater.* **2010**, *9*, 868.
(17) Diederich, F.; Kivala, M. *Adv. Mater.* **2010**, *22*, 803.
(18) Tobe, Y.; Furukawa, R.; Sonoda, M. **2001**, *21*, 4072.
(19) Shvo, Y.; Hazum, E. *J. Chem. Soc., Chem. Commun.* **1974**, *9*, 336.
(20) Cetini, G.; Rossetti, R.; Sappa, E. *J. Organomet. Chem.* **1967**, *8*, 149.
(21) Allison, N. T.; Fritch, J. R.; Vollhardt, K. P. C.; Walborsky, E. C. *J. Am. Chem. Soc.* **1983**, *105*, 1384.
(22) Meyer, A.; Gorguesa, A.; Le Floc, Y.; Pineau, Y.; Guillevic, J.; Le Marouille, J. *Tetrahedron Lett.* **1981**, *22*, 5181.
(23) Pannell, K. H.; Crawford, G. M. *J. Coord. Chem.* **1973**, *2*, 251.
(24) Hanson, B. E.; Mancini, J. S. *Organometallics* **1983**, *2*, 126.
(25) Eisler, S.; Tykwinski, R. R. *J. Am. Chem. Soc.* **2000**, *122*, 10736.
(26) Luu, T.; Morisaki, Y.; Cunningham, N.; Tykwinski, R. R. *J. Org. Chem.* **2007**, *72*, 9622.
(27) Luu, T.; Elliott, E.; Slepkov, A. D.; Eisler, S.; McDonald, R.; Hegmann, F. A.; Tykwinski, R. R. *Org. Lett.* **2005**, *7*, 51.
(28) Diederich, F.; Rubin, Y.; Knobler, C. B.; Whetten, R. L.; Schriver, K. E.; Houk, K. N.; Li, Y. *Science* **1989**, *245*, 1088.
(29) Rubin, Y.; Kahr, M.; Knobler, C. B.; Diederich, F.; Wilkins, C. L. *J. Am. Chem. Soc.* **1991**, *113*, 495.
(30) Eisler, S.; Slepkov, A. D.; Elliott, E.; Luu, T.; McDonald, R.; Hegmann, F. A.; Tykwinski, R. R. *J. Am. Chem. Soc.* **2005**, *127*, 2666.
(31) Tobe, Y.; Fujii, T.; Naemura, K. *J. Org. Chem.* **1994**, *59*, 1236.
(32) Tobe, Y.; Fujii, T.; Matsumoto, H.; Naemura, K.; Achiba, Y.; Wakabayashi, T. *J. Am. Chem. Soc.* **1996**, *118*, 2758.
(33) Tobe, Y.; Umeda, R.; Iwasa, N.; Sonoda, M. *Chem. Eur. J* **2003**, *9*, 5549.

(34) Movsisyan, L. D.; Franz, M.; Hampel, F.; Thompson, A. L.; Tykwinski, R. R.; Anderson, H. L. *J. Am. Chem. Soc.* **2016**, *138*, 1366.
(35) Kohn, D. R.; Movsisyan, L. D.; Thompson, A. L.; Anderson, H. L. *Org. Lett.* **2017**, *19*, 348.
(36) Anthony, J.; Boldi, A. M.; Rubin, Y.; Hobi, M.; Gramlich, V.; Knobler, C. B.; Seiler, P.; Diederich, F. *Helv. Chim. Acta* **1995**, *78*, 13.
(37) Zhao, Y.; Slepkov, A. D.; Akoto, C. O.; McDonald, R.; Hegmann, F. A.; Tykwinski, R. R. *Chem. Eur. J* **2005**, *11*, 321.
(38) Platonov, A. Y.; Evdokimov, A. N.; Kurzin, A. V.; Maiyorova, H. D. *J. Chem. Eng. Data* **2002**, *47*, 1175.
(39) Anderson, H. L. *Inorg. Chem.* **1994**, *33*, 972.
(40) Eglinton, G; Galbraith, A, R. *Chem. Ind.* **1956**, 737.
(41) Diederich, F. *Helv. Chim. Acta* **1994**, *77*, 1441.
(42) Choice, T. F.; Modeling, P. M. *HyperChem(TM) Prof. 7.51, Hypercube, Inc., 1115 NW 4th Street, Gainesville, Florida 32601, USA*.
(43) Saito, S.; Takahashi, E.; Nakazono, K. *Org. Lett.* **2006**, *8*, 5133.
(44) Movsisyan, L. D.; Kondratuk, D. V.; Franz, M.; Thompson, A. L.; Tykwinski, R. R.; Anderson, H. L. *Org. Lett.* **2012**, *14*, 3424.
(45) Marini, A.; Munnoz-Losa, A.; Biancardi, A.; Mennucci, B. *J. Phys. Chem. B* **2010**, *114*, 17128.
(46) Reichardt, C. *Chem. Rev.* **1994**, *94*, 2319.
(47) Szafert, S.; Gladysz, J. A. *Chem. Rev.* **2006**, *106*, 1.
(48) Chalifoux, W. A.; McDonald, R.; Ferguson, M. J.; Tykwinski, R. R. *Angew. Chem. Int. Ed.* **2009**, *48*, 7915.
(49) Yang, S.; Kertesz, M. *J. Phys. Chem. A* **2006**, *110*, 9771.
(50) Palatinus, L.; Van Der Lee, A. *J. Appl. Crystallogr.* **2008**, *41*, 975.
(51) Palatinus, L. *Acta Crystallogr. Sect. B Struct. Sci. Cryst. Eng. Mater.* **2013**, *69*, 1.
(52) Palatinus, L.; Chapuis, G. *J. Appl. Crystallogr.* **2007**, *40*, 786.
(53) Betteridge, P. W.; Carruthers, J. R.; Cooper, R. I.; Prout, K.; Watkin, D. J. *J. Appl. Crystallogr.* **2003**, *36*, 1487.
(54) Cooper, R. I.; Thompson, A. L.; Watkin, D. J. *J. Appl. Crystallogr.* **2010**, *43*, 1100.
(55) Groom, C. R.; Bruno, I. J.; Lightfoot, M. P.; Ward, S. C. *Acta Crystallogr. Sect. B Struct. Sci. Cryst. Eng. Mater.* **2016**, *72*, 171.
(56) Jones, G. B.; Wright, J. M.; Plourde, G. W.; Hynd, G.; Huber, R. S.; Mathews, J. E. *J. Am. Chem. Soc.* **2000**, *122* (9), 1937.
(57) Anthony, J.; Boldi, A. M.; Rubin, Y.; Knobler, C. B.; Hobi, M.; Diederich, F. *Synth.* **1995**, *78*, 13.

Chapter 4

Dibromoolefin rotaxanes

4.1. Introduction 122

4.2. Synthesis of macrocycles 124

4.3. Synthesis of TIPS-D1 and rotaxane formation 128

4.4. Synthesis of TIPS-D2 and rotaxane formation 133

4.5. Attempted synthesis of catenanes 134

4.6. Template-directed approaches towards dibromoolefin catenanes 137

4.7. Conclusions 140

4.8. Experimental data for known compounds 141

4.9. Experimental data for novel compounds 148

4.10. References 161

Chapter 4 – Dibromoolefin rotaxanes

4.1 - Introduction

A number of masked alkyne equivalents (MAEs) have been used as components in synthetic strategies approaching cyclocarbons (**Chapter 1**). However, as far as we are aware, the dibromoolefin has never been used for this purpose. The development of this group as a MAE occurred after interest in pristine cyclocarbons subsided due to synthetic difficulties.[1–3] The 'unmasking' reaction for this MAE is the Fritsch-Buttenberg-Wiechell (FBW) rearrangement (see **Chapter 5)**. This rearrangement has developed from an exotic 19th century reaction[4–6] into a valuable methodology for synthesising polyynes.[7–9] We believe the extensive use of this rearrangement in polyyne synthesis and the successful preparation of dibromoolefin rotaxanes *via* active metal template (AMT) synthesis by our group (**Scheme 4.1**)[10] sets a strong precedent for the preparation of a dibromoolefin-masked cyclocarbon catenane.

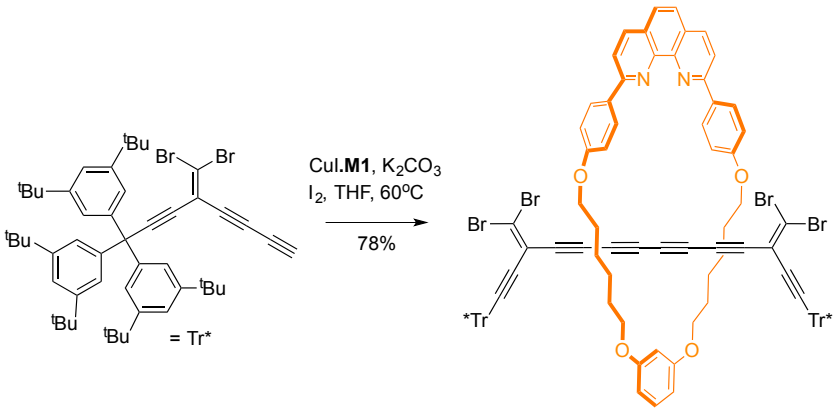

Scheme 4.1. Dibromoolefin oligoyne and dibromoolefin rotaxane prepared by Movsisyan *et al*.[10]

For a rotaxane to remain threaded the mechanical bond must lock the dumbbell in place. In *The Nature of a Mechanical Bond*[11] the importance of repulsive forces in maintaining an interlocked topology is highlighted. To prepare a masked cyclocarbon catenane, it is necessary to prepare a rotaxane intermediate with a small enough macrocycle that the dibromoolefin group can act as a stopper (**Figure 4.1iii**). Previously in our group, synthetic efforts have centred upon coordinating metals to the phenanthroline to decrease the cavity size sufficiently that unthreading of the threaded component is prevented. This strategy was unsuccessful. A rotaxane with terminal acetylenes in the stopper groups has not been isolated in previous investigations.

The use of a smaller macrocycle is an elegant way to circumvent the problem of unthreading. Developing a new series of macrocycles with smaller cavity sizes is highly valuable in the context of our wider objective of preparing masked cyclocarbon catenanes *via* any MAE. Most MAE groups are too small to act as stoppers for pre-existing phenanthroline macrocycles. Most macrocycles that have been used for AMT rotaxane formation have been considerably larger than the dibromoolefin group.[12] The dibromoolefin group is perfect for performing these optimising experiments because it has a short, well-understood synthesis in comparison to many other MAE groups. The insights into rotaxane formation, deprotection and coupling could then be applied to other MAEs.

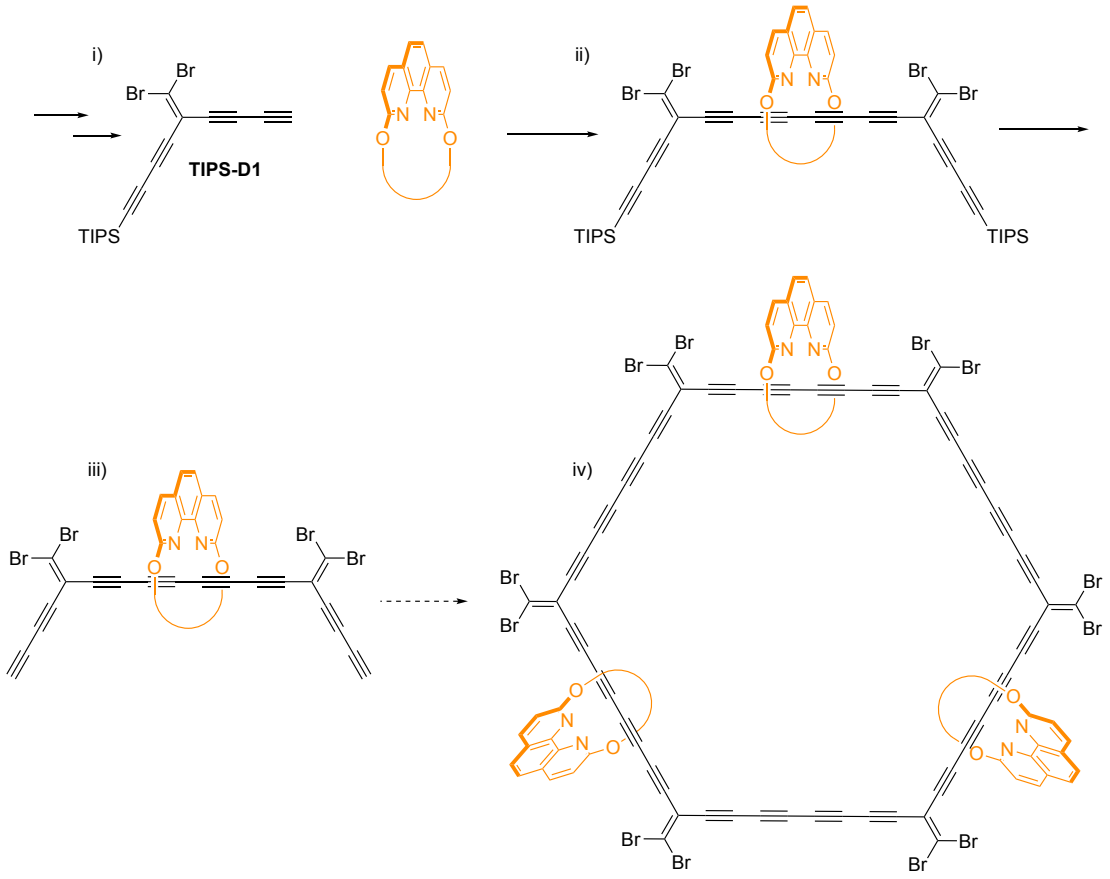

Figure 4.1. Planned dibromoolefin rotaxane preparation and subsequent catenane formation.

The synthesis of a multicomponent target like the dibromoolefin catenane (**Figure 4.1iv**) requires careful molecular design. The tuning of all components of this complex system will provide useful insights into the AMT reaction, dibromoolefin chemistry, phenanthroline chemistry and macrocycle formation. Our initial synthetic plan was to use the previously synthesised asymmetric dibromoolefin building block

TIPS-D1 because it previously provided good yields of rotaxanes. A rotaxane with a longer acetylenic dumbbell is also synthesised in order to try and improve the molecular design. In this chapter, we begin to explore the approach of templating the cyclisation step, which links to the work detailed in **Chapter 2**.

4.2 – Synthesis of macrocycles

A range of macrocycles have been used in previous dibromoolefin rotaxane syntheses (**Figure 4.2**).[13] These macrocycles were all too large to prevent unthreading when the bulky silyl protecting group was removed. A combination of crystal structures and Hyperchem modelling was used to estimate the cavity sizes of these macrocycles (**Figure 4.2**).[13]

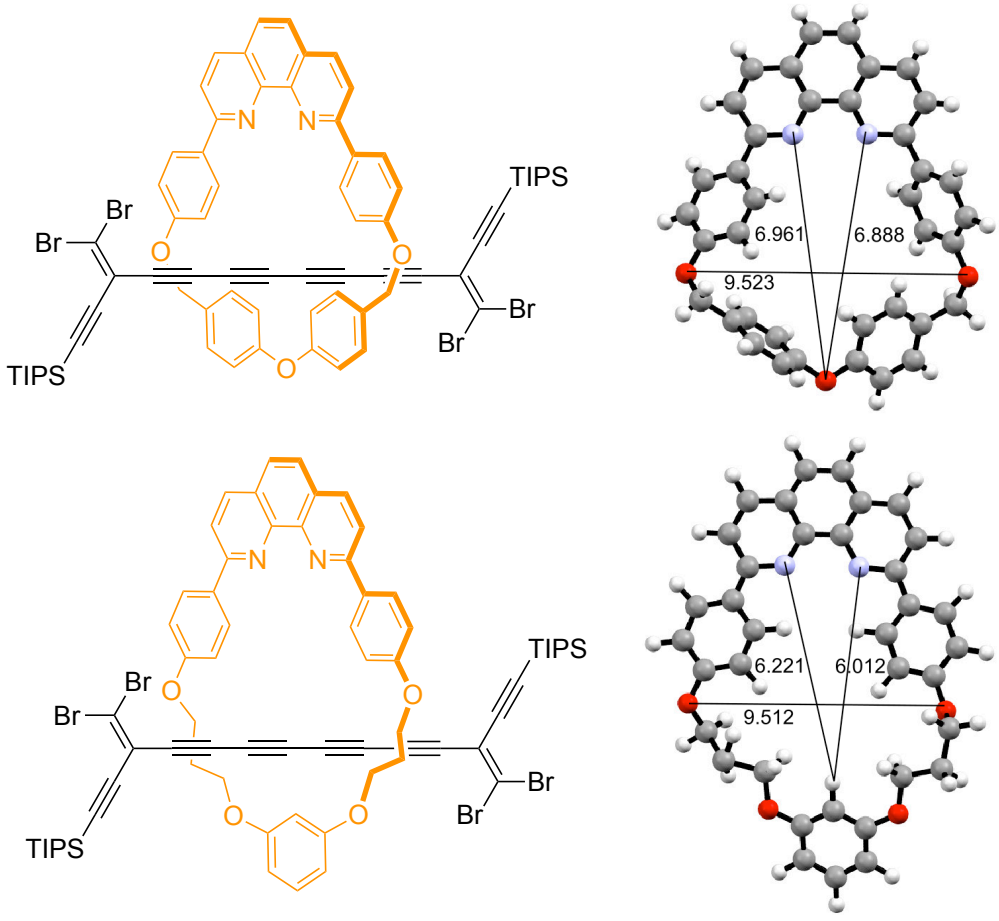

Figure 4.2. Two previously prepared rotaxanes[13] and the cavity sizes of their macrocycles (in Å), determined from crystal structure of **M2** and Hyperchem™ geometry optimisation (MM+ forcefield).

Passive metal templated (PMT) rotaxane formation is primarily a thermodynamically driven process.[14] In contrast, AMT rotaxane formation is a kinetically driven reaction. The reaction takes place faster through the ring than anywhere else in solution due to

the capture of the metal ion in the catalytic site. The practical consequence is that, as opposed to PT products, the interlocked product is kinetically more favoured than the non-interlocked components, but not necessarily more thermodynamically stable.[15]

The macrocycle needs to be sufficiently small that unthreading of the dibromoolefin dumbbell is prevented after removal of the TIPS group. However, this requirement must also be balanced with the efficiency of rotaxane formation. Smaller macrocycles generally reduce the coupling efficiency when preparing polyyne rotaxanes, although not as dramatically as with passive-templated synthesis.[10] This contrasts with the results obtained by Goldup *et al*. for the synthesis of rotaxanes *via* an active template copper-catalysed azide−alkyne cycloaddition (CuAAC) reaction, where smaller macrocycles afforded better yields.[16] These contrasting results may arise from the nature of the different transition states; the macrocycle must be large enough to accommodate the transition state for the reaction to be efficient. A series of macrocycles with subtle variation in cavity size were designed in order to find the 'sweet spot' of coupling efficiency and slippage prevention.

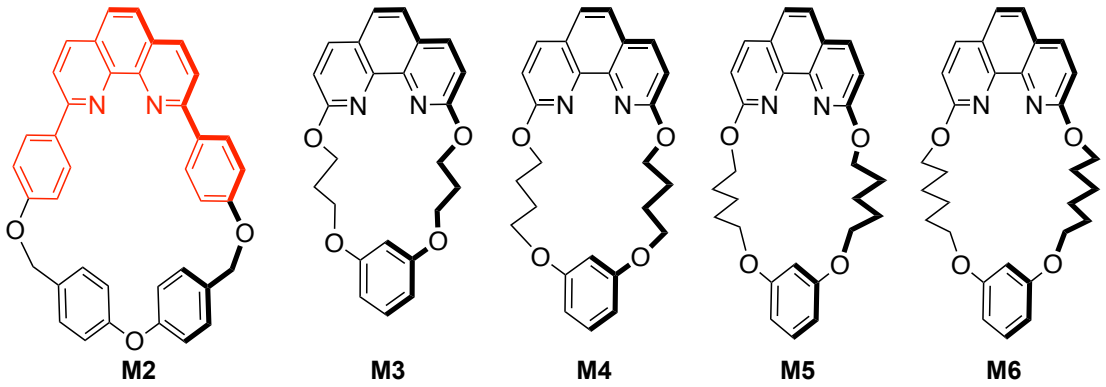

Figure 4.3. New macrocycle designs **M3-M6** and previously synthesized **M2**.[10]

All previously synthesised macrocycles were based on a phenyl-substituted phenanthroline (red in **Figure 4.3**). This intrinsically added a wide point of the cavity that presented a problem when using the small dibromoolefin as a stopper (**Figure 4.2**). Therefore, a direct oxygen substitution of phenanthroline was used to form a new family of smaller phenanthroline macrocycles; oxygen-substituted phenanthroline **4.4** was the key intermediate. A series of straps of different length could be synthesised in order to approach the optimum sized macrocycle. It is difficult

to predict the exact cavity size of these flexible macrocycles because their size is dependent on the conformation they adopt. However, it is clear that all of them are smaller than **M2** due to the loss of the phenyl-substituted phenanthroline moiety, as shown in the modelling**.**

In order to access the desired oxygen-substituted phenanthroline **4.4**, 2,9-dichloro-1,10-phenanthroline **4.3** had to be synthesised (**Scheme 4.2**). Until recently, this compound required a laborious six-step synthesis.[17] However, in 2012, Guo and coworkers[18] reported a convenient three-step synthesis with improved yields. 1,10-Phenanthroline was heated at 110 °C with excess dibromopropane in chlorobenzene and salt **4.1** was isolated a yellow precipitate in excellent yield. But, the second step was unreliable, Guo and coworkers' conditions, using KO^{t}Bu and *t*-BuOH, were irreproducible and the solidification of *t*-BuOH was highly impractical.

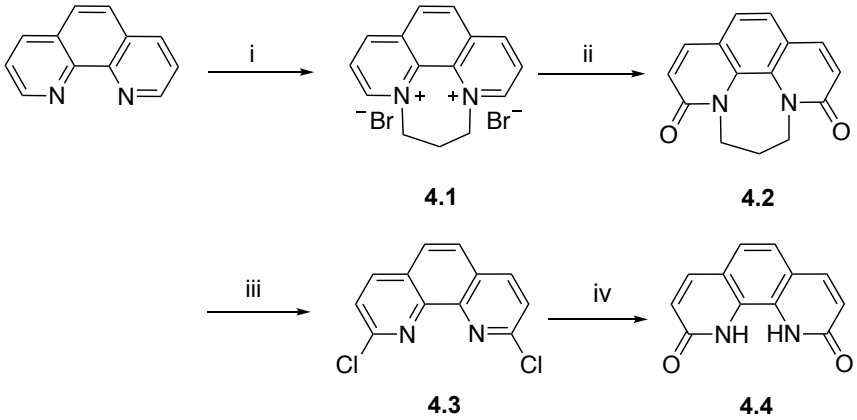

Scheme 4.2. Synthesis of phenanthroline **4.4**. i) Dibromopropane, chlorobenzene, 120 °C, 5 h, 93% ii) $[K_3Fe(CN)_6]$, NaOH, H_2O, 0-5 °C, 2 h, 38% iii) PCl_5, $POCl_3$, 110 °C, 7 h, 85% iv) H_2SO_4, H_2O, 120 °C, 4 h, 84%.

Although phenanthroline derivative **4.2** was successfully isolated *via* Guo's method, when scaling up, Bijin and coworkers'[19] procedure was utilised and found to be more reliable. This procedure utilised aqueous potassium ferricyanide and sodium hydroxide and yielded phenanthroline derivative **4.2** in 38% yield. Chlorination following the procedure of Guo and coworkers yielded 2,9-dichloro-1,10-phenanthroline **4.3** in 85% yield after heating with PCl_5 in $POCl_3$ at 110 °C.[18] In 2008, Krapcho and coworkers reported the facile acid hydrolysis of 2,9-dichloro-1,10-phenanthroline.[20] This procedure was followed and the desired phenanthroline

building block **4.4** was isolated in 84% yield. This molecule was suitable for forming a range of macrocycles which did not possess the additional phenyl moieties.

In order to prepare a series of macrocycles of tunable size, it is important to choose a molecular design where the size of the macrocycle can be adjusted by one carbon at a time. As a series of dibromoalkyl compounds can be used to achieve the required diversity, we prepared a range of substituted resorcinol compounds **S_3 – S_6** (**Scheme 4.3**). These strap compounds were synthesised by the reaction of resorcinol with various length dibromoalkyl compounds and K_2CO_3 in acetone at 60 °C.

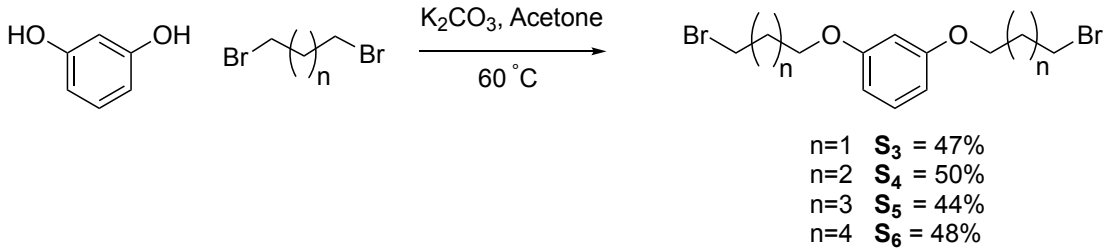

Scheme 4.3. Synthesis of straps **S_3-S_6**.

After the complete synthesis of the series of straps, macrocycles were prepared from phenanthroline **4.4** and straps **S_3 – S_6**. The macrocycles were synthesised by adding both reagents in high dilution to Cs_2CO_3 in DMF at 60 °C (≈2 mM), yielding macrocycles **M3-M6** in moderate yields. The high-dilution conditions lead to a preference in formation of the macrocycle over polymerisation by lowering the concentration of the mono-substituted intermediate and favouring the intramolecular reaction over a second substitution.[21] Generally, the smaller macrocycles were prepared in lower yields than the larger macrocycles. This is because the conformation required to cyclise is slightly less probable, with fewer degrees of freedom of the alkyl chain.

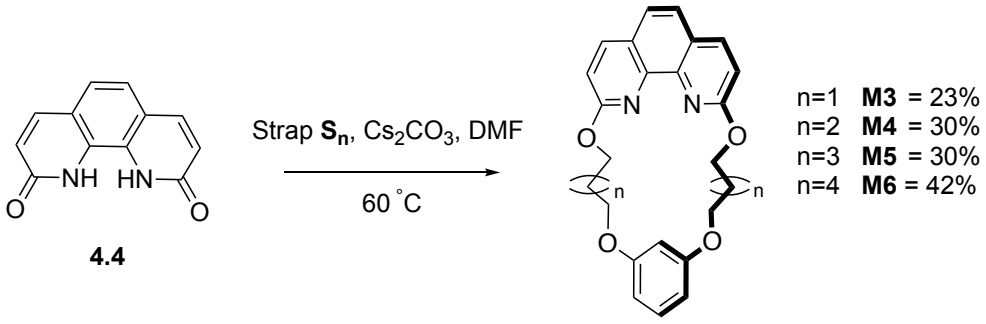

Scheme 4.4. Synthesis of macrocycles **M3-M6**

The ^{1}H NMR spectra of the macrocycles exhibit some clear trends (**Figure 4.4**). The area of the spectrum containing the phenanthroline signals ($H_{a\text{-}c}$) remains unchanged in all spectra. The protons from the resorcinol moiety of the macrocycle ($H_{j,k}$) change considerably and are clearly split in **M3** in comparison to **M6**, where they overlap. The chemical shift of the alkyl protons is highly dependent on their distance from an oxygen atom and can be assigned accordingly ($H_{d\text{-}i}$).

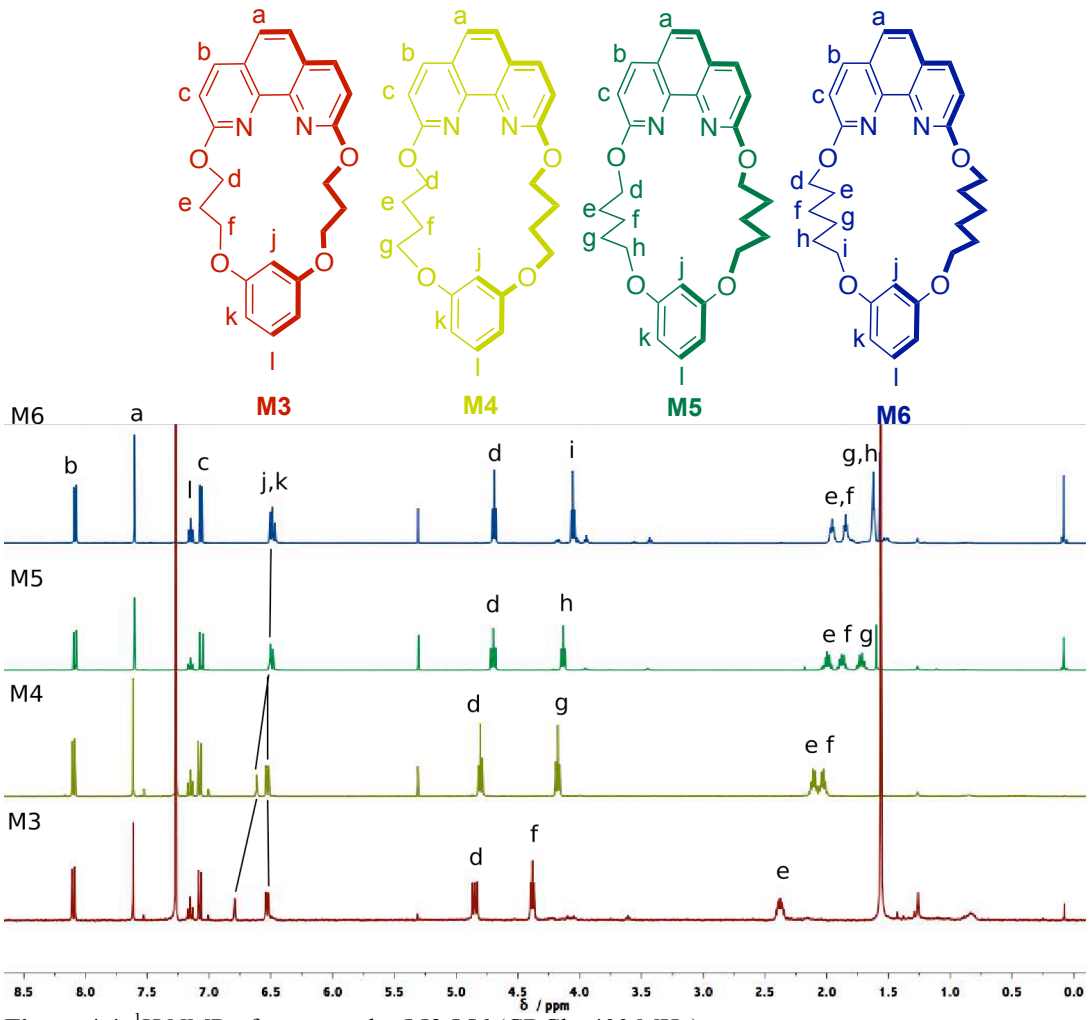

Figure 4.4. ^{1}H NMR of macrocycles **M3-M6** ($CDCl_3$, 400 MHz).

4.3 – Synthesis of dibromoolefin TIPS-D1 and rotaxane formation

The molecular design of dibromoolefin **4.7** was chosen to incorporate two different silyl protecting groups because they can be removed separately and mildly in the synthetic path. The dibromoolefin **4.7** had been prepared previously in our group from a published procedure by Tykwinkski and coworkers[1] as part of our attempts to make dibromoolefin rotaxanes. The same synthetic route was taken but modified in order to improve yields. TIPS-acetylene was converted to TIPS-propargylic acid **4.5** in

excellent yield (99%). Conjugated ketones can be formed directly *via* a Friedel-Crafts type acylation and this methodology was used to furnish ketone **4.6** in 57% yield. The acid **4.5** was chlorinated with $SOCl_2$ overnight and the product was reacted with 1,4-bis(trimethylsilyl)-butadiyne yielding ketone **4.6** as an unstable brown oil. The reaction crude was passed through silica plug and the product was used in the next stage without further purification. Reaction of this ketone under Ramirez's conditions gave dibromoolefin **4.7** as a stable yellow oil in excellent yield (**Scheme 4.5**).

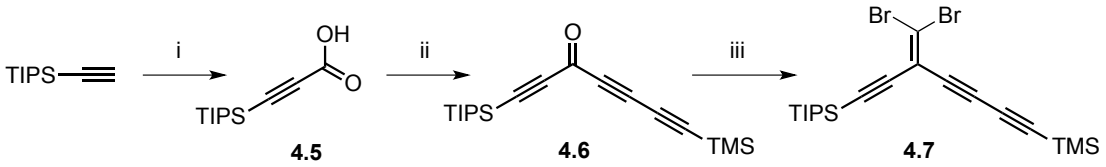

Scheme 4.5. Synthesis of **4.7**. i) a) MeLi, THF, 0 °C, 1 h. b) CO_2, -78 ºC, 1 h, 99% ii) a) $SOCl_2$, 25 °C, 12 h. b) 1,4- bis TMS butadiyne, $AlCl_3$, CH_2Cl_2, 0 °C, 2 h, 57% iii) PPh_3, CBr_4, CH_2Cl_2, 25 °C, 90 %.

The TMS-deprotection of **4.7** was always performed directly before the rotaxane formation as the terminal diyne **TIPS-D1** was unstable. It had to be treated with care and never kept in the solid phase. Homocoupling was used instead of Cadiot-Chodkiewicz coupling due to the instability of the halogenated diyne. Rotaxanes **M6⊂(TIPS-D1)$_2$** and **M5⊂(TIPS-D1)$_2$** were prepared from their corresponding macrocycles in moderate yield *via* an AMT coupling reaction (**Scheme 4.6**). In contrast, rotaxane formation with macrocycles **M3** and **M4** was not possible. A small peak was observed by MALDI mass spectrometry of **M4⊂(TIPS-D1)$_2$**, but this was not isolable. The intermediate in AMT coupling is likely to be highly sterically congested due to the small macrocycle cavity size. We propose that this steric congestion prevents the rotaxane from forming in **M3** and **M4**.

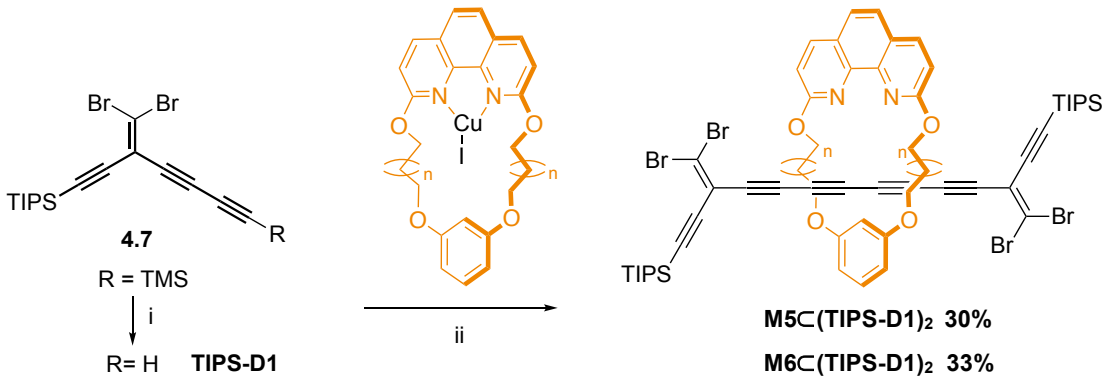

Scheme 4.6. Rotaxane Synthesis. i) K_2CO_3, THF/MeOH, 25 °C, 30 min, 100% ii) a) CuI, MeCN, CH_2Cl_2, 25 °C, 30 min. b) K_2CO_3, I_2, THF, 60 °C.

Threading a polyyne through the macrocycle induces a notable chemical shift change in macrocycle protons, which has been observed previously (**Figure 4.5**).[10,22] The π-system of the polyyne has a significant magnetic effect depending on the relative orientation.[23] This effect can be observed in protons *a* and *d*. However, the most notable examples is proton *j*; the overlapping signal in macrocycle **M5** is highly split in rotaxane **M5⊂(TIPS-D1)$_2$.** This proton shifts the most as it points into the macrocyclic cavity. These shifts confirm the rotaxane is one interlocked entity rather than a mixture of macrocycle and dumbbell. The ^{13}C NMR and MALDI mass spectrometry are also consistent with the proposed structure. This is the first polyyne rotaxane formed with this type of smaller macrocycle. Very similar shifts are observed in **M6/M6⊂(TIPS-D1)$_2$**.

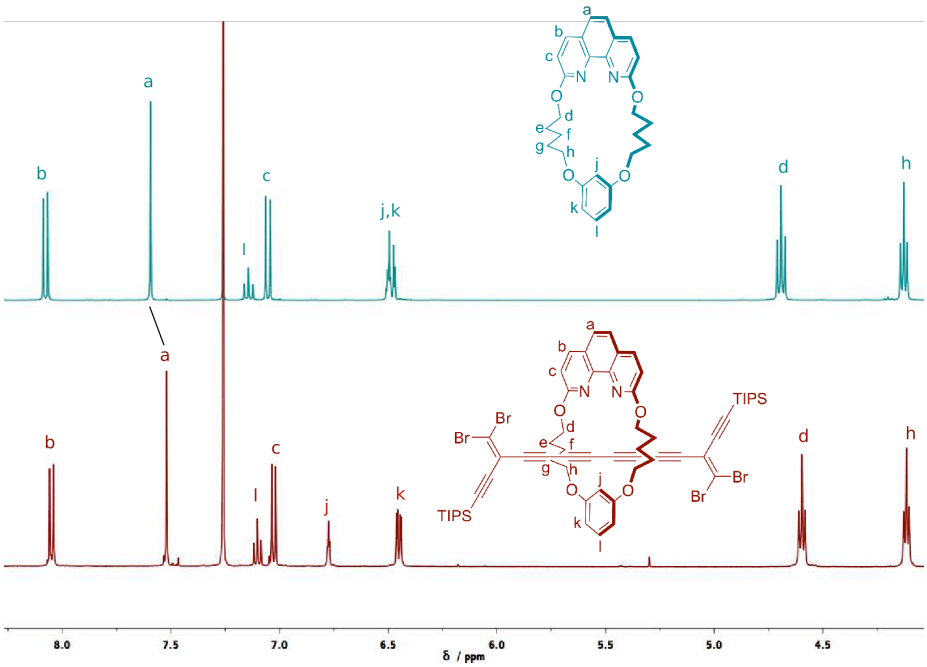

Figure 4.5. ^{1}H NMR of **M5** and **M5⊂(TIPS-D1)$_2$** ($CDCl_3$, 500 MHz).

The deprotection of rotaxanes was initially performed using TBAF in CH_2Cl_2. The dumbbell appeared to slip from the macrocycle after the addition of TBAF to rotaxane **M6⊂(TIPS-D1)$_2$**., two products were observed *via* TLC analysis and crude ^{1}H NMR showed the reversal of the characteristic shift in the macrocycle protons. In contrast, the product from deprotection of rotaxane **M5⊂(TIPS-D1)$_2$**. appeared to remain interlocked. For further confirmation, the reaction was performed in an NMR tube and monitored. The NMR experiment showed a subtle shift in macrocycle protons and the loss of the TIPS peak after 15 minutes (**Figure 4.6**). After this positive result, the

deprotection was run on a larger scale and the fully deprotected **M5⊂(D1)$_2$** was isolated after purification with a silica plug (**Scheme 4.7**). When the same reaction was performed on the naked dumbbell **(TIPS-D1)$_2$** the reaction had to be performed at 0 °C in order to prevent complete decomposition.[13] Once again, the difference in reactivity highlights the effect of 'stabilisation by encapsulation'. The rotaxane **M5⊂(D1)$_2$** is slightly unstable in the solid state, but is stable for at least 24 hours in the solid state. This contrasts with the naked deprotected dumbbell **(D1)$_2$**, which is highly unstable in the solid state.[13]

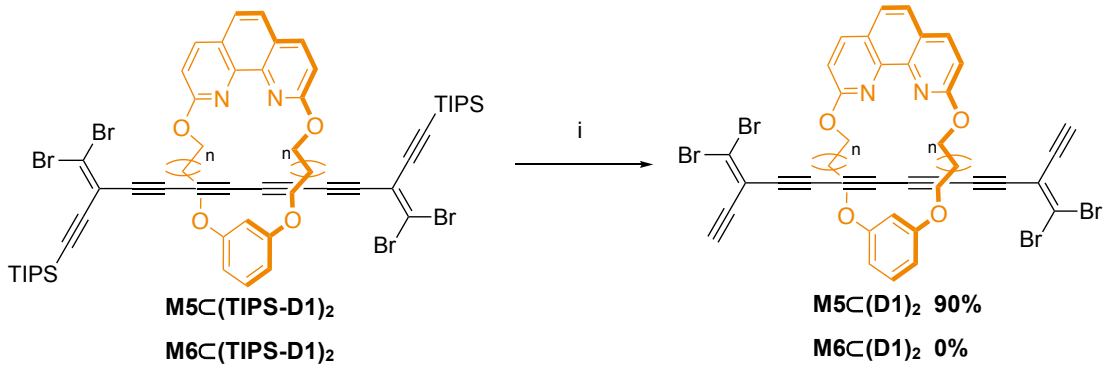

Scheme 4.7. Rotaxane deprotection i) TBAF, CH_2Cl_2, 25 °C, 15 min.

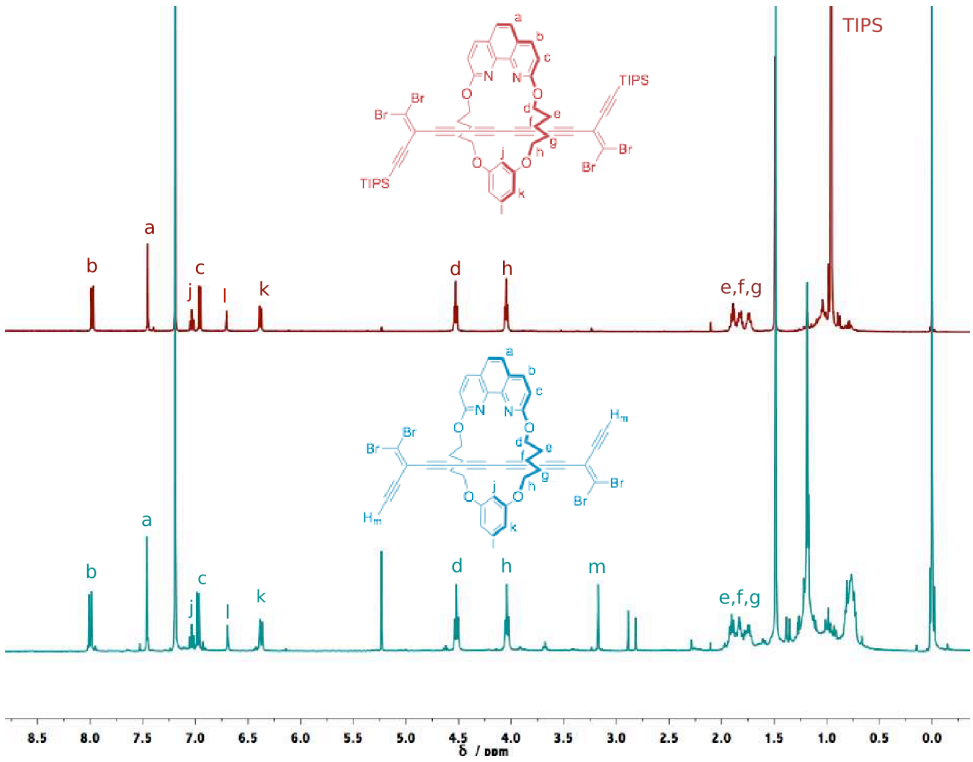

Figure 4.6. ^{1}H NMR of **M5⊂(TIPS-D1)$_2$** and **M5⊂(D1)$_2$** ($CDCl_3$, 500 MHz).

The only stable deprotected rotaxane resulting from these experiments was **M5⊂(D1)$_2$**. The size of macrocycle **M5** can be estimated by modelling (**Figure 4.7**).

It is clearly smaller than the macrocycles shown in **Figure 4.2**, which supports the experimental evidence regarding unthreading. It is also possible to estimate the size of the dibromoolefin group by modelling (**Figure 4.7**). This method only provides an estimate as there is significant flexibility in the macrocycle conformation. The bromine atom has a larger van der Waals radius than the other atoms in the macrocycle, so the distance measured during modelling is comparatively underestimated when the distance between the centre of the atoms is measured (**Figure 4.7**). If the van der Waals radius of bromine (1.85 Å) is added to the estimated dibromoolefin size and the van der Waals radii of nitrogen and hydrogen (1.60 Å and 1.20 Å)[24] are subtracted from the macrocyclic cavity size, the dibromoolefin is too large to be able to slip through the macrocyclic cavity. Molecular dynamics simulations were also performed on this rotaxane to see if unthreading occurred. The dumbbell remained threaded after being heated from 0 K to 500 K over 10 ps, maintained at 500 K for 50 ps and cooled to 298 K over 10 ps. This fully deprotected rotaxane was used to approach cyclic structures (**Section 4.5**).

(6.743 – 1.60 – 1.20) = 3.943 Å *Macrocycle cavity size estimate*

(5.259 + 1.85) = 7.109 Å *Dibromoolefin group size estimate*

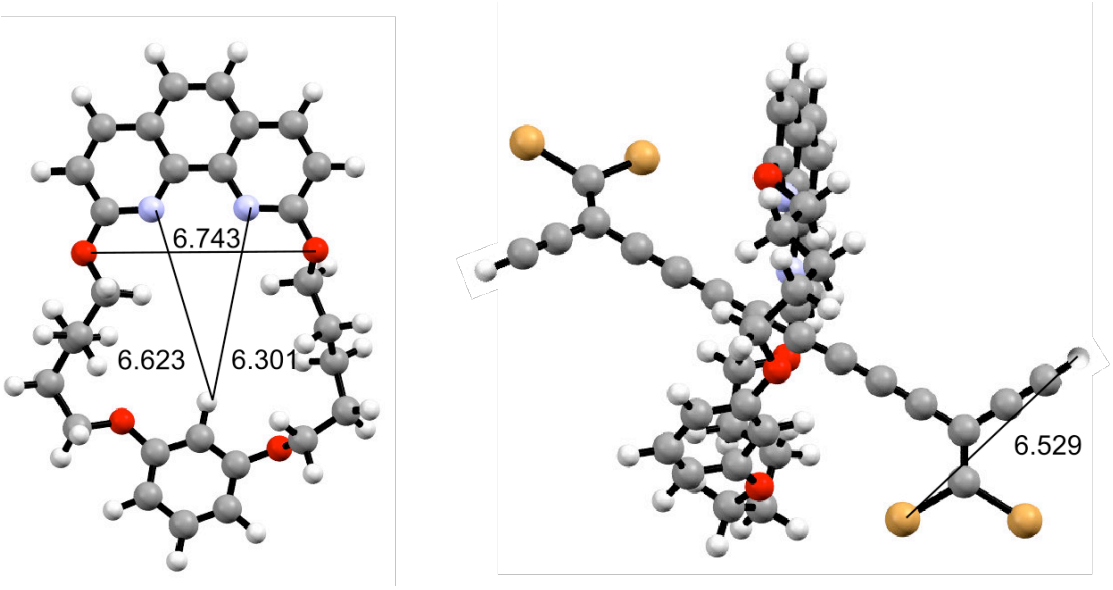

Figure 4.7. Macrocycle **M5** and estimated macrocycle cavity size, rotaxane **M5⊂(D1)$_2$** and estimated size of dibromoolefin MAE (in Å), modelled using Hyperchem™ (MM+ forcefield).

4.4 – Synthesis of dibromoolefin TIPS-D2 and rotaxane formation

Novel dibromoolefin **4.12** was designed to yield the longer analogous terminal dibromoolefin rotaxane **M5⊂(TIPS-D2)$_2$**. This new molecular design could reduce steric hindrance, as well as the electronic effect of the dibromoolefin moiety on the terminal acetylene. These two factors may make it easier to couple the deprotected rotaxane and form catenanes.

In the first step, TIPS-propargylic aldehyde was subjected to Ramirez's conditions and furnished dibromoolefin **4.8** in excellent yield.[1,25] TIPS-butadiyne **4.9** was prepared *via* an elimination of dibromoolefin **4.8** with LDA in good yield.[26] Diyne **4.9** was handled with care and deprotonated with MeLi and CO_2 gas was bubbled through the reaction mixture to form carboxylic acid **4.10** in very good yield.[27] The subsequent Friedel-Crafts acylation furnished novel ketone **4.11** in good yield. Finally, Ramirez's conditions were used to prepare novel dibromoolefin **4.12** in good yield.

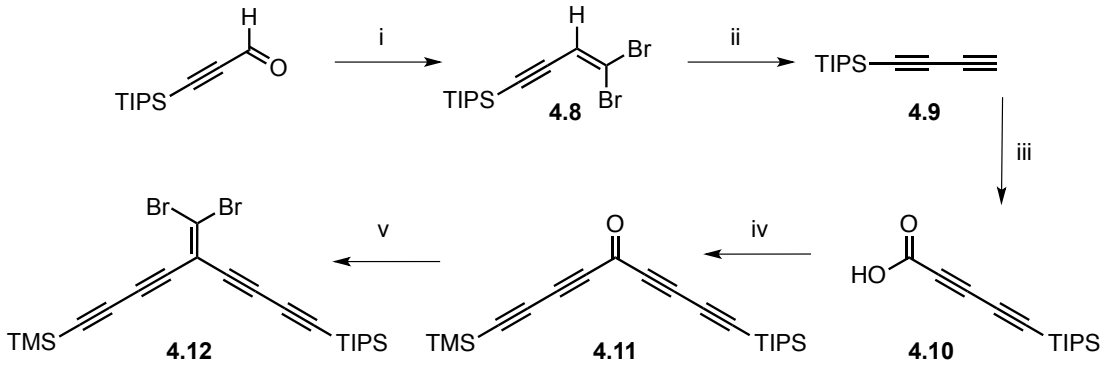

Scheme 4.9. Synthesis of dibromoolefin **4.12**. i) PPh_3, CBr_4, CH_2Cl_2, 25 °C, 100% ii) LDA, THF, -78 °C, 80% iii) a) MeLi, THF, 0 °C b) CO_2, -78 °C, 88% iv) a) $SOCl_2$, 12 h, 25 °C. b) 1,4-bis TMS butadiyne, $AlCl_3$, CH_2Cl_2, 0 °C, 2 h, 70% v) PPh_3, CBr_4, CH_2Cl_2, 25 °C, 100 %.

Our previous experiments had suggested that macrocycle **M5** was the optimum size for avoiding unthreading. For this reason, all rotaxane formations were performed with macrocycle **M5**. Our typical active metal template conditions yielded rotaxane **M5⊂(TIPS-D2)$_2$** in 25% yield (**Scheme 4.10**). This reaction was less clean than with the shorter analogue **TIPS-D1** and required extensive purification. It appeared that a very similar rotaxane side product was also formed. MALDI mass spectrometry suggested that this product had one fewer carbon atom. Indeed, Tykwinski and

coworkers have reported a loss of one carbon atom in some coupling reactions.[1] However, this is not well understood. **M5⊂(TIPS-D2)$_2$** was purified *via* silica column chromatography, size exclusion chromatography and recycling gel permeation chromatography (GPC). The purified rotaxane **M5⊂(TIPS-D2)$_2$** had the expected increased number of carbons in the ^{13}C NMR spectrum, a similar ^{1}H NMR to its shorter relative and the expected MALDI mass spectrum.

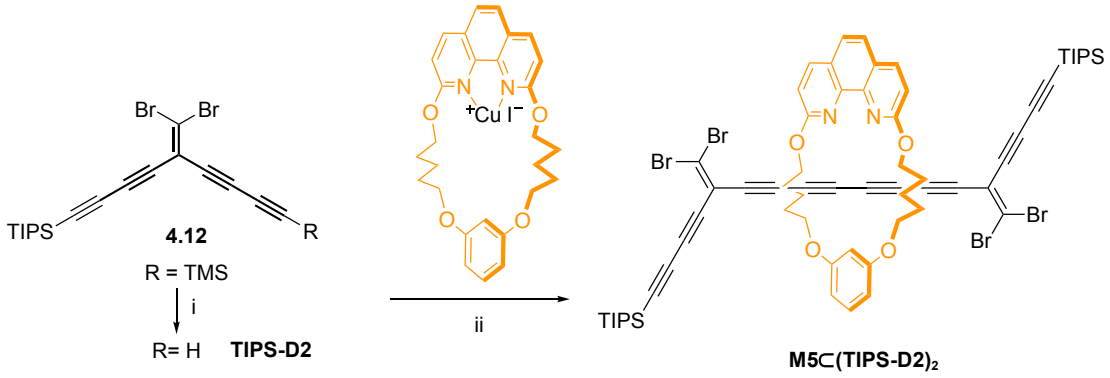

Scheme 4.10. Synthesis of longer rotaxane **M5⊂(TIPS-D2)$_2$** i) K_2CO_3, THF/MeOH, 25 °C, 15 min, 90% ii) K_2CO_3, I_2, THF, 60 °C, 24 h, 25%.

We subjected this rotaxane to deprotection with TBAF to prepare a precursor for catenane formation. This reaction worked very quickly and yielded the desired deprotected rotaxane **M5⊂(D2)$_2$** in good yield without unthreading of the dibromoolefin dumbbell.

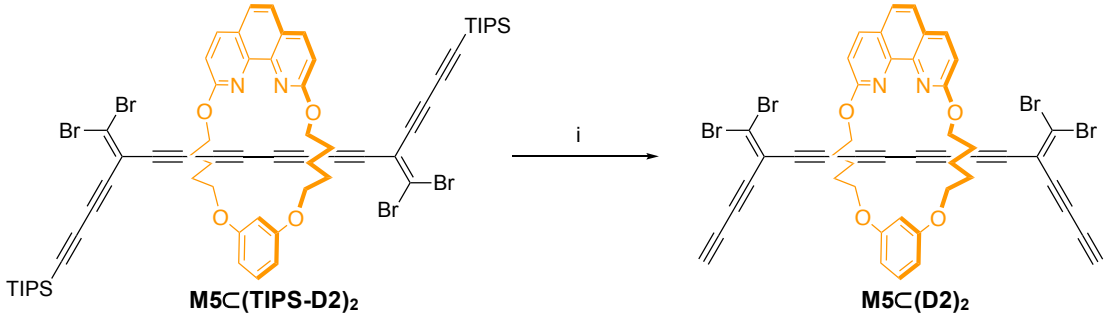

Scheme 4.11. Deprotection of **M5⊂(TIPS-D2)$_2$** i) TBAF, CH_2Cl_2, 25 °C, 15 min, 85%.

4.5 – Attempted synthesis of dibromoolefin catenanes

When preparing cyclic compounds in homocoupling reactions, high dilution conditions are used to favour cyclisation over polymerisation[28], including new phase-transfer methods.[29] Many different conditions can be used for alkyne homocouplings, ranging from old methods such as Glaser-Hay[30,31] and Eglinton couplings[32] to more

modern copper and palladium methods with various phosphine ligands.[28,33] Many different coupling conditions were screened in various attempts to form catenanes from **M5⊂(D1)$_2$** and **M5⊂(D2)$_2$.** However, all of the reaction conditions resulted in intractable black soot, with no evidence of catenane formation (**Scheme 4.12**). The reactions were monitored by TLC, ^{1}H NMR and MALDI mass spectrometry and the starting material was always consumed rapidly.

Throughout this thesis our most commonly used conditions for homocoupling were Glaser-Hay modified conditions (CuCl/TMEDA, CH_2Cl_2).[31] However, these conditions did not yield any catenanes or longer rotaxanes (**Table 4.1**, **Scheme 4.12**). TMEDA is a fairly nucleophilic base, so may result in side reactions with the fragile rotaxane. In **Chapter 3**, Eglinton couplings were used to couple dicobalt complexes of acetylenes. However, these conditions were also unsuccessful at preparing catenanes ($Cu(OAc)_2$, Pyridine, N_2).[28,32] A catalyst with a lower turnover may preferentially favour cyclisation over polymerisation. Copper chloride and pyridine is a less active catalytic system but is longer lived. However, the application of this catalytic system to rotaxanes **M5⊂(D1)$_2$** and **M5⊂(D2)$_2$** was also unsuccessful. When preparing cyclic strained acetylenic porphyrin nanorings, modified palladium conditions are frequently used [$PdCl_2(PPh_3)_2$, CuI, DIPA, toluene, benzoquinone (BQ)].[34,35] However, the application of these conditions for catenane formation was also unsuccessful. It is possible that the copper in these reaction mixtures is coordinating to the phenanthroline and this is precipitating the compound or somehow hindering its desired reactivity. For that reason, copper-free coupling conditions were employed, these conditions were also unsuccessful ($Pd_2(dba)_3$, tri(2-furyl)phosphine, toluene, NEt_3, 50 °C).[33]

Table 4.1. Attempted cyclisation conditions trialled with both rotaxanes **M5⊂(D1)$_2$** and **M5⊂(D2)$_2$**

Reaction conditions	Outcome
CuCl/TMEDA, CH_2Cl_2, air[31]	Unsuccessful
$Cu(OAc)_2$, pyridine, N_2[28,32]	Unsuccessful
CuCl, pyridine, air[36]	Unsuccessful
$PdCl_2(PPh_3)_2$, CuI, DIPA, toluene	Unsuccessful
$Pd_2(dba)_3$, tri(2-furyl)phosphine, toluene, BQ, NEt_3, 50 °C[33]	Unsuccessful

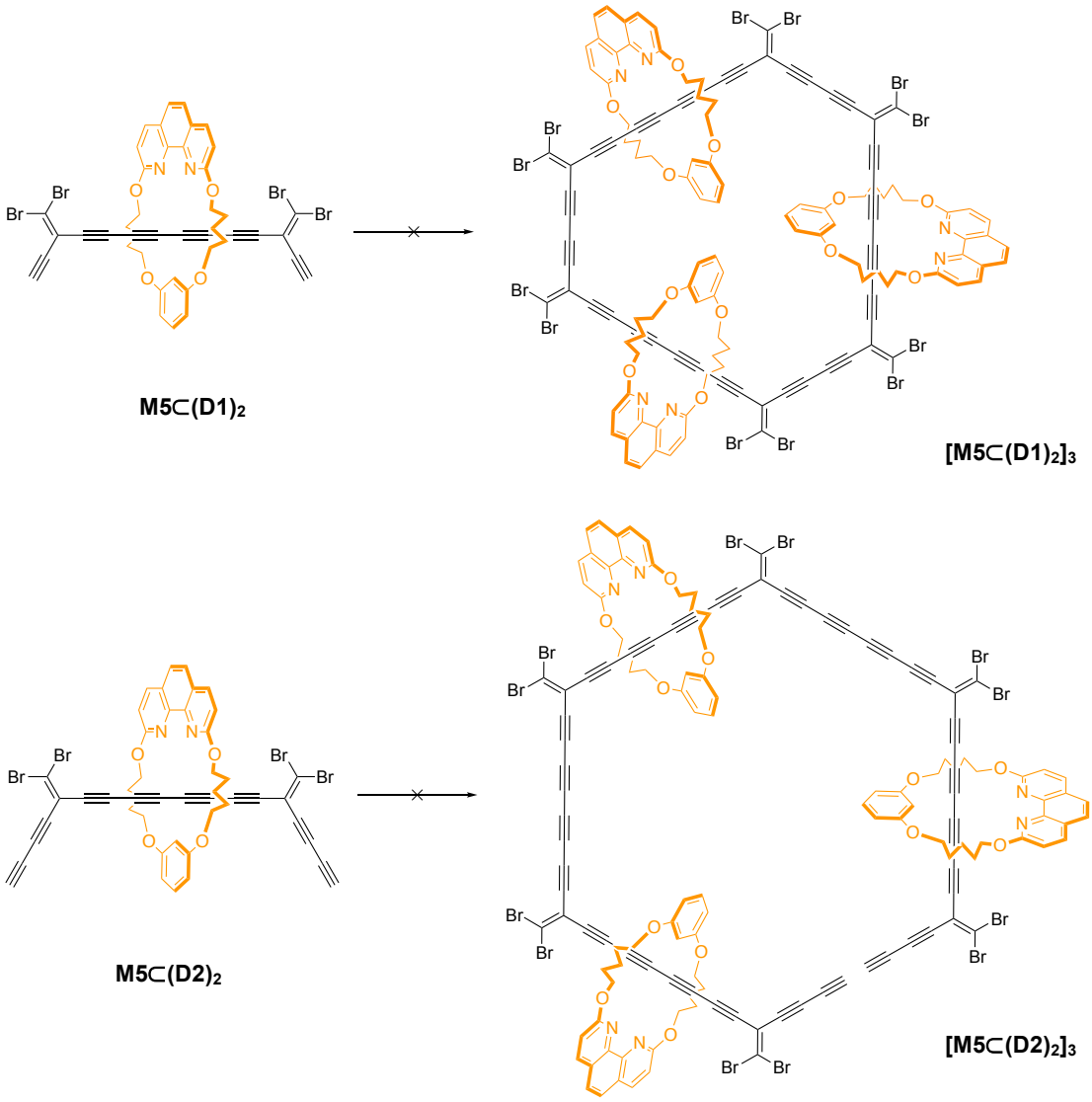

Scheme 4.12. Attempted catenane formation.

The homocoupling of a monodeprotected species is a simpler reaction for probing coupling conditions, with fewer possible products and a lower entropic demand. Additionally, if the desired [3]rotaxane was successfully isolated it may offer a degree of preorganisation and subsequently lead to the desired catenane. Therefore, monodeprotected rotaxane **M5⊂(TIPS-D1)(D1)** was synthesised *via* a statistical deprotection by careful addition of TBAF in a mixture of CH_2Cl_2:$CHCl_3$:EtOH (50:50:1). Careful separation of bis-protected, mono-protected and fully deprotected rotaxanes by column chromatography led to isolation of monodeprotected **M5⊂(TIPS-D1)(D1)** in 35% yield. Subsequent [3]rotaxane synthesis was unsuccessful, despite exposure to a broad range of conditions (**Table 4.2, Scheme 4.13**).

Table 4.2. Attempted homocoupling conditions for rotaxane **M5⊂(TIPS-D1)(D1)**

Reaction conditions	Outcome
CuCl/TMEDA, CH_2Cl_2, air[31]	Unsuccessful
$Cu(OAc)_2$, pyridine, N_2[28,32]	Unsuccessful
CuCl, pyridine, air[36]	Unsuccessful
$PdCl_{2(}PPh_{3)2}$, CuI, DIPA, toluene	Unsuccessful
$Pd_2(dba)_3$, Tri(2-furyl)phosphine, toluene, BQ, NEt_3, 50 °C[33]	Unsuccessful

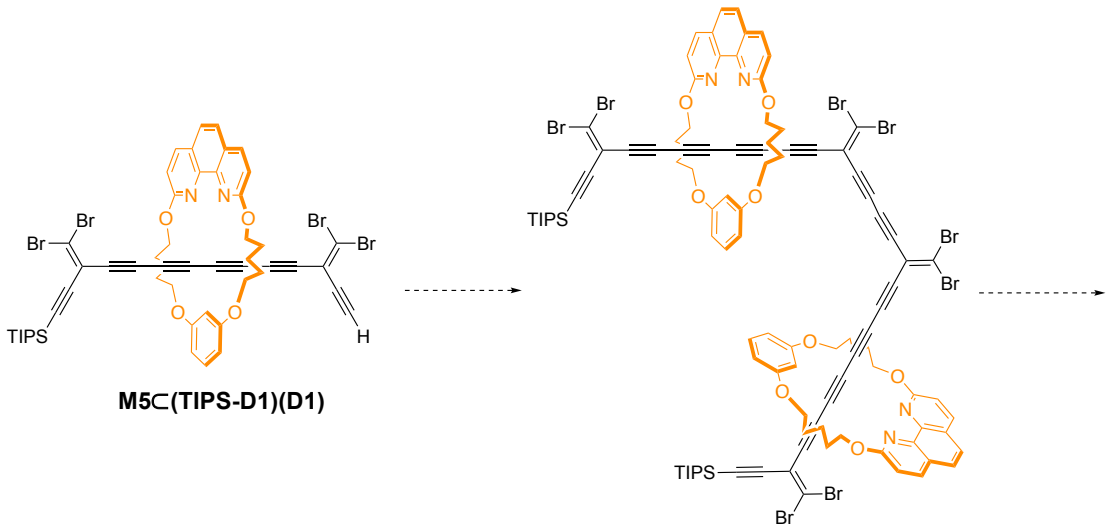

Scheme 4.13. Attempted [3]rotaxane formation.

The failure of the homocoupling of **M5⊂(TIPS-D1)(D1)** was unexpected because single acetylenes adjacent to dibromoolefins in unthreaded species have been coupled successfully (**Chapter 5**). The only possible explanations seem to be that steric hindrance from the macrocycle prevented the reaction or the rotaxanes are too unstable to the reaction conditions.

4.6 – Template-directed approaches towards dibromoolefin catenanes

The arrangement of acetylenic dumbbells around a central core was explored in **Chapter 2**. A new molecular design with linked macrocycles was chosen to favour catenane formation. Molecular modelling was performed using Hyperchem to test the feasibility of the molecular design and predicted that a core comprising two macrocycles was of suitable size for templating catenane formation (**Figure 4.8**). The acetylenic dumbells could reach one another to couple without significant strain.

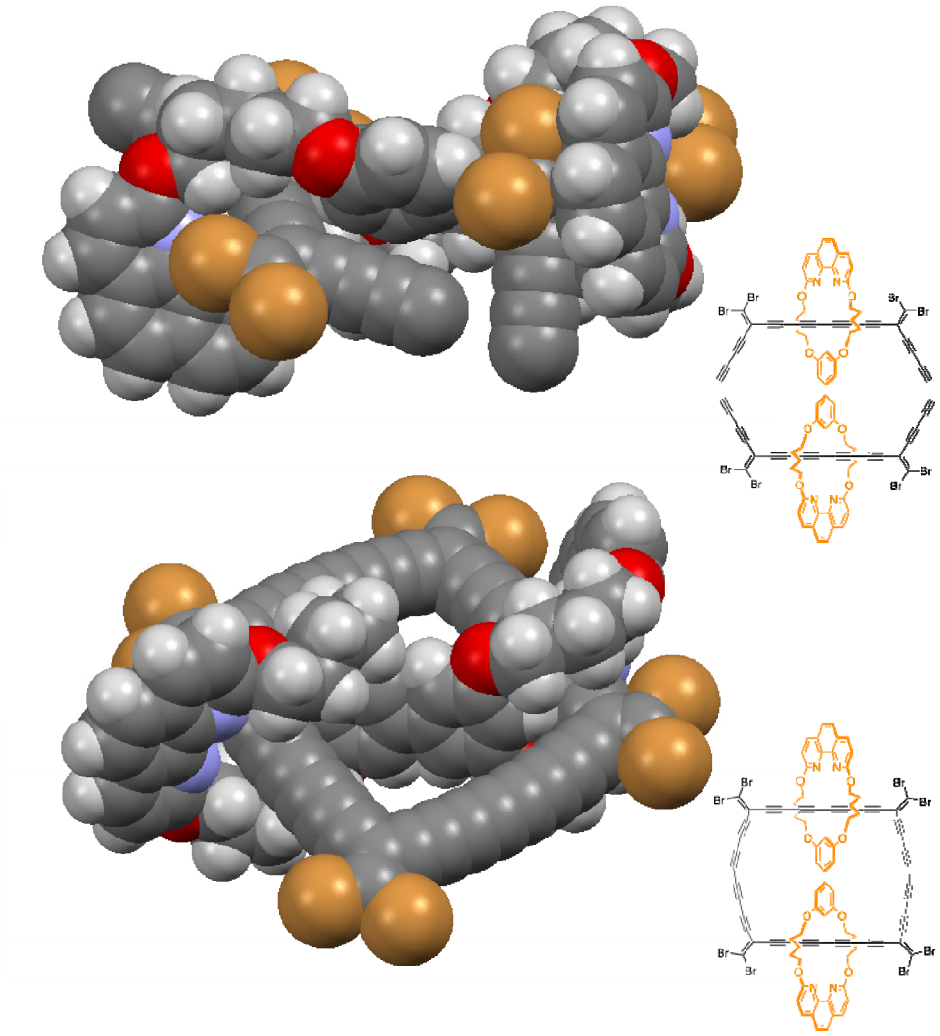

Figure 4.8. Hyperchem^{TM} modeling of desired template [3]rotaxane and catenane (MM^{+} forcefield).

In order to synthesise this linked macrocyclic core, a coupling point must be introduced to the macrocycle. For this reason, macrocycle $\mathbf{M_{5Br}}$ was synthesised *via* a similar synthetic route to previous macrocycles. Analogously to the non-brominated strap compounds, $\mathbf{S5_{Br}}$ was prepared by alkylating a resorcinol derivative in a moderate yield (**Scheme 4.14**). This macrocycle contained a bromine atom that could be used to initiate a coupling between two macrocycles and result in a linked core. It is possible to both link the macrocycles first and then form a rotaxane or link two rotaxanes together after a AMT reaction (similarly to **Chapter 2**). We initially pursued the macrocycle linking route and did not attempt the alternative strategy due to time constraints.

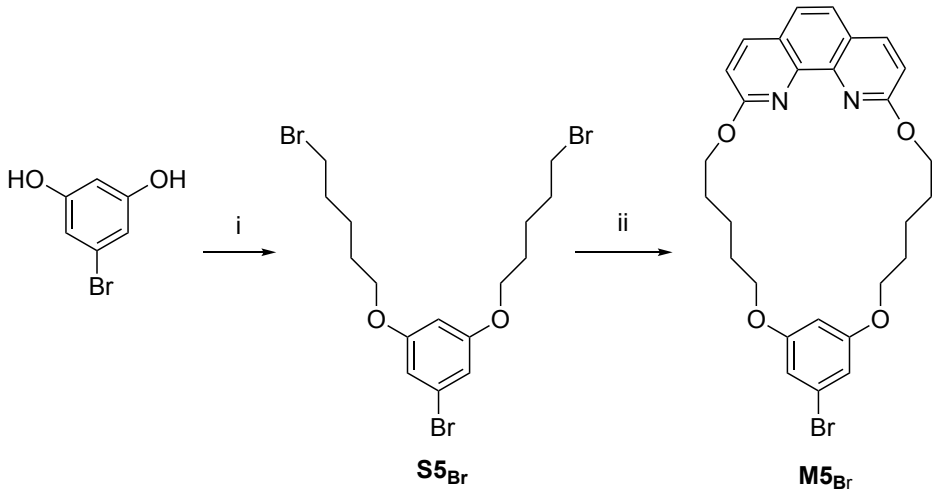

Scheme 4.14. Synthesis of $\mathbf{M5_{Br}}$ i) Dibromopentane, K_2CO_3, acetone, 60 °C, 48 h, 50% ii) Phenanthroline 4.4, Cs_2CO_3, DMF, 60 °C, 24 h, 22%.

The planned synthetic route relied on a homocoupling of the macrocycle $\mathbf{M5_{Br}}$ *via* an Ullmann type coupling.[37] However, many Ullmann type conditions utilise extremely high temperatures, which were difficult to achieve.[38] Yamamoto couplings with Ni(0) can also be used to homocouple aryl bromides.[39,40] However, the catalysts are highly air sensitive and had fairly poor substrate scope. One-pot Suzuki protocols have also been reported where an *in situ* borylation and subsequent coupling can result in very efficient yields.[41,42] When these conditions were trialled a mixture of desired $\mathbf{(M5)_2}$, $\mathbf{M_{Br}}$ and $\mathbf{M_{Bpin}}$ was obtained, which was very challenging to purify. Thus, the reaction was performed stepwise and $\mathbf{(M5)_2}$ was prepared in two steps in a combined good yield.

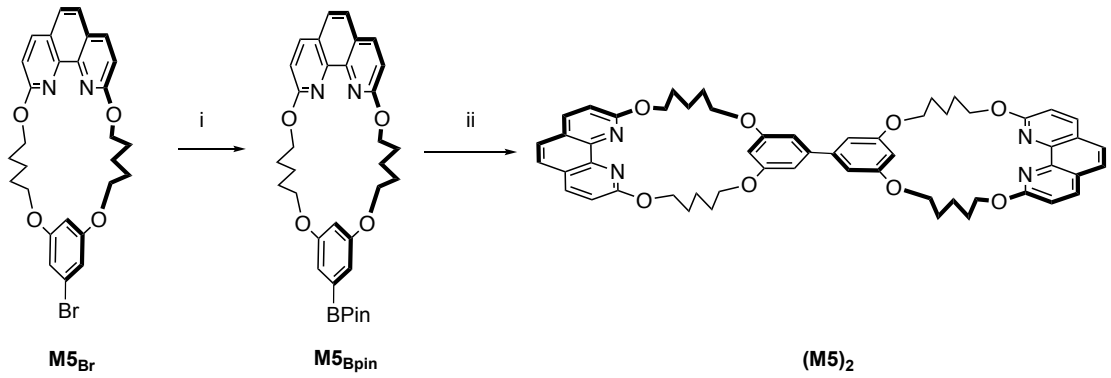

Scheme 4.15. Synthesis of bis-macrocycle $\mathbf{(M5)_2}$. i) $\mathbf{M5_{Br}}$, B_2Pin_2, $PdCl_2$(dppf), dppf, KOAc, DMF, 80 °C, 12 h, 98% ii) $\mathbf{M5_{Br}}$, $PdCl_2$(dppf), Na_2CO_3, THF/H_2O, 80 °C, 18 h, 61%.

After isolation of bis-macrocycle **(M5)$_2$**, copper insertion was attempted so active metal template synthesis could be pursued. This resulted in a highly insoluble complex, despite testing with other Cu(I) sources. Unfortunately, time restrictions meant that this could not be investigated further. If more time had been available, further efforts would have been made at rotaxane formation from bis-macrocycle **(M5)$_2$**. Additionally, we would have tried to explore the alternative route of forming a rotaxane from **M5$_{Br}$** first and then linking the macrocycles.

4.7 – Conclusions

A series of carefully designed macrocycles have been synthesised with considerably smaller macrocyclic cavities than pre-existing phenanthroline macrocycles. These macrocycles offer opportunities to utilise small MAEs in masked cyclocarbon synthesis. Dibromoolefin rotaxanes were systematically prepared from these novel macrocycles and the macrocycle size was found to have a large effect on rotaxane yield. It is not possible to synthesise rotaxanes from very small macrocycles. These investigations resulted in the successful synthesis of two TIPS-capped rotaxanes and the successful deprotection of one of these species. The isolation of a rotaxane with terminal acetylene end groups offers significant promise for the objective of preparing cyclocarbon catenanes.

A new carbon-rich dibromoolefin building block was synthesised with a terminal butadiyne in the molecular design. The successful rotaxane formation demonstrates the level of tolerance of our synthetic methods and our increased ability to design and build complex carbon-rich molecules from the bottom up. All attempts at coupling rotaxanes together were unsuccessful. Cyclisation and [3]rotaxane preparation was not successful despite a wide variety of reaction conditions. A linked macrocycle was synthesised in order to overcome this obstacle. However, time constraints stopped further testing of this new system.

4.8 – Experimental data for known compounds

4,8-Dibromo-4,5,6,7,8,9-hexahydro-4^{1}*H*-[1,4]diazepino[1,2,3,4-*lmn*][1,10]phenanthroline-4,8-diium-4^{1},9-diide - **4.1**[18]

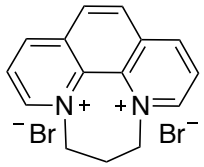

A solution of 1,10-phenanthroline monohydrate (10.0 g, 60.8 mmol) in chlorobenzene (50 mL) was heated at 70 °C. To the solution, 1,3-dibromopropane (30.8 mL, 300 mmol) was added dropwise over 15 min, the temperature was raised to 120 °C. During the course of the reaction, a yellow solid precipitated from the reaction mixture. After 4 h, the mixture was allowed to cool to room temperature and the yellow precipitate was collected, washed with petroleum ether and dried *in vacuo* to yield **4.1** as a yellow solid (18.2 g, 93%). As in lit.[18]

^{1}H NMR (D_2O, 400 MHz): δ 9.50 (dd, *J* = 1.2, 5.8 Hz, 2H), 9.28 (dd, *J* = 1.2, 8.6 Hz, 2H), 8.41 (s, 2H), 8.37 (d, ^{4}J = 2.7 Hz, 2H), 4.99 (t, ^{3}J = 7.0 Hz, 4H), 3.27 (quint, ^{3}J = 6.7 Hz, 2H).

^{13}C NMR (D_2O, 100 MHz): δ = 150.9, 147.4, 134.2, 133.6, 130.3, 127.4, 60.5, 31.0.

6,7-Dihydro-*3H*-1,4-diazepino[1,2,3,4-*lmn*][1,10]phenanthroline-3,9(*5H*)-dione - **4.2**[19]

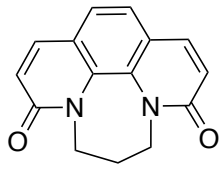

$[K_3Fe(CN)_6]$ (123.5 g, 375.0 mmol, 10.0 equiv) was dissolved in water (200.1 mL) and NaOH (56.4 g, 1.40 mol, 34 equiv) was added with stirring. The flask was placed in an ice/water bath. A solution of phenanthroline **4.1** (16.0 g, 41.9 mmol) in water (25.0 mL) was added dropwise, maintaining a temperature between 0–5 °C. The mixture was stirred for 2 h. It was then neutralised with HCl (4 M) to pH 7–8 with simultaneous cooling and concentrated under reduced pressure. The resulting brown solid was dissolved in CH_2Cl_2 then filtered through a silica plug (CH_2Cl_2) and purified by column chromatography (silica, CH_2Cl_2), yielding **4.2** as a yellow solid (4.00 g, 38%). As in lit.[19]

^{1}H NMR (400 MHz, $CDCl_3$): δ = 7.72 (d, ^{3}J = 9.6 Hz, 2H), 7.37 (s, 2H), 6.81 (d, ^{3}J = 9.2 Hz, 2H), 4.39 (s, 4H), 2.43-2.49 (m, 2H).

^{13}C NMR ($CDCl_3$, 100 MHz): 162.8, 139.0, 132.3, 123.3, 123.0, 122.9, 45.9, 25.9.

2,9-Dichloro-1,10-phenanthroline - **4.3**[18]

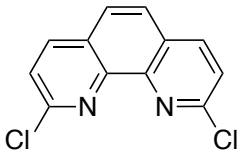

Compound **4.2** (500 mg, 1.98 mmol) was suspended in $POCl_3$ (6.00 mL) and PCl_5 (0.826 g, 3.96 mmol) was added in one portion. The mixture was degassed and heated to reflux (110 °C) under a nitrogen atmosphere for 8 h. The excess $POCl_3$ was quenched with ice. The resulting suspension was neutralised with aqueous NaOH (4 M) with cooling. The brown precipitate obtained was dried under vacuum, purified by column chromatography (silica, CH_2Cl_2), then recrystallized from methanol (300 mL) to afford **4.3** (400 mg, 85%) as a yellow solid. As in lit.[18]

^{1}H NMR ($CDCl_3$, 400 MHz): δ 8.22 (d, ^3J = 8.3 Hz, 2H), 7.83 (s, 2H), 7.65 (d, ^3J = 8.3 Hz, 2H).
^{13}C NMR ($CDCl_3$, 100 MHz): δ = 177.3, 159.3, 152.4, 139.8, 127.4, 127.1.

1,10-Dihydro-1,10-phenanthroline-2,9-dione - **4.4**[20]

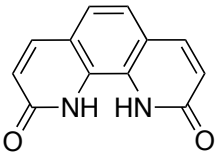

A mixture of **4.3** (375 mg, 1.46 mmol) and 64% H_2SO_4 (2 mL conc acid and 2 mL H_2O) was heated in an oil bath at 120 °C for 5 h. The mixture was cooled, allowed to stand for one hour and then neutralised with $NaHCO_3$, the solid was then collected by filtration, washed with water and dried to afford **4.4** as a white solid (270 mg, 84%). As in lit.[20]

^{1}H NMR (DMSO-d_6): δ = 11.70 (br, s), 8.00 (d, ^3J = 9.5 Hz, 2H), 7.47 (s, 2H), 6.65 (d, ^3J = 9.5 Hz, 2H).
^{13}C NMR (DMSO-d_6): δ = 161.8, 140.9, 126.2, 122.5, 121.3, 119.6.

3-(Triisopropylsilyl)propiolic acid - **4.5**[1]

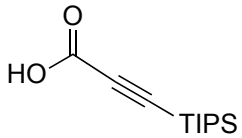

A solution of triisopropylsilylacetylene (3.00 mL, 2.43 g, 13.4 mmol) in THF (100 mL) was cooled under N_2 to 0 °C. A solution of MeLi (2.2 M in diethyl ether, 8.50 mL, 18.7 mmol) was added and the mixture was stirred for 1 h and then cooled to –78 °C and CO_2 gas was bubbled into the solution for 1 h. The reaction mixture was quenched by the slow addition of aqueous $KHSO_4$ (2 M, 30 mL), warmed to 20 °C, and extracted with EtOAc. The combined organic layers were washed with

brine, dried ($MgSO_4$) and concentrated to a yellow oil that was diluted with toluene (50 mL), passed through a silica plug and eluted with EtOAc (300 mL). The filtrate was concentrated to afford acid **4.5** (3.01 g, 99%) as a yellow oil that crystallised to a pale yellow solid *in vacuo*. As in lit.[1]

^{1}H NMR (400 MHz, $CDCl_3$) δ 10.92 (br, s, 1 H), 1.21-1.02 (m, 21 H)
^{13}C NMR (100 MHz, $CDCl_3$) δ 157.7, 96.1, 95.1, 18.6, 11.1.

1-(Triisopropylsilyl)-7-(trimethylsilyl)hepta-1,4,6-triyn-3-one - **4.6**[1]

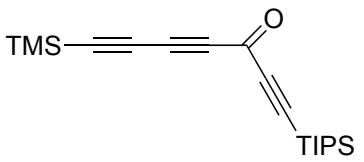

Acid **4.5** (3.00 g, 13.3 mmol) was dissolved in $SOCl_2$ (7.00 mL, 97.2 mmol) in a flask equipped with $CaCl_2$ drying tube and stirred at 20 °C for 20 h. The $SOCl_2$ was removed *in vacuo* and 1,4- bis(trimethylsilyl)butadiyne (2.69 g, 13.9 mmol) added and the resulting mixture was dissolved in dry CH_2Cl_2 (15 mL). To this solution was added slowly $AlCl_3$ (2.02 g, 15.1 mmol) at 0 °C under a N_2 atmosphere and then stirred at 0 °C for 4 h. The reaction was quenched with ice/HCl (10%) (100 mL) at 0 °C and allowed to warm to 20 °C. The aqueous layer was extracted with Et_2O (150 mL), washed with brine (2 × 50 mL) and dried over $MgSO_4$. The solvent was removed *in vacuo*, the crude product passed through a silica plug (hexane: CH_2Cl_2 1:1) and the solvent removed *in vacuo* to yield crude ketone **4.6** (2.50 g, 57%) as a brown oil which decomposed at room temperature over days. As in lit.[1]

^{1}H NMR (400 MHz, $CDCl_3$) δ 1.09 (s, 21H), 0.18 (s, 9H)
^{13}C NMR (100MHz, $CDCl_3$) δ 159.0, 104.6, 99.1, 98.8, 85.8, 75.4, 74.2, 18.5, 11.1, –0.8.

(5-(Dibromomethylene)-7-(triisopropylsilyl)hepta-1,3,6-triyn-1-yl)trimethylsilane - **4.7**[1]

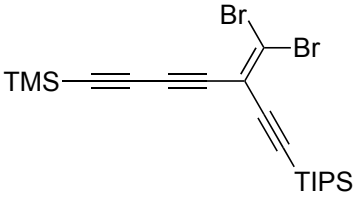

To a solution of CBr_4 (8.65 g, 26.1 mmol) in CH_2Cl_2 (200 mL) was added PPh_3 (13.2 g, 52.2 mmol) and the mixture stirred for 1 h under a N_2 atmosphere. Ketone **4.6** (2.00, 6.53 mmol) was dissolved in CH_2Cl_2 (50 mL), added dropwise, and the

mixture stirred at 20 °C for 2 h under a N_2 atmosphere. The reaction mixture was concentrated *in vacuo* to ca. 50 mL and then hexanes were added to precipitate the Ph_3PO as a white solid along with an oily residue. The supernatant was decanted and filtered through a pad of silica. The oily residue left in the flask was dissolved in minimal CH_2Cl_2 and hexanes were added; the heterogeneous mixture was then decanted and the supernatant filtered through silica (this procedure was repeated three times). The solvent was removed *in vacuo* and the crude product purified by column chromatography (silica, hexanes) to yield dibromoolefin **4.7** (3.90 g, 90%) as a yellow oil. As in lit.[1]

^{1}H NMR (400 MHz, $CDCl_3$) δ 1.09 (s, 21H), 0.21 (s, 9H);
^{13}C NMR (100MHz, $CDCl_3$) δ 113.6, 112.3, 101.0, 100.8, 94.9, 87.3, 80.1, 72.4, 18.6, 11.2, – 0.5

(3-(Dibromomethylene)hepta-1,4,6-triyn-1-yl)triisopropylsilane - **TIPS-D1**[1]

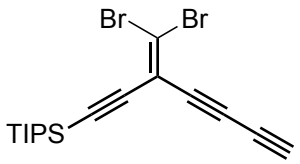

To a solution of **4.7** (132 mg, 0.272 mmol) in THF (5 mL)/MeOH (5 mL) was added K_2CO_3 (37.6 mg, 0.272 mmol). The reaction mixture was stirred at 20 °C for 30 min and passed through a silica plug (hexanes) yielding dibromoolefin **TIPS-D1** as a yellow oil (110 mg, 0.268 mmol, 98%). As in lit.[1]

^{1}H NMR (400 MHz, $CDCl_3$) δ 2.10 (s, 1H), 1.09 (s, 21H).

(m-Bis[(4-bromopropyl)oxy]benzene) **- S_3**[10]

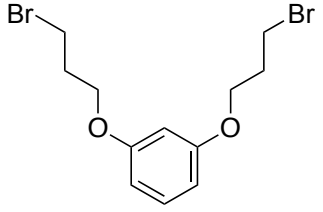

Resorcinol (6.00 g, 54.5 mmol), 1,3-dibromopropane (16.7 mL, 163 mmol) and K_2CO_3 (19.1 g, 138 mmol) were suspended in acetone (250 mL). The reaction mixture was heated for 72 h at 65 °C. The reaction mixture was cooled, water (100 mL) was added and the organic phase was extracted with EtOAc (3 × 150 mL). Organic fractions were combined and solvent was removed. The crude product was purified by column chromatography (silica, hexane/EtOAc 15:1) followed by recrystallisation from EtOAc affording the product **S_3** (4.80 g, 25%) as a white solid. As in lit.[10]

^{1}H NMR (400 MHz, $CDCl_3$): δ 7.18 (t, ^3J = 8.2 Hz, 1H), 6.54–6.47 (m, 3H), 4.09 (t, ^3J = 5.8 Hz, 4H), 3.60 (t, ^3J = 6.5 Hz, 4H), 2.36-2.30 (m, 4H).
^{13}C NMR (100 MHz, $CDCl_3$): δ 160.1, 130.1, 107.1, 101.7, 65.4, 32.5, 30.2.

(m-Bis[(4-bromobutyl)oxy]benzene) - **S_4 strap** [10]

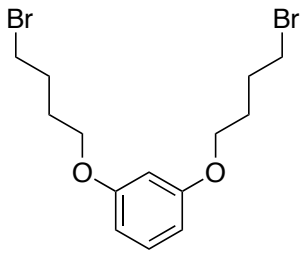

Resorcinol (800 mg, 7.27 mmol), 1,4-dibromobutane (5.19 mL, 43.6 mmol) and K_2CO_3 (5.02 g, 13.7 mmol) were suspended in acetone (200 mL). The reaction mixture was heated for 72 h at 65 °C and the solvent was removed. The crude was purified by column chromatography (Petroleum ether: CH_2Cl_2, 3:2) affording the product **S_4** (1.20 g, 50%) as a white solid. As in lit.[10]

^{1}H NMR (400 MHz, $CDCl_3$) δ 7.16 (t, ^3J = 8.2, 1H), 6.49 (dd, J = 2.4 Hz, J = 5.8 Hz, 2H), 6.44 (t, J = 2.4 Hz), 3.97 (t, ^3J = 6.1 Hz, 4H), 3.49 (t, ^3J = 6.6, 4H,), 2.10–2.02 (m, 4H), 1.97–1.90 (m, 4H).
^{13}C NMR (100 MHz, $CDCl_3$): δ 160.2, 130.0, 106.9, 101.6, 66.9, 33.6, 29.6, 28.0.

(m-Bis[(4-bromohexyl)oxy]benzene) **- S_6 strap** [10]

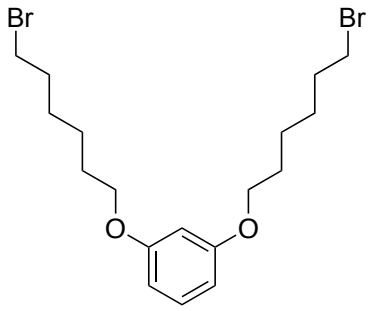

Resorcinol (845 mg, 7.45 mmol), 1,6-dibromohexane (7.15 mL, 44.7 mmol) and K_2CO_3 (5.20 g, 37.7 mmol) were dissolved in acetone (300 mL). The reaction mixture was heated for 72 h at 65 °C and the solvent removed. The crude was purified by column chromatography (hexanes/CH_2Cl_2 3:2) affording the product **S_6** (1.60 g, 49%) as a white solid. As in lit.[10]

^{1}H NMR (400 MHz, $CDCl_3$) δ 7.16 (t, ^3J = 8.1 Hz, 1H), 6.50-6.45 (m, 3H), 4.12 (t, ^3J = 6.5 Hz, 4H), 3.43 (t, ^3J = 6.4 Hz, 4H), 1.95-1.75 (m, 8H), 1.54-1.49 (m, 8H). As in lit.[10]
^{13}C NMR (100 MHz, $CDCl_3$) δ 25.21, 27.82, 28.99, 32.59, 33.68, 67.55, 101.32, 106.54, 129.68, 160.17.

(4,4-Dibromobut-3-en-1-yn-1-yl)triisopropylsilane - **4.8**[1]

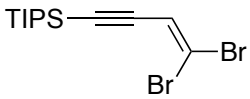

A solution of CBr_4 (12.6 g, 38.1 mmol) in CH_2Cl_2 (40 mL) was transferred with a canula to a solution of PPh_3 (19.9 g, 76.1 mmol) in CH_2Cl_2 (50 mL) and the resulting mixture stirred at 20 °C under a N_2 atmosphere for 1 h. A solution of aldehyde **2.1** (4.00 g, 19.03 mmol) in CH_2Cl_2 (100 mL) was added and the reaction stirred for 30 min. The mixture was concentrated to a minimum and hexanes were added to precipitate the Ph_3PO salt as a white solid along with an oily residue. The supernatant was decanted and passed through a silica plug. The oily residue left in the flask was dissolved in the minimum amount of CH_2Cl_2 and petroleum ether was added. The heterogeneous mixture was then decanted and the supernatant filtered through a silica plug (this procedure was repeated three times). The solvent was removed *in vacuo* and the product was passed through a silica plug (silica, hexanes) to yield dibromoolefin **4.8** as a yellow oil (3.90 g, 10.7 mmol, 56%). As in lit.[1]

^{1}H NMR (400 MHz, $CDCl_3$) δ 6.51 (s, 1H), 1.00 (s, 21H)
^{13}C NMR (100 MHz, $CDCl_3$) δ 120.2, 103.2, 102.7, 101.0, 18.8

Buta-1,3-diyn-1-yltriisopropylsilane - **4.9**[26]

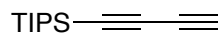

A solution of LDA was prepared *via* addition of *n*-BuLi (1.6 M, 11.2 mL, 17.9 mmol) to diisopropylamine (2.78 mL, 19.6 mmol) in THF (10 mL) at -78 °C, this was stirred for 5 min. Dibromoolefin **4.8** (1.98 g, 5.41 mmol) was added over 5 min at -78 °C. The reaction was stirred for 30 min at –78 °C and quenched at -78 °C with saturated NH_4Cl (aq) (15 mL). The mixture was extracted with hexanes (100 mL) and the layers separated. The organic phase was washed with H_2O (50 mL), brine (50 mL), and dried over $MgSO_4$. The solvent was removed *in vacuo* and the crude product was purified by column chromatography (silica, CH_2Cl_2/hexanes 1:10) to yield diyne **4.9** (1.13 g, 100% as a brown oil. As in lit.[26]

^{1}H NMR (400 MHz, $CDCl_3$) δ 2.07 (s, 1H), 1.09 (s, 21H)
^{13}C NMR (100 MHz, $CDCl_3$) δ 89.1, 82.1, 68.7, 65.6, 18.6, 11.3

5-(Triisopropylsilyl)penta-2,4-diynoic acid - **4.10**[27]

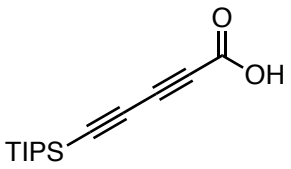

A solution of diyne **4.9** (1.30 g, 6.29 mmol) in THF (70 mL) was cooled under N_2 to 0 °C. A solution of MeLi (1.6 M in Et_2O, 5.50 mL, 8.80 mmol) was added and the mixture was stirred for 1 h and then cooled to –78 °C and CO_2 gas was bubbled into the solution for 1 h. The reaction mixture was quenched by the slow addition of (2.0 M) aqueous $KHSO_4$ (2.0 M, 30 mL), warmed to 20 °C, and extracted with EtOAc. The combined organic layers were washed with brine, dried over $MgSO_4$ and concentrated to a yellow oil that was diluted with toluene (50 mL), passed through silica plug and eluted with EtOAc (300 mL). The filtrate was concentrated to afford carboxylic acid **4.10** (1.37 g, 87%) as a brown oil. As in lit.[27]

^{1}H NMR (400 MHz $CDCl_3$) δ 8.59 (br, 1H), 1.06-1.00 (m, 21H)
^{13}C NMR (100 MHz, $CDCl_3$) δ 158.3, 109.1, 78.2, 67.0, 64.9, 17.9, 16.8.

TIPS-Dibromorotaxane **M2⊂(TIPS D1)$_2$**[10]

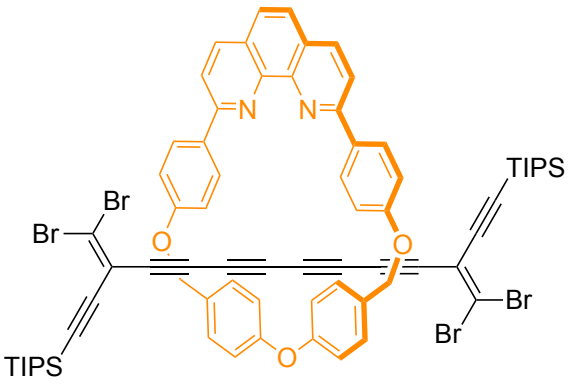

To a solution of macrocycle **M2** (55.1 mg, 98.7 μmol) in CH_2Cl_2 (4 mL) a solution of CuI (18.9 mg, 98.7 μmol) in acetonitrile (4 mL) was added and the mixture was stirred for 1 h at 20 °C. The solvents were removed *in vacuo* and the residue re-dissolved in THF (4 mL). To the solution of protected dibromoolefin **4.7** (120 mg, 0.247 mmol) in a 1:1 mixture of THF and methanol (20 mL) was added K_2CO_3 (34.0 mg, 0.247 mmol). The reaction mixture was stirred at 20 °C for 10 min. Solvents were reduced to approx. 5 mL and the mixture was passed through a silica plug (hexanes). The solvent volume was reduced to approx. 5 mL *in vacuo*, ~ 20 ml THF was added and solvent was reduced to approx. 5 mL This procedure was repeated 3 times. This mixture of deprotected **TIPS-D1** was added to a mixture of CuI·**M2** complex, K_2CO_3 (54.5 mg, 395 μmol) and I_2 (27.8 mg, 109 mmol) in THF (4 mL). The reaction mixture was flushed with nitrogen, and heated at 65 °C for 2 d. After cooling to 20 °C, the reaction was

quenched by the addition of KCN (25.0 mg, 384 mmol, in 2 mL H_2O), diluted with CH_2Cl_2 (4 mL) the organic phase separated, washed with H_2O and the solvents were removed. Column chromatography (silica, hexanes:EtOAc 20:1) afforded the rotaxane **M2⊂(TIPS D1)$_2$** as a dark yellow oil (30 mg, 22%). As in lit.[10]

^{1}H NMR (500 MHz, $CDCl_3$) δ 8.19 (d, ^3J = 8.3 Hz, 2H), 7.97 (d, 4H, ^3J = 8.7 Hz), 7.88 (d, ^3J = 8.4 Hz, 2H), 7.70 (s, 2H), 7.31 (d, ^3J = 9.1 Hz, 8H), 6.93 (d, ^3J = 8.7 Hz, 4H), 5.31 (s, 4H), 1.06–1.05 (m, 42H)

^{13}C NMR (125 MHz, $CDCl_3$) δ 159.4, 158.4, 157.8, 146.7, 136.3, 134.2, 134.0, 129.9, 127.4, 125.6, 122.4, 120.4, 116.3, 114.5, 113.2, 101.4, 100.6, 80.9, 73.9, 71.5, 70.5, 67.2, 65.6, 18.7, 11.2.

MALDI TOF MS $C_{72}H_{81}N_2O_3Si_2Br_4$ Calc ($[M+H]^+$) = 1385.15, Found *m/z* = 1385.71; $C_{72}H_{80}N_2O_3Si_2Br_3$ ($[M–Br]^-$) = 1305.23, Found *m/z* =1304.94; $C_{72}H_{81}N_2O_3Si_2Br_2$ Calc ([M+H–2Br] = 1225.31, found *m/z* = 1225.21

4.9 – Experimental data for novel compounds

(m-Bis[(4-bromopentyl)oxy]benzene) - **S$_5$**

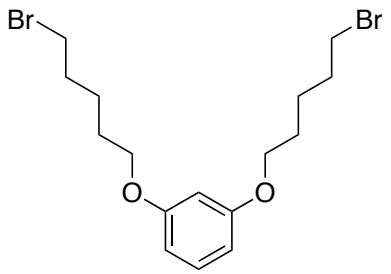

Resorcinol (800 mg, 7.27 mmol), 1,5-dibromopentane (5.91 mL, 43.6 mmol) and K_2CO_3 (5.02 g, 13.7 mmol) were suspended in acetone (200 mL). The reaction mixture was heated at 65 °C for 72 h and the solvent was removed. The crude was purified by column chromatography (silica, petroleum ether: CH_2Cl_2, 3:2) affording **S$_5$** (1.50 g, 44%) as a white solid.

^{1}H NMR (400 MHz, $CDCl_3$) δ 7.17 (t, ^3J = 8.2 Hz, 1H), 6.53 – 6.42 (m, 3H), 3.96 (t, ^3J = 6.3 Hz, 4H), 3.45 (t, ^3J = 6.8 Hz, 4H), 2.01 – 1.89 (m, 4H), 1.86 – 1.75 (m, 3H), 1.70 – 1.57 (m, 4H), 1.55 (s, 3H).

^{13}C NMR (100 MHz, $CDCl_3$) δ 160.4, 130.1, 106.9, 101.6, 67.8, 33.9, 32.7, 28.7, 25.1

EI HRMS: *m/z* 409.0191 (Calc. for $C_{16}H_{25}{}^{79}Br^{81}Br$ 409.0195), 407.0212 (Calc. for $C_{16}H_{25}{}^{79}Br_2$ 407.0215), 411.0169 (Calc. for $C_{16}H_{25}{}^{81}Br_2$ 411.0174),

Macrocycle **M3**

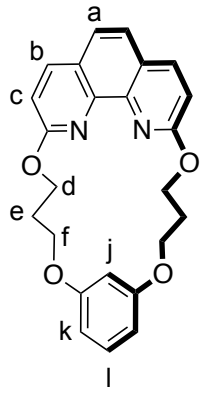

1,10-Dihydroxyphenanthroline (100 mg, 0.471 mmol) and **S$_3$** (165.9 mg, 0.471 mmol) were dissolved in DMF (100 mL) and added dropwise under N_2 to a suspension of Cs_2CO_3 (0.55 g, 2.35 mmol) in DMF (200 mL) over a 6 h at 60 °C, this was then heated for a further 12 h. The DMF was removed *in vacuo* and then the residue was dissolved in CH_2Cl_2/MeOH (150 mL) and washed with water (3x100 mL). The organic layer was then dried with $MgSO_4$ and purified *via* column chromatography (silica, CH_2Cl_2) yielding macrocycle **M3** as a white solid (44 mg, 0.109 mmol, 23%).

^{1}H NMR (400 MHz, $CDCl_3$): 8.07 (d, ^3J = 8.4 Hz, 2H, H_b), 7.61 (s, 2H, H_a), 7.15 (t, ^3J = 8.4 Hz, 1H, H_l), 7.07 (d, ^3J = 8.4 Hz, 2H, H_c), 6.79 (t, ^4J = 2.1 Hz, 1H, H_j) 6.53 (dd, J = 8.4 Hz, 2.1 Hz, 2H, H_k), 4.84 (t, ^3J = 6.8 Hz, 4H, H_d), 4.38 (t, ^3J = 6.8 Hz, 4H, H_f), 2.38 (m, 4H, H_e).
^{13}C NMR (100 MHz, $CDCl_3$): 162.7, 160.7, 143.4, 139.4, 125.6, 123.8, 113.8, 108.8, 102.7, 66.3, 64.2, 30.3.
HRMS ESI: $C_{24}H_{22}O_4N_2$ $[M]^+$ Calc – 403.164, Found *m/z* – 403.164

Macrocycle **M4**

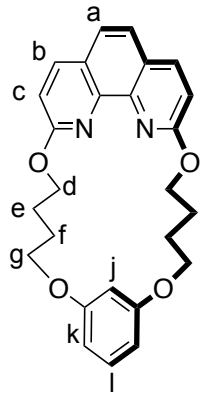

1,10-Dihydroxyphenanthroline (200 mg, 0.942 mmol) and **S$_4$** (358 mg, 0.942 mmol) were dissolved in DMF (100 mL) and added dropwise under N_2 to a solution of Cs_2CO_3 (1.84 g, 5.65 mmol) in DMF (300 mL) over 6 h at 60 °C, this was then heated for a further 12 h. The DMF was removed *in vacuo* and then the residue was dissolved in CH_2Cl_2/MeOH (150 mL) and washed with water (3 × 100 mL). The organic layer was then dried with $MgSO_4$ and purified *via* column chromatography (silica, CH_2Cl_2) yielding macrocycle **M4** as a white solid (124 mg, 0.282 mmol, 30%).

^{1}H NMR (400 MHz, $CDCl_3$): 8.08 (d, ^3J = 9.0 Hz, 2H, H_b), 7.61 (s, 2H, H_a), 7.14 (t, ^3J = 8.4 Hz, 1H, H_l), 7.07 (d, ^3J = 8.9 Hz, 2H, H_c), 6.61 (t, ^4J = 2.1 Hz, 1H, H_j) 6.51

(dd, ^3J = 8.4 Hz, 2.2 Hz, 2H, H_k), 4.79 (t, ^3J = 6.4 Hz, 4H, H_d), 4.16 (t, ^3J = 6.5 Hz, 4H, H_g), 2.13-1.98 (m, 8H, $H_{e,f}$).

^{13}C NMR (100 MHz, $CDCl_3$): 162.7, 160.3, 143.3, 139.3, 125.5, 123.6, 113.7, 109.3, 100.7, 67.8, 65.2, 25.7, 25.5.

HRMS ESI: $C_{26}H_{27}O_4N_2$ $[M+H]^+$ Calc – 431.196, Found *m/z* – 431.196

Macrocycle **M5**

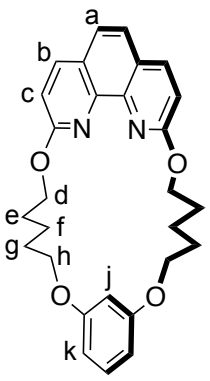

1,10-Dihydroxyphenanthroline (447 mg, 2.11 mmol) and **S$_5$** (878 mg, 2.11 mmol) were dissolved in DMF (100 mL) and added dropwise under N_2 to a solution of Cs_2CO_3 (4.12 g, 12.6 mmol) in DMF (300 mL) over 6 h at 60 °C, this was then heated for a further 12 h. The DMF was removed *in vacuo* and then the residue was dissolved in CH_2Cl_2/MeOH (150 mL) and washed with water (3 × 100 mL). The organic layer was then dried with $MgSO_4$ and purified *via* column chromatography (silica, CH_2Cl_2) yielding macrocycle **M5** as a white solid (295 mg, 0.633 mmol, 30%)

^{1}H NMR (400 MHz, $CDCl_3$) δ 8.09 (d, ^3J = 8.7 Hz, 2H, H_b), 7.61 (s, 2H, H_a), 7.16 (t, J = 7.9, 0.7 Hz, 1H, H_l), 7.07 (d, ^3J = 8.7 Hz, 2H, H_c), 6.55 – 6.44 (m, 3H, $H_{j,k}$), 4.71 (t, ^3J = 7.2 Hz, 4H, H_d), 4.14 (t, ^3J = 6.1 Hz, 4H, H_h), 2.09 – 1.78 (m, 8H, $H_{e,g}$), 1.80 – 1.66 (m, 4H, H_f)

^{13}C NMR (100 MHz, $CDCl_3$): 162.8, 160.4, 143.3, 139.2, 125.3, 123.5, 113.6, 107.9, 102.5, 68.3, 65.9, 28.8, 28.6, 22.9

HRMS ESI: $C_{28}H_{31}O_4N_2$ $[M+H]^+$ Calc – 459.227, Found *m/z* – 459.227

Macrocycle **M6**

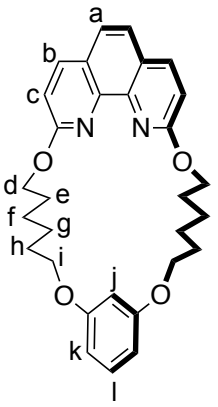

1,10-Dihydroxyphenanthroline (100 mg, 0.471 mmol) and **S$_6$** (205 mg, 0.471 mmol) were dissolved in DMF (100 mL) and added dropwise under N_2 to a solution of Cs_2CO_3 (0.55 g, 2.35 mmol) in DMF (200 mL) over 6 h at 60 °C, this was then heated for a further 12 h. The DMF was removed *in vacuo* and then the residue was dissolved in CH_2Cl_2/MeOH (150 mL) and

washed with water (3 × 100 mL). The organic layer was then dried with $MgSO_4$ and purified *via* column chromatography (silica, CH_2Cl_2) yielding macrocycle **M6** as a white solid (95 mg, 0.195 mmol, 42%).

^{1}H NMR (400 MHz, $CDCl_3$): 8.07 (d, ^3J = 8.4 Hz, 2H, H_b), 7.59 (s, 2H, H_a), 7.13 (t, ^3J = 8.4 Hz, 1H, H_l), 7.04 (d, ^3J = 8.4 Hz, 2H, H_c), 6.46 (m, 3H, $H_{j,k}$), 4.68 (t, ^3J = 6.8 Hz, 4H, H_d), 4.04 (t, ^3J = 6.8 Hz, 4H, H_i), 1.93 (m, 4H, H_e), 1.83 (m, 4H, H_h), 1.54 (m, 8H, $H_{f,g}$)
^{13}C NMR (100 MHz, $CDCl_3$): 161.6, 159.1, 142.0, 138.0, 128.9, 124.1, 122.3, 112.4, 107.0, 99.9, 66.9, 64.7, 28.1, 27.3, 24.7, 24.2.
HRMS ESI: $C_{30}H_{35}O_4N_2$ $[M+H]^+$ Calc – 487.259, Found *m/z* – 487.259

TIPS-dibromorotaxane **M6⊂(TIPS-D1)$_2$**

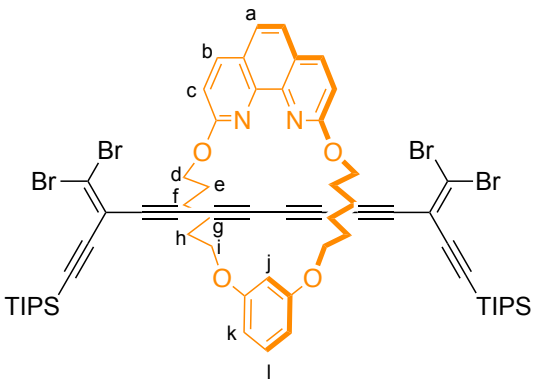

To a solution of macrocycle **M6** (17 mg, 34.9 µmol) in CH_2Cl_2 (4 mL) a solution of CuI (6.65 mg, 34.9 µmol) in acetonitrile (4 mL) was added and the mixture was stirred for 1 h at 20 °C. The solvents were removed *in vacuo* and the residue re-dissolved in THF (4 mL). To a solution of protected dibromoolefin **4.7** (42.3 mg, 87.2 µmol) in a 1:1 mixture of THF and methanol (20 mL) was added K_2CO_3 (12 mg, 34.9 µmol). The reaction mixture was stirred at 20 °C for 10 min, then the reaction was quenched by addition of saturated NH_4Cl (aq) (50 mL), the organic phase was extracted by Et_2O (3 × 50 mL), organic phases were combined, washed with brine (50 mL) and dried over $MgSO_4$. Solvents were removed to the minimum and the mixture was passed through silica plug (hexanes). The solvent volume was reduced to approx. 5 mL, THF (20 mL) was added and solvent was reduced to approx. 5 mL. This procedure was repeated 3 times. In the end this mixture was added to a mixture of CuI·**M6** complex, K_2CO_3 (48 mg, 139 µmol) and I_2 (10.8 mg, 38.9 µmol) in THF (4 mL). The reaction mixture was flushed with nitrogen, and stirred in a Schlenk tube at 65 °C for 2 d. After cooling to 20 °C, the reaction was quenched by the addition of KCN (10 mg, 34.9 µmol, in 2 mL H_2O), diluted with CH_2Cl_2 (4 mL)

the organic phase separated, washed with H_2O and the solvents were removed. Column chromatography (silica, hexanes:EtOAc 20:1) afforded the rotaxane **M6⊂(TIPS-D1)$_2$** as a dark yellow oil (15 mg, 30%).

^{1}H NMR (500 MHz, $CDCl_3$) δ 7.98 (d, ^3J = 8.7 Hz, 2H, H_b), 7.45 (s, 2H, H_a), 7.08 (t, ^3J = 8.2 Hz, 1H, H_l), 7.02 (d, ^3J = 8.7 Hz, 2H, H_c) 6.66 (t, ^4J = 2.6 Hz, 1H, H_k), 6.45 (dd, J = 8.2, 2.5 Hz, 2H, H_k), 4.75 (t, J = 7.0 Hz, 4H, H_d), 4.05 (t, J = 6.3 Hz, 4H, H_i), 1.94 – 1.87 (m, 8H, $H_{e,h}$), 1.65-1.63 (m, 8H, $H_{f,g}$), 1.05 (s, 42H, H_{TIPS}).
^{13}C NMR (100 MHz, $CDCl_3$) δ 163.1, 160.6, 144.0, 139.0, 129.8, 125.5, 123.6, 115.1, 113.6, 113.0, 108.0, 102.0, 100.4, 80.3, 74.8, 71.7, 68.2, 66.4, 66.3, 29.8, 28.0, 26.3, 25.7, 18.9, 11.3.
MALDI TOF MS: $C_{64}H_{67}N_2O_4Si_2Br_4$ Calc ($[M+H]^+$) = 1313.20, Found *m/z* = 1313.33; $C_{64}H_{67}N_2O_4Si_2Br_3$ ([M–Br+H]) = 1234.20, Found *m/z* =1234.39

TIPS-dibromorotaxane **M5⊂(TIPS D1)$_2$**

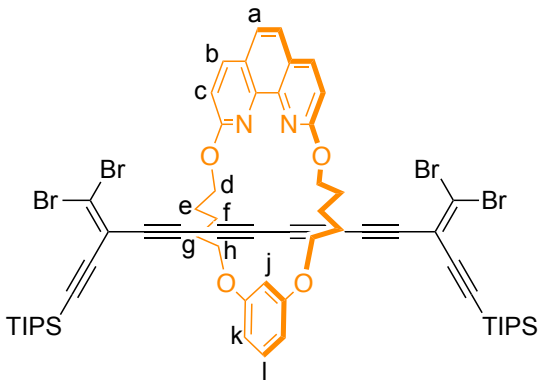

To a solution of macrocycle **M5** (20 mg, 43.1 µmol) in CH_2Cl_2 (4 mL) a solution of CuI (8.22 mg, 43.1 µmol) in acetonitrile (4 mL) was added and the mixture was stirred for 1 h at 20 °C. The solvents were removed *in vacuo* and the residue re-dissolved in THF (4 mL). To a solution of protected dibromoolefin **4.7** (120 mg, 246 µmol) in a 1:1 mixture of THF and methanol (20 mL) was added K_2CO_3 (40 mg, 246 µmol). The reaction mixture was stirred at 20 °C for 10 min, then the reaction was quenched by addition of saturated NH_4Cl (aq) (50 mL), the organic phase was extracted by Et_2O (3 × 50 mL), organic phases were combined, washed with brine (50 mL) and dried over $MgSO_4$. Solvents were reduced to approx. 5 mL and the mixture was passed through silica plug (hexanes). The solvent volume was reduced to approx. 5 mL *in vacuo*, THF (20 mL) was added and solvent was reduced to approx. 5 mL: This procedure was repeated 3 times. This mixture was added to a mixture of CuI·**M5** complex, K_2CO_3 (30 mg, 217 µmol) and I_2 (15 mg, 58 µmol) in THF (4 mL). The reaction mixture was flushed with nitrogen, and stirred in a Schlenk

tube at 65 °C for 2 d. After cooling to 20 °C, the reaction was quenched by the addition of KCN (10 mg, 34.9 µmol, in 2 mL H_2O), diluted with CH_2Cl_2 (4 mL) the organic phase separated, washed with H_2O and the solvents were removed. Column chromatography (silica, hexanes:EtOAc 20:1) afforded the rotaxane **M5⊂(TIPS D1)$_2$** as a dark yellow oil (25 mg, 33%).

^{1}H NMR (400 MHz, $CDCl_3$) δ 8.06 (d, ^3J = 8.7 Hz, 2H, H_c), 7.53 (s, 2H, H_a), 7.11 (t, ^3J = 8.2 Hz, 1H, H_l) 7.03 (d, ^3J = 8.4 Hz, 2H, H_a), 6.78 (t, ^4J = 2.5 Hz, 1H, H_j), 6.46 (dd, J = 8.2, 2.4 Hz, 2H, H_k), 4.60 (t, ^3J = 7.0 Hz, 4H, H_d), 4.12 (t, ^3J = 6.2 Hz, 4H, H_h), 2.01 – 1.83 (m, 12H, $H_{e,f,g}$), 1.03 (s, 42H, H_{TIPS}).
^{13}C NMR (125 MHz, $CDCl_3$) δ 162.9, 160.3, 144.7, 139.0, 129.9, 125.3, 123.4, 114.0, 113.5, 111.5, 107.0, 104.0, 101.3, 100.7, 81.6, 73.8, 73.6, 68.2, 67.2, 66.6, 29.8, 29.7, 23.1, 18.8, 11.3.
MALDI TOF MS: $C_{62}H_{73}N_2O_4Si_2Br_4$ Calc ($[M+H]^+$) = 1286.20, Found *m/z* = 1286.29; $C_{62}H_{73}N_2O_4Si_2Br_3$ ([M–Br+H]) = 1207.20, Found *m/z* =1207.33

Deprotected rotaxane **M5⊂(D1)$_2$**

Dibromorotaxane **9** (20 mg, 15.5 umol) was dissolved in CH_2Cl_2 (10 mL). TBAF (1.0 M, 31 µL) was added. The reaction was stirred for 5 minutes. The reaction mixture was passed through a silica plug (CH_2Cl_2:EtOAc 1:1). This yielded deprotected dibromorotaxane **M5⊂(D1)$_2$** as a yellow solid (15 mg, 90%).

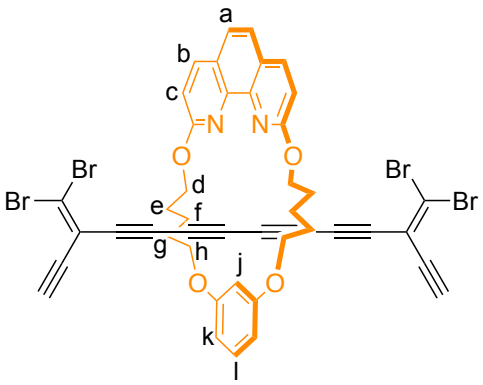

^{1}H NMR (400 MHz, $CDCl_3$) δ 8.07 (d, ^3J = 8.7 Hz, 2H, H_c), 7.53 (s, 2H, H_a), 7.12 (t, ^3J = 8.3 Hz, 2H, H_j), 7.04 (d, J = 8.5 Hz, 2H, H_a), 6.77 (t, ^4J = 2.3 Hz, 1H, H_l), 6.44 (dd, J = 8.2, 2.4 Hz, 2H, H_k), 4.59 (t, J = 6.9 Hz, 4H, H_d), 4.11 (t, J = 6.3 Hz, 4H, H_h), 3.24 (s, 2H, $H_{terminal}$), 1.99 – 1.69 (m, 12H, $H_{e,f,g}$).
^{13}C NMR (125 MHz, $CDCl_3$) δ 162.8, 160.3, 144.7, 138.9, 129.8, 125.2, 123.3, 114.7, 112.4, 111.2, 106.7, 103.5, 84.9, 82.3, 73.5, 72.9, 68.0, 67.1, 66.5, 29.9, 29.7, 23.1.

MALDI TOF MS: $C_{44}H_{32}N_2O_4Br_4$ Calc ($[M]^+$) = 971.91, Found *m/z* = 972.09; $C_{48}H_{33}N_2O_4Br_4$ ($[M\text{-}Br]^-$) = 892.90, Found *m/z* = 892.02.

Monodeprotected rotaxane **M5⊂(TIPS D1)(D1)**

Dibromorotaxane **M5⊂(TIPS D1)$_2$** (20 mg, 15.5 µmol) was dissolved in CH_2Cl_2 (10 mL). TBAF (1.0 M, 15 µL) was added. The reaction was stirred at 20 °C for 5 min. The reaction mixture was purified by column chromatography (silica, PE:EtOAc 1:1). This yielded monodeprotected dibromorotaxane **M5⊂(TIPS D1)(D1)** as a yellow solid (8 mg, 35%).

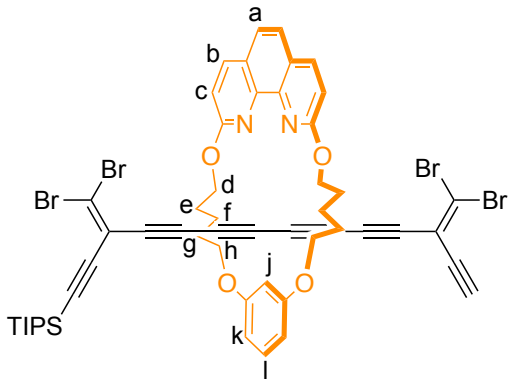

^{1}H NMR (400 MHz, $CDCl_3$) δ 8.06 (d, ^3J = 8.7 Hz, 2H, H_c), 7.52 (s, 2H, H_a), 7.10 (t, ^3J = 8.3 Hz, 2H, H_l), 7.04 (d, J = 8.5 Hz, 2H, H_a), 6.77 (t, ^4J = 2.3 Hz, 1H, H_j), 6.37 (dd, J = 8.2, 2.4 Hz, 2H, H_k), 4.52 (t, J = 6.9 Hz, 4H, H_d), 4.04 (t, J = 6.3 Hz, 4H, H_h), 3.17 (s, 1H, $H_{terminal}$), 1.99 – 1.69 (m, 12H), 1.05 (s, 21H, H_{TIPS}).

^{13}C NMR (125 MHz, $CDCl_3$) δ 162.8, 160.3, 144.7, 138.9, 129.8, 128.9, 128.8, 125.2, 123.3, 114.7, 114.5, 114.0, 113.4, 112.4, 111.3, 106.8, 103.7, 101.3, 100.6, 84.8, 82.4, 81.4, 78.4, 73.9, 73.4, 73.1, 72.8, 68.3, 68.1, 67.1, 66.5, 66.5, 29.9, 29.7, 29.6, 29.1, 23.1, 18.7, 11.2.

MALDI TOF MS: $C_{53}H_{53}N_2O_4SiBr_4$ Calc ($[M+H]^+$) = 1129.04, Found *m/z* = 1129.21; $C_{53}H_{53}N_2O_4SiBr_3$ ([M–Br+H]) = 1048.13, Found *m/z* =1048.34

1-(Triisopropylsilyl)-9-(trimethylsilyl)nona-1,3,6,8-tetrayn-5-one - **4.11**

Acid **4.10** (1.37 g, 5.47 mmol) was dissolved in $SOCl_2$ (2.5mL, 34.7 mmol) in a flask equipped with a $CaCl_2$ drying tube and stirred at 20 °C for 20 h. The $SOCl_2$ was removed *in vacuo*, 1,4-bis(trimethylsilyl)butadiyne (1.12 g, 5.74 mmol) added and the resulting mixture dissolved in dry CH_2Cl_2 (15 mL). To this solution was added slowly $AlCl_3$ (0.88 g,

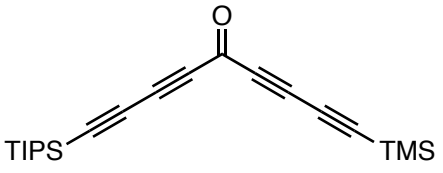

6.54 mmol) at 0 °C under a N_2 atmosphere and then stirred at 0 °C for 4 h. The reaction was quenched with ice/HCl (10%) (100 mL) at 0 °C and allowed to warm to 20 °C. The organic layer was extracted with Et_2O (150 mL), washed with brine (2 × 50 mL) and dried over $MgSO_4$. The solvent was removed *in vacuo*, the crude product passed through a silica plug (hexane: CH_2Cl_2 1:1) and the solvent removed *in vacuo* to yield crude ketone **4.11** (1.12 g, 58%) as a brown oil which decomposed slowly.

^{1}H NMR (400 MHz $CDCl_3$) 1.13-1.00 (m, 21H), 0.18 (s, 9H)
^{13}C NMR (100 MHz, $CDCl_3$) δ 159.1, 101.0, 99.3, 88.2, 86.4, 78.1, 73.7, 19.4, 19.3, 19.3, 12.0, 0.0.
EI HRMS: *m*/*z* 354.1839 (Calc. for $C_{21}H_{30}OSi_2$ 354.1840) $[M\text{-}H^+]^=$

(5-(Dibromomethylene)-9-(triisopropylsilyl)nona-1,3,6,8-tetrayn-1-yl)trimethylsilane - **4.12**

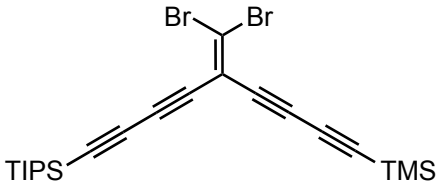

To a solution of CBr_4 (2.09 g, 6.32 mmol) in CH_2Cl_2 (40 mL) was added PPh_3 (3.31 g, 12.64 mmol) and the mixture stirred for 1 h under a N_2 atmosphere. Ketone **4.11** (1.12g, 3.16 mmol) was dissolved in CH_2Cl_2 (50 mL), added dropwise, and the mixture stirred at 20 °C for 2 h under a N_2 atmosphere. The reaction mixture was concentrated *in vacuo* to ca. 50 mL and then hexanes were added to precipitate the Ph_3PO as a white solid along with an oily residue. The supernatant was decanted and filtered through a silica plug (hexanes). The oily residue left in the flask was dissolved in minimal CH_2Cl_2 and hexanes were added; the heterogeneous mixture was then decanted and the supernatant filtered through a silica plug (this procedure was repeated three times). The solvent was removed *in vacuo* and the crude product purified by column chromatography (silica, hexanes) to yield dibromolefin **4.12** (740 mg, 46 %) as a brown oil.

^{1}H NMR (400 MHz $CDCl_3$) 1.13-1.00 (m, 21H), 0.18 (s, 9H)
^{13}C NMR (100 MHz, $CDCl_3$) 114.3, 112.7, 96.0, 93.6, 88.9, 87.1, 71.8, 70.6, 18.8, 11.4, 0.0.

EI HRMS: *m/z* 510.021 (Calc. for $C_{22}H_{30}{}^{79}Br^{81}BrSi_2$ 510.021) $[M\text{-}H^+]^=$ 508.023 (Calc. for $C_{22}H_{30}{}^{79}Br_2Si_2$ 508.023) $[M\text{-}H^+]^=$ 512.019 (Calc. for $C_{22}H_{30}{}^{81}Br_2Si_2$ 512.019) $[M\text{-}H^+]$

Extended rotaxane **M5⊂(TIPS D2)$_2$**

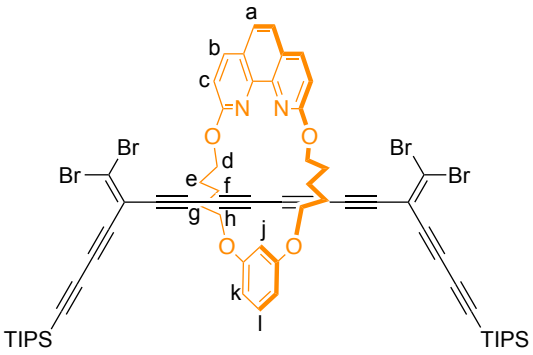

To a solution of macrocycle **M5** (20 mg, 43.1 µmol) in CH_2Cl_2 (4 mL) a solution of CuI (8.22 mg, 43.1 µmol) in acetonitrile (4 mL) was added and the mixture was stirred for 1 h at 20 °C. The solvents were removed *in vacuo* and the residue re-dissolved in THF (4 mL). To the solution of dibromolefin **4.12** (56 mg, 110 µmol) in a 1:1 mixture of THF and methanol (20 mL) was added K_2CO_3 (2.4 mg, 17.4 µmol). The reaction mixture was stirred at 20 °C for 10 min, then the reaction was quenched by addition of saturated NH_4Cl (50 mL), the organic phase was extracted by Et_2O (3 × 50 mL), organic phases were combined, washed with brine (50 mL) and dried over $MgSO_4$. Solvents were reduced to approx. 5 mL and the mixture was passed through silica plug (hexanes). The solvent volume was reduced to approx. 5 mL *in vacuo*, ~ 20 ml THF was added and solvent was reduced to approx. 5 mL: This procedure was repeated 3 times. In the end this mixture was added to a mixture of CuI·**M5** complex, K_2CO_3 (29 mg, 220 µmol) and I_2 (12.4 mg, 48 µmol) in THF (4 mL). The reaction mixture was flushed with nitrogen, and stirred in a Schlenk tube at 65 °C for 2 d. After cooling to 20 °C, the reaction was quenched by the addition of KCN (10 mg, 34.9 µmol, in 2 mL H_2O), diluted with CH_2Cl_2 (4 mL) the organic phase separated, washed with H_2O and the solvents were removed. Column chromatography (silica, hexanes:EtOAc 20:1) afforded the rotaxane **M5⊂(TIPS D2)$_2$** as a dark yellow oil (17 mg, 25%).

^{1}H NMR (400 MHz, $CDCl_3$) δ 8.05 (d, ^3J = 9.1 Hz, 2H, H_c), 7.52 (s, 2H, H_a), 7.10 (t, ^3J = 8.2 Hz, 1H, H_l) 7.03 (d, ^3J = 9.1 Hz, 2H, H_b), 6.79 (t, ^4J = 2.5 Hz, 1H, H_j), 6.45 (dd, J = 7.9, 2.5 Hz, 2H, H_k), 4.60 (t, ^3J = 7.0 Hz, 4H, H_d), 4.11 (t, ^3J = 6.4 Hz, 4H, H_h), 1.99 – 1.79 (m, 12H), 1.03 (s, 42H).

MALDI TOF MS: $C_{66}H_{73}N_2O_4Si_2Br_4$ Calc ($[M+H]^+$) = 1333.17, Found *m/z* = 1334.44; $C_{66}H_{73}N_2O_4Si_2Br_3$ ([M–Br+H]) = 1254.17, Found *m/z* =1254.39; $C_{66}H_{73}N_2O_4Si_2Br_2$ Calc ([M–2Br] = 1174.17, found *m/z* = 1174.35

Deprotected rotaxane **M5⊂(D2)$_2$**

Dibromorotaxane **M5⊂(TIPS-D2)$_2$** (17 mg, 15.5 µmol) was dissolved in CH_2Cl_2 (10 mL). TBAF (1M, 31.1 µL) was added. The reaction was stirred at 20 °C for 5 min. The reaction mixture was passed through a silica plug (CH_2Cl_2:EtOAc 1:1). This yielded deprotected dibromorotaxane **M5⊂(D2)$_2$** as a yellow solid (13 mg, 90%).

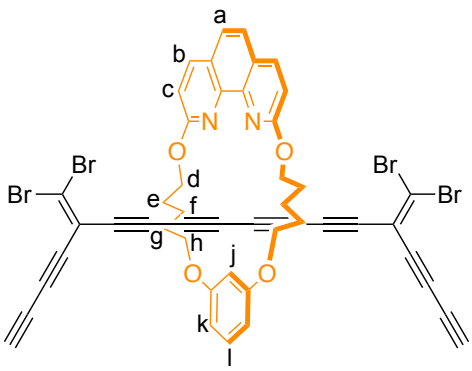

^{1}H NMR (400 MHz, $CDCl_3$) δ 8.07 (d, ^3J = 8.1 Hz, 2H, H_c), 7.54 (s, 2H, H_a), 7.11 (t, ^3J = 7.2 Hz, 1H, H_l) 7.03 (d, ^3J = 8.1 Hz, 2H, H_b), 6.77 (t, ^4J = 2.5 Hz, 1H, H_j), 6.44 (dd, *J* = 7.9, 2.5 Hz, 2H, H_k), 4.60 (t, ^3J = 7.0 Hz, 4H, H_d), 4.12 (t, ^3J = 6.4 Hz, 4H, H_h), 2.60 (s, 2H), 1.99 – 1.79 (m, 12H).
MALDI TOF MS: $C_{48}H_{33}N_2O_4Br_4$ Calc ($[M+H]^+$) = 1020.90, Found *m/z* = 1022.36; $C_{48}H_{33}N_2O_4Br_4$ ([M–Br+H]) = 941.90, Found *m/z* = 942.26.

1-Bromo-3,5-bis((5-bromopentyl)oxy)benzene – **S$_{5\text{-Br}}$**

3-Bromoresorcinol (350 mg, 1.86 mmol), 1,5-dibromopentane (1.48 mL, 11.1 mmol) and K_2CO_3 (1.07 g, 7.80 mmol) were suspended in acetone (120 mL). The reaction mixture was heated at 65 °C for 72 h and the solvent was removed. The crude was purified by column chromatography (Pet ether: CH_2Cl_2, 3:2) affording the product **S$_{5\text{-Br}}$** (450 mg, 50%) as a white solid.

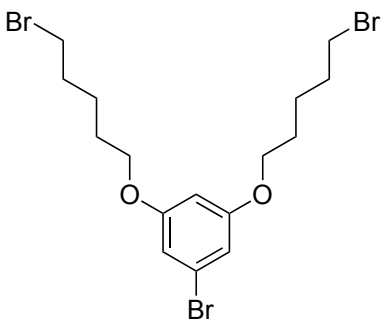

^{1}H NMR (400 MHz, $CDCl_3$) δ 6.64 (d, ^3J = 2.6 Hz, 2H), 6.36 (t, ^3J = 82.6 Hz, 1H), 3.93 (t, ^3J = 6.3 Hz, 4H), 3.45 (t, ^3J = 6.8 Hz, 4H), 1.97 – 1.93 (m, 4H), 1.82 – 1.77 (m, 4H), 1.66 – 1.59 (m, 4H).

^{13}C NMR (100 MHz, $CDCl_3$) δ 160.8, 123.1, 110.5, 100.8, 68.1, 33.8, 32.2, 28.5, 25.0.

EI HRMS: *m/z* 486.9294 (Calc. for $C_{16}H_{24}{}^{79}Br_2{}^{81}Br$ 486.9300), 488.9272 (Calc. for $C_{16}H_{24}{}^{79}Br^{81}Br_2$ 488.92722).

Macrocycle **M5$_{Br}$**

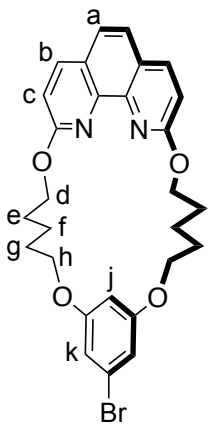

1,10-Dihydroxyphenanthroline **4.4** (196 mg, 0.923 mmol) and strap **S$_{5\text{-}Br}$** (450 mg, 0.923 mmol) were dissolved in DMF (100 mL) and added dropwise under N_2 to a suspension of Cs_2CO_3 (1.81 g, 5.54 mmol) in DMF (300 mL) over 6 h at 60 °C, this was then heated for a further 12 h. The DMF was removed *in vacuo* and then the residue was dissolved in CH_2Cl_2/MeOH (150 mL) and washed with water (3x100 mL). The organic layer was then dried with $MgSO_4$ and purified via column chromatography (CH_2Cl_2) yielding macrocycle **M5$_{Br}$** as a white solid (110 mg, 0.205 mmol, 22%)

^{1}H NMR (400 MHz, $CDCl_3$) δ 8.09 (d, ^3J = 8.7 Hz, 2H, H_c), 7.61 (s, 2H, H_a), 7.06 (d, ^3J = 8.7 Hz, 2H, H_b), 6.64 (d, ^4J = 1.9 Hz, 2H, H_k), 6.41 (t, ^4J = 2.3 Hz, 2H, H_j), 4.68 (t, J = 7.2 Hz, 4H, H_d), 4.10 (t, J = 6.1 Hz, 4H, H_h), 2.02 – 1.94 (m, 4H, H_e), 1.89 – 1.83 (m, 4H, H_g), 1.73- 1.66 (m, 4H, H_f).

^{13}C NMR (100 MHz, $CDCl_3$) δ = 162.9, 160.9, 143.6, 139.4, 125.4, 123.7, 113.6, 111.5, 101.9, 68.8, 66.0, 28.9, 28.6, 22.9.

HRMS ESI: $C_{28}H_{30}O_4N_2Br^{79}[M]^+$ Calc – 537.138, Found *m/z* – 537.138 $C_{28}H_{30}O_4N_2Br^{81}[M]^+$ Calc – 539.136, Found *m/z* – 539.136.

Macrocycle **M5$_{BPin}$**

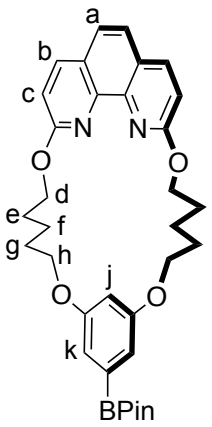

Macrocycle **M5$_{Br}$** (80 mg, 148.0 µmol), B_2Pin_2 (41.3 mg, 160 µmol), $PdCl_2$(dppf) (18.2 mg, 22.3 µmol, 0.15 equiv.), KOAc (43.6 mg, 440 µmol) and dppf (12.3 mg, 22.3 µmol) were loaded into a schlenk tube and dried *in vacuo* for 10 min. DMF (12 mL) was added. The mixture was pump-purge degassed three times and then heated to 80 °C for 18 h. The reaction mixture was added to CH_2Cl_2 (30 mL), washed with water (3 × 10mL) and dried over $MgSO_4$. The organic layer was evaporated, and the crude product was purified by column chromatography (silica, $CHCl_3$:methanol 100:1) to yield the crude macrocycle **M5$_{BPin}$** as a colourless oil (85 mg, 98%).

^{1}H NMR (400 MHz, $CDCl_3$) δ 8.09 (d, ^3J = 8.7 Hz, 2H, H_c), 7.61 (s, 2H, H_a), 7.06 (d, ^3J = 8.7 Hz, 2H, H_b), 6.64 (d, ^4J = 1.9 Hz, 2H, H_k), 6.41 (t, ^4J = 2.3 Hz, 1H, H_j), 4.68 (t, ^3J = 7.2 Hz, 4H, H_d), 4.10 (t, ^3J = 6.1 Hz, 4H, H_h), 2.02 – 1.94 (m, 4H, H_e), 1.89 – 1.83 (m, 4H, H_g), 1.73- 1.66 (m, 4H, H_f), 1.51 (s, 18H, H_{BPin}).

Bis macrocycle (**M5)$_2$**

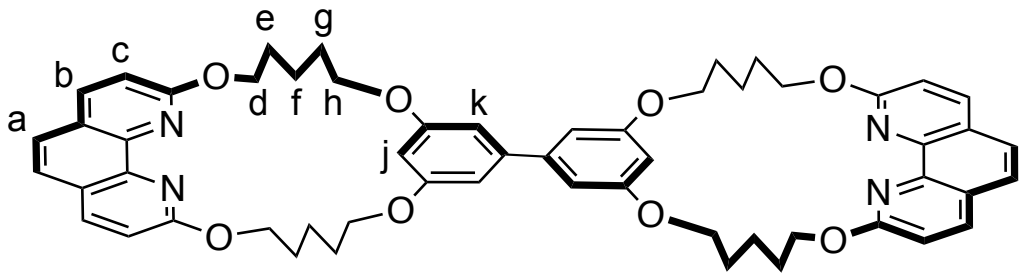

Macrocycle **M5$_{Br}$** (60.1 mg, 111 µmol), macrocycle **M5$_{BPin}$** (85 mg, 145 µmol), $PdCl_2$(dppf) (4.53 mg, 5.55 µmol, 0.05 equiv.) and Na_2CO_3 (23.5 mg, 222 µmol) were loaded into a Schlenk tube and dried *in vacuo* for 10 minutes. THF/H_2O 2:1 (9 mL) was added. The mixture was pump-purge degassed three times and then heated to 80 °C for 18 h. The reaction mixture was added to CH_2Cl_2 (30 mL), washed with water (3 × 10mL) and dried over $MgSO_4$. The organic layer was evaporated, and the crude product was purified by column chromatography (silica, CH_2Cl_2/methanol 100:2) and then *via* a SEC column to yield the bis-macrocycle (**M5)$_2$** as a white solid (62 mg, 61%).

^{1}H NMR (400 MHz, $CDCl_3$) δ 8.07 (d, ^{3}J = 9.1 Hz, 2H, H_c), 7.59 (s, 2H, H_a), 7.05 (d, ^{3}J = 8.2 Hz, 2H, H_b), 6.68 (d, ^{4}J = 2.4 Hz, 2H, H_k), 6.49 (t, ^{4}J = 2.4 Hz, H_j), 4.69 (t, ^{3}J = 7.2 Hz, 4H, H_d), 4.16 (t, ^{3}J = 6.1 Hz, 4H, H_h), 2.02 – 1.94 (m, 4H, H_e), 1.92 – 1.85 (m, 4H, H_g), 1.76- 1.68 (m, 4H, H_f).

^{13}C NMR (100 MHz, $CDCl_3$) δ = 162.8, 160.5, 143.7, 143.3, 139.2, 125.4, 123.5, 113.6, 107.1, 101.6, 68.6, 66.0, 28.8, 28.7, 22.9.

MALDI TOF MS: $C_{56}H_{58}N_4O_4K$Calc ($[M+K]^+$) = 953.39, Found *m/z* = 954.10

4.9 – References

(1) Eisler, S.; Slepkov, A. D.; Elliott, E.; Luu, T.; McDonald, R.; Hegmann, F. A.; Tykwinski, R. R. *J. Am. Chem. Soc.* **2005**, *127*, 2666.
(2) Chalifoux, W.; Tykwinski, R. R. *Nat. Chem.* **2010**, *2*, 967.
(3) Bichler, P.; Chalifoux, W. A.; Eisler, S.; Shi Shun, A. L. K.; Chernick, E. T.; Tykwinski, R. R. *Org. Lett.* **2009**, *11*, 519.
(4) Fritsch, P. *Liebigs Ann. Chem.* **1894**, *272*, 319.
(5) Buttenberg, W. P. *Liebigs Ann. Chem* **1894**, *272*, 324.
(6) Wiechell, H. Von. *Liebigs Ann. Chem.* **1894**, *272*, 337.
(7) Eisler, S.; Tykwinski, R. R. *J. Am. Chem. Soc.* **2000**, *122*, 10736.
(8) Luu, T.; Morisaki, Y.; Cunningham, N.; Tykwinski, R. R. *J. Org. Chem.* **2007**, *72*, 9622.
(9) Chalifoux, W. A.; McDonald, R.; Ferguson, M. J.; Tykwinski, R. R. *Angew. Chem. Int. Ed.* **2009**, *48*, 7915.
(10) Movsisyan, L. D.; Franz, M.; Hampel, F.; Thompson, A. L.; Tykwinski, R. R.; Anderson, H. L. *J. Am. Chem. Soc.* **2016**, *138*, 1366.
(11) Bruns, C. J.; Stoddart, J. F. *The Nature of the Mechanical Bond: From Molecules to Machines*, 1st ed.; John Wiley & Sons, 2017.
(12) Denis, M.; Goldup, S. M. *Nat. Rev. Chem.* **2017**, *1*, 61.
(13) Movsisyan, L. D. Polyyne Rotaxanes, University of Oxford, 2014.
(14) Dichtel, W. R.; Miljanic, O. S.; Zhang, W. Y.; Spruell, J. M.; Patel, K.; Aprahamian, I.; Heath, J. R.; Stoddart, J. F. *Acc. Chem. Res.* **2008**, *41*, 1750.
(15) Lewis, J. E. M.; Beer, P. D.; Loeb, S. J.; Goldup, S. M. *Chem. Soc. Rev.* **2017**, *46*, 2577.
(16) Lahlali, H.; Jobe, K.; Watkinson, M.; Goldup, S. M. *Angew. Chem. Int. Ed.* **2011**, *50*, 4151.
(17) Krapcho, A. P.; Lanza, J. B. *Org. Prep. Proced. Int.* **2007**, *39*, 603.
(18) Guo, H. C.; Zheng, R. H.; Jiang, H. J. *Org. Prep. Proced. Int.* **2012**, *44*, 392.
(19) Li, B.; Qin, X.; You, J.; Cong, X.; Lan, J. *Org. Biomol. Chem.* **2013**, *11*, 1290.
(20) Krapcho, A. P.; Sparapani, S. *J.Heterocyclic Chem.* **2008**, *45*, 1167.
(21) Yudin, A. K. *Chem. Sci.* **2015**, *6*, 30.
(22) Movsisyan, L. D.; Kondratuk, D. V.; Franz, M.; Thompson, A. L.; Tykwinski, R. R.; Anderson, H. L. *Org. Lett.* **2012**, *14*, 3424.
(23) Wannere, C. S.; Schleyer, P. V. R. *Org. Lett.* **2003**, *5*, 605.
(24) Rowland, R. S.; Taylor, R. *J. Phys. Chem.* **1996**, *100*, 7384.
(25) Ramirez, F.; Desai, N. B.; McKelvie, N. *J. Am. Chem. Soc.* **1962**, *84*, 1745.
(26) Morisaki, Y.; Luu, T.; Tykwinski, R. R. *Org. Lett.* **2006**, *8*, 689.
(27) Luu, T.; Medos, B. J.; Graham, E. R.; Vallee, D. M.; McDonald, R.; Ferguson, M. J.; Tykwinski, R. R. *J. Org. Chem.* **2010**, *75*, 8498.
(28) Naveen; Babu, S. A.; Kaur, G.; Aslam, N. A.; Karanam, M. *RSC Adv.* **2014**, *4*, 18904.
(29) Bédard, A. C.; Collins, S. K. *J. Am. Chem. Soc.* **2011**, *133*, 19976.
(30) Glaser, C. *Chem. Ber.* **1869**, *2*, 422.
(31) Hay, A. S. *J. Org. Chem.* **1962**, *27*, 3320.
(32) Eglinton, G; Galbraith, A, R. *Chem. Ind.* **1956**, 737.
(33) Wagner, R. W.; Johnson, T. E.; Li, F.; Lindsey, J. S. *J. Org. Chem.* **1995**, *60*, 5266.
(34) Hoffmann, M.; Wilson, C. J.; Odell, B.; Anderson, H. L. *Angew. Chem. Int. Ed.* **2007**, *46*, 3122.

(35) Roche, C.; Luo, Q.; Gil-Ramírez, G.; Jiang, H. W.; Kohn, D. R.; Xiong, Y.; Thompson, A. L.; Anderson, H. L. *J. Org. Chem.* **2017**, *82*, 7446.
(36) Anderson, H. L. *Chem. Commun.* **1999**, *23*, 2323.
(37) Ullmann, F. *Chem. Ber.* **1898**, *31*, 1697.
(38) Bergeron-Brlek, M.; Giguère, D.; Shiao, T. C.; Saucier, C.; Roy, R. *J. Org. Chem.* **2012**, *77*, 2971.
(39) Yamamoto, T.; Morita, A.; Miyazaki, Y.; Maruyama, T.; Wakayama, H.; Zhou, Z. H.; Nakamura, Y.; Kanbara, T.; Sasaki, S.; Kubota, K. *Macromolecules* **1992**, *25*, 1214.
(40) Yamamoto, T.; Koizumi, T. *Synlett.* **2007**, *48*, 5449.
(41) Ishiyama, T.; Murata, M.; Miyaura, N. *J. Org. Chem.* **1995**, *60*, 7508.
(42) Dzhevakov, P. B.; Topchiy, M. A.; Zharkova, D. A.; Morozov, O. S.; Asachenko, A. F.; Nechaev, M. S. *Adv. Synth. Catal.* **2016**, *358*, 977.

Chapter 5

Preparing polyynes on surfaces

5.1. Introduction 164

5.2. Synthesis of linear dibromoolefins 169

5.3. Crystallography 173

5.4. Generation and imaging of polyynes from dibromoolefins 176

5.5. Synthesis of linear dichloroolefins 181

5.6. Conclusions 183

5.7. Experimental data for known compounds 184

5.8. Experimental data for novel compounds 192

5.9. References 194

Parts of this chapter have been submitted to *Nature Chemistry*. (N. Pavliček, P. Gawel, D.R. Kohn, Z. Majzik, Y. Xiong, G. Meyer, H.L. Anderson, L. Gross). The images in this chapter and all scanning probe microscopy was performed by N. Pavliček, Z. Majzik, G. Meyer and L. Gross at IBM Zurich. Interpretation and analysis of images was performed by all authors. Crystallography was performed by Yaoyao Xiong, who collected and refined the data.

Chapter 5 – Preparing polyynes on surfaces

5.1 – Introduction

Throughout this thesis our objective has been to stabilise highly reactive π–systems, and ultimately to stabilise cyclocarbons. In **Chapters 2-4** we focused on encapsulation as a strategy to macroscopically prepare rotaxanes and catenanes for investigation of their properties. However, there is an alternative strategy: molecules too reactive to be studied using traditional solution chemistry have been stabilised on metallic (e.g. copper and gold) surfaces and studied using scanning probe microscopy (SPM). Highly reactive molecules can be investigated in this way because SPM instruments can operate at low temperatures and surfaces can be prepared with a decoupling layer of NaCl. Much of the pioneering work in this area has been carried out by Leo Gross and coworkers at IBM Zurich research institute.[1–3]

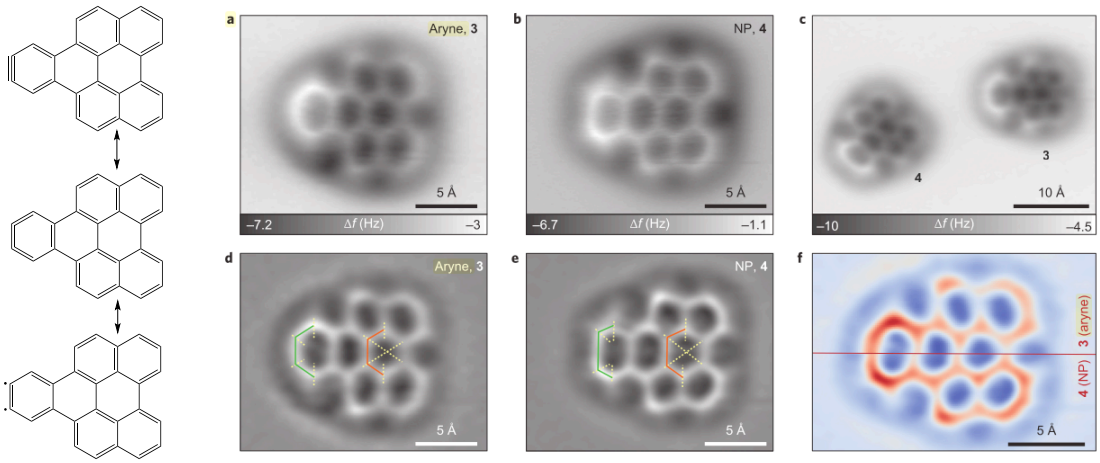

Figure 5.1. Structure and bond-length evaluation of aryne and naphthoperylene (NP) molecules. a,b, AFM imaging of individual aryne 3, Δz = −1.1Å) (a) and NP molecules 4, Δz = −0.78 Å) (b). c, AFM image of an aryne 3 and an NP molecule 4 close to each other (Δz = −1.0Å). d,e, The Laplace-filtered representations of a and b emphasise their differences. Solid and dashed lines highlight differences in the apparent bond lengths. f, To facilitate direct comparison, clipped and zoomed-in data from d and e are shown in the top (aryne 3) and bottom (NP 4) parts, respectively. The right-most bond on the symmetry axis was used to align both images. g–i, Colour-coded C–C bond orders for Kekulé depictions 3a, 3b and 3c, respectively. i is also valid for NP molecules (4) (adapted with permission from reference 1. Copyright 2015 Nature Publishing Group).

Examples of highly reactive molecules that have been prepared on surfaces include an aryne (**Figure 5.1**)[1], a diradical[2] (**Figure 5.2**) and triangulene.[3] These species have been isolated individually on an inert layer of NaCl at 5 K, which circumvents their high reactivity. In all of these examples a precursor molecule was adsorbed onto the

surface and the highly reactive molecule of interest was prepared by atomic manipulation. In this chapter, the first attempts to apply these SPM techniques to prepare *sp*-hybridised materials are detailed, in collaboration with Leo Gross and his group.

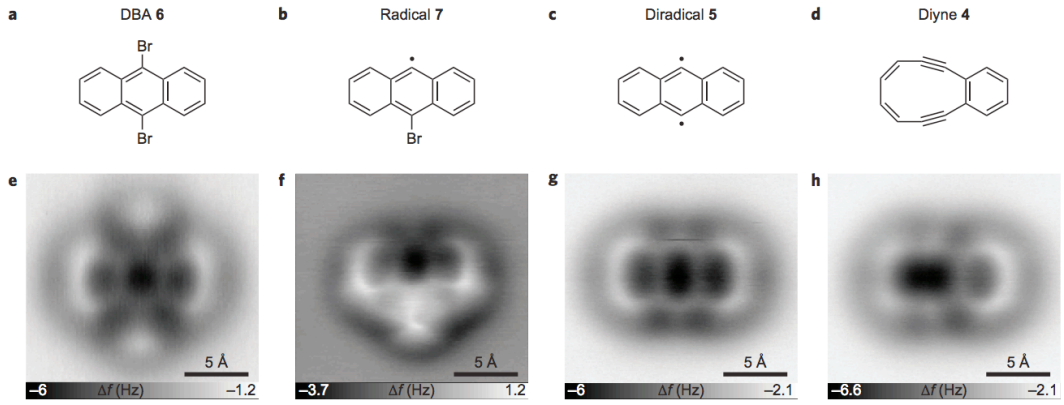

Figure 5.2. a-d, Chemical structures of the reaction products of successive tip-induced debromination of DBA 6. e-h, corresponding constant-height AFM images of molecules a-d on NaCl(2ML)/Cu(111) using a CO tip (adapted with permission from reference 2. Copyright 2016 Nature Publishing Group).

The field of SPM began in 1981 with the invention of the scanning tunnelling microscope (STM). This was developed by G. Binnig and H. Rohrer at IBM, and resulted in their award of the 1986 Nobel Prize in Physics.[4] The microscope relies on the quantum mechanical effect of tunnelling. Setting a bias voltage between a conducting tip and a conducting surface can allow electrons to tunnel through the vacuum barrier between the two conductors. The exponential distance dependence of the magnitude of this tunnelling results in very high spatial resolution, as sub-nanometre changes in tip-sample distance result in relatively large changes in tunnelling current. STM allows imaging of molecular electronic structure at very high resolution but does not necessarily allow molecules themselves to be identified. A highly important technique for atomic identification is inelastic electron tunnelling spectroscopy (IETS), a form of vibrational spectroscopy pioneered by the Ho group.[5] This technique yields energies of molecular vibrational modes that can serve as molecular fingerprints and even distinguish between different isotopes.[6,7]

For neutral molecules, the HOMOs or LUMOs can be visualised by applying a positive or negative bias voltage. To improve the imaging of these orbitals it is beneficial to use a thin isolating layer of NaCl or another inert layer such as xenon.

Functionalising the tip with a small molecule, such as CO, can significantly improve the resolution of the image in STM. STM images *atomic-scale* bodies on surfaces. However, resolving single atoms in an adsorbed molecule remains a great challenge because the tunnelling current is primarily sensitive to the local electron density of states close to the Fermi level.

A complementary scanning probe microscopy technique is known as atomic force microscopy (AFM), developed in 1986 by G. Binnig, C. Gerber and C. Quate.[8] This technique combines elements of a stylus profilometer and a STM, and was initially developed as a contact-based measurement technique to extend STM to insulating samples. The force acting between a cantilevered probe and a surface is used to image the surface with very high resolution. However, for atomic resolution of molecules, contact-based techniques have been superseded by non-contact AFM, which has allowed true atomic resolution of insulating surfaces.[9]

The development of non-contact AFM with tip-functionalisation has made it possible for molecules to be visualised on an atomic level and has made AFM a valuable characterisation technique for molecules with unknown structure.[10,11] The images of molecules are typically obtained in constant height mode. The intermolecular force field (made up of electrostatic, Van der Waals, Pauli repulsion) of the molecule induces a change in the frequency of the rapidly oscillating tip as the tip is scanned across the molecule. The magnitude of this frequency change allows the topography of the molecule to be mapped and subsequently imaged. The use of a functionalised tip and low oscillation amplitudes leads to very high resolution and the tip apex allows atomic level Pauli repulsion to be imaged (**Figure 5.3).**[12] Tip functionalisation is crucial for obtaining such high resolution and the most frequently used tip is CO. The protruding oxygen has a very small radius and its behaviour is very well understood.[13] However, a wide variety of tips can be used to provide different information about the molecule of interest.

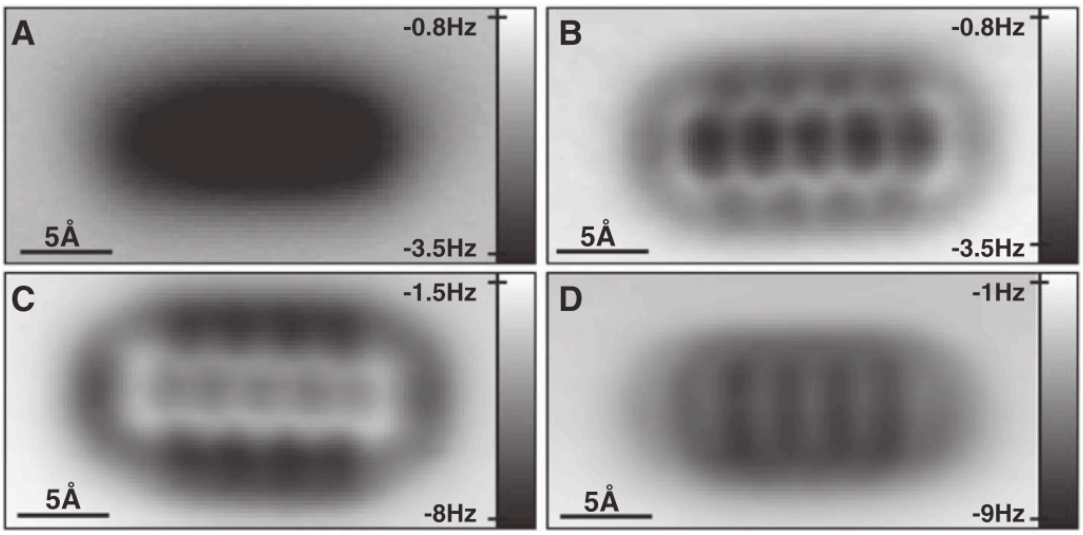

Figure 5.3. Constant-height AFM images of pentacene on NaCl(2ML)/Cu(111) using different tip modifications.Ag tip, z = –0.7Å, A = 0.6Å; (B) CO tip, z = +1.3Å, A = 0.7Å; (C) Cl tip, z = –1.0Å, A = 0.7Å; and (D) pentacene tip, z = +0.6Å, A = 0.5Å. The z values are given with respect to a STM set point of I = 2 pA, V = 200 mV above the NaCl(2 ML)/Cu(111) substrate (adapted with permission from reference 12. Copyright 2011 Science Publishing Group).

Alongside imaging, Gross and coworkers have become adept at molecular manipulation and have performed unprecedented manipulations using their combined AFM/STM setup, which approached the level of control predicted in Richard Feynmann's famous lecture '*There's plenty of room at the bottom'*. For this reason, we believed they were the perfect research group to collaborate with for pursuing our goals of preparing and probing a cyclocarbon on a surface.

There are several different important manipulation techniques that can be used to control atomic movement, bond-forming and bond-breaking with precise control. These key methods are the tip-adsorbate force, tunnelling current induced electron attachment and inelastic energy transfer to the adsorbate (IET). It is generally thought that the most important mechanism for bond formation and dissociation is IET. This is a process where energy is transferred from electrons that are tunnelling between tip and substrate to a molecule, normally causing the weakest bond to break, provided that the electron energy is sufficiently high. This process often leads to the breaking of carbon-halogen or carbon-hydrogen bonds due to their lower bond strength.[14,15] The prior examples of breaking carbon-halogen bonds with IET led to the development of our synthetic strategy that is outlined in this chapter.

The Fritsch-Buttenberg-Wiechell (FBW) rearrangement[16–18] is a well-established method for acetylene synthesis and the second step of the more widely known Corey-Fuchs[19] reaction. The FBW rearrangement has developed from a niche 19th century reaction, heating diarylvinyl chlorides with sodium ethoxide in ethanol at 200 °C, to a highly important synthetic method with broad functional group tolerance. (**Scheme 5.1)**. In 2000, Tykwinski and coworkers were the first to migrate alkyne, which triggered a renaissance of applications for this reaction in carbon-rich chemistry.[20] The development of one-pot procedures[21,22] has only widened its utility and it is now one of the most important methodologies in polyyne synthesis and synthetic attempts towards carbyne.[23] Investigation into the mechanism of the FBW rearrangement suggests it normally follows an anionic mechanism with a sequence of halogen-metal exchange of a 1,1-dihaloolefin **1b**, formation of a carbenoid intermediate **2**, carbene **3** formation and subsequent rearrangement (**Scheme 5.1)**.[24] The presence of intermediate **2** in the mechanism was confirmed by isotopic labelling experiments.[25] α-Elimination of MX to form the carbene **3** and simultaneous migration of a substituent from the adjacent carbon then yields the alkyne **4**.[26] It is not possible to characterise intermediates in this final step, however various isotopic studies have confirmed the mechanistic path.[27,28] In contrast, numerous mechanistic studies suggested the group *trans* to the halide (R_2 in **2**) migrated preferentially, which contradicts the existence of a carbene intermediate.[29–31] There was also a postulated radical mechanism by Kunishima and coworkers who treated a dihaloolefin with single electron transfer reagent samarium iodide.[32] Due to synthetic limitations, the alkyne group was absent from these earlier studies, however, Tykwinski *et al.* investigated the alkyne groups migratory aptitude in 2008. It was found that the alkynyl group migrated more efficiently than all other groups except the anisyl group.[27]

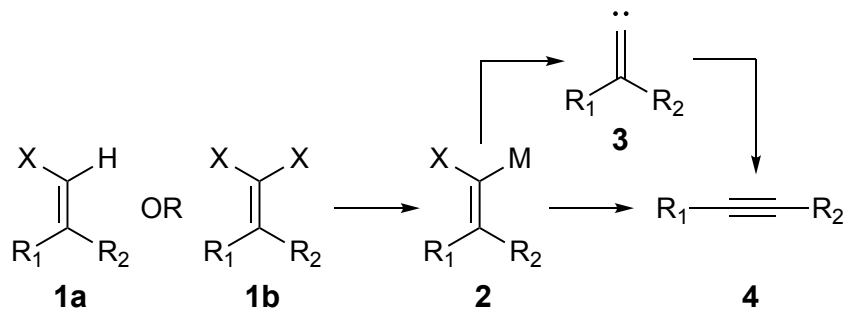

Scheme 5.1. FBW rearrangement (R_1, R_2 = aryl, alkyl, alkenyl, alkynyl).

We set out to investigate FBW rearrangements on surfaces. The aims of this work were to learn more about the mechanism and scope of this reaction and to develop a methodology for the synthesis and characterization of long polyynes under well-controlled conditions. In this work, we have generated tri-, tetra-, hexa- and octaynes (**5-8**) by atomic manipulation on bilayer NaCl islands on Cu(111) (**Scheme 5.7**). The tip of a low temperature qPlus-based[33] STM/AFM was used to cleave the C-Br bonds of precursors **5(Br2)**, **6(Br4)**, **7(Br4)** and **8(Br4)** one-by-one using suitable voltage pulses.[1,2,34–36] This approach is of interest for preparing and stabilising planar polyynes and cyclocarbons *via* planar dibromoolefins (**Scheme 5.2**).

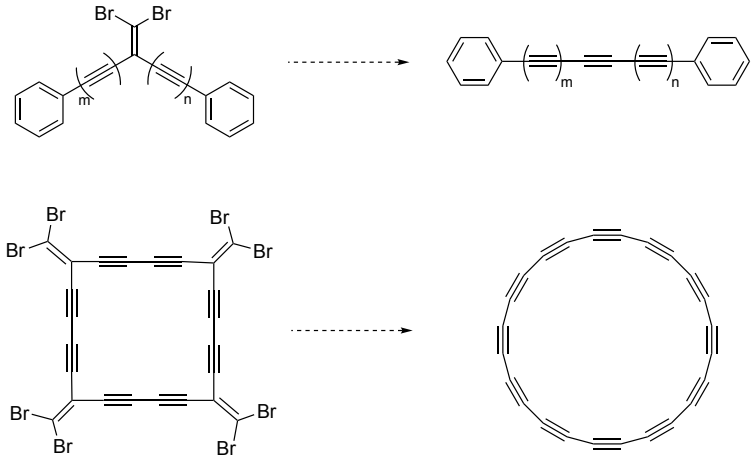

Scheme 5.2. Hypothesised surface-stabilised rearrangement.

5.2 – Synthesis of linear dibromoolefins

We believed atomic manipulation could break the C-Br bonds of dibromoolefins and potentially initiate the FBW rearrangement. Initiating and controlling the FBW rearrangement on a surface would be the first skeletal rearrangement on a surface and would represent a step forward in increased bottom-up control of reactivity. If one or more rearrangements can be performed successfully on linear dibromoolefins this would give us great confidence that cyclic analogues could be prepared and cyclocarbons could be prepared on the surface *via* this approach.

Phenyl-substituted dibromoolefins have been synthesised previously to prepare aryl-capped polyynes for non-linear optics.[37,38] Dibromoolefin formation was primarily used as a means to circumvent low stability of terminal polyynes (particularly triynes and longer). First, phenyl acetylene was lithiated at low temperature and ethyl formate

was added slowly to form alcohol **5.1**. This alcohol was taken forward without purification and oxidised overnight with PCC in CH_2Cl_2 yielding ketone **5.2** in good yield over two steps. The desired dibromoolefin **5(Br2)** was prepared in good yield by forming an ylid using Ramirez' conditions and adding ketone **5(Br2)**.

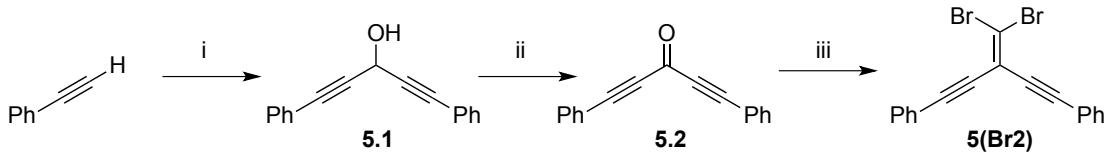

Scheme 5.3. Synthesis of **5(Br2)**: i) *n*-BuLi, THF, –78 °C, then EtO_2CH, 2 h, 25 °C; ii) PCC, mol. sieves, celite, CH_2Cl_2, 20 h, 25 °C, 44% (two steps); iii) CBr_4, PPh_3, CH_2Cl_2, 20 h, 25 °C, 79%.

Dibromoolefin **5(Br2)** was sent to our collaborators in Zurich and SPM atomic manipulation experiments were performed with it, which showed the rearrangement successfully occurring on the surface (**Figure 5.10**). After this successful result, longer linear molecules were prepared to see if the rearrangement could be done twice on the surface within one molecule and to prove its reproducibility. The tetrayne precursor **6(Br4)** had never previously been synthesised. Morisaki and coworkers synthesised dibromoolefin **5.7** but then performed a FBW rearrangement and further functionalization.[21] Their synthetic route was followed with few modifications to prepare dibromoolefin **5.7** (**Scheme 5.4**).

Alcohol **5.4** was synthesised from TMS-acetylene and aldehyde **5.3**. This alcohol was oxidised immediately after crude purification to yield ketone **5.5**. The ketone was treated with Ramirez's conditions to yield the dibromoolefin **5.6**. Deprotection occurred cleanly and quickly to yield the deprotected dibromoolefin **5.7**. Glaser-Hay conditions were used to prepare tetrayne precursor **6(Br4)** in good yield.[39,40] This molecule was fully characterised and single crystals were grown and measured (**Section 5.3**). This general synthetic pathway was followed in the synthesis of **7(Br4)** and **8(Br4)** with slightly different substrates.

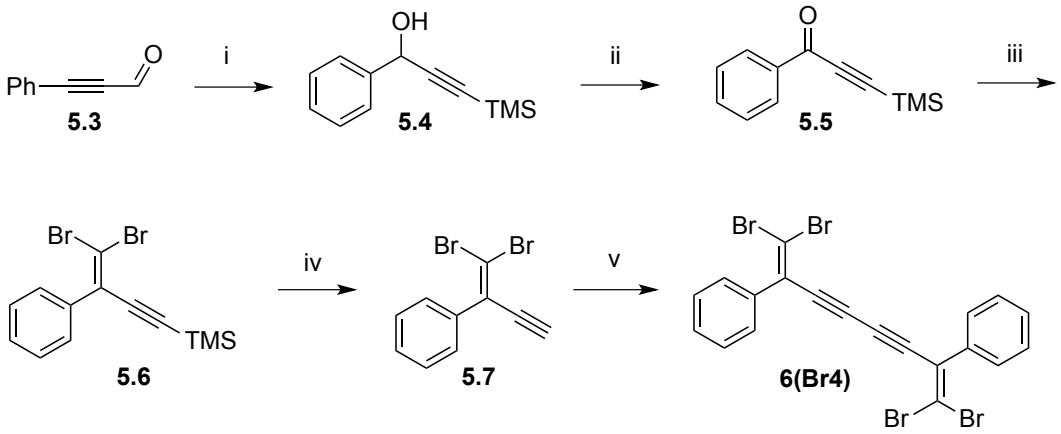

Scheme 5.4. Synthesis of **6(Br4)**: i) *n*-BuLi, THF, –78 °C, trimethylsilylacetylene, 25 °C, 30 mins; ii) PCC, molecular sieves, celite, CH_2Cl_2, 25 °C, 12 h, 81% (two steps); iii) CBr_4, PPh_3, CH_2Cl_2, 25 °C, 3 h, 79%; iv) K_2CO_3, THF/MeOH, 25 °C, 30 mins, 86%; v) CuCl, TMEDA, CH_2Cl_2, 25 °C, 2 h, 58%.

Hexayne precursor **7(Br4)** was synthesised by a similar synthetic route, which had been used previously in Luu and coworkers diarylpolyyne synthesis (**Scheme 5.5**).[37] This synthesis was repeated with few modifications and **7(Br4)** was isolated in excellent yield. Single crystals of **7(Br4)** were grown (**Section 5.3**).

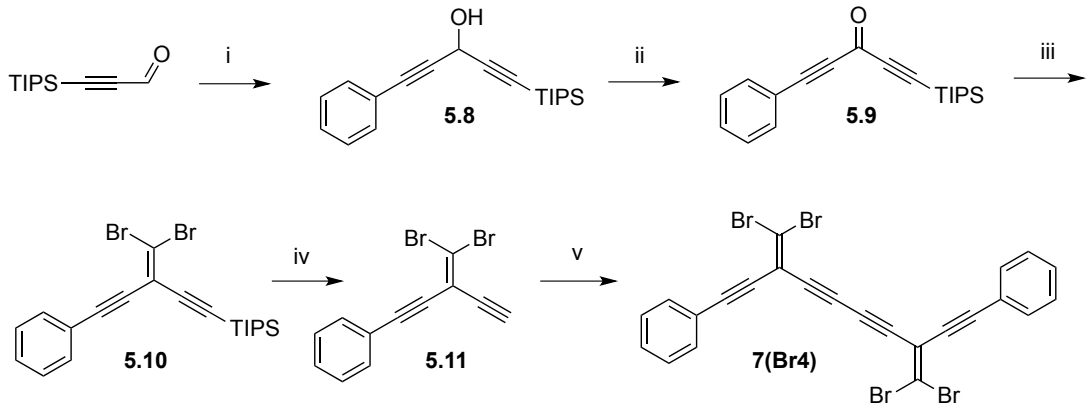

Scheme 5.5. Synthesis of **7(Br4)**: i) PhC≡CLi, THF, 25 °C, 2 h, 74%; ii) PCC, molecular sieves, celite, CH_2Cl_2, 25 °C, 12 h, 89%; iii) CBr_4, PPh_3, CH_2Cl_2, 25 °C, 3 h, 79%; iv) K_2CO_3, THF/MeOH, 25 °C, 30 mins, 99%; v) CuCl, TMEDA, CH_2Cl_2, 25 °C, 3 h, 92%.

To complete the series of dibromoolefins, **8(Br4)** was synthesised, which had been synthesised previously in Luu and coworkers diarylpolyyne synthesis (**Scheme 5.6**).[37] The synthesis was repeated with few modifications and **8(Br4)** was isolated. Single crystals of **8(Br4)** were grown (**Section 5.3**).

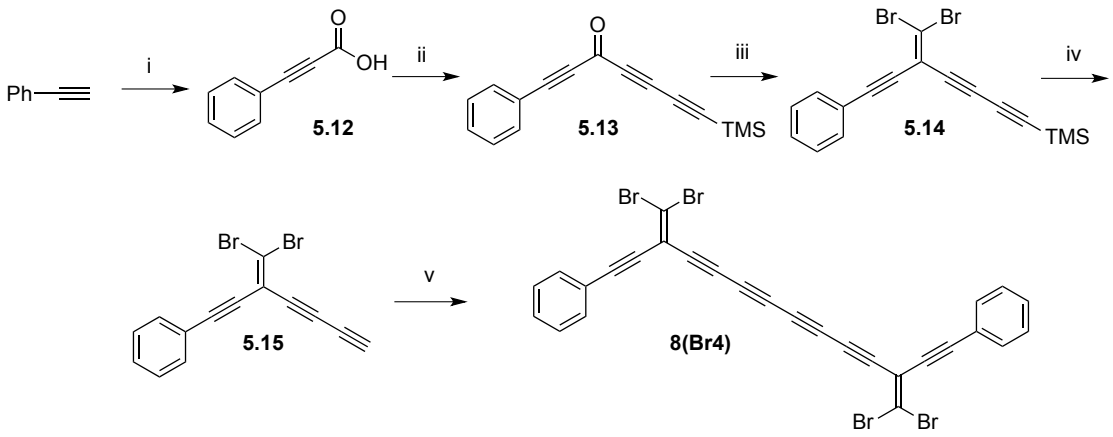

Scheme 5.6. Synthesis of **8(Br4)**: i) MeLi, THF, 1 h, –78 °C, then CO_2, 1 h, 58%; ii) $SOCl_2$, 12 h, $AlCl_3$, 1,4-trimethylsilylbutadiyne, CH_2Cl_2, 0 °C, 4 h, 64% (two steps); iii) CBr_4, PPh_3, CH_2Cl_2, 25 °C, 12 h, 70%; iv) K_2CO_3, THF/MeOH, 25 °C, 15 min, CuCl, TMEDA, CH_2Cl_2, 25 °C, 3 h, 44% (two steps).

The on-surface generation of polyynes *via* the FBW rearrangement results in the corresponding polyynes **5-8** from the dibromoolefin precursors (**Scheme 5.7**). The technique, mechanisms and insights from these voltage-induced rearragements are discussed further in **Section 5.4.**

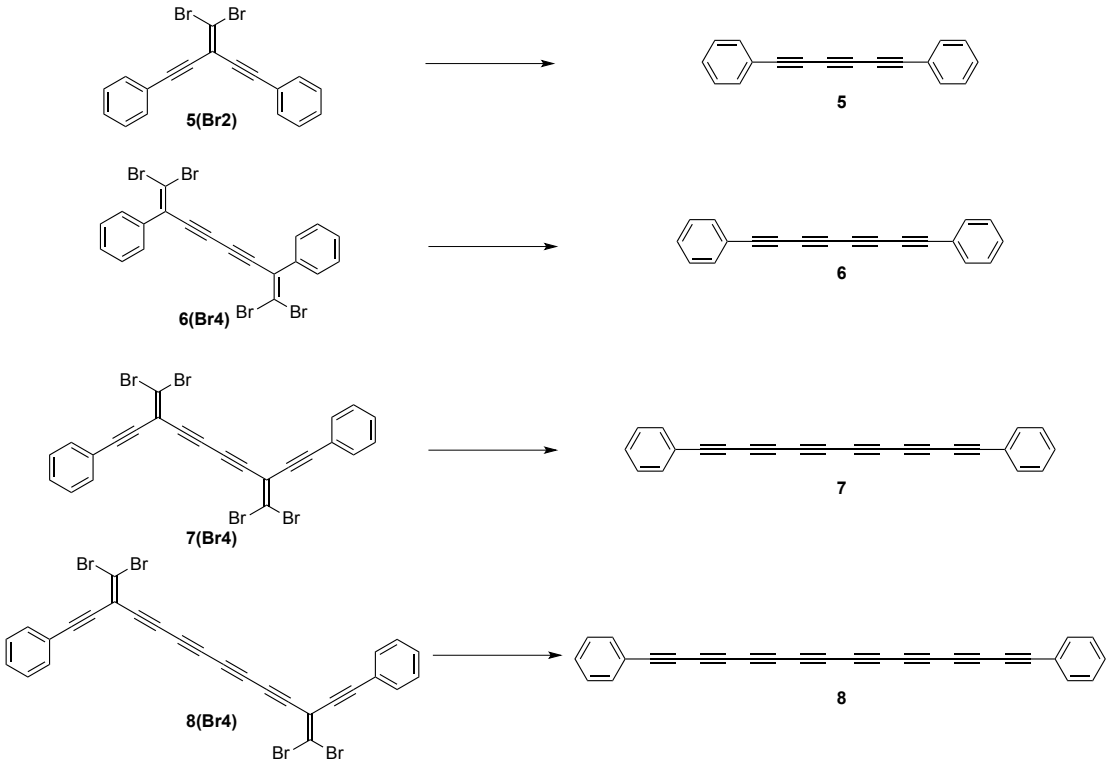

Scheme 5.7. On surface generation of polyynes **5,6,7,8.**

5.3 – Crystallography

Single crystal X-ray diffraction data were collected at 150 K using an Oxford Diffraction/Agilent SuperNovae A (Cu) X-ray source by Yaoyao Xiong. The raw frame data were integrated and reduced using CrysAlisPro (Agilent Technologies, 2010). The structure was solved using charge flipping[41,42] with the SuperFlip method.[43] It was refined by full-matrix least-squares on F^2 in CRYSTALS by Yaoyao Xiong. Crystals of **6(Br4)** suitable for X-ray diffraction studies were grown from slow vapor diffusion of petroleum ether into a CH_2Cl_2 solution of the compound at 25 °C. (**Figure 5.4**, **Figure 5.5**). The size of the bromine atom forces the phenyl to rotate to avoid a steric clash.

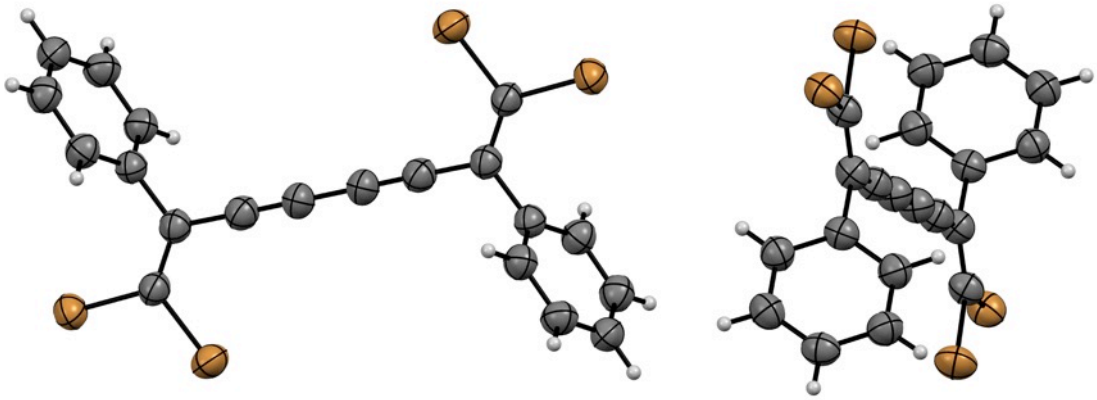

Figure 5.4. ORTEP plot of **6(Br4)**. Atomic displacement parameters at 150 K are drawn at 50% probability level.

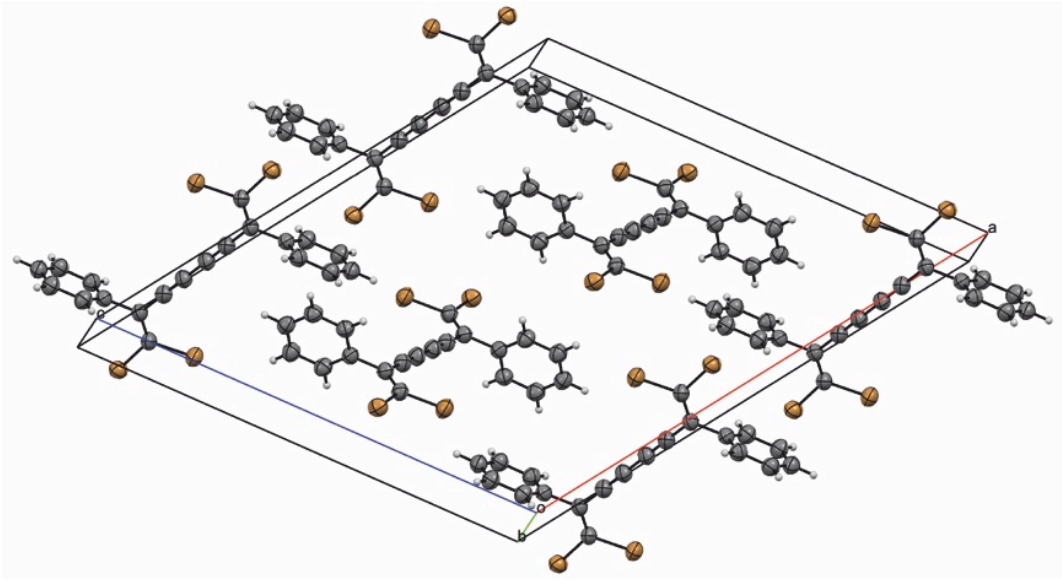

Figure 5.5. ORTEP plot of **6(Br4)**, unit cell. Atomic displacement parameters at 150 K are drawn at 50% probability level.

Crystals of **7(Br4)** suitable for X-ray diffraction studies were grown from slow vapor diffusion of petroleum ether into a CH_2Cl_2 solution of the compound at 25 °C. (**Figure 5.6**, **Figure 5.7**). Dibromoolefin **7(Br4)** is far more planar than **6(Br4)**.

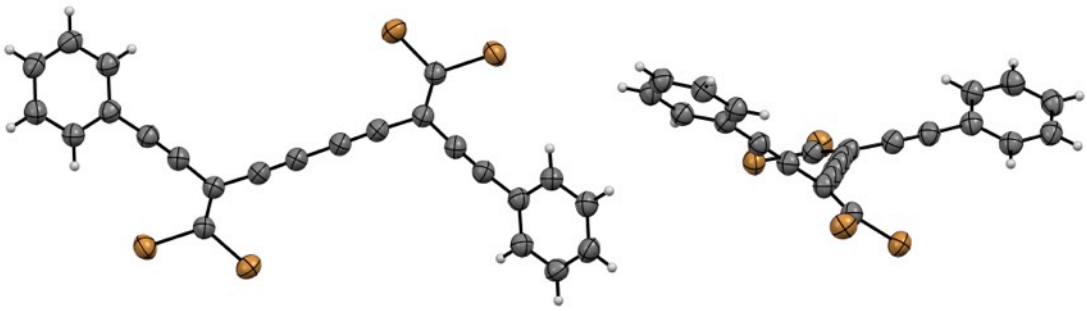

Figure 5.6. ORTEP plot of **7(Br4)**. Atomic displacement parameters at 150 K are drawn at 50% probability level.

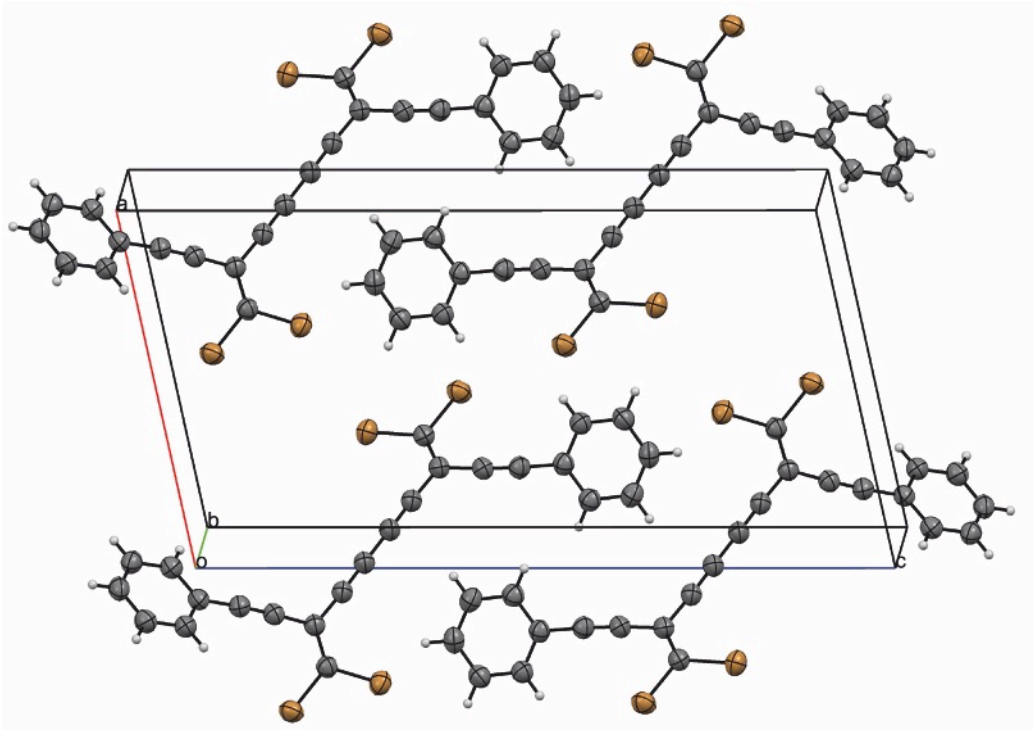

Figure 5.7. ORTEP plot of **7(Br4)** unit cell. Atomic displacement parameters at 150 K are drawn at 50% probability level.

Crystals of **8(Br4)** suitable for X-ray diffraction studies were grown from slow evaporation of the compound in a solvent mixture of CH_2Cl_2 and CH_3OH at 0 °C (**Figure 5.8**, **Figure 5.9**).

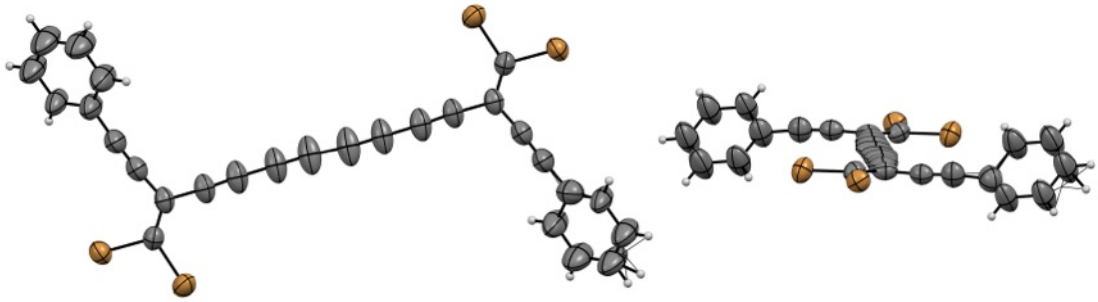

Figure 5.8. ORTEP plot of **8(Br4)**. Atomic displacement parameters at 150 K are drawn at 50% probability level.

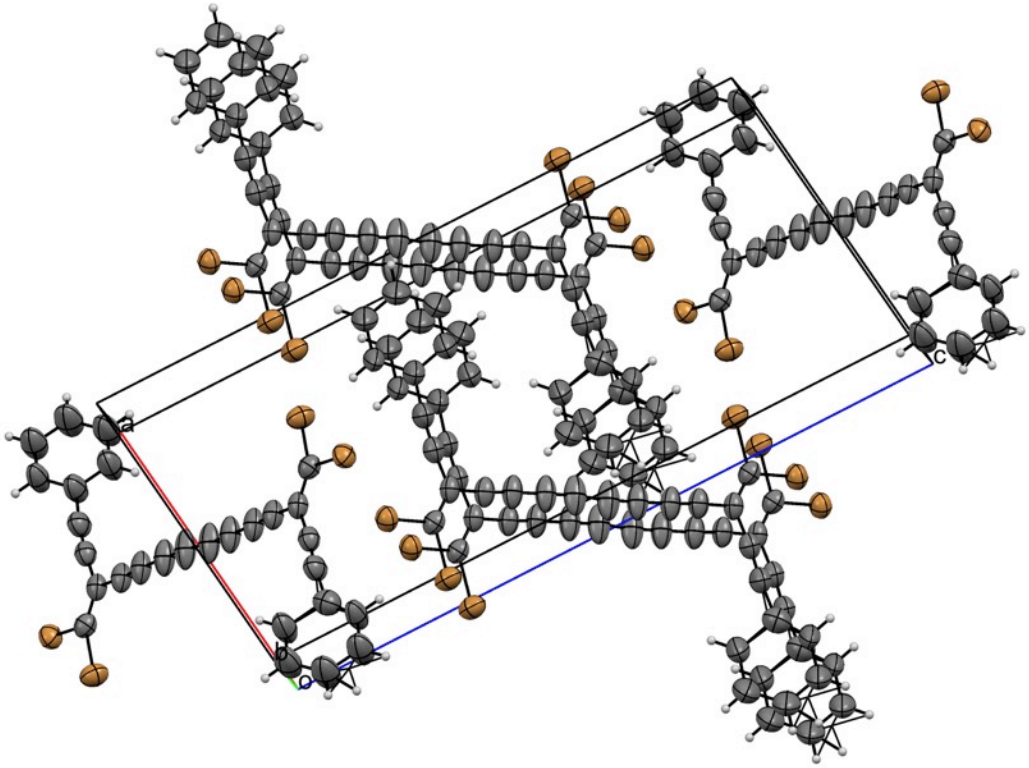

Figure 5.9. ORTEP plot of **8(Br4)** unit cell. Atomic displacement parameters at 150 K are drawn at 50% probability level.

All of the crystal structures are solved with high quality data. The bond lengths and angles all fall within expected ranges. The molecules stack efficiently and in the planar molecules **7(Br4)** and **(8Br4)** the conformation of these molecules could lead to a Diels-Alder type decomposition pathway.[44] This could explain the limited stability of these molecules.

5.4 – Generation and imaging of polyynes from dibromoolefins

The generation of phenyl triyne **5** from precursor **5(Br2)** was investigated by scanning probe microscopy (**Figure 5.10**). The structure of the dibromoolefin **5(Br2)** can be clearly distinguished from the AFM image (**Figure 5.10a**). In particular, the triple bonds and the attached Br atoms can be assigned by their pronounced and characteristic contrast, as reported in the literature.[2,45] A voltage pulse at $V \geq 1.7$ V was used to cleave the first C-Br bond. The detached Br atom remains nearby, but can be moved out of the frame by vertical manipulation.[2,33] A higher voltage pulse ($V \geq 2.1$ V) was used to cleave the second C-Br bond, resulting directly in formation of triyne **5**; the three triple bonds are clearly visible in the AFM image (**Figure 5.10c**).

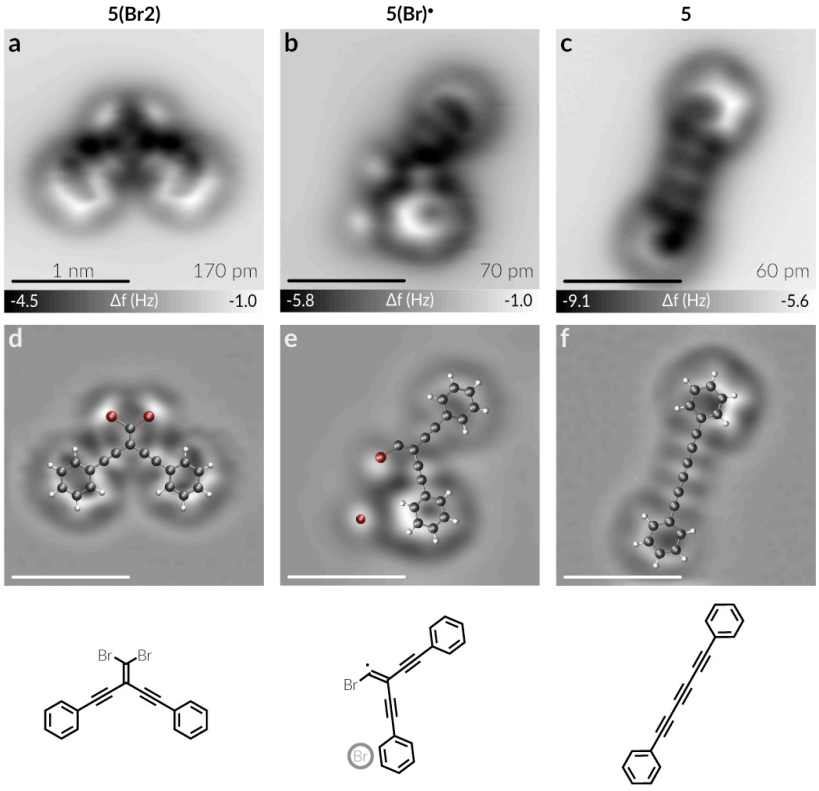

Figure 5.10. On-surface reaction to generate triyne **5** from precursor **5(Br2)**: a, b, and c show AFM images of precursor **5(Br2)**, intermediate radical **5(Br)•** and triyne **5**, respectively. Molecular structures are shown below for comparison, with the detached Br atom shown in a grey circle.

The double layer of NaCl decoupling the reaction from the Cu(111) surface seems to be essential for these FBW rearrangements. When the reaction was performed on a bare Cu(111) surface, radical intermediates reacted with the substrate, preventing the final rearrangement from occurring (**Figure 5.11**). The thin insulating layer of NaCl

also facilitates orbital imaging by STM because it reduces the electronic coupling between the molecule and the surface.[34,46]

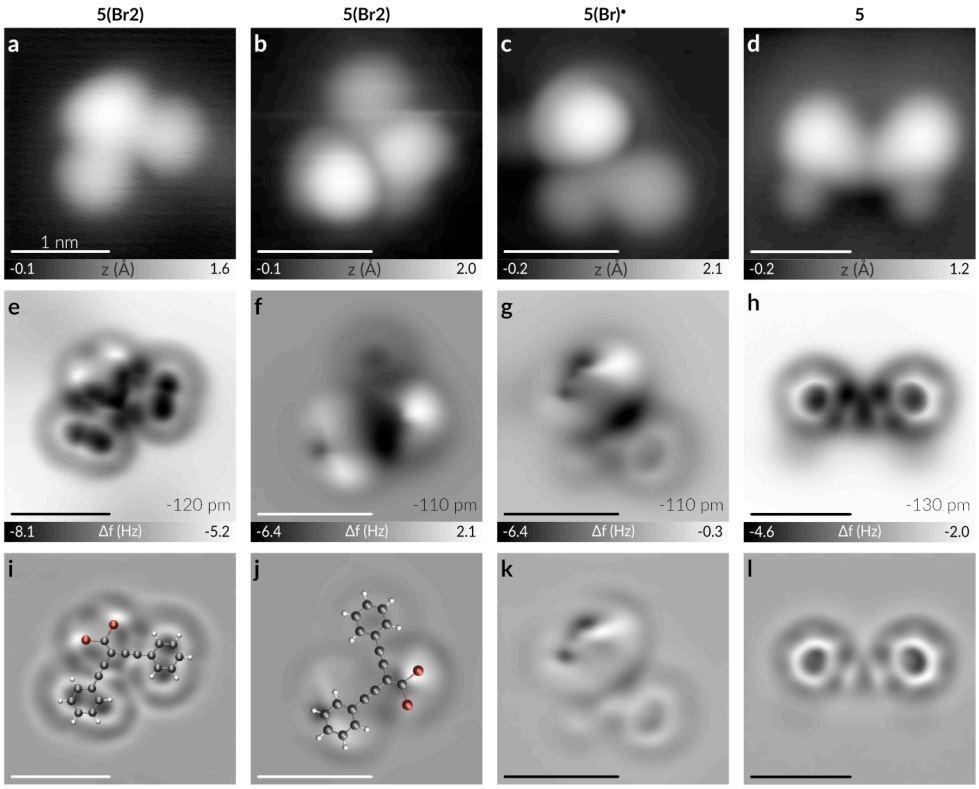

Figure 5.11. Debromination of **5(Br2)** adsorbed on Cu(111). a-d, STM images. e-h (i-l), Corresponding (Laplace-filtered) AFM images; ball-and-stick models are overlaid in panels i and j.

Three intermediates were observed and characterised during formation of hexayne **7** from **7(Br4)** (**Figure 5.12**). The AFM image of **7(Br4)** agrees well with its X-ray crystal structure (**Figure 5.6**); the triple bonds and the Br atoms have the expected characteristic contrast, similar to **5(Br2)**. Two consecutive voltage pulses at $V \geq 1.4$ V were applied to remove one of the two Br atoms at each olefin unit. The corresponding radical **7(Br3)•** and diradical **7(Br2)2•** were clearly observed (**Figure 5.12b** and **Figure 5.12c**, respectively). We found that these radicals are always formed as the isomer with the bromine atoms pointing towards the centre of the molecule. Next, a higher voltage pulse ($V \geq 2.0$ V) was applied to cleave the third C-Br bond, leading immediately to a FBW rearrangement to form a tetrayne moiety on the left-hand side of the molecule (**Figure 5.12d**). Finally, a fourth voltage pulse ($V \geq 2.0$ V) was applied to produce hexayne **7** (**Figure 5.12e**). The ability to visualise each step of a mechanism and induce the next step with such precision is a significant

development for atomic manipulation. This rearrangement is arguably the most impressive achievement of bottom-up control of a chemical reaction to date.

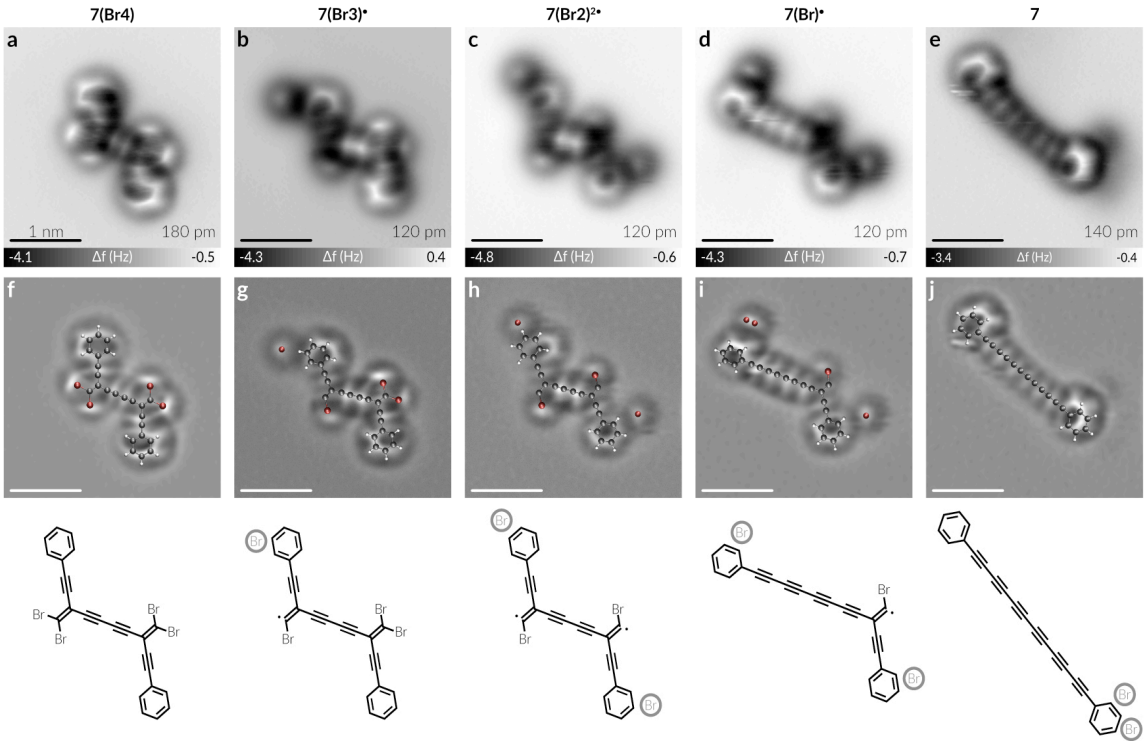

Figure 5.12. On-surface reaction to generate hexayne **7** from precursor **7(Br4)** illustrated by AFM images (top) and corresponding chemical structures (bottom) as a visual aid. a, Precursor **7(Br4)**. b, Radical 7**(Br3)•**. c, Diradical **7(Br2)2•.** d, Intermediate **7(Br)•** after the first FBW rearrangement, resulting in a tetrayne moiety. e, Hexayne **7** after second FBW rearrangement. f-j corresponding Laplace-filtered images with ball and stuck models overlaid as a visual aid. Molecular structures are shown below for comparison, with the detached Br atom shown in a grey circle.

The on-surface manipulation method yielding tetrayne **6** proceeded similarly to the formation of **7**, but it was more difficult to image the intermediates in these reactions due to the non-planar geometry of **6(Br4)** (**Figure 5.13**). Dibromoolefins **5(Br2)**, **7(Br4)**, and **8(Br4)** are relatively flat, both on the surface and in the solid state (**Section 5.3**). In contrast, the two phenyl rings of **6(Br4)** are twisted out of the plane of the dibromoolefin by 70 ° in the solid state (**Figure 5.4**) and are clearly twisted in the AFM images too. The on-surface manipulation method yielding octayne **8** proceeded similarly to the formation of **7**, but it was more difficult to image the intermediates in these reactions due to the instability of **8(Br4)**. This dibromoolefin showed signs of decomposition while handling during the synthesis and some molecules fragmented considerably during sublimation. Nonetheless, numerous molecules were found intact and visualised normally (**Figure 5.14**).

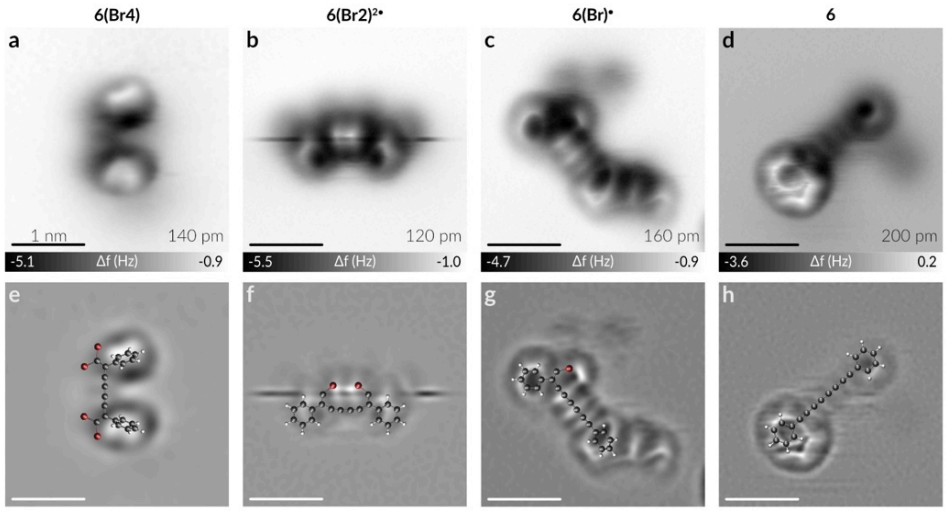

Figure 5.13. Synthesis of tetrayne **6** from precursor **6(Br4)** illustrated by a typical sequence of AFM images (a-d) and corresponding Laplace-filtered images (e-h) with ball-and-stick models are overlaid as a visual aid. Figure created by Niko Pavlicek.

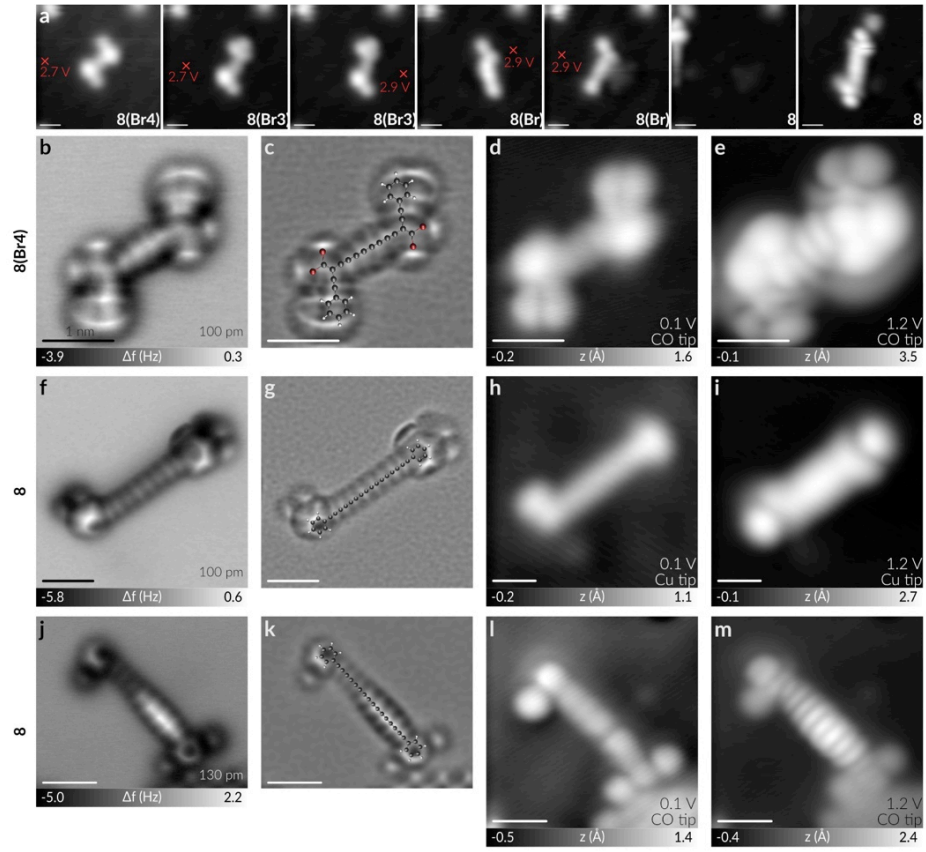

Figure 5.14. Synthesis of octayne **8** from precursor **8(Br4)**. a, Series of STM images illustrating the atomic manipulation procedure (1 pA, 1.0 V). Manipulation steps were performed at the positions indicated by red crosses at the indicated voltages. b-e, Characterization of **8(Br4)**. It is apparent that the molecule jumps between two azimuthal orientations. f-m, Characterization of two different octayne **8** molecules. Figure created by Niko Pavlicek.

The higher voltage required to break the C-Br bonds in radicals **5(Br)•**, **7(Br2)2•,** and **7(Br3)•**, compared to **5(Br2)**, **7(Br4)** and **7(Br3)•**, indicates that cleavage of the second C-Br bond in the vinyl radical (C=C•-Br moiety) is the rate determining step of the rearrangement. Although the mechanisms of FBW rearrangements are normally drawn with carbene intermediates (**3** in **Scheme 5.1**), we did not observe them in these reactions under our experimental conditions and time scale (10 s). The 1,2-bond migration appears to occur spontaneously after (or simultaneously with) cleavage of the second C-Br bond, even at 5 K. There has been some discussion about the bond angles in vinyl radicals of the type R_2C=C•-X because these species can be linear or bent, depending on the substituents R and X.[47] The high resolution of images of **5(Br)•**, **7(Br2)2•**, and **7(Br)•** show that the C=C•-Br is bent. This is the first time that the geometry of a vinyl radical has been visualised by AFM.

Polyynes **5**-**8** were characterised by AFM, STM and scanning tunnelling spectroscopy (STS, **Figure 5.15**). Isolated polyynes are frequently observed in slightly curved conformations on the surface, as often observed for longer polyynes, both in solution and in the solid state.[48] In general, for a neutral molecule, the LUMO and HOMO are imaged by applying a positive or negative sample voltage, to tunnel *via* the negative or positive ion resonance (NIR or PIR, respectively).[34] Our collaborators recorded images of the LUMO orbitals (NIR) of all the polyynes; those of **7** and **8** are particularly well resolved with a CO and a Br tip, respectively, and it is possible to see the characteristic nodes in the middle of every triple bond in excellent agreement with DFT calculated frontier molecular orbitals (**Figure 5.15**). They also recorded clear images for the HOMO (PIR) of 7 and 8 (**Figure 5.15**). The STS traces show that the LUMO energies of the polyynes decrease for longer polyynes as expected (**Figure 5.15 m,n**). Note the error of ± 0.2 V involved in determining the resonance energies.[49]

To the best of our knowledge, this is the first time that a skeletal rearrangement has been observed on a surface and the first time that a polyyne has been structurally characterised by STM and AFM. The results shown here represent a large breakthrough in the field of atomic manipulation by scanning probe microscopy.

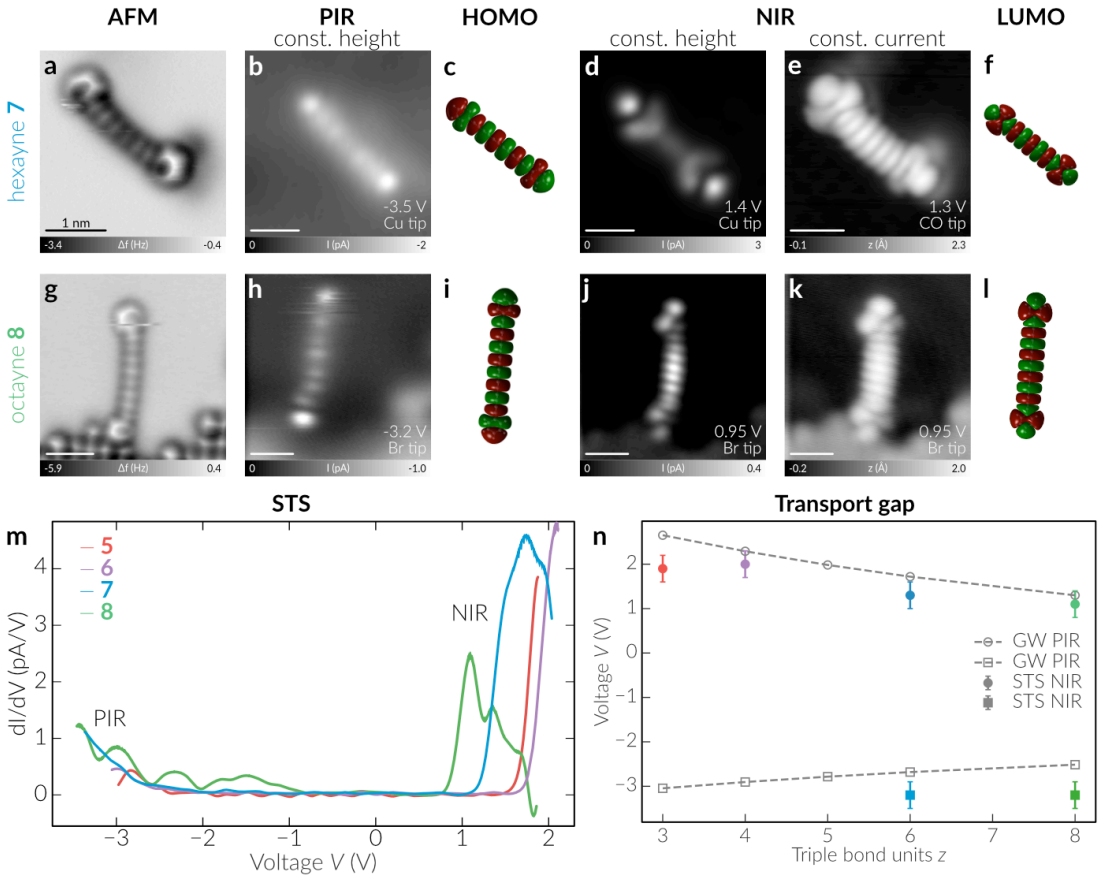

Figure 5.15. Characterization of polyynes **5–8** on the NaCl surface using AFM, STM, and STS. Experimental HOMO and LUMO maps from positive and negative ion resonance (PIR and NIR) STM images, respectively, are compared with orbital densities from DFT calculations (B3LYP/6-31G(d), isovalues 0.0004). a,g, AFM image of hexayne **7** (repeated and rotated from Fig. 3e) and octayne 8 (anchored at a step edge of a three-monolayer thick NaCl island). b,g, Constant height STM images corresponding to PIR of **7** and **8**. c,i, calculated HOMO orbitals of 7 and 8 in vacuum. d,j, Constant height STM images corresponding to NIR of 7 and 8. e,k, Constant current STM images corresponding to NIR of **7** and 8. f,l, calculated LUMO orbitals of 7 and 8 in vacuum. m, Typical STS curves for polyynes **5–8**. n, Transport gap as a function of triple bond units z. Zero voltage of theoretical values corresponds to a work function of 4.0 eV for bilayer NaCl on Cu(111). Figure created by Niko Pavlicek.

5.5 – Synthesis of linear dichloroolefins

Dichloroolefins are more soluble than dibromoolefins and are likely to be easier to sublime onto the surface due to their lower molecular weight. We have concerns about the stability of cyclocarbon precursors after the decomposition of **8(Br2)** was observed. The C-Cl bond is stronger than the C-Br bond and has not been broken by IET in an atomic manipulation surface method before. Preparing analogous dichloroolefins would be an excellent model for investigating this due to the

successful rearrangement of analogous dibromoolefins. If the rearrangement is possible and the C-Cl bond is selectively broken this will expand the molecular toolkit of atomic manipulation even further and simultaneously assist with synthesising cyclic precursors.

Dichloroolefins are far less prevalent in the literature than dibromoolefins and there are very limited examples of dichloroolefination. Stachulski and coworkers reported a highly efficient, mild dichloroolefination in acetonitrile in 1988.[50] The only example in the literature of an acetylene-conjugated ketone as a substrate was reported by Chauvin and coworkers in 2011.[51] However, despite the similarity of the system, these conditions were incompatible with ketone **5.2 (Scheme 5.8)**. We attempted pre-formation of an ylid and reducing the reaction temperature, but our screening consistently resulted in the destruction of the starting material and resulted in unidentifiable byproducts. However, when using a more similar substrate to Chauvin and coworkers the reaction was successful (**Scheme 5.9**). Ketone **5.5** was transformed into dichloroolefin **5.15** in excellent yield. TMS-protected dichloroolefin **5.15** was deprotected and immediately coupled using Glaser-Hay conditions, yielding **6(Cl4)** in excellent yield.

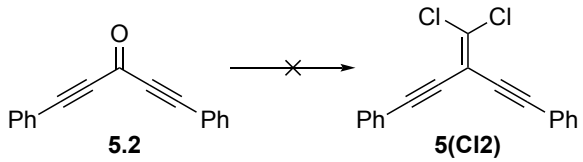

Scheme 5.8. Failed synthesis of **5(Cl2)**

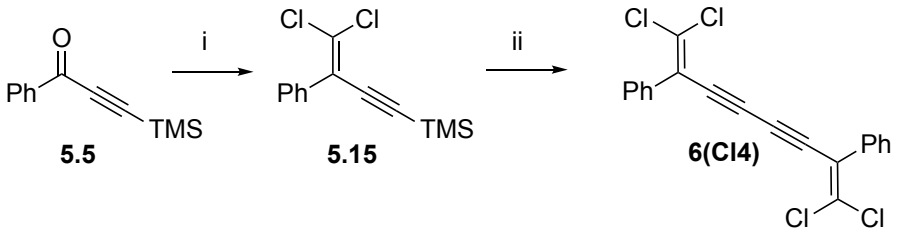

Scheme 5.9. Synthesis of **6(Cl4)**. i) CCl_4, PPh_3, MeCN, 0 °C, 2 h, 88% ii) a) K_2CO_3, THF/MeOH, 30 25 °C, 30 mins b) CuCl, TMEDA, CH_2Cl_2, 25 °C, 1 h, 92%.

Dichloroolefin **6(Cl4)** was fully characterised and sent to our collaborators in Zurich for investigation. The results of these experiments are still outstanding at the time of writing this thesis.

5.6 – Conclusions

We have synthesised a series of polyynes **5**–**8** using atomic manipulation on a surface, starting from the corresponding dibromoolefins. The intermediates, and all the final polyynes, were characterised using AFM, STM, and STS. The core transformation in this approach is the FBW rearrangement, initiated by the dissociation of the Br from the vinyl radical (C=C$^{\bullet}$-Br). This is the first report of any 1,2-shift triggered by atomic manipulation on a surface. In the case of **5** and **7**, we were able to image all of the vinyl radical intermediates and these radicals were found to be persistent on the surface at 5 K. We do not observe any carbene intermediates, which indicates that these FBW rearrangements proceed via a mechanism in which the 1,2-migration occurs simultaneously with cleavage of the second C-Br bond.

We demonstrated that complex molecular skeletal rearrangements can be triggered by atom manipulation. To the best of our knowledge, this is the first time that a FBW rearrangement has been observed on a surface and that a polyyne has been structurally characterised by STM and AFM. The precision of the synthesis and wealth of information provided by this approach opens new opportunities for the on-surface fabrication of novel molecules and atomic scale devices. The same methodology could result in the isolation of cyclocarbons if a suitable cyclic precursor can be successfully synthesised and sublimed onto the surface.

5.7 – Experimental data for known compounds

1,5-Diphenylpenta-1,4-diyn-3-ol – **5.1**[52]

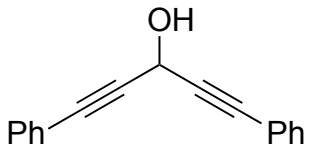

n-BuLi (1.6 M in hexanes), (33.5 mL, 54.0 mmol) was added slowly to a solution of phenylacetylene (5.40 mL, 49.0 mmol) in dry THF (100 mL) at –10 °C. After 1 h stirring at –10 °C, ethyl formate (2.00 mL, 24 mmol) was added *via* syringe over 1 h. The reaction mixture was kept at –10 °C for an additional hour and then allowed to warm to room temperature. Saturated NH_4Cl (aq)(100 mL) was added and aqueous phase was extracted with Et_2O (3x50 mL). The organic phase was washed with water (50 mL) and brine (50 mL) and dried over $MgSO_4$. Evaporation of solvent gave **5.1** as a pale brown oil, which was used in next step without further purification. As in lit.[52]

^{1}H NMR (400 MHz, $CDCl_3$) δ = 2.73 (d, ^3J = 7.4 Hz, 1H), 5.59 (d, ^3J = 7.4 Hz, 1H), 7.31–7.37 (m, 6H), 7.50 (m, 6H).
^{13}C NMR (100 MHz, $CDCl_3$) δ = 53.3, 84.6, 86.2, 122.1, 128.5, 129.0, 132.0.

1,5-Diphenylpenta-1,4-diyn-3-one – **5.2**[52]

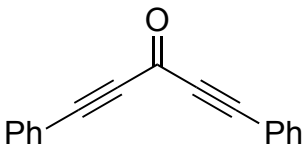

Celite (7.00 g), powdered molecular sieves 4 Å (7.00 g), and PCC (7.70 g, 35.0 mmol) were added in that order to the solution of **5.1** in CH_2Cl_2 (250 mL) at 25 °C. After 15 h, the reaction mixture was passed through a silica plug and celite and then purified by column chromatography (silica, petroleum ether/EtOAc 95:5) to yield **5.2** (2.40 g, 44% over 2 steps) as a pale yellow oil. As in lit.[52]

^{1}H NMR (400 MHz, $CDCl_3$) δ = 7.42 (t, ^3J = 7.4 Hz, 4H), 7.50 (t, ^3J = 7.5 Hz, 2H), 7.66 (d, ^3J = 7.1 Hz, 4H).
^{13}C NMR (100 MHz, $CDCl_3$) δ = 89.5, 91.8, 119.6, 128.8, 131.4, 133.5, 160.9.

(3-(Dibromomethylene)penta-1,4-diyne-1,5-diyl)dibenzene – **5(Br2)**[52]

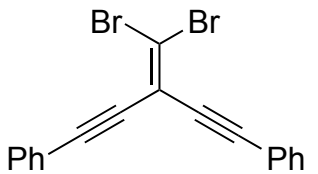

A solution of CBr_4 (5.80 g, 17.4 mmol) in CH_2Cl_2 (250 mL) was transferred to the flask of PPh_3 (9.10 g, 34.7 mmol) under a N_2 atmosphere and the resulting mixture

stirred at 20 °C for 1 h. A solution of ketone **5.2** (2.00 g, 8.70 mmol) in CH_2Cl_2 (40 mL) was added dropwise to the solution of ylid and the reaction mixture was stirred for 15 h. The reaction mixture was concentrated to ca. 50 mL and hexanes were added to precipitate the Ph_3PO as a white solid. The supernatant was decanted and passed through a silica plug. The oily residue was dissolved in MeOH (50 mL) at 50 °C and then cooled to –50 °C. The precipitate was filtered and dried under high vacuum to give **5(Br2)** (2.64 g, 79%) as a white solid. As in lit.[52]

^{1}H NMR (400 MHz, $CDCl_3$) δ = 7.33–7.40 (m, 6H), 7.55 (dd, ^3J = 7.8, 1.7 Hz, 4H).
^{13}C NMR (100 MHz, $CDCl_3$) δ = 86.2, 95.9, 122.3, 128.6, 129.4, 131.8.

Phenylpropanal – **5.3**[53]

To a stirred solution of phenylacetylene (3.00 g, 3.22 mL, 29.4 mmol) in Et_2O (75 mL) at 0 °C was added *n*-BuLi (20.1 mL, 1.6 M in hexane, 32.3 mmol) dropwise over 5 min. Then dry DMF (3.41 mL, 44.0 mmol) was added at –78 °C. The reaction mixture was allowed to warm up slowly to 0 °C over a period of 2 h. The reaction mixture was quenched at 0 °C by pouring it into a solution of ice and HCl (10%, 15 mL). After stirring for 1 h, the organic phase was separated and the aqueous phase was extracted with ether. The organic layers were combined, dried over $MgSO_4$, filtered and concentrated under reduced pressure. The residual oil was purified by column chromatography (silica, pentane/Et_2O 10:1 → 5:1) to afford aldehyde **5.3** (2.60 g, 68 %) as an orange oil. As in lit.[53]

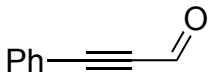

^{1}H NMR (400 MHz, $CDCl_3$) δ 9.42 (s, 1H), 7.59-7.62 (m, 2H), 7.47-7.51 (m, 1H), 7.38-7.42 (m, 2H).
^{13}C NMR (100 MHz, $CDCl_3$) δ = 176.8, 133.4, 131.3, 128.8, 119.4, 95.1, 88.5.

1-Phenyl-3-(trimethylsilyl)prop-2-yn-1-one – **5.5**[38]

n-BuLi (1.6 M in hexanes), (9.09 mL, 14.55 mmol) was added to trimethylsilylacetylene (3.20 mL, 2.20 g, 22.4 mmol) in freshly distilled THF (40 mL) at –78 °C. After stirring for 1 h at this temp, benzaldehyde (2.00 mL, 2.08 g, 19.6 mmol) was added in THF (10 mL). After stirring for 1 h and warming to room temperature, the

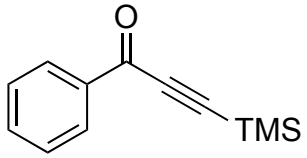

reaction was quenched by adding saturated NH_4Cl (aq)(20 mL). The mixture was extracted twice with Et_2O (50 mL), the combined org. phases were washed with H_2O and saturated NH_4Cl (aq)(20 mL), and dried over $MgSO_4$. Solvent was removed *in vacuo* and purified by passing through a silica plug (hexanes:CH_2Cl_2 1:1), which yielded the alcohol, which was immediately taken forward for oxidation.

To a solution of the alcohol, CH_2Cl_2 (150 mL) celite (4.51 g), molecular sieves (4.51 g), and PCC (6.00 g, 27.8 mmol) were added in that order and the reaction mixture stirred at 20 °C overnight. The mixture was filtered through a silica plug (CH_2Cl_2) and the solvent removed in *vacuo* to yield ketone **5.5** (3.23 g, 15.9 mmol, 81% over two steps) as a yellow oil. As in lit.[38]

^{1}H NMR (400 MHz, $CDCl_3$) δ 8.13-8.16 (m, 2H), 7.59-7.63 (m, 1H), 7.47-7.51 (m, 2H), 0.33 (s, 9H).
^{13}C NMR (100 MHz, $CDCl_3$) δ 177.8, 136.6, 134.4, 129.8, 128.7, 101.0, 89.0, -0.5.

(4,4-Dibromo-3-phenylbut-3-en-1-yn-1-yl)trimethylsilane – **5.6**[21]

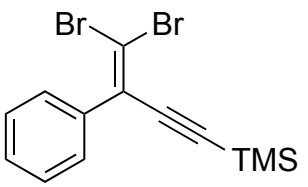

To a solution of CBr_4 (8.19 g, 24.7 mmol) in CH_2Cl_2 (30 mL) was added PPh_3 (12.9 g, 49.4 mmol) in CH_2Cl_2 (40 mL) and the resulting mixture stirred at 20 °C under a N_2 atmosphere for 1 h. A solution of ketone **5.5** (2.50 g, 12.4 mmol) in CH_2Cl_2 (30 mL) was added and the reaction was stirred for 4 h. The reaction mixture was concentrated and hexanes were added to precipitate the Ph_3PO as a white solid along with an oily residue. The supernatant was decanted and passed through a silica plug (hexane). The oily residue left in the flask was dissolved in ca. 50 mL of CH_2Cl_2 and hexane was added; the heterogeneous mixture was then decanted and the supernatant passed through a silica plug (this procedure was repeated three times). The solvent was removed *in vacuo* yielding **5.6** (2.95 g, 8.23 mmol 79%) as a yellow oil. As in lit.[21]

^{1}H NMR (400 MHz, $CDCl_3$) δ 7.43-7.46 (m, 2H), 7.35-7.41 (m, 3H), 0.21 (s, 9H).
^{13}C NMR (100 MHz, $CDCl_3$) δ 138.0, 131.2, 128.9, 128.5, 104.4, 103.5, 100.5, -0.1.

(1,1-Dibromobut-1-en-3-yn-2-yl)benzene – **5.7**[21]

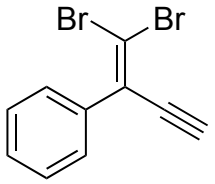

A solution of dibromoolefin **5.6** (2.00 g, 5.58 mmol) was dissolved in 1:1 MeOH/THF mixture (10 mL). K_2CO_3 (750 mg, 5.43 mmol) was added in one portion. The reaction was stirred at 25 ºC for 30 min. The reaction mixture was evaporated and then redissolved in CH_2Cl_2/petroleum ether (1:1) and passed through a silica plug. Dibromoolefin **5.7** was isolated as a colourless oil (1.37 g, 4.79 mmol, 86%). As in lit.[21]

^{1}H NMR (400 MHz, $CDCl_3$) δ 7.43-7.46 (m, 2H), 7.36-7.41 (m, 3H), 3.61 (s, 1H).
^{13}C NMR (100 MHz, $CDCl_3$) δ 137.9, 129.0, 128.7, 128.6, 101.1, 86.9, 82.9.

1-Phenyl-5-(triisopropylsilyl)penta-1,4-diyn-3-ol – **5.8**[54]

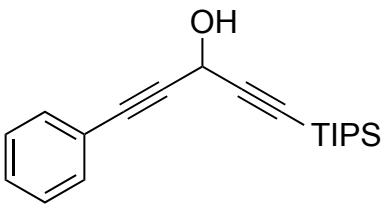

n-BuLi (1.6 M in hexanes), (9.09 mL, 14.6 mmol) was added to phenylacetylene (1.52 ml, 14.4 mmol) in THF (40 ml) at –78 °C. After stirring for 1 h at –78 °C, aldehyde **2.1** (3.00 g, 14.3 mmol) in THF (10 mL) was added. After stirring for 1 h, the reaction was quenched by adding saturated NH_4Cl (aq)(20 mL). The mixture was extracted twice with Et_2O (50 mL), the combined org. phases were washed with H_2O (20 mL), and dried over $MgSO_4$. Evaporation *in vacuo* and passing through a silica plug yielded **5.8** as a yellow oil (3.27 g, 10.47 mmol, 74%). As in lit.[54]

^{1}H NMR (400 MHz, $CDCl_3$) δ 7.45 (m, 2H), 7.32 (m, 3H), 5.34 (d, ^3J = 7.3 Hz), 2.23 (d, ^3J = 7.7 Hz), 1.08-1.12 (m, 21H).
^{13}C NMR (100 MHz, $CDCl_3$) δ 132.1, 129.0, 128.6, 122.3, 104.2, 86.6, 86.5, 84.4, 53.4, 19.8, 11.4.

1-Phenyl-5-(triisopropylsilyl)penta-1,4-diyn-3-one – **5.9**[54]

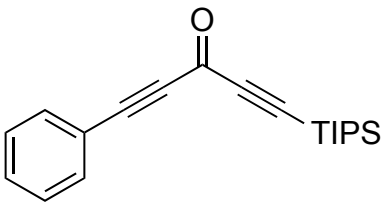

To a solution of alcohol **5.8** (3.37 g, 10.5 mmol) in CH_2Cl_2 (150 mL) celite (4.51 g), molecular sieves (4.51 g), and PCC (4.51 g, 21.0 mmol) were added in that order and the reaction mixture stirred at 20 °C

overnight. The mixture was passed through a silica plug (CH_2Cl_2) and the solvent removed in *vacuo* to yield ketone **5.9** (2.90 g, 9.34 mmol, 89%) as a yellow oil. As in lit.[54]

^{1}H NMR (400 MHz, $CDCl_3$) δ 7.50-7.52 (m, 2H), 7.32-7.38 (m, 3H), 1.09-1.13 (s, 21H).
^{13}C NMR (100 MHz, $CDCl_3$) δ 160.6, 133.6, 131.5, 128.9, 119.8, 105.4, 97.9, 91.7, 89.8, 18.7, 11.3.

(Dibromomethylene)-5-phenyl,1,4-diyn-1-yltriisopropylsilane – **5.10**[54]

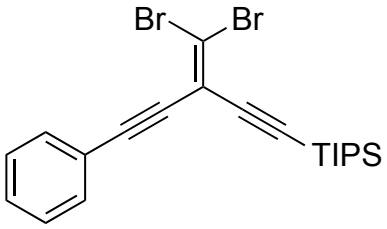

To a solution of CBr_4 (5.13 g, 15.4 mmol) in CH_2Cl_2 (30 mL) was added PPh_3 (8.11 g, 30.9 mmol) in CH_2Cl_2 (40 mL) and the resulting mixture stirred at 20 °C under a N_2 atmosphere for 1 h. A solution of ketone **5.9** (2.40 g, 7.73 mmol) in CH_2Cl_2 (30 mL) was added and the reaction was stirred for 4 h. The reaction mixture was concentrated and hexanes were added to precipitate the Ph_3PO as a white solid along with an oily residue. The supernatant was decanted and passed through a silica plug (hexane). The oily residue left in the flask was dissolved in ca. 50 mL of CH_2Cl_2 and hexane was added; the heterogeneous mixture was passed through a silica plug (this procedure was repeated three times). The solvent was removed *in vacuo* yielding dibromoolefin **5.10** (2.84 g, 6.09 mmol, 79%) as a yellow oil. As in lit.[54]

^{1}H NMR (400 MHz, $CDCl_3$) δ 7.50-7.52 (m, 2H), 7.32-7.38 (m, 3H), 1.09-1.13 (s, 21H).
^{13}C NMR (100 MHz, $CDCl_3$) δ 131.8, 129.2, 128.7, 122.7, 114.7 108.6, 102.2, 99.2, 95.7, 86.3, 18.8, 11.3.

(3-(Dibromomethylene)penta-1,4-diyn-1-yl)benzene – **5.11**[37]

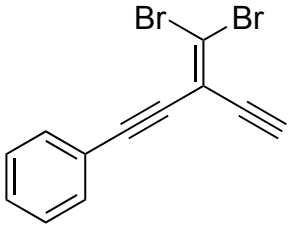

To a solution of dibromoolefin **5.10** (0.500 g, 1.07 mmol) in wet THF (20 mL THF and 10 μL H_2O) was added TBAF (1.07 mL, 1.0 M in THF, 1.07 mmol) dropwise. The solution was stirred at 0 °C for 30 min. The reaction was quenched

with saturated NH_4Cl (aq)(10 mL) and extracted with hexanes (20 mL). The organic phase was washed with H_2O (10 mL), brine (10 mL), and dried over $MgSO_4$. The solvent was removed *in vacuo* and the crude product passed through a silica plug (Hexane:CH_2Cl_2 1:1) to yield dibromoolefin **5.11** (0.330 g, 1.06 mmol, 99%) as a yellow oil. As in lit.[37]

^{1}H NMR (400 MHz, $CDCl_3$) δ 7.50-7.53 (m, 2H), 7.31-7.39 (m, 3H), 3.52 (s, 1H).
^{13}C NMR (100 MHz, $CDCl_3$) δ 131.8, 129.6, 128.7, 113.2 108.2, 102.2, 96.4, 86.1, 84.2, 80.4.

3,8-Bis(dibromomethylene)-1,10-diphenyl-deca-1,4,6,9-tetrayne – **7(Br2)**[37]

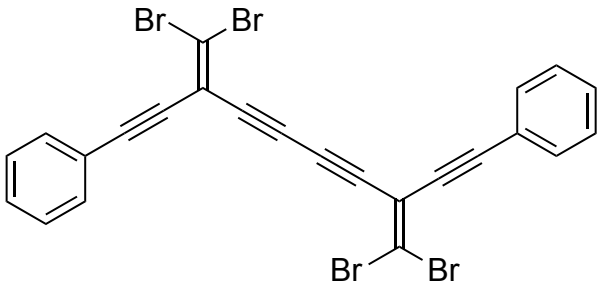

Dibromoolefin **5.11** (600 mg, 1.93 mmol) was dissolved in CH_2Cl_2 (50 mL) and CuCl (191 mg, 1.93 mmol) was added. This was stirred vigorously in air and TMEDA (0.21 g, 0.27 mL, 1.83 mmol) was added in one portion. The progress of the reaction was monitored by TLC and quenched after 2 h by passing through a silica plug (100 mL). The reaction mixture was purified by column chromatography (silica, CH_2Cl_2:Hexane 1:2) to give **7(Br2)** (550 mg, 92%) as a a light yellow solid. As in lit.[37]

^{1}H NMR (400 MHz, $CDCl_3$) δ 7.52-7.55 (m, 4H), 7.33-7.39 (m, 6H).
^{13}C NMR (100 MHz, $CDCl_3$) δ 131.9, 129.7, 128.7, 122.0, 113.6, 111.9, 97.1, 85.1, 80.7, 79.6.

3-Phenylpropiolic acid - **5.12**[55]

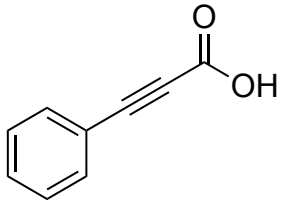

A solution of phenylacetylene (2.00 mL, 1.86 g, 18.2 mmol) in THF (100 mL) was cooled under N_2 to 0 °C. A solution of MeLi (2.2 M in diethyl ether, 10.8 mL, 23.6 mmol) was added and the mixture was stirred for 1 h and then cooled to –78 °C and CO_2 gas was bubbled into the solution for 1 h. The reaction mixture was quenched by the slow addition of ~2.0 M aqueous $KHSO_4$ (30 mL), warmed to 20 °C,

and extracted with EtOAc. The combined organic layers were washed with brine, dried ($MgSO_4$) and concentrated to a yellow oil that was diluted with toluene (50 mL), passed through a silica plug and eluted with EtOAc (300 mL). The filtrate was concentrated to afford 3-phenylpropiolic acid **5.12** (1.55 g, 10.6 mmol, 58%) as a yellow oil that crystallised to a pale yellow solid *in vacuo*. As in lit.[55]

^{1}H NMR (400 MHz, $CDCl_3$) δ 10.32 (bs, 1H), 7.60-7.62 (m, 2H), 7.46-7.48 (m, 1H), 7.37-7.41 (m, 2H).
^{13}C NMR (100 MHz, $CDCl_3$) δ 158.1, 133.5, 131.3, 128.9, 119.4, 89.1, 80.3.

1-Phenyl-7-(trimethylsilyl)hepta-1,4,6-triyn-3-one - **5.13**[37]

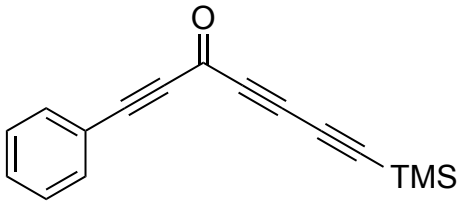

Acid **5.12** (1.00 g, 6.84 mmol) was dissolved in $SOCl_2$ (1.92 mL, 47.9 mmol) in a flask equipped with $CaCl_2$ drying tube and stirred at 20 °C for 20 h. The $SOCl_2$ was removed *in vacuo* and 1,4-bis(trimethylsilyl)butadiyne (1.39 g, 7.18 mmol) added and the resulting mixture was dissolved in dry CH_2Cl_2 (25 mL). To this solution was added slowly $AlCl_3$ (1.09 g, 8.20 mmol) at 0 °C under a N_2 atmosphere and then stirred at 0 °C for 4 h. The reaction was quenched with ice/HCl (10%) (100 mL) at 0 °C and allowed to warm to 20 °C The organic layer was extracted with Et_2O (150 mL), washed with brine (2 × 50 mL) and dried over $MgSO_4$. The solvent was removed *in vacuo*, the crude product passed through a silica plug (hexane: DCM 1:1) and the solvent removed *in vacuo* to yield crude ketone **5.13** (1.09 g, 64%) as a brown oil which decomposed slowly. As in lit.[37]

^{1}H NMR (400 MHz, $CDCl_3$) δ 7.61-7.63 (m, 2H), 7.48-7.50 (m, 1H), 7.38-7.42 (m, 2H), 0.26 (s, 9H).
^{13}C NMR (100 MHz, $CDCl_3$) δ 159.7, 133.7, 131.7, 128.9, 119.4, 99.5, 92.9, 89.4, 86.0, 76.0, 74.3, – 0.5.

(5-(Dibromomethylene)-7-phenylhepta-1,3,6-triyn-1-yl)trimethylsilane - **5.14**[37]

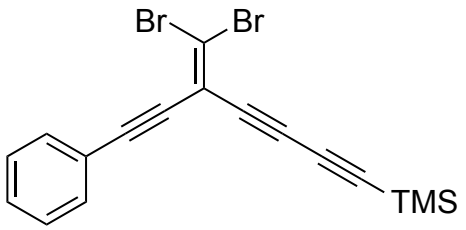

To a solution of CBr_4 (2.91 g, 8.77 mmol) in CH_2Cl_2 (200 mL) was added PPh_3 (4.60 g, 17.6 mmol) and the mixture stirred for 1 h under a N_2 atmosphere. The ketone **5.13** (1.10 g, 4.38 mmol) was dissolved in CH_2Cl_2 (50 mL), added dropwise, and the mixture stirred at 20 °C for 2 h under a N_2 atmosphere. The reaction mixture was concentrated *in vacuo* to ca. 50 mL and then hexanes were added to precipitate the phosphine salts as a white solid along with an oily residue. The supernatant was decanted and filtered through a silica plug. The oily residue left in the flask was dissolved in minimal CH_2Cl_2 and hexanes were added; the heterogeneous mixture was then decanted and the supernatant filtered through silica (this procedure was repeated three times). The solvent was removed *in vacuo* and the crude product purified by column chromatography (silica, hexanes) to yield dibromoolefin **5.14** (1.25 g, 70%) as an off-white solid. As in lit.[37]

^{1}H NMR (400 MHz, $CDCl_3$) δ 7.48-7.52 (m, 2H), 7.31-7.39 (m, 3H), 0.23 (s, 9H). **^{13}C NMR** (100MHz, $CDCl_3$) δ 131.9, 129.6, 128.7, 122.1, 96.7, 95.4, 87.4, 85.4, 80.5, 72.4,– 0.3.

3,12-Bis(dibromoethylene)-1,14-diphenyl-tetradeca-1,4,6,8,10,13-heaxyne - **8(Br2)**[37]

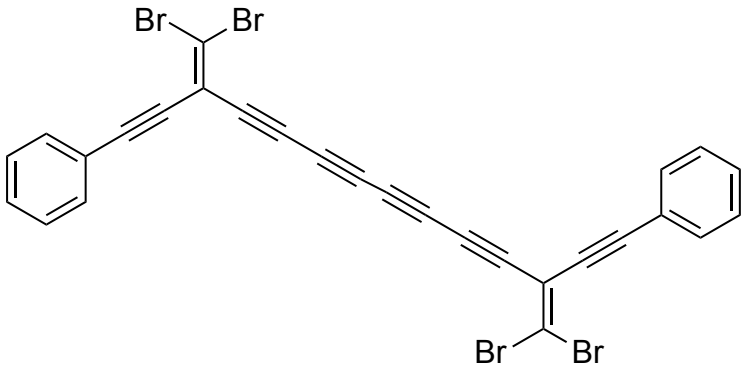

To a solution of dibromoolefin **5.14** (585 mg, 1.45 mmol) in THF (10 mL)/MeOH (10 mL) was added K_2CO_3 (37.6 mg, 0.272 mmol). The reaction mixture was stirred for 30 mins then passed through a silica plug yielding the dibromoolefin **5.15** as a yellow oil. Dibromoolefin **5.15** was immediately dissolved in CH_2Cl_2 (50 mL) and CuCl (143 mg, 1.45 mmol) was added. This was stirred vigorously in air and TMEDA (0.162 g, 0.210 mL, 1.37 mmol) was added in one portion. The progress of the reaction was

monitored by TLC and quenched after 2 h by passing through a silica plug (100 mL). The reaction mixture was purified by column chromatography (silica, CH_2Cl_2:Hexane 1:2) to give **8(Br2)** (200 mg, 44%) as an orange solid. As in lit.[37]

^{1}H NMR (400 MHz, $CDCl_3$) δ 7.50-7.53 (m, 4H), 7.33-7.39 (m, 6H).
^{13}C NMR (100 MHz, $CDCl_3$) δ 131.7, 129.6, 128.5, 121.6, 113.4, 113.9, 97.4, 84.6, 80.1, 73.9, 70.4, 64.7.

5.8 – Experimental data for novel compounds

(Perbromoocta-1,7-dien-3,5-diyne-2,7-diyl)dibenzene – **6(Br4)**

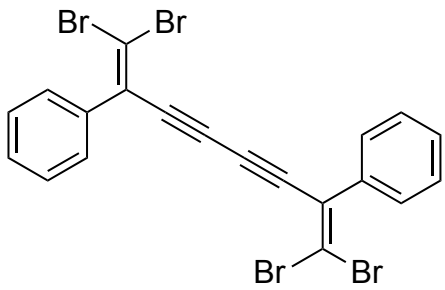

Dibromoolefin **5.7** (1.30 g, 4.54 mmol) was dissolved in CH_2Cl_2 (50 mL) and CuCl (260 mg, 2.63 mmol) was added. The mixture was stirred vigorously in air and TMEDA (0.395 mL, 2.63 mmol) was added in one portion. The progress of the reaction was monitored by TLC and quenched after 2 h by addition of water. The organic layer was washed with water (3 × 100 mL) and dried with $MgSO_4$. The reaction mixture was purified by column chromatography (silica, CH_2Cl_2 : hexane, 1:2) to yield **6(Br4)** (870 mg, 1.53 mmol, 58%) as a light yellow solid.

^{1}H NMR (500 MHz, $CDCl_3$) δ 7.36–7.40 (m, 10H, Ar-*H*).
^{13}C NMR (125 MHz, $CDCl_3$) δ 138.0, 131.2, 128.9, 128.5, 104.4, 103.5, 100.5, –0.1
EI HRMS *m/z* 569.7467 (Calc. for $C_{20}H_{10}{}^{79}Br_2{}^{81}Br_2$ 569.7475), 567.7483 (Calc. for $C_{20}H_{10}{}^{79}Br_3{}^{81}Br$ 567.7496), 571.7455 (Calc. for $C_{20}H_{10}{}^{79}Br^{81}Br_3$ 571.7455).

(4,4-Dichloro-3-phenylbut-3-en-1-yn-1-yl)trimethylsilane - **5.15**

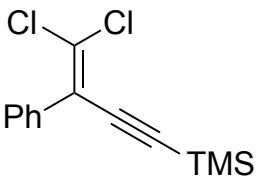

PPh_3 (1.16 g, 4.44 mmol) and CCl_4 (0.20 mL, 2.20 mmol) were added to a solution of ketone **5.5** (0.225 g, 1.11 mmol) in anhydrous CH_3CN (20 mL) at 0 °C. After stirring for 2 h at 25 °C, the orange solution was diluted with diethyl ether, washed with water and with brine, dried over $MgSO_4$, and evaporated to dryness.

After purification by column chromatography (silica, EtOAc/pentane, 5:95), the dichloroolefin **5.15** was isolated as a colorless oil (260 mg, 88%)

^{1}H NMR (400 MHz, $CDCl_3$): δ 7.53-7.49 (m, 2H, Ar-*H*), 7.42-7.36 (m, 3H, Ar-*H*), 0.26 (s, 9H, ($SiCH_3$)$_3$).
^{13}C NMR (100 MHz, $CDCl_3$): δ 135.8, 129.3, 128.8, 128.7, 128.5, 124.0, 104.4, 101.7, 0.1.

(Perchloroocta-1,7-dien-3,5-diyne-2,7-diyl)dibenzene - **6(Cl4)**

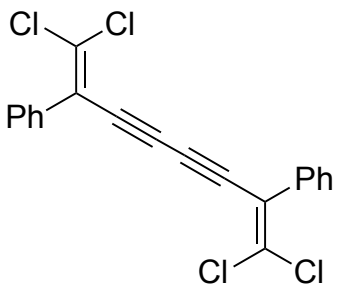

To a solution of dichloroolefin **5.15** (150 mg, 0.557 mmol) in THF (10 mL)/MeOH (10 mL) was added K_2CO_3 (77.0 mg, 0.557 mmol). The reaction mixture was stirred for 30 mins then passed through a silica plug (hexanes) yielding the deprotected dichloroolefin as a white solid. This was immediately dissolved in CH_2Cl_2 (50 mL) and CuCl (55 mg, 0.557 mmol) was added. This was stirred vigorously in air and TMEDA (0.061 g, 0.078 mL, 0.53 mmol) was added in one portion. The progress of the reaction was monitored by TLC and quenched after 2 h by passing through a silica plug (hexane). The reaction mixture was purified by column chromatography (silica, CH_2Cl_2:Hexane 1:2) to yield dichloroolefin **6(Cl4)** (104 mg, 95%) as a white solid.

^{1}H NMR (400 MHz, $CDCl_3$) δ 7.34-7.52 (m, 10H, Ar-*H*).
^{13}C NMR (100 MHz, $CDCl_3$) δ 134.9, 131.4, 129.2, 129.0, 128.8, 123.2, 81.7, 81.6.
EI HRMS: *m*/*z* 392.958 (Calc. for $C_{20}H_{10}{}^{35}Cl_3{}^{37}Cl$ 392.958), 390.960 (Calc. for $C_{20}H_{10}{}^{35}Cl_4$ 390.960), 394.955 (Calc. for $C_{20}H_{10}{}^{35}Cl_2{}^{37}Cl_2$ 395.955).

5.9 – References

(1) Pavliček, N.; Schuler, B.; Collazos, S.; Moll, N.; Pérez, D.; Guitián, E.; Meyer, G.; Peña, D.; Gross, L. *Nat. Chem.* **2015**, *7*, 623.
(2) Schuler, B.; Fatayer, S.; Mohn, F.; Moll, N.; Pavliček, N.; Meyer, G.; Peña, D.; Gross, L. *Nat. Chem.* **2016**, *8*, 220.
(3) Pavliček, N.; Mistry, A.; Majzik, Z.; Moll, N.; Meyer, G.; Fox, D. J.; Gross, L. *Nat. Nanotechnol.* **2017**, *12*.
(4) Binnig, G.; Rohrer, H.; Gerber, C.; Weibel, E. *Appl. Phys. Lett.* **1982**, *40*, 178.
(5) Stipe; Rezaei; Ho. *Science* **1998**, *280*, 1732.
(6) Lee, H. J.; Ho, W. *Science* **1999**, *286*, 1719.
(7) Lauhon, L. J.; Ho, W. *J. Phys. Chem. A* **2000**, *104*, 2463.
(8) Binnig, G.; Quate, C. F. *Phys. Rev. Lett.* **1986**, *56*, 930.
(9) Gross, L.; Wang, Z. L.; Ugarte, D.; Mohn, F.; Moll, N.; Heer, W. a; Vincent, P.; Liljeroth, P.; Journet, C.; Meyer, G.; Binh, V. T.; Poot, M.; Zant, H. S. J. Van Der; Aguasca, A.; Bachtold, A.; Kim, K.; Zettl, A.; Hung, P.; Postma, H. W. C.; Bockrath, M.; Blase, X.; Roche, S. *Science* **2009**, *325*, 1110.
(10) Schuler, B.; Meyer, G.; Peña, D.; Mullins, O. C.; Gross, L. *J. Am. Chem. Soc.* **2015**, *137*, 9870.
(11) Schuler, B.; Zhang, Y.; Collazos, S.; Fatayer, S.; Meyer, G.; Pérez, D.; Guitián, E.; Harper, M. R.; Kushnerick, J. D.; Peña, D.; Gross, L. *Chem. Sci.* **2017**, *8*, 2315.
(12) Moll, N.; Gross, L.; Mohn, F.; Curioni, A.; Meyer, G. *New J. Phys.* **2010**, *12*, 125020.
(13) Ellner, M.; Pavlicek, N.; Pou, P.; Schuler, B.; Moll, N.; Meyer, G.; Gross, L.; Perez, R. *Nano Lett.* **2016**, *16*, 1974.
(14) Kim, Y.; Komeda, T.; Kawai, M. *Phys. Rev. Lett.* **2002**, *89*, 126104.
(15) Hla, S.-W.; Bartels, L.; Meyer, G.; Rieder, K.-H. *Phys. Rev. Lett.* **2000**, *85*, 2777.
(16) Fritsch, P. *Liebigs Ann. Chem.* **1894**, *272*, 319.
(17) Buttenberg, W. P. *Liebigs Ann. Chem* **1894**, *272*, 324.
(18) Wiechell, H. Von. *Liebigs Ann. Chem.* **1894**, *272*, 337.
(19) Corey, E. J.; Fuchs, P. L. *Tetrahedron Lett.* **1972**, No. 36, 3769.
(20) Eisler, S.; Tykwinski, R. R. *J. Am. Chem. Soc.* **2000**, *122*, 10736.
(21) Morisaki, Y.; Luu, T.; Tykwinski, R. R. *Org. Lett.* **2006**, *8*, 689.
(22) Luu, T.; Morisaki, Y.; Cunningham, N.; Tykwinski, R. R. *J. Org. Chem.* **2007**, *72*, 9622.
(23) Jahnke, E.; Tykwinski, R. R. *Chem. Commun.* **2010**, *46*, 3235.
(24) Stang, P. J. *Chem. Rev.* **1978**, *78*, 383.
(25) Pritchard, J, G, Bothner-By, A, A. *J. Phys. Chem.* **1960**, *64*, 1271.
(26) Knorr, R. *Chem. Rev.* **2004**, *104*, 3795.
(27) Bichler, P.; Chalifoux, W. A.; Eisler, S.; Shi Shun, A. L. K.; Chernick, E. T.; Tykwinski, R. R. *Org. Lett.* **2009**, *11*, 519.
(28) Sahu, B.; Muruganantham, R.; Namboothiri, I. N. N. *Eur. J. Org. Chem* **2007**, *2007*, 2477.
(29) Bothner-By, A. *J. Am. Chem. Soc.* **1955**, *77*, 3293.
(30) Curtin, D. Y, Flynn, E.W, Nystrom, R. *J. Am. Chem. Soc.* **1958**, *80*, 4599.
(31) Kobrich, G, Reitz, G, Schumacher, U. *Chem. Ber* **1972**, *105*, 1674.
(32) Kunishima, M.; Hioki, K.; Ohara, T.; Tani, S. *J. Chem. Soc.-Chem. Commun.* **1992**, *1992*, 219.

(33) Giessibl, F. J. *Appl. Phys. Lett.* **1998**, *73*, 3956.
(34) Pavliček, N.; Gross, L. *Nat. Rev. Chem.* **2017**, *1* (5), 1.
(35) Mohn, F.; Schuler, B.; Gross, L.; Meyer, G. *Appl. Phys. Lett.* **2013**, *102*, 1.
(36) Schuler, B.; Liu, W.; Tkatchenko, A.; Moll, N.; Meyer, G.; Mistry, A.; Fox, D.; Gross, L. *Phys. Rev. Lett.* **2013**, *111*, 1.
(37) Luu, T.; Elliott, E.; Slepkov, A. D.; Eisler, S.; McDonald, R.; Hegmann, F. A.; Tykwinski, R. R. *Org. Lett.* **2005**, *7*, 51.
(38) Tykwinski, R. R.; Luu, T. *Synth.* **2012**, *44*, 1915.
(39) Hay, A. S. *J. Org. Chem.* **1962**, *27*, 3320.
(40) Naveen; Babu, S. A.; Kaur, G.; Aslam, N. A.; Karanam, M. *RSC Adv.* **2014**, *4*, 18904.
(41) Palatinus, L.; Van Der Lee, A. *J. Appl. Crystallogr.* **2008**, *41*, 975.
(42) Palatinus, L. *Acta Crystallogr. Sect. B Struct. Sci. Cryst. Eng. Mater.* **2013**, *69*, 1.
(43) Palatinus, L.; Chapuis, G. *J. Appl. Crystallogr.* **2007**, *40*, 786.
(44) Hoye, T. R.; Baire, B.; Niu, D.; Willoughby, P. H.; Woods, B. P. *Nature* **2012**, *490*, 208.
(45) Oteyza, D. G. De; Gorman, P.; Chen, Y.-C.; Wickenburg, S.; Riss, A.; Mowbray, D. J.; Etkin, G.; Pedramrazi, Z.; Tsai, H.-Z.; Rubio, A.; Crommie, M. F.; Fischer, F. R. **2014**, *1434*, 1434.
(46) Repp, J.; Meyer, G.; Stojković, S. M.; Gourdon, A.; Joachim, C. *Phys. Rev. Lett.* **2005**, *94* (26803), 1.
(47) Galli, C.; Guarnieri, A.; Koch, H.; Mencarelli, P.; Rappoport, Z. **1997**, *3263*, 4072.
(48) Szafert, S.; Gladysz, J. A. *Chem. Rev.* **2006**, *106*, 1.
(49) Pavliček, N.; Swart, I.; Niedenführ, J.; Meyer, G.; Repp, J. *Phys. Rev. Lett.* **2013**, *110* (136101), 1.
(50) Burton, G.; Elder, J. S.; Fell, S. C. M.; Stachulski, A. V. *Tetrahedron Lett.* **1988**, *29*, 3003.
(51) Maraval, V.; Leroyer, L.; Harano, A.; Barthes, C.; Saquet, A.; Duhayon, C.; Shinmyozu, T.; Chauvin, R. *Chem. Eur. J.* **2011**, *17*, 5086.
(52) Philp, D.; Gramlich, V.; Seiler, P.; Diederich, F. *J. Chem. Soc. Perkin Trans* **1995**, *2*, 875.
(53) Hayashi, R.; Mutoh, Y.; Kasama, T.; Saito, S. *J. Org. Chem.* **2015**, *80*, 7536.
(54) Auffrant, A.; Diederich, F.; Boudon, C.; Gisselbrecht, J. P.; Gross, M. *Helv. Chim. Acta* **2004**, *87*, 3085.
(55) Parsons, P. J.; Jones, D. R.; Padgham, A. C.; Allen, L. A. T.; Penkett, C. S.; Green, R. A.; White, A. J. P. *Chem. Eur. J.* **2016**, *22*, 3981.

Chapter 6

Conclusions and future work

6.1. Conclusions 198

6.2. Future Work 199

6.3. References 203

Chapter 6 – Conclusions and future work

6.1 - Conclusions

The synthesis of pristine cyclo[*n*]carbons from the corresponding masked precursors has been attempted many times by other research groups (**Section 1.2.2**).[1–4] However, the isolation or experimental analysis of these *sp*-allotropes of carbon has proven extremely difficult due to their inherent instability. New methods of stabilisation offer the best chance of isolating cyclocarbons and in doing so, successfully overcoming the challenges these molecules impose. This thesis summarises a range of important developments in the pursuit of cyclocarbons. We have prearranged extended *sp*-hybridised π-systems around a central hub, unmasked MAEs in unprecedented systems, prepared the first ever rotaxane with terminal acetylene stoppers and designed precursors for the controlled on-surface synthesis of polyynes.

The previous research in carbon-rich chemistry was reviewed in **Chapter 1**. The history of carbon-rich molecules, experimental and theoretical studies of cyclocarbons and the previous work in 'stabilisation by encapsulation' were evaluated to guide our efforts at stabilising and synthesising cyclocarbons.

In **Chapter 2** we investigated the arrangement of polyynes around a central porphyrin hub. For the first time, polyynes were arranged around a central core in the synthesised porphyrin-polyyne [3]- and [5]rotaxanes, paving the way for a template-directed synthesis of polycatenane cyclocarbons.[5] If a masked alkyne equivalent (MAE) group was used in conjunction with this strategy, the template effect of the central hub could be used to favour cyclisation over polymerisation, as in Anderson's porphyrin nanorings.[6,7]

In **Chapter 3** the chemistry of the dicobalt tetracarbonyl MAE was studied. Extended triisopropylsilyl end-capped polyynes (including up to 20 contiguous *sp*-hybridised carbon atoms) were prepared from the corresponding tetracobalt complexes by removing the masking dicobalt tetracarbonyl diphenylphosphinomethane moieties. Alkyne unmasking was achieved under mild conditions with elemental iodine at room temperature, making it possible to obtain fragile polyynes in unparalleled yields. The electronic and magnetic effects of the dicobalt MAE on the conjugated alkyne π-

system were probed *via* IR, UV-vis and NMR spectroscopies, DFT calculations and X-ray crystallography. Our efforts to prepare rotaxanes were unsuccessful so far. However, further work in this area is of the utmost importance, due to the facile unmasking of this MAE.

In **Chapter 4** a series of phenanthroline macrocycles for forming rotaxanes with small MAE groups was carefully designed. This family of macrocycles will be used in future synthetic efforts to facilitate the use of small MAEs in rotaxane formation. The very first rotaxane with terminal acetylene containing stoppers was also prepared using the dibromoolefin MAE, which is a critical hurdle in this project. It may be possible to prepare dibromoolefin catenanes with suitable conditions. However, conditions were not found that yielded cyclic structures during the period of this work.

In **Chapter 5** a series of intelligently designed molecules were synthesised to establish the scope of newly developed on-surface synthesis of polyynes *via* the Fritsch-Buttenberg-Wiechell rearrangement. We show that single polyyne molecules can be fabricated on a surface at low temperature from dibromoolefins using atomic manipulation and studied by scanning probe microscopic methods. This work is the first controlled skeletal rearrangement on a surface and represents a significant breakthrough in on-surface synthesis. We visualise the HOMO and LUMO of polyynes for the first time, demonstrating the power of this technique for probing electronic structure. This method also has great potential for future synthesis of carbyne and cyclocarbons and is currently the object of further research. At the time of writing, we are yet to successfully isolate expanded perhaloradialenes. However, continued efforts to prepare these cyclocarbon precursors are of critical importance.

6.2 – Future Work

Our findings in this thesis have revealed promising avenues for continued research in the pursuit of cyclocarbons. We believe that the ease of unmasking the dicobalt group justifies the reopening of rotaxanation trials on these substrates. The unmasking conditions for this MAE are milder than any other known alternative. The instability of cyclocarbons make this result highly significant. A cobalt carbonyl cyclocarbon

catenane **6.4** has a greater probability of successful unmasking than an alternative masked catenane which requires harsher unmasking conditions (**Scheme 6.1**).

Active-metal templated homocoupling reactions require an oxidant. The most commonly used oxidant for this reaction is elemental iodine, which unmasks the dicobalt MAE. Therefore, a reductive Cadiot-Chodkiewicz cross coupling with a brominated compound **6.2** could be used to circumvent this problem (**Scheme 6.1**).[8,9] We briefly attempted to functionalise cobalt substrates with bromine, but further research in this area could aid the pursuit of cobalt-masked rotaxanes and catenanes. Alternatively other acetylene cross-coupling methods could be applied.

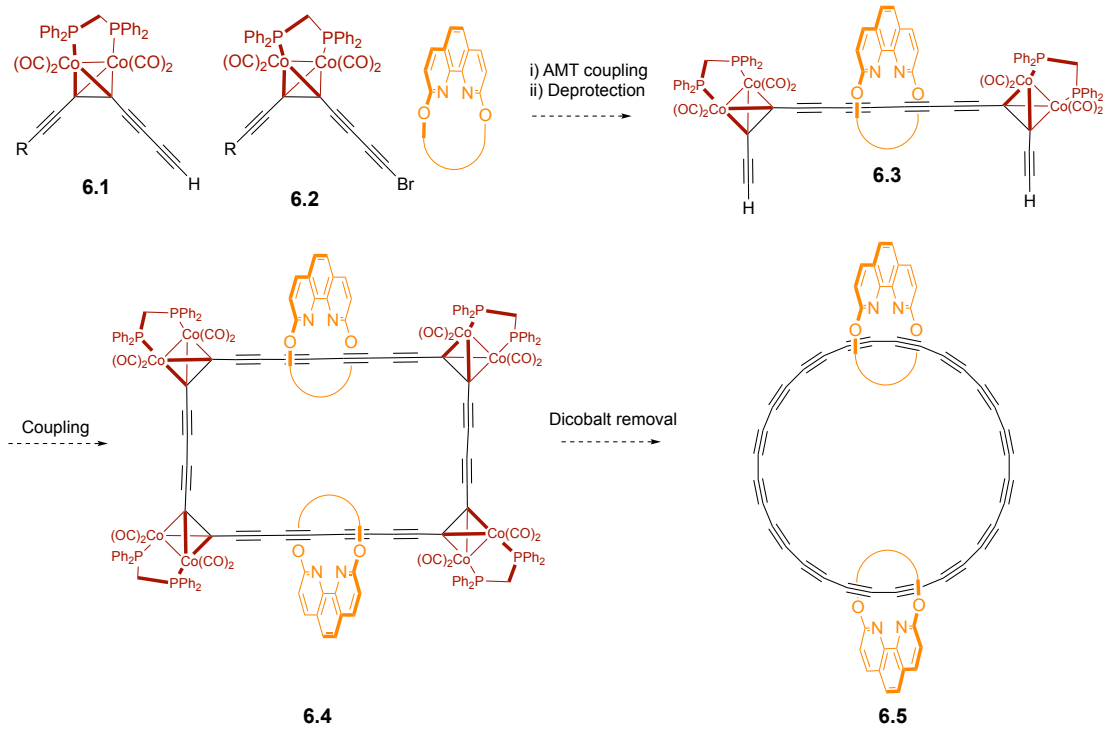

Scheme 6.1. Proposed route to cyclocarbons *via* Cadiot-Chodkiewicz coupling.

Several other MAEs remain unexplored. We were recently sent a sample of 11,12-dichloro[4.3.2]propella-1,3,11-triene **6.6** by Professor Yoshito Tobe from Osaka University (**Scheme 6.2**).[3] We performed some preliminary experiments using this MAE and isolated butadiyne **6.9**. In future, we plan to screen this oligoyne with active metal template rotaxane formation conditions. This MAE offers promise for cyclocarbon catenane unmasking due to the reliability of its removal in numerous projects and the possibility of doing photochemical reactions at low temperatures.[10–12]

The UV light that triggers unmasking could leave an unmasked cyclocarbon catenane intact and prove to be better tolerated than chemical unmasking methods.

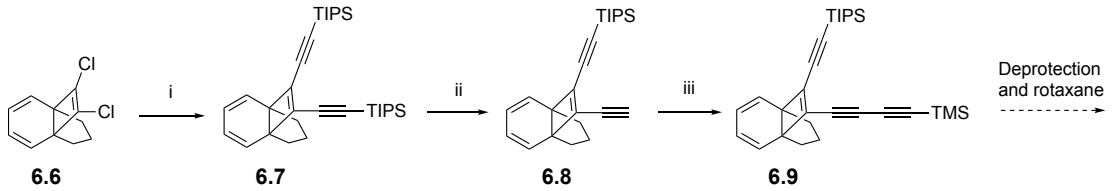

Scheme 6.2. Rotaxane precursor synthesis. i) $Pd(PPh_3)_4$, $BuNH_2$, TIPS-acetylene, CuI, THF, 25 °C, 18 h, 99%. ii) TBAF (1 eq.), $CHCl_3$, EtOH (1%), 35% iii) CuCl, TMEDA, TMS-acetylene, CH_2Cl_2, 25 °C, 3h, 89%.

Recently, Thamattoor and coworkers have studied the benzylidene-phenylacetylene rearrangement in functionalised phenanthrenes.[13,14] This moiety offers promise for use in cyclocarbon synthesis for several reasons. The large steric bulk, short synthetic pathway (**Scheme 6.3**) and facile photochemical rearrangement make it very suitable for application in cyclocarbon catenane synthesis. This MAE offers a short, scalable synthetic route for preparing oligoynes. If rotaxane formation is possible with this group it provides a novel route towards masked cyclocarbon catenanes.

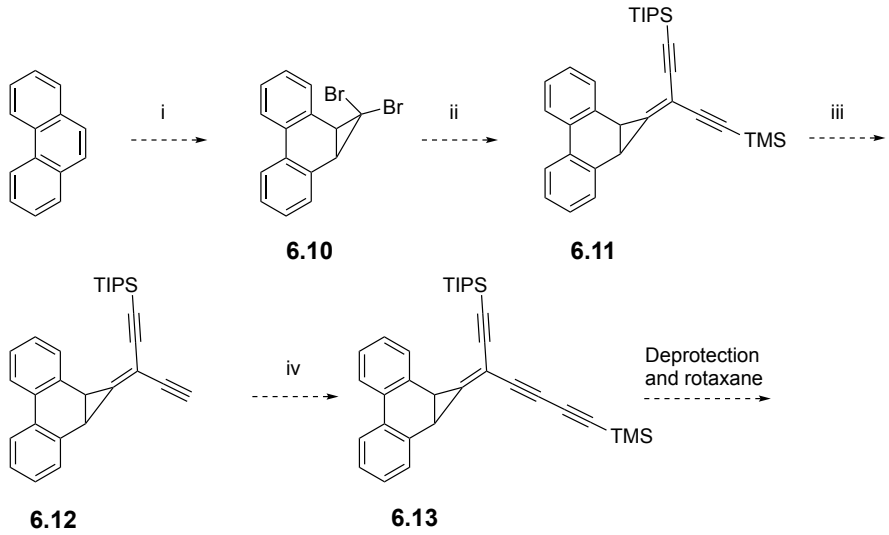

Scheme 6.3. Planned route using the functionalised phenanthrene MAE. i) $CHBr_3$, CH_2Cl_2, NaOH, $PhCH_2NEt_3Cl$ ii) *n*–BuLi, –100 °C, then ketone **3.5**, -70 °C, then TsCl, THF iii) TBAF (1 M), $CHCl_3$, EtOH (1%) iv) CuCl, TMEDA, TMS-acetylene, CH_2Cl_2, 25 °C.

Finally, we plan to continue to develop the controlled on-surface synthesis of carbon rich compounds. Our preparation of polyynes from dibromoolefins was highly successful and led us to believe the same rearrangement would be possible on

perbromoradialenes. Our initial synthetic attempts towards perbromoradialenes have been unsuccessful. However, continued synthetic efforts in this area are ongoing. We believe that the poor volatility and stability of these compounds could be an issue and that dichloroolefin analogues could provide an alternative. As detailed in **Section 5.5**, a dichlorooolefin tetrayne precursor **6(Cl4)** was synthesised. Experiments are currently being performed on this compound.

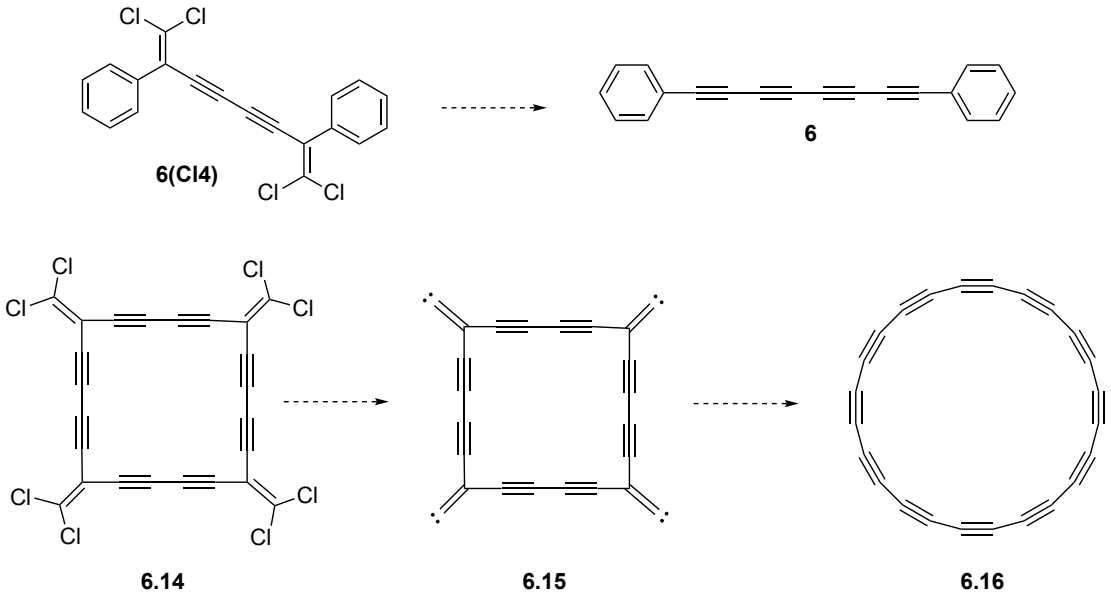

Scheme 6.4. Synthesis of polyynes and cyclocarbons *via* dichloroolefin precursors

In summary, novel methods of stabilising *sp*-carbon chains hold enormous promise for the isolation of cyclocarbons and other carbon-rich compounds. The wait for cyclocarbons is nearly over.

6.3 - References

(1) Rubin, Y.; Diederich, F. *J. Am. Chem. Soc.* **1989**, *11*, 6870.
(2) Rubin, Y.; Knobler, C. B.; Diederich, F. *J. Am. Chem. Soc.* **1990**, *12*, 4966.
(3) Tobe, Y.; Fujii, T.; Matsumoto, H.; Tsumuraya, K.; Noguchi, D.; Nakagawa, N.; Sonoda, M.; Naemura, K. *J. Am. Chem. Soc.* **2000**, *122*, 1762.
(4) Adamson, G. A.; Rees, C. W. *J. Chem. Soc. Perkin Trans* **1996**, *2*, 1535.
(5) Kohn, D. R.; Movsisyan, L. D.; Thompson, A. L.; Anderson, H. L. *Org. Lett.* **2017**, *19*, 348.
(6) Hoffmann, M.; Wilson, C. J.; Odell, B.; Anderson, H. L. *Angew. Chem. Int. Ed.* **2007**, *46*, 3122.
(7) O'Sullivan, M. C.; Sprafke, J. K.; Kondratuk, D. V; Rinfray, C.; Claridge, T. D. W.; Saywell, A.; Blunt, M. O.; O'Shea, J. N.; Beton, P. H.; Malfois, M.; Anderson, H. L. *Nature* **2011**, *469*, 72.
(8) Shi, W.; Lei, A. *Tetrahedron Lett.* **2014**, *55*, 2763.
(9) Movsisyan, L. D.; Franz, M.; Hampel, F.; Thompson, A. L.; Tykwinski, R. R.; Anderson, H. L. *J. Am. Chem. Soc.* **2016**, *138*, 1366.
(10) Tobe, Y.; Fujii, T.; Naemura, K. *J. Org. Chem.* **1994**, *59*, 1236.
(11) Tobe, Y.; Fujii, T.; Matsumoto, H.; Naemura, K.; Achiba, Y.; Wakabayashi, T. *J. Am. Chem. Soc.* **1996**, *118*, 2758.
(12) Tobe, Y.; Matsumoto, H.; Naemura, K.; Achiba, Y.; Wakabayashi, T. *Angew. Chem. Int. Ed. Engl.* **1996**, *35*, 1799.
(13) Moore, K. A.; Vidaurri-Martinez, J. S.; Thamattoor, D. M. *J. Am. Chem. Soc.* **2012**, *134*, 20037.
(14) Maurer, D. P.; Fan, R.; Thamattoor, D. M. *Angew. Chem. Int. Ed.* **2017**, *56*, 4499.